UNIVERSITEIT VAN PRETORIA
UNIVERSITY OF PRETORIA
YUNIBESITHI YA PRETORIA
Denkleiers • Leading Minds • Dikgopolo tša Dihlalefi

Potential anticancer actions of cholecalciferol on a cervical squamous carcinoma cell line

Sachin Bhoora

(15104533)

Thesis submitted in fulfilment of part of the requirements for the degree

Master of Science (Chemical Pathology)

Faculty of Health Sciences

University of Pretoria

Supervisor: Dr R. Punchoo

Department of Chemical Pathology, Faculty of Health Sciences, University of Pretoria, South Africa

Co-supervisor: Prof T.S. Pillay

Department of Chemical Pathology, Faculty of Health Sciences, University of Pretoria, South Africa

October 2020

Executive Summary

Cervical cancer is the fourth most common female malignancy worldwide and is substantively higher in low-income and middle-income countries. In South Africa, cervical cancer is a leading cause of mortality amongst women.

The anti-cancer actions of the vitamin D and its numerous metabolites are an active field of research. The family of vitamin D metabolites regulate numerous cellular pathways which are implicated in tumorigenesis. Pre-clinical studies and clinical studies have yielded promising, although conflicting results in various cancers.

Some healthy and cancerous tissue express an autocrine vitamin D metabolising system (VDMS) which is capable of tightly regulating intracellular metabolism and growth. The VDMS expresses activating and inactivating enzymes and a vitamin D receptor (VDR). At the cellular level, the VDMS can activate and inactivate vitamin D precursors and transduce signals to the nucleus to regulate various cell health genes, including cell growth, metabolism and survival. Healthy and cancerous cervical tissue express a VDMS.

The anti-cancer actions of cholecalciferol, an early precursor of activated vitamin D, is poorly studied in cervical cancer. This study aimed to characterise cholecalciferol's action on cell growth, cell death and the VDMS in a high-grade cervical cancer cell line, SiHa.

SiHa cell cultures were treated with a range of cholecalciferol doses (26 nM, 104 nM, 260 nM and 2600 nM) for 72 hours. Cell count and viability were assessed by crystal violet and trypan blue assays, respectively. Cell proliferation was enumerated by Ki67 nuclear antigen and the cell cycle profile analysed by flow cytometry. Apoptotic cell death was investigated by measuring mitochondrial membrane potential ($\Delta\Psi m$), phosphatidylserine (PS) externalisation, effector caspase activation and evaluation of DNA damage markers by flow cytometric analysis. The biochemical markers microtubule-associated proteins 1A/1B light chain 3B-II (LC3-II) and lactate dehydrogenase (LDH) were also measured by flow

cytometry and spectrophotometric analysis to identify autophagic cell death and necrosis, respectively. In addition, brightfield microscopy and transmission electron microscopy (TEM) were respectively used to characterise morphological and ultrastructural features of apoptosis, autophagic cell death and necrosis. The VDMS in SiHa control and experimental cultures were characterised by the investigation of intracellular gene and protein expression of the cholecalciferol activating (CYP2R1 and CYP27A1) and inactivating (CYP24A1) enzymes, and the VDR. Qualitative microscopical analysis evaluated classical characteristics of cell death and semi-quantitative analysis of apoptosis was performed. Data were analysed using a one-way ANOVA and Bonferroni *post-hoc* test. $p < 0.05$ was considered statistically significant.

A significant decrease in cell count and cell viability was identified in SiHa cell cultures treated with 2600 nM cholecalciferol. Furthermore, significant increase in biochemical markers of apoptosis were identified including, decreased $\Delta\Psi m$; PS exposure; terminal caspase activation; and nuclear damage at 2600 nM cholecalciferol treatment of SiHa cell cultures. Moreover, the biochemical findings were supported by brightfield microscopy and TEM, which observed classical apoptotic features *viz.* membrane blebbing, apoptotic bodies and nuclear fragmentation. Also, a significantly increased number of apoptotic cells were enumerated. There was no evidence of autophagic cell death and necrosis. Additionally, a significant increase in 25-hydroxylase (CYP2R1) gene and protein expression was identified in SiHa cells treated with 2600 nM cholecalciferol. Conversely, a significant decrease in 1α-hydroxylase (CYP27B1) gene and protein expression was identified in SiHa cells treated with 2600 nM cholecalciferol. Furthermore, significant increase in both 24-hydroxylase (CYP24A1) and VDR expression at gene and protein levels were observed in 2600 nM experimental SiHa cultures.

In conclusion, cholecalciferol exerts growth inhibition and apoptosis in SiHa cells at 2600 nM. This is accompanied by CYP2R1 and VDR upregulation which suggests autocrine activation to calcidiol and intracellular nuclear signalling, respectively. It is therefore hypothesised that calcidiol synthesised *de novo* binds to VDR and induces apoptosis in SiHa cell line.

Keywords: Vitamin D, cholecalciferol, cervical cancer, anti-cancer, SiHa, vitamin D receptor, vitamin D metabolism, calcidiol, apoptosis

Acknowledgements

Firstly, I would like to sincerely thank my supervisor, Dr Rivak Punchoo. Thank you for consistently supporting me throughout these years and for always encouraging me to do my best. Thank you for believing in me, even when I did not believe in myself. I am eternally grateful. Secondly, many thanks to my co-supervisor, Prof. T.S. Pillay, for his support, practical suggestions and review of draft versions of this thesis.

A special thank you to my family and friends for their unparalleled love and support during my MSc. Most importantly, I would like to thank my parents for their continuous care and support, and enabling me to achieve my personal and educational goals.

Lastly, I would like to acknowledge the National Research Foundation (NRF) and the University of Pretoria's post-graduate bursary for funding my studies.

This project was funded by the South African Research Medical Research Council (SAMRC) and the School of Medicine Research Committee of the University of Pretoria (SOM RESCOM).

Declaration

I, Sachin Bhoora, declare that this dissertation, which I hereby submit for MSc in Chemical Pathology at the University of Pretoria, is my own work and has not previously been submitted by me for a degree at this or any other tertiary institution.

Signature: _____ Date: 26 January 2021

Research Outputs

Conference Outputs

Poster Presentations

Conference:	The 56th congress of the Microscopy Society of Southern Africa (MSSA)
Title:	Cholecalciferol inhibits cell growth and induces apoptosis in SiHa cells
Authors:	S. Bhoora, T.S. Pillay and R. Punchoo
Date:	1st -5th December 2019
Venue:	Club Mykonos Resort (Langebaan, Western Cape, South Africa)
ISBN:	978-0-6398435-0-6

Accepted abstracts

Conference:	IFCC WorldLab Congress (*postponed*)
Title:	Cholecalciferol induces apoptosis and regulates the vitamin D metabolic pathways in the SiHa cervical cancer cell line
Authors:	S. Bhoora, T.S. Pillay and R. Punchoo
Presentation type:	Poster
Date:	1st -5th December 2021
Venue:	Seoul, South Korea

Conference postponed due to COVID-19 pandemic

Table of Contents

Executive Summary ii

Acknowledgements v

Research Outputs vii

List of Figures xiii

List of Tables xv

List of Abbreviations xvi

1. Introduction 1

2. Literature review 3

2.1 Cervical cancer epidemiology 3

2.2 Risk factors for cervical cancer 3

2.3 Cervical cancer tumorigenesis 4

2.4 The screening and diagnosis of cervical cancer 5

2.5 Preventing and treating cervical dysplasia, and early and advanced cervical cancer 6

2.6 The SiHa cervical cancer cell line 7

2.7 Vitamin D in the body 7

2.7.1 Activation and inactivation of vitamin D 7

2.7.2 Vitamin D transport in the body 9

2.7.3 Vitamin D status of the body 10

2.7.4 The physiology of vitamin D 10

2.7.5 Genomic and non-genomic actions of vitamin D 11

2.7.6 The pleiotropic actions of vitamin D in the body 12

2.8 The VDMS in cancer 14

2.8.1 Altered VDR expression in cancer 15

2.8.2 Altered 25-hydroxylase expression in cancer 16

2.8.3 Altered CYP27B1 expression in cancer 16

2.8.4 Altered CYP24A1 expression in cancer 17

2.8.5 A summary of changes in expression of the VDMS in cancer 18

2.9 The mechanisms of anti-cancer action of vitamin D metabolites 20

2.9.1 Vitamin D inhibits cell proliferation in cancer 20

2.9.2 The role of vitamin D in inducing cell cycle arrest in cancer 20
2.9.3 Apoptotic cell death 27
2.9.4 Autophagic cell death 33
2.9.5 Necrotic cell death 37
2.10 Vitamin D and cervical cancer in vitro 38
3. Aims and objectives 39
3.1 Aims 39
3.2 Objectives 39
4. Materials and methods 41
4.1 Basic cell culture techniques 41
4.1.1 Materials 41
4.1.2 Cell line and cell culturing 41
4.1.3 Cryopreservation and retrieval of cells 42
4.1.4 Seeding cells for experiments 43
4.1.5 Determination of optimal treatment range and incubation period 44
4.1.6 Control and experimental cultures 45
4.2 Cell health assays 47
4.2.1 Crystal violet assay 47
4.2.2 Trypan blue exclusion assay 48
4.2.3 Count and viability assay 49
4.3 Ki67 cell proliferation assay 51
4.3.1 Principle of the assay 51
4.3.2 Materials and method 51
4.4 Cell cycle analysis 52
4.4.1 Principle of the assay 52
4.4.2 Materials and method 52
4.5 Assessment of apoptosis 53
4.5.1 Mitochondrial membrane potential ($\Delta\Psi m$) assay 53
4.5.2 Annexin V detection assay 54
4.5.3 Caspase 3/7 detection assay 55
4.5.4 DNA damage analysis 56
4.6 Autophagy detection assay 57
4.6.1 Principle of the assay 57
4.6.2 Materials and method 58
4.7 Necrosis detection assay 59

4.7.1 Principle of the assay 59
4.7.2 Materials and method 59
4.8 Analysis of cell morphology 60
4.8.1 Brightfield microscopy using haematoxylin and eosin (H&E) staining 60
4.8.2 Transmission electron microscopy 62
4.9 Analysis of gene and protein expression 64
4.9.1 Quantitative polymerase chain reaction (qPCR) 64
4.9.2 Western blots 70
4.10 Statistics 75
4.10.1 Sample size 76
4.10.2 Quantitative data analysis 76
4.10.3 Qualitative and semi-quantification data analysis for microscopy studies 76
5. Results 78
5.1 Optimal incubation period for cholecalciferol treatments in SiHa cells determined by cell enumeration and viability 78
5.2 Cell proliferation measured by Ki67 proliferation marker expression 81
5.3 Cell cycle analysis using Muse™ Cell Cycle assay 82
5.4 Biochemical investigation of modes of cell death 85
5.4.1 Biochemical markers of early apoptosis 85
5.4.2 Biochemical markers of late apoptosis 89
5.4.3 Autophagic cell death 92
5.4.4 Necrotic cell death based on LDH release 94
5.5 Cell morphology and cell ultrastructure of cholecalciferol-treated SiHa cells 95
5.5.1 Qualitative assessment of cell morphology using Brightfield microscopy 96
5.5.2 Cell ultrastructure assessed using transmission electron microscopy (TEM) 102
5.6 Evaluation of gene and protein expression of the VDMS 105
5.6.1 Effects of cholecalciferol on gene and protein expressions of the 25-hydroxylases (CYP2R1 and CYP27A1) in SiHa cell line 105
5.6.2 Effects of cholecalciferol on gene and protein expressions of 1α-hydroxylase (CYP27B1) in SiHa cell line 108
5.6.3 Effects of cholecalciferol on gene and protein expressions of VDR in SiHa cell line 109
5.6.4 Effects of cholecalciferol on gene and protein expressions of 24-hydroxylase (CYP24A1) in SiHa cell line 110
6. Discussion 113

6.1 Rationale for investigating the anti-cancer actions of vitamin D in cervical cancer 113

6.2 Cholecalciferol inhibited cell count and viability in the SiHa cell line 113

6.3 Cholecalciferol did not decrease Ki67 expression in SiHa cells 115

6.4 Cholecalciferol did not disrupt cell cycling but increased the sub-G_1 population of SiHa cells 116

6.5 Cholecalciferol upregulated early and late biochemical and morphological markers of intrinsic apoptosis in SiHa cell line 117

6.5.1 Cholecalciferol induced mitochondrial damage in SiHa cell line 118

6.5.2 Cholecalciferol induced phosphatidylserine externalisation in SiHa cells 119

6.5.3 Cholecalciferol induced terminal caspase activation in SiHa cell line 120

6.5.4 Cholecalciferol induced significant DNA damage in SiHa cell line 122

6.5.5 Summary: cholecalciferol treatment induced intrinsic apoptosis in SiHa cell line 122

6.6 Cholecalciferol treatment did not induce autophagic cell death and necrosis in SiHa cell line 123

6.7 Cholecalciferol did not increase or decrease the large multinucleated (LMNC) sub-population in SiHa cells 123

6.8 Cholecalciferol induced perturbations of gene and protein expression in the VDMS in SiHa cell line 124

6.8.1 The VDMS in cervical tissue 124

6.8.2 Cholecalciferol induces significant CYP2R1 gene and protein expression in SiHa cell line 125

6.8.3 Cholecalciferol significantly downregulated CYP27B1 gene and protein expression in SiHa cell line 127

6.8.4 Cholecalciferol significantly upregulated VDR gene and protein expression in SiHa cell line 128

6.8.5 Cholecalciferol significantly upregulated CYP24A1 gene and protein expression in SiHa cell line 129

6.9 A proposed mechanism of cholecalciferol action on the VDMS and induction of intrinsic apoptosis in SiHa cell line 130

6.10 Limitations of the study 131

7. Conclusion 133

8. References 135

Appendices 162

Appendix A: Growth inhibitory studies conducted over 24 hours, 48 hours and 72 hours showing the GI_{50} concentration 162

Appendix B: Crystal Violet Staining Solution (0.5%) 163

Appendix C: Excitation and emission spectra of Muse™ Assays 164

Appendix D: Preparation of assay and fixation buffers for the Muse™ Ki67 proliferation assay 165

Appendix E: Muse™ Caspase 3/7 detection assay reagents 165

Appendix F: Muse™ Multi-Colour DNA Damage assay 166

Appendix G: LDH reagent preparation 166

Appendix H: H&E reagent preparation 167

Appendix I: Morphological criteria assessed in control and experimental cultures by H&E stained microscopy 167

Appendix J: Morphological criteria semi-quantified in control and apoptotic cells by H&E stained microscopy 169

Appendix K: Preparation of embedding solution for TEM analysis 170

Appendix L: Ultrastructural criteria used in the assessment of control and experimental SiHa cells analysed by TEM 170

Appendix M: qPCR Primer optimisations 171

Appendix N: Efficiency plots 177

Appendix O: Western blot reagents 178

Appendix P: An example of a BCA protein assay standard curve 178

Appendix Q: Optimised antibody concentrations 179

Appendix R: Ethics approval letter 180

Appendix S: Biostatistician clearance letter 181

List of Figures

Figure 1. Progression of cervical dysplasia to cervical cancer mediated by HPV infection..... 5
Figure 2. Pathway of vitamin D_3 metabolism in the human body. 9
Figure 3. The activation of vitamin D in the endocrine axis and the autocrine vitamin D metabolising system (VDMS). 14
Figure 4. Altered expression of the VDMS in cancer 19
Figure 5. The cell cycle 21
Figure 6. Calcitriol regulation of p21 and p27 expression in the G_1 phase of the cell cycle[6] 25
Figure 7. Biochemical and morphological parameters present during apoptotic cell death[163] 31
Figure 8. Intracellular process of autophagy[179] 34
Figure 9. A simplified outline of methodological techniques aligned with each research objective in this study. 46
Figure 10. Overview of the steps performed to identify differential expression of genes of the VDMS in control and experimental SiHa cells..... 66
Figure 11. Manual RNA isolation protocol using QIAzol lysis reagent 67
Figure 12. Overview of workflow for Western Blot experiments 72
Figure 13. The wet transfer sandwich orientation 74
Figure 14. Cell count using the crystal violet assay 78
Figure 15. Cell viability semi-quantified by trypan blue dye exclusion in SiHa control and experimental cultures at 24, 48 and 72 hours 79
Figure 16. Cell viability in SiHa control and experimental cell cultures at 24, 48 and 72 hours..... 80
Figure 17. Effects of cholecalciferol Ki67 cell proliferation marker in SiHa cells..... 82
Figure 18. Effects of cholecalciferol on the cell cycle profile SiHa control and experimental cultures 84
Figure 19. Mitochondrial membrane potential ($\Delta\Psi m$) in SiHa control and experimental cell cultures..... 86
Figure 20. Annexin V binding in SiHa control and experimental cell cultures 88

Figure 21. Activation of caspases -3 and -7 activation in SiHa control and experimental cell cultures 90
Figure 22. DNA damage in SiHa control and experimental cell cultures 92
Figure 23. LC3-II intensity detected the induction of autophagic cell death 94
Figure 24. Necrotic cell death assessed using the lactate dehydrogenase (LDH) release assay 95
Figure 25. Light microscopy images of haematoxylin and eosin (H&E) stained SiHa cultures 97
Figure 26. Brightfield micrograph of H&E stained SiHa cells treated with 2600 nM cholecalciferol 98
Figure 27. Giant multinucleated cells (outlined) present in control and experimental SiHa cell cultures 99
Figure 28. Semi-quantification of morphological features of apoptosis in SiHa control and experimental cultures. 101
Figure 29. Giant multinucleated cells in SiHa cell cultures 102
Figure 30. Transmission electron micrographs of SiHa control and experimental cultures 103
Figure 31. Transmission electron micrographs in solvent control and 2600 nM cholecalciferol treatment in SiHa 104
Figure 32. Gene and protein expression of CYP2R1 in SiHa control and experimental cultures 106
Figure 33. Gene and protein expressions of CYP27A1 enzyme in SiHa cell cultures treated with cholecalciferol 107
Figure 34. CYP27B1 gene and protein expression in SiHa cells 109
Figure 35. Vitamin D receptor (VDR) gene and protein expression in SiHa control and experimental cultures 110
Figure 36. Effects of cholecalciferol on CYP24A1 gene and protein expression in SiHa control and experimental cultures 111
Figure 37. Proposed hypothesis for the induction of apoptosis by cholecalciferol in the SiHa cell line. 131

List of Tables

Table 1. Studies identifying G_0/G_1 cell cycle arrest induced by calcitriol and/or vitamin D analogues *in vitro* 24
Table 2. List of the appropriate seeding density for each experiment in the most suitable cell culture plate for the experiment. 44

List of Abbreviations

$1,25(OH)_2D_3$	1,25-Dihydroxycholecalciferol (calcitriol)
$25(OH)D_3$	25-Hydroxycholecalciferol (calcidiol)
7-AAD	7-Aminoactinomycin D
APAF-1	Apoptotic Protease Activating Factor
ATCC	American Type Culture Collection
ATM	Ataxia-telangiecsta mutated
ATR	ATM-and-Rad3 related
BAD	BCL-2-associated death promoter
BAK	BCL-2 homologous antagonist killer
BAX	BCL-2-associated X
BCA	Bicinchoninic acid
BCL	B-Cell lymphoma
BCL-XL	B-Cell lymphoma-extra large
BCL-2	B-Cell lymphoma protein 2
BCL-W	B-Cell lymphoma-2 like 2 protein
BFL-1	B-Cell lymphoma-2 related protein A1
BLAST	Basic Local Alignment Search Tool
BME	Basal Medium Eagle
BSA	Bovine serum albumin
calcitriol-MARRS	Calcitriol-Membrane-associated rapid response steroid-binding protein
CDKI	Cyclin dependent kinase inhibitor
CDK	Cyclin dependent kinase
cDNA	complementary DNA
CFKAR	Caspase-8 and FADD-like apoptosis regulator

CIN	Cervical intraepithelial neoplasia
CIP	Cdk interacting protein
Ct	Cycle threshold
CYP24A1	Cytochrome P450 Family 24 Subfamily A Member 1
CYP27A	Cytochrome P450 Family 27 Subfamily A Member 1
CYP27B1	Cytochrome P450 Family 27 Subfamily B Member
CYP2R1	Cytochrome P450 Family 2 Subfamily R Member 1
Cyt C	Cytochrome C
DAP-3	Death associated protein 3
DDR	DNA damage response
DISC	Death-inducing signalling complex
DMSO	Dimethyl sulfoxide
DNA	Deoxyribonucleic Acid
DSB	Double stranded break
dsDNA	Double-stranded DNA
E	Efficiency
E2F-1	Elongation factor 2
ECL	Enhanced chemiluminescence
EDTA	Ethylenediaminetetraacetic acid
EMT	Epithelial-mesenchymal transition
ELISA	Enzyme-linked immunosorbent assay
FADD	FAS-associated protein with a death domain
FasL	Fas ligand
FasR	Fas receptor
FCS	Foetal calf serum
FGF-23	Fibroblast growth factor-23
FI	Fluorescence intensity

FS	Forward scatter
G_0	Resting phase / Quiescent phase
G_1	Gap 1 phase
G_2	Gap 2 phase
GADD45α	Growth arrest and DNA damage inducible alpha
Gy	Gray
H&E	Haematoxylin and eosin
HPV	Human papilloma virus
HRP	Horseradish peroxidase
IGFBP-3	Insulin growth factor binding protein-3
IOM	Institute of Medicine
KIP	Kinase inhibitory protein
LC3	Microtubule-associated 1A/1B-Light Chain 3
LDH	Lactate dehydrogenase
LMNC	Large multinucleated cell
M	Mitosis
MAPK	Mitogen activated protein kinase
MCL1	B-Cell lymphoma-2 family apoptosis regulator
miRNA	micro-RNA
ml	Millilitre
MOMP	Mitochondrial outer membrane permeabilization
MPER	Mammalian protein extraction buffer
MRN	Mre11-Rad50-Nbs1 protein complex
mRNA	Messenger ribonucleic acid
mTORC1	Mammalian target of rapamycin complex 1
MTT	3-(4,5-Dimethylthiazol-2-Yl)-2,5-Diphenyltetrazolium bromide
NCCP	National Cancer Control Programme

NAD^+	Nicotinamide adenine dinucleotide
NR1I	Nuclear hormone receptor 1I
Pap	Papanicolaou
PBS	Phosphate buffer solution
PDCD4	Programmed cell death 4
PI	Propidium iodide
PI3k	Phosphatidylinositol 3-kinase
PKC	Protein kinase c
PS	Phosphatidylserine
pRB	Retinoblastoma protein
PTEN	Phosphatase and tensin homologue deleted on chromosome 10
PTH	Parathyroid hormone
PVDF	Polyvinylidene fluoride
RCD	Regulated cell death
RANK	Nuclear factor-kb
RANKL	Nuclear factor-kb ligand
RNA	Ribonucleic acid
RPMI	Roswell Park Memorial Institute
rRNA	ribosomal RNA
RT-qPCR	Real-time quantitative polymerase chain reaction
RXR	Retinoid x receptor
ROS	Reactive oxygen species
S	Synthesis
SCC	Squamous cell carcinoma
SDS	Sodium dodecyl sulphate
SEM	Standard error mean
SIL	Squamous intraepithelial lesions

SPARC	Secreted protein acidic and rich in cysteine
TEM	Transmission electron microscopy
Ta	Annealing temperature
Tm	Melting temperature
TNFα	Tumour necrosis factor α
TMRE	Tetramethylrhodamine ethyl ester
TRPV6	Transient receptor potential cation channel, subfamily V, member 6
UTR	Untranslated region
UVB	Ultraviolet B
VDBP	Vitamin D binding protein
VDR	Vitamin D receptor
VDREs	Vitamin D response elements
VIA	Visual inspection with acetic acid
VILI	Visual inspection with Lugol’s iodine

1. Introduction

Cervical cancer is the fourth most common female malignancy worldwide and is substantively higher in low-income and middle-income countries.[1-2] Although primary prevention strategies are advocated, the incidence and prevalence in sub-Sahara regions of developing African countries is sub-optimal in curbing disease incidence and prevalence.[1,3] In South Africa, cervical cancer is a leading cause of mortality in women. In 2018, age standardised statistics published by the International Agency for Research on Cancer (IARC) showed that cervical cancer had the second-highest incidence rate of 12,1% (n = 12983) and mortality rate of 9,8% (n = 5595) in South Africa.[4]

The role of vitamin D in bone mineral metabolism is well-characterised and the pleomorphic actions of the vitamin D metabolites on extra-skeletal tissue is an evolving area of research.[5] Notably, the anti-cancer actions of the vitamin D is a growing field of research with potentially useful clinical applications in primary and adjunctive secondary treatment of cancer.[5-6] Pre-clinical and clinical studies have yielded inconsistent findings on the protective action of vitamin D against tumorigenesis in various cancers. Pre-clinical studies have identified anti-cancerous mechanisms which include dysregulation of cell proliferation, induction of cell death, attenuation of tumour invasion and metastasis and promotion of cellular differentiation.[5-6] Clinical trials have shown most substantial evidence of vitamin D's anti-cancerous action in breast, colon and prostate cancers.[6]

The vitamin D family of hormones are secosteroids endogenously synthesised from steroid precursors (7-dehydrocholesterol) and also supplemented by dietary intake.[7] The fully activated endogenous metabolite, calcitriol (1,25-dihydroxycholecalciferol; $1,25(OH)_2D_3$) is formed from sequential hydroxylation reactions of cholecalciferol catalysed by cytochrome-P450 enzymes present in the liver (25-hydroxylase) and kidney (1α-hydroxylase).[8] Calcitriol binds to the intracellular vitamin D receptor (VDR) and regulates the expression of genes implicated in cellular metabolism and growth.[7]

Interestingly, a similar autocrine system of vitamin D enzymes and receptor has been identified in selective tissues, for example, cervical tissue.[9-11] This system is referred to as the vitamin D metabolising system (VDMS) and functions to regulate vitamin D metabolism and actions in an autocrine and/or paracrine manner. The VDMS therefore carefully regulates cellular physiology related to vitamin D responsive genes, for example, genes regulating cell proliferation and cell differentiation. Normal and cancerous cervical tissue express a VDMS[9] and this suggests that vitamin D regulates cellular growth and cell death, in both healthy and cancerous cervical cells and cervical tissue. The potential role of vitamin D and the VDMS in regulating cell growth and cell death are poorly studied in cervical cancer. Furthermore, the regulation of the VDMS by early vitamin D pre-hormones, for example, cholecalciferol, are also poorly explored in the literature.

The relevance of cervical cancer to our geographic context, coupled to the inexpensive, relatively non-toxic and ready availability of vitamin D pharmaceuticals invites investigation of the role of vitamin D and vitamin D metabolites in cervical cancer. This study therefore investigated the effect of cholecalciferol on growth, cell death and the regulation of the VDMS in a high grade cervical squamous carcinoma cell line, SiHa. This study will contribute to the narrow field which explores the anti-cancer actions of vitamin D and its metabolites in cancerous cervical tissue. More specifically, the findings may suggest further investigation of vitamin D's action on other *in vitro* cervical cancer cell lines. In addition, this study may inform potential clinical translational research of vitamin D's anti-cancer actions in the South African population.

2. Literature review

2.1 Cervical cancer epidemiology

Cervical cancer is the fourth most common cancer amongst females in the world,[12] and is a major global health challenge.[2] In South Africa, cervical cancer is the leading cause of cancer related death in women.[2,4] In 2018, there was an estimated 569 847 new diagnoses of cervical cancer and 311 265 deaths worldwide,[1] however; there is a great disparity in incidence and mortality with geographic location.[12] Low-income countries accounted for approximately 90% of the 270 000 deaths due to cervical cancer in 2015.[13]

Population-based screening programs have led to a worldwide decline in the incidence and mortality of cervical cancer in recent years.[14] The implementation of these programmes in high-income countries in Europe and North America has significantly decreased the incidence of cervical cancer.[15-16] In countries with poor health resources, limited access to healthcare and ineffective screening programmes, for example, Eastern Europe and Central Asia, data demonstrates rapid increase in premature cervical cancer mortality.[12,17] Furthermore, where data are available in Africa, for example, sub-Saharan Africa, Uganda and Zimbabwe, an increase in the incidence and mortality are reported for cervical cancer.[12,18]

2.2 Risk factors for cervical cancer

The Human Papilloma Virus (HPV) is the critical aetiological agent of cervical cancer.[19] Approximately 99.7% of cervical cancer cases result from persistent infection with high-risk oncogenic strains of HPV.[4] There are 15 oncogenic high-risk strains, and HPV 16 and 18 are responsible for the majority of cases.[20] Most infections are short-lived and spontaneously resolve. HPV resolution requires an intact immunological system.[21] In the natural evolution of HPV infection, cervicitis usually lasts approximately 8-13 months in young women, and then spontaneously resolves.[22]

HPV is transmitted through sexual activity, and the risk factors such as immunosuppression (especially, due to human immunodeficiency virus infection), smoking, high parity, early sexual debut, multiple sexual partners and the use of oral contraceptives increase transmission.[2]

2.3 Cervical cancer tumorigenesis

DNA alterations underpin the progression of HPV infected epithelial tissue to invasive cancer.[23] The virus integrates its genome into the host's genome and takes control of the host's transcriptional machinery.[23-24] This enables self-replication and spread of virions in the epithelium layer of the cervix.[23-24] HPV encodes oncoproteins E6 and E7 that disrupt cellular function of host cells. In particular, these oncoproteins inhibit the function of tumour suppressor proteins, p53 and retinoblastoma (pRB), which permit the progression to invasive cancer.[24-25]

In approximately 90% of patients, HPV is cleared by the immune system within 5-10 years post-infection.[26-27] Patients only present with cervical cancer approximately 15 years after latent infection, which demonstrates the slow progression of this malignancy.[26-27] Cervical cancer is characterised by a pre-malignant phase that is identified by cytological examination of exfoliated cervical cells.[21] Cervical cancer is confirmed on histological examination of cervical biopsies.[21] The pre-malignant phase is characterised by dysplastic changes of squamous cells in the cervical epithelium.[28] These changes are known as cervical intraepithelial neoplasia (CIN).[28] CIN is histologically graded according to severity and ranges from CIN1 (mild dysplasia) to CIN2 (moderate dysplasia) to CIN3 (severe dysplasia/carcinoma in situ) (Figure 1).[21] CIN1 is typically cleared by the patient's immune system; however, CIN1 lesions that do not regress may progress into CIN 2 and CIN 3 within 3 years following primary HPV infection.[28]

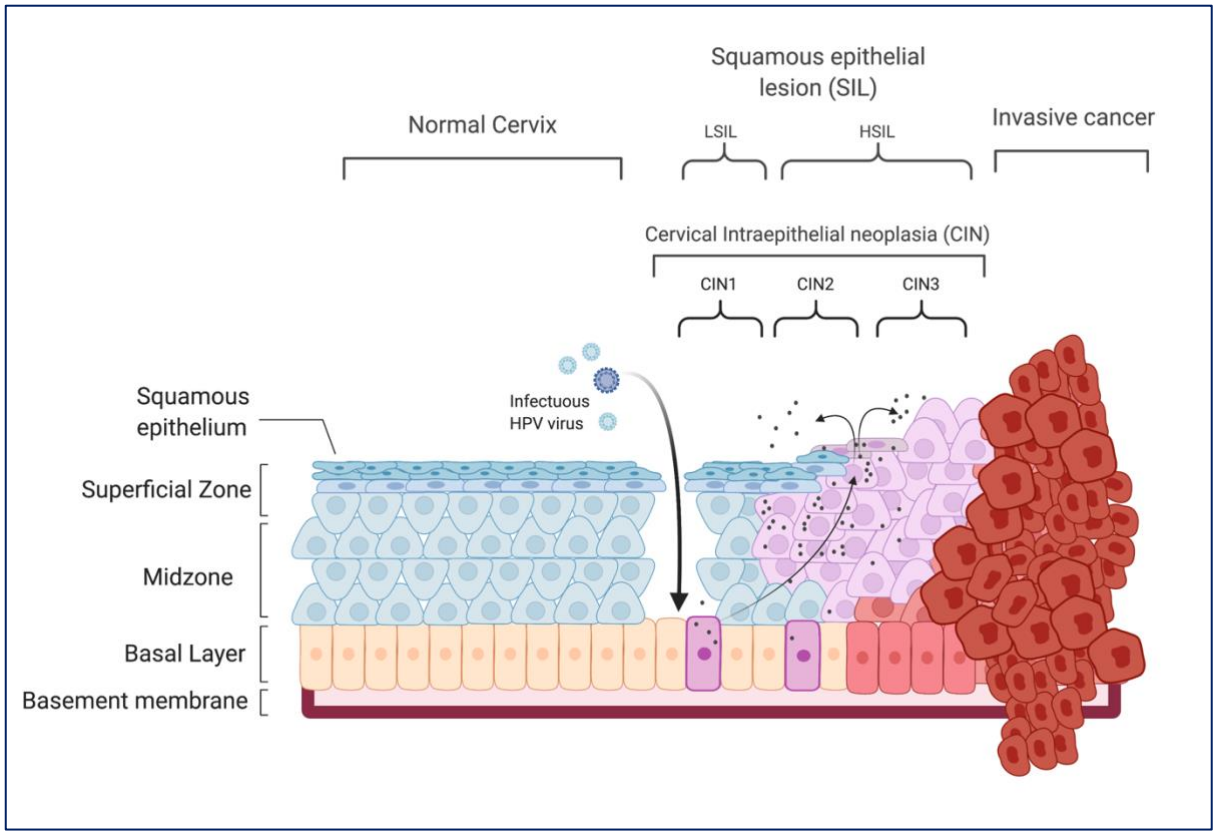

Figure 1. Progression of cervical dysplasia to cervical cancer mediated by HPV infection.

Early dysplastic changes (dysplasia) are termed cervical intraepithelial neoplasia (CIN) and are graded 1-3 based on their severity and invasion of the midzone of the cervix epithelium. These CIN categories can be further classified into squamous intraepithelial lesions (SIL) of low grade (CIN1) and high grade (CIN 2 and CIN3). High-grade SIL can progress to cervical cancer and invade the basement membrane. (Source: personal collection; adapted from Woodman *et al.*[21]). Image created using BioRender.com.

2.4 The screening and diagnosis of cervical cancer

Cervical cancer screening involves cervical cytology and/or HPV testing and/or tissue biopsy.[29] Screening of early-stage lesions and HPV infection can detect common types of cervical cancer, adenocarcinoma and squamous cell carcinoma.[29] Early treatment of the disease prevents the progression to invasive cancer and thus reduces cervical cancer mortality.[20,30]

The first screening method developed was cytology-based and named eponymously the Papanicolaou (Pap) smear test.[30] Since then, countries which have adopted this screening method have significantly reduced their cervical cancer incidence and mortality rates.[31] HPV testing is a polymerase chain reaction (PCR) test that identifies

most, but not all, high-risk subtypes of HPV DNA. HPV testing demonstrates a higher sensitivity and reproducibility compared to cytology.[32]

Generally, guidelines in the United States of America suggest co-testing with Pap smear and HPV to screen for cervical cancer.[33] If both tests are positive for cervical cellular abnormality, then the patient is referred for colposcopy.[32-33] However, recommendations for screening approaches vary between female age groups and co-morbid patient factors, such as HIV-infected patients or those receiving immunosuppressive medication.[29]

In South Africa, the National Department of Health launched a health policy called National Cancer Control Programme (NCCP) to address the local burden of cervical cancer. Under the policy, women over 30 years are given access to three free Pap smears during their lifetime, should they remain asymptomatic.[3] However, this programme was ineffective due to a lack of health care workers, a shortage of equipment and poor follow-up of patients with abnormal cytology.[3] HPV testing is expensive and not yet freely available in South Africa - and only offered by a limited number of diagnostic laboratories.[34] The National Department of Health does not endorse other screening modes for cervical cancer, such as visual inspection with acetic acid (VIA) and visual inspection with Lugol's iodine (VILI), in the current cervical cancer control policy.[3,18] The current challenges of delivering and expanding screening programmes and initiatives in South Africa may strongly play a role in cervical cancer incidence and mortality in the country.

2.5 Preventing and treating cervical dysplasia, and early and advanced cervical cancer

Prior to the advent of HPV vaccinations, prevention of cervical cancer relied on preventing HPV infection by sexual abstinence, mutual monogamy of virgins and the use of condoms.[2,13] Today, three globally available HPV vaccinations include bivalent, quadrivalent and 9-valent vaccinations, each with increasing numbers of target antigens against oncogenic HPV strains.[30] Data suggests that high-coverage vaccination of school girls between 9-12 years of age will cost effectively benefit

cervical cancer prevention.[18] In the UK, the quadrivalent vaccination is routinely offered to girls aged 12-13 years, whereas girls as young as 9 years are vaccinated in USA.[30] In South Africa, a national HPV vaccination programme was initiated in 2014 and aimed to vaccinate school girls aged 9-10 years with quadrivalent Cervrix HPV vaccine.[35]

Patients infected with the HPV virus, require secondary prevention. These include screening for pre-invasive abrasions and early diagnosis of dysplastic cervical cancerous change and cervical cancer.[2,21] Early diagnosis allows for early treatment and management of the carcinoma with improved clinical outcomes.[20] The success and effectiveness of the secondary preventative methods depend mainly on the population coverage and the efficiency of the screening technique employed.[2,21]

Lastly, once diagnosed with cervical cancer, tertiary methods of management are required. These methods include radiotherapy, surgery and chemotherapy.[18] Once cervical cancer reaches an incurable stage, palliative care is the only option, which is focussed on symptomatic relief and hospice care.[3]

2.6 The SiHa cervical cancer cell line

According to the American Type Culture Collection (ATCC),[36] the SiHa cell line is a human cervical cancer cell line derived from a 55-year-old Japanese woman. It is classified as a grade II squamous cell carcinoma. The genome has 1 to 2 copies of HPV 16 integrated into it. Approximately 24% of the cells in the SiHa cell line are hyper-triploid and have a modal chromosomal number of 71. The oncogenes p53 and pRB are present in this cell line.

2.7 Vitamin D in the body

2.7.1 Activation and inactivation of vitamin D

Vitamin D is a steroid hormone which is endogenously synthesised from steroid precursors, such as cholecalciferol (vitamin D_3) and ergocalciferol (vitamin D_2). Cholecalciferol is synthesised non-enzymatically from 7-dehydrocholesterol present in

skin stores when ultraviolet B rays from sunlight penetrates the skin.[7] Ergocalciferol is obtained from vitamin D fortified foods or vitamin D supplements.[7] Vitamins D_2 and D_3 are activated endogenously and exert similar physiological actions in the human body.[8] Both precursors are similarly metabolised and only differ in their chemical composition and potency: D_2 is less potent than D_3.[8] In most cases, vitamin D_2 and D_3 are collectively referred to as vitamin D as they both contribute to the vitamin D stores in the body. For the sake of clarity, all vitamin D compounds will be referred to by their scientific name or chemical identifier throughout this thesis.

Vitamin D is activated by two sequential hydroxylation reactions in the body.[7] These activation hydroxylation reactions are catalysed by cytochrome p450 (CYP) enzymes located primarily in the liver and kidney, respectively.[8]

The first activation reaction of cholecalciferol (Figure 2) and ergocalciferol is catalysed by 25-hydroxylase enzymes in the liver to form calcidiol (25-hydroxycholecalciferol; $25(OH)D_3$) and ergodiol ($25(OH)D_2$), respectively. To date, six 25-hydroxylase enzymes have been identified in humans, and include CYP2R1, CYP27A1, CYP3A4, CYP2C11, CYP2J1 and CYP2D25.[8] The predominant 25-hydroxylases are CYP2R1 and CYP27A1, as they are the largest contributors to calcidiol and ergodiol synthesis in the body.[8] Between the two 25-hydroxylases, the liver microsomal CYP2R1 is considered the major physiologically relevant 25-hydroxylase, as it contributes to 50% of the 25-hydroxylated vitamin D pool in the human body.[37]

The second hydroxylation reaction takes place in the kidney where $25(OH)D_3$ and $25(OH)D_2$ are hydroxylated by 1α-hydroxylase (CYP27B1) to form the most bioactive compound, calcitriol, ($1,25(OH)_2D_3$, also referred to as $1α,25(OH)_2D_3$; Figure 2).[37] Unlike the 25-hydroxylases, there is only one 1α-hydroxylase enzyme. This enzyme's expression and activity is carefully regulated to maintain by calcium and phosphate homeostasis.[5] Furthermore, this enzyme is expressed in extra-renal tissues, conferring calcitriol synthesis in these tissues.[38-39] The relevance of this extra-renal synthesis will be discussed later.

$25(OH)D_3$ and $1,25(OH)_2D_3$ are inactivated by hydroxylation of carbon-24 in the kidney by 24-hydroxylase (CYP24A1) enzyme.[5] CYP24A1 is best-characterised vitamin D

catabolic enzyme and catabolises 25(OH)D_3 and 1,25(OH)$_2D_3$ by either a 24-oxidase pathway or a 23-hydroxylase pathway.[37] The final product of the 24-oxidase pathway is the biologically inactive calcitroic acid (1α,24,25(OH)$_3D_3$), whereas the 23-hydroxylase pathway produces biologically active 1α,25R(OH)$_2D_3$-26,23S-lactone.[40] The 24-hydroxylase and the 1α-hydroxylase enzymes are reciprocally expressed in vitamin D target tissues, such as the kidney, to regulate 1,25(OH)$_2D_3$ levels. In addition, another 24-hydroxylase enzyme (CYP3A4) has been reported; however, data on this enzyme is limited and preliminary findings indicate that CYP3A4 has a lower specificity for vitamin D metabolites in comparison to CYP24A1.[41]

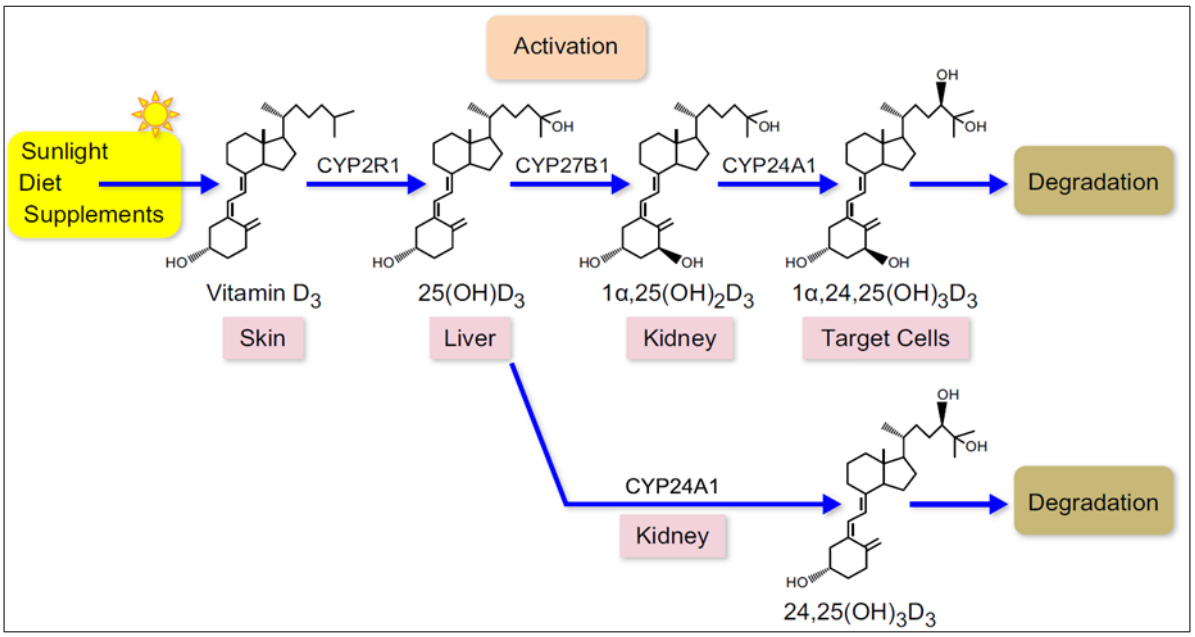

Figure 2. Pathway of vitamin D_3 metabolism in the human body.

Cholecalciferol is synthesised in the skin from 7-dehydrocholesterol precursors under UVB sunlight exposure (not shown) and undergoes sequential hydroxylations in the liver and kidney, respectively. Both the intermediate metabolite, calcidiol (25(OH)D_3) and calcitriol (1,25(OH)$_2D_3$), synthesised in the kidney are catabolised by CYP24A1, 24-hydroxylase enzyme, to maintain vitamin D homeostasis. Source: Pike *et al*.[42] (University of Pretoria institutional copyright clearance obtained from the Clinical Key Health database)

2.7.2 Vitamin D transport in the body

The 25-hydroxylated vitamin D metabolites (25(OH)D_3 and 25(OH)D_2) are transported in the bloodstream complexed to vitamin D binding protein (DBP) to target tissues, such as the kidney.[5] DBP is a serum glycoprotein that transports all vitamin D metabolites and has a high affinity for 25(OH)D_3 and a lower affinity to 1,25(OH)$_2D_3$.[43]

Additionally, DBP also has higher affinity for vitamin D_3 compared to that of vitamin D_2 metabolites[44] preventing its premature degradation. This difference in binding affinity may explain the lower biological activity of vitamin D_2 (as free 25(OH)D_2 will degrade) and the longer half-life of 25(OH)D_3 compared to 25(OH)D_2 in humans.[44]

2.7.3 Vitamin D status of the body

The 25-hydroxylated vitamin D metabolites (25(OH)D_3 and 25(OH)D_2) are the most abundant vitamin D metabolites in the body.[45] Vitamin D reserve or status is defined by the quantity of 25(OH)D_3 and 25(OH)D_2, also termed total vitamin D, measured in the human body.[46-47] There is currently no consensus on optimal serum 25(OH)D_3 and 25(OH)D_2 levels in the body. However, it was agreed by two independent expert panels, the Endocrine Society and Institute of Medicine (IOM), that serum total vitamin D levels should not fall below 30 nM, irrespective of age and gender.[48] In addition, the current definition of vitamin D deficiency is a serum concentration less than 50 nM (20 ng/ml) because at this cut-point concentration and below, optimal bone health, muscular function and calcium homeostasis are impaired and physiological compensatory mechanisms to regulate these functions are activated.[48]

2.7.4 The physiology of vitamin D

2.7.4.1 The endocrinology of vitamin D

Activated vitamin D, calcitriol, principally functions in the small intestine, bone and the kidney.[5] In the intestine, calcitriol enhances absorption of dietary calcium and phosphate by increasing the expression of the epithelial calcium channel (transient receptor potential cation channel, subfamily V, member 6 [TRPV6]) and calcium-binding protein, calbindin 9K.[5] In the bone, calcitriol has osteolytic action *in vitro*, promoting osteoclast differentiation through the upregulation of receptor activator of nuclear factor-kB ligand (RANKL) in osteoblasts.[49] However, the physiological relevance of bone resorption by calcitriol is uncertain. In the kidney, calcitriol stimulates 24-hydroxylase synthesis, thereby catalysing its own degradation in states of elevated calcitriol levels, and thereby maintaining calcitriol levels within a healthy serum reference range.[5]

Renal synthesis of calcitriol, which is catalysed by 1α-hydroxylase, is regulated by several mechanisms.[49] Calcitriol synthesis is enhanced by low serum phosphate concentrations, low $1,25(OH)_2D_3$ concentration and by high concentration of parathyroid hormone (PTH). Hypophosphatemia and PTH increase $1,25(OH)_2D_3$ synthesis by increasing 1α-hydroxylase synthesis in the kidney. In hypocalcaemia, PTH is stimulated and increases renal $1,25(OH)_2D_3$ synthesis.[49] In contrast, calcitriol is suppressed by high concentrations of bone-derived fibroblast growth factor 23 (FGF-23).[5] FGF23 is produced by osteocytes in states of high serum calcitriol and phosphate levels and is also stimulated by PTH.[5] FGF-23 regulates phosphate and calcitriol homeostasis by acting on the kidney. It increases phosphate excretion by inhibiting the sodium–phosphate cotransporter expression and inhibits renal 1α-hydroxylase, thereby reducing calcitriol synthesis.[49]

2.7.5 Genomic and non-genomic actions of vitamin D

2.7.5.1 Nuclear vitamin D receptor

In vitamin D target tissues, $1,25(OH)_2D_3$ exerts its action by binding to a specific cytosolic receptor called vitamin D receptor (VDR).[50] VDR is a member of the NR1I receptor super family and functions as a transcription factor in target cells upon binding its ligand.[42,51] VDR is 427 amino acids long and C4-type zinc fingers that bind to DNA. Upon ligand binding, VDR dimerises with retinoid X receptor (RXR) and this heterodimer translocates into the nucleus.[42,51] In the nucleus, VDR binds to a specific consensus sequence of DNA, known as vitamin D response elements (VDRE).[52-53] Once bound to VDREs, the VDR-RXR complex recruits co-activators or co-repressors to either enhance or suppress transcription of vitamin D target genes, respectively.[5,42]

2.7.5.2 Non-genomic rapid response vitamin D receptor

Recent studies suggest that vitamin D metabolites may modulate non-genomic rapid responses by targeting signal transduction pathways responsible for enhancing intracellular calcium stores and increasing cell exocytosis/ATP secretion.[54] These rapid responses directly target cytosolic proteins and do not involve gene transcription and protein translation.[54] These rapid actions are thought to be mediated by VDRs located on the surface of the plasma membrane.[55] Two types of $1,25(OH)_2D_3$ receptors have been reported. Firstly, immunohistochemistry and confocal microscopy revealed that the classic cytosolic VDR localises to the lipid raft caveolae-enriched microdomain of the plasma membrane.[55] Secondly, the calcitriol-membrane-associated rapid response, steroid binding protein ($1,25(OH)_2D_3$-MARRS) has been reported in osteoblasts, chondrocytes and other cell types.[56-58] $1,25(OH)_2D_3$-MARRS is a member of disulfide isomerase protein family and is thought to also facilitate the non-genomic response of vitamin D in these cells.[54] However, the complete function of these receptors and their binding affinity compared to cytosolic VDR is poorly characterised, and thus their role remains unclear.

2.7.6 The pleiotropic actions of vitamin D in the body

Over the past few decades, the discovery of VDR expression in various extra-skeletal tissues that are not involved in the classic role of calcium homeostasis, has raised questions about the potential role of vitamin D at these extra-skeletal sites. Since then, research has expanded to include the biological actions of vitamin D which extend beyond bone mineral homeostasis. $1,25(OH)_2D_3$ has been reported to confer protective actions in cardiovascular disease, augment innate and adaptive immune functions, and protect against tumorigenesis.[59] This review will only consider the role of the vitamin D metabolites in cancer.

The actions of vitamin D are mediated by the vitamin D metabolising system (VDMS) or components of the VDMS. The VDMS consists of activating enzymes (25-hydroxylases and 1α-hydroxylase), 24-hydroxylase catabolic enzymes as well as VDR. Earlier studies demonstrated nearly ubiquitous VDR expression in the body.[6] Subsequent studies that showed that various cell types also express a functional

VDMS.[59-60] Notably healthy cervical tissue expresses an intact VDMS as reported by the Human Protein Atlas.[61]

Thus, $1,25(OH)_2D_3$ can function both as an endocrine (systemic) hormone when systemically metabolised, or exert biological function as an autocrine, paracrine or autocrine hormone when it is locally synthesised (Figure 3).[42] The localised regulation of vitamin D homeostasis at the cellular level in selective tissues therefore represents a finely tuned homeostatic intracellular milieu in which vitamin D exerts genomic and non-genomic biological actions. At a cellular level, vitamin D regulates various metabolic processes and cellular events, for example, cellular differentiation, cell growth and cell death.[5-6]

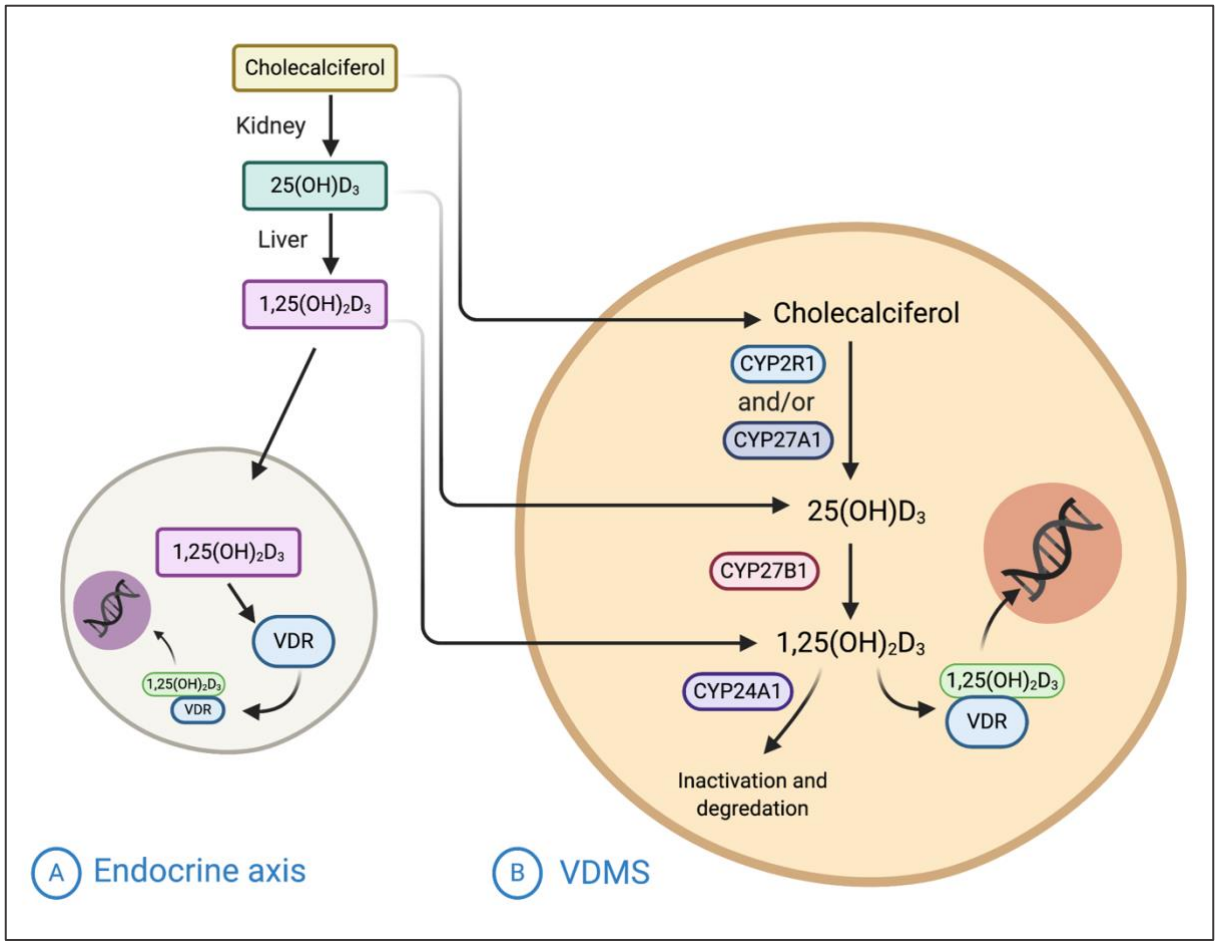

Figure 3. The activation of vitamin D in the endocrine axis and the autocrine vitamin D metabolising system (VDMS).

In the endocrine axis (A), cholecalciferol is activated in the liver and kidney, respectively, to form the active metabolite, calcitriol. Calcitriol travels in the blood to target cells, where it binds to VDR, translocates to the nucleus and mediates its genomic actions. In cells with an autocrine VDMS (B), precursor metabolites enter the cell from the blood and are activated by the autocrine VDMS to form calcitriol. Calcitriol then binds to VDR to mediate the genomic response. Furthermore, active vitamin D metabolites are inactivated and broken down intracellularly by CYP24A1. (Source: personal collection; adapted from Pike *et al.* [42] and Feldman *et al.*[6]). Image created using BioRender.com.

2.8 The VDMS in cancer

Healthy cells acquire mutations which initiate them to become tumorigenic and ultimately transform to a malignant phenotype.[62] During tumorigenesis, a key hallmark is also the dysregulation of intracellular biochemical signalling pathways. The elements of the VDMS – such as vitamin D activators, inactivators and the VDR – are also impacted during cancer development.[60,63] These alterations affect synthesis and catabolism of vitamin D and thereby, disrupt appropriate cell signalling by the VDR

ultimately reducing the cell's optimal responsiveness to vitamin D.[60,63] The next section will explore the alterations in the expression of the VDMS during carcinogenesis.

2.8.1 Altered VDR expression in cancer

VDR protein levels decline as tumours progressively de-differentiate and assume malignant phenotypes. For example, breast, skin, ovarian and colon cancers demonstrate a negative correlation between VDR expression and malignant phenotype.[64-66] This pattern of VDR expression suggests that VDR intracellular signalling confers protection against the development and progression of cancer.

To date, five mechanisms for VDR abrogation during carcinogenesis have been identified. Firstly, the Snail family of transcription factors, in particular Snail1 and Snail2 have been reported to inhibit VDR expression. Snail transcription factors are frequently overexpressed in cancers and enable epithelial-mesenchymal transition (EMT), tumour invasion and metastases.[67] In colon and breast cancer cells, Snail1 and Snail2 were shown to bind to E-boxes in the promoter region of *VDR* and recruit cop-repressors, thereby decreasing *VDR* transcription.[68-69] Secondly, oncogenic *Ras* mutations, such as *K-Ras* and *H-Ras* suppressed VDR transcription in mouse and human colon cancer cell lines, respectively.[70-71] Furthermore, parietal epithelial cell lines and keratinocytes with *K-Ras* and *H-Ras* mutations showed reduced VDR activity by phosphorylation of RXR. This prevented RXR binding to VDR and thus lead to impaired overall transcriptional activity of the VDR-RXR complex.[72] Thirdly, p53 mutants were shown to physically bind to VDR and redirect the VDR transactivation profile to support cell growth and prevent cell apoptosis.[73] Fourthly, overexpression of miRNA-125b attenuated VDR translation in MCF-7 breast cancer cells.[74] This is consistent with a finding of an inverse relationship between vitamin-D induced growth suppression and miRNA-125b expression in melanoma cell lines.[75] Finally, epigenetic modifications of the *VDR* gene promoter region by methylation of CpG islands caused a decrease in *VDR* expression in breast cancer cell lines.[76] These findings were supported by treatment of DNA methyltransferase inhibitors which rescued the VDR anti-proliferative action in these breast cancer cells.[76] Collectively, these studies demonstrate the potentially wide array of mechanisms which suppress VDR expression and increase tumorigenesis.

2.8.2 Altered 25-hydroxylase expression in cancer

The impact of 25-hydroxylases in carcinogenesis is not well documented as studies generally investigate the anti-cancer effects using activated vitamin D metabolites and their synthetic analogues, and not the precursor hormone. The action of precursor vitamin D metabolites, for example, cholecalciferol, therefore, is poorly characterised in cancer. In addition, there are numerous 25-hydroxylase enzymes[8] and therefore it is analytically challenging to characterise these multiple enzyme functions. Moreover, the cellular expression of the 25 hydroxylases is variable between tissues[37] and is not widely expressed as the VDMS is restricted to selected tissue.

CYP2R1 and CYP27A1 25-hydroxylases have been shown to be expressed by cervical, ovarian and prostate cancer cell lines. Kloss *et al.* have demonstrated expression of 25-hydroxylase in HeLa cervical cancer and OVCAR3 ovarian cancer cells lines.[10] However, the authors did not indicate which 25-hydroxylase enzymes were investigated. In a study by our research group, CYP27A1 and CYP2R1 expression was observed in HeLa cells and interestingly, only CYP27A1 expression was increased in response to 2600 nM cholecalciferol treatment.[77] This suggests that cervical cancer cells demonstrate differential biological activity between the 25-hydroxylases in cervical cancer *in vitro*. In prostate cancer RWPE-1 cells, CYP27A1 expression increased by treatment with 10^{-5} M cholecalciferol.[78] The latter two studies collectively show that early vitamin D precursor administration can upregulate synthesis of calcidiol by the autocrine VDMS present in the cancerous cell lines. However, more data is needed to characterise the role of these 25-hydroxylase enzymes in cancers and carcinogenesis.

2.8.3 Altered CYP27B1 expression in cancer

The expression CYP27B1 at extra-renal sites suggests that calcitriol can be locally synthesised from circulatory supply of calcidiol in a tissue specific manner.[60] In cancer, CYP27B1 expression declines as tumours de-differentiate. Thus, the autocrine synthesis of calcitriol by CYP27B1 (using calcidiol substrate) declines in cancerous tissue, with progressive loss of autocrine calcitriol synthesis in advanced malignancies.[79] This inverse relationship between CYP27B1 expression and the

degree of malignant phenotype was observed in skin, lung, parathyroid, colon and prostate cancers.[65,80-84]

The underlying mechanisms which cause a reduction in CYP27B1 expression in cancer cells remain unclear. One possible mechanism is the role of a pro-inflammatory tumour microenvironment. Pro-inflammatory cytokines, interleukin-6 and tumour necrosis factor α (TNFα), lead to a reduction in CYP27B1 expression in colon cancer cell lines.[85] This finding suggests that a pro-inflammatory tumour microenvironment down-regulates CYP27B1 expression, and consequently reduces autocrine calcitriol synthesis, conferring increased tumorigensis.[60]

2.8.4 Altered CYP24A1 expression in cancer

In contrast to VDR and CYP27B1 expression, CYP24A1 expression in positively correlated with cancer progression.[60,63] CYP24A1 catabolises $1,25(OH)_2D_3$ and therefore attenuates of $1,25(OH)_2D_3$ signalling, thereby causing a decrease in anti-cancer actions of vitamin D.[8,60,63] CYP24A1 thus has been proposed as a potential oncogene.[60,79] Albertson *et al.*[86] demonstrated amplification of the 20q13.2-20q13.3 locus, which encompasses the *CYP24A1* gene, in breast cancer patients. This finding was supported by an independent study in colon cancer tissue.[87] Interestingly, CYP24A1 was only amplified in malignant tissues but not benign colonic tumours, suggesting that CYP24A1 expression may be important for cancer initiation and early-stage cancer progression to malignant phenotype.[88]

Additional mechanisms of CYP24A1 upregulation have been identified. Firstly, CYP24A1 has been identified as a microRNA-125b target, which results in downregulation of CYP24A1 protein translation. Breast cancer biopsies analysed by immunohistochemistry revealed an inverse association of CYP24A1 protein expression and miRNA-125b levels.[89] Also, in an investigation of a panel of 27 lung cancer cell lines, the cell lines with reduced miR-17-miR -92 cluster expression demonstrated upregulated of CYP24A1 expression in the lung cancer cell lines.[90] These findings suggest that CYP24A1 levels are also influenced by dysregulated miRNA expression. Secondly, casein kinase 2 signalling pathway upregulated CYP24A1 expression in prostate cancer and portended poor prognosis.[91] Thirdly,

epigenetic modifications of the gene promoter region of *CYP24A1* also increases CYP24A1 expression as observed in lung and prostate cancers. [92-93]

2.8.5 A summary of changes in expression of the VDMS in cancer

In summary, autocrine regulation of the VDMS is important in tumorigenesis (Figure 6). Studies on cancer cell lines and cancerous tissue show a pattern of regulation of vitamin D activating enzymes and VDR, which respectively decrease autocrine synthesis of calcitriol and disrupt intracellular signalling by VDR. In addition, these studies show increased catabolic CYP24A1 expression which degrades activated vitamin D. Collectively, this pattern of VDMS expression in cancer suggests that vitamin D is protective against cancer at an autocrine and/or paracrine level. Furthermore, from the aforementioned discussion it is evident that multiple intracellular mechanisms (summarised in Figure 4) mediate regulation of the VDMS in cancerous cells and tissue, which confer an increased risk of tumour initiation and progression.

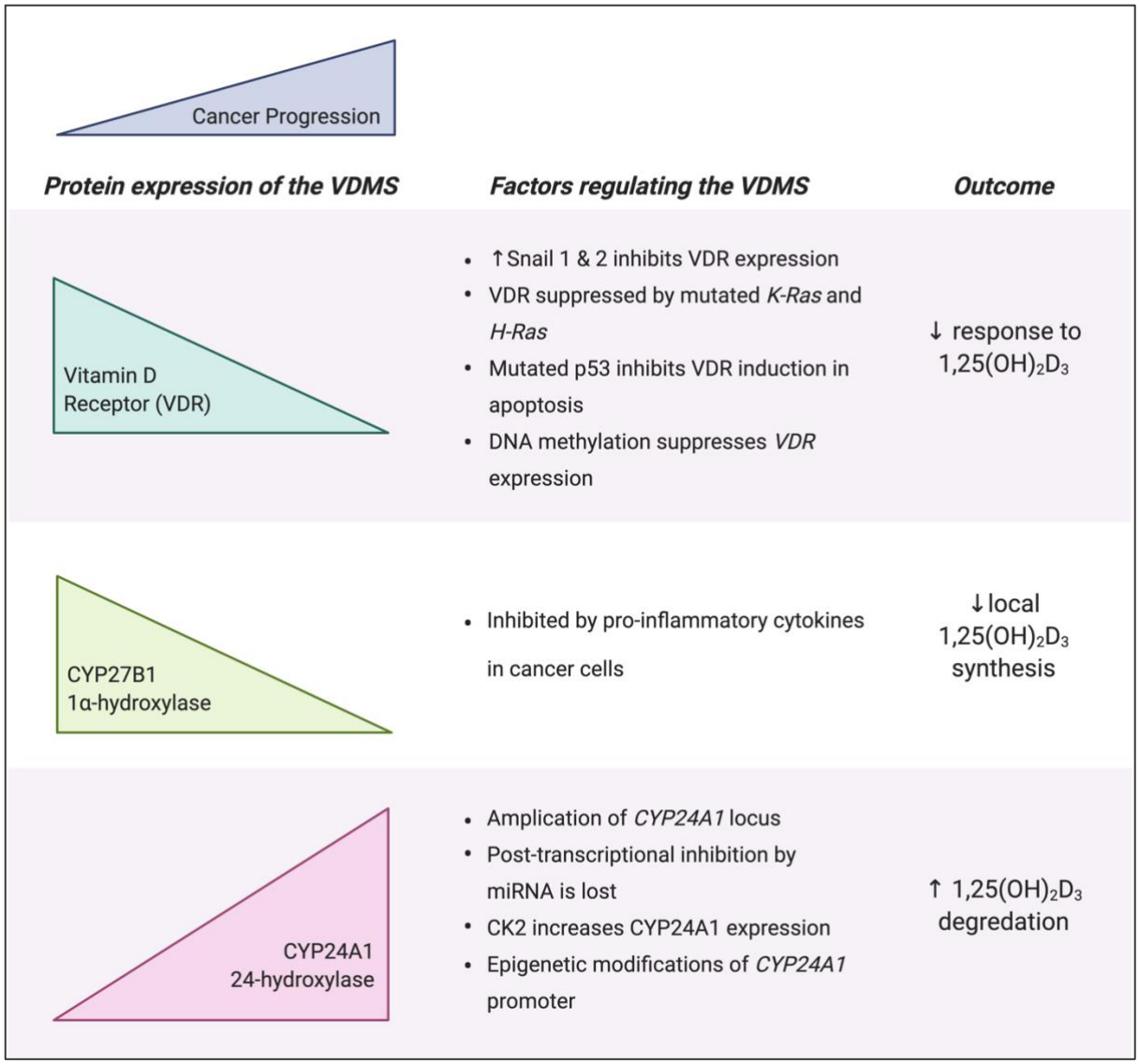

Figure 4. Altered expression of the VDMS in cancer

Cancer cells with malignant phenotypes demonstrate decreased VDR, CYP27A1 and increased CYP24A1 levels. The altered VDMS expression pattern decreases autocrine synthesis of calcitriol, increases catabolism of calcitriol and decreases signalling of calcitriol by VDR. This pattern favours tumorigenesis in cells expressing the VDMS. (Source: Personal collection). Image created using BioRender.com.

2.9 The mechanisms of anti-cancer action of vitamin D metabolites

Almost four decades ago, epidemiological data on sunlight (UVB) exposure and low latitude, both are factors which result in higher vitamin D production, showed lower incidence in colorectal cancer.[94] At the same time, Colston *et al.*[95] demonstrated a reduction in the growth rate of melanoma cell cultures treated with $1,25(OH)_2D_3$. Since then, numerous pre-clinical studies on the anti-cancer actions of vitamin D metabolites have shown promising results.[6,96] However, the mechanism of anti-cancer action of vitamin D metabolites remain elusive. The current data suggests that vitamin D and its metabolites induces cell death, reduces cell proliferation and inhibits tumour metastases and angiogenesis.[6,79,97-98] This section will review current data on the mechanisms of anti-cancer action of vitamin D and its metabolites.

2.9.1 Vitamin D inhibits cell proliferation in cancer

The anti-proliferative of vitamin D metabolites are well characterised and have been reported in cell lines derived from colon,[99] breast[100] and prostate[101] cancers. To date, various mechanisms of anti-proliferation by vitamin D metabolites have been reported.[102-104] The most commonly reported and best-described mechanism is direct targeting of cell cycle regulators to induce cell cycle arrest and therefore inhibit cell growth.[97-98] These direct actions on cell cycle regulators will be reviewed in detail.

2.9.2 The role of vitamin D in inducing cell cycle arrest in cancer

2.9.2.1 The cell cycle

Most cells in the body are not actively proliferating, but instead reside in 'out-of-cycle' states while a minority of cells, such as cancer cells, are actively cycling.[62] Most functional cells, such as neurons, have irreversibly withdrawn from the cycle into terminally differentiated states and will not undergo cell replication by mitosis throughout their lifetime. On the other hand, some cells may reversibly withdraw from the cell cycle and enter the 'quiescent' G_0 phase. These cells and may resume cell division depending on tissue milieu.[105]

The cell cycle consists of four sequential phases (Figure 5). The two important phases of the cell cycle are the DNA synthesis (S phase) and mitosis (M phase) phases, where DNA is duplicated and where two daughter cells are formed, respectively.[106] The G_1 and G_2 phases separate the S and M phases, respectively. The G_1 phase begins directly after mitosis and during this phase the cell is sensitive to mitogenic and growth inhibitory signals for DNA synthesis.[106] The G_2 phase is the gap phase between DNA synthesis and mitosis and is a period when the cell prepares for entry into mitosis. In mitosis (M phase), cells undergo karyokinesis (separation of chromosomes) and cytokinesis (cell division) to form two identical daughter cells.[107] Upon division, the two daughter cells may temporarily enter the quiescent G_0 phase depending factors such as mitogen deprivation or contact inhibition due to high cell density.[105] Checkpoints in the cell cycle maintain the correct sequential progression through the cell cycle and eliminate unhealthy cell.[105]

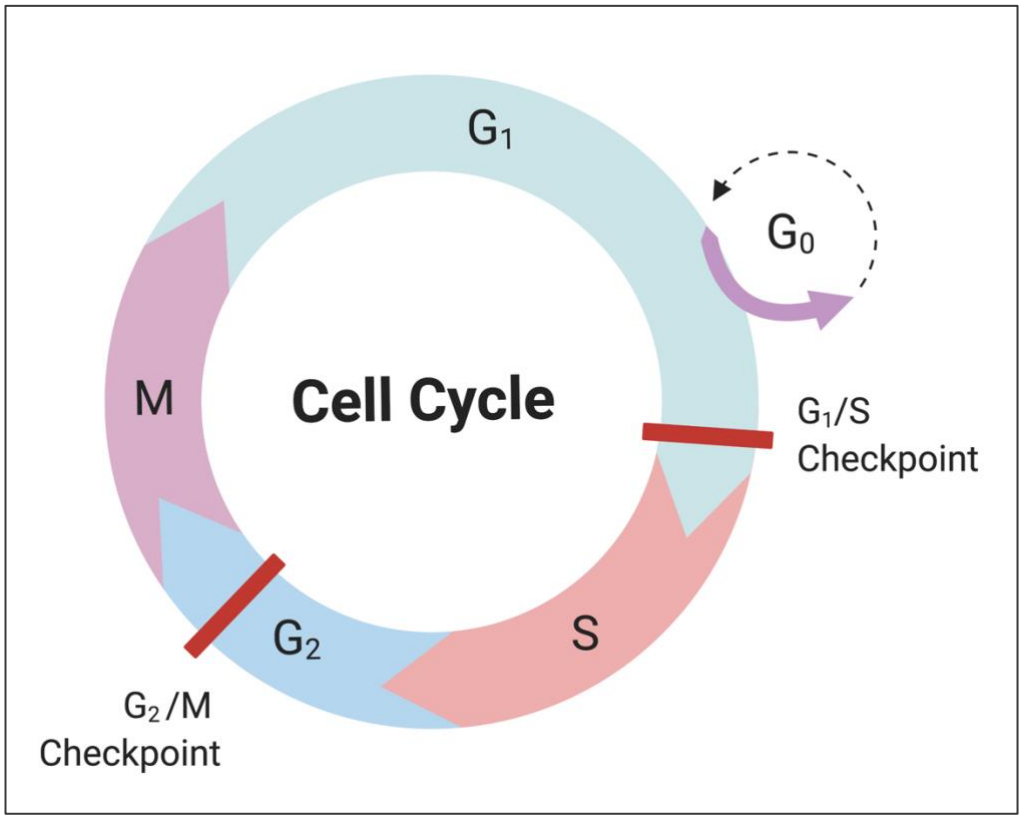

Figure 5. The cell cycle

The cell cycle consists of four active phases which terminate at the end of mitosis (M) phase. The G_0 phase is a quiescent phase in which the cell is not actively dividing. At the G_1/S and G_2/M phase boundaries lie checkpoint mechanisms that halt the cell cycle until all requirements for the phase are met before cell cycling proceeds. (Source: personal collection). Image created using BioRender.com.

2.9.2.2 Regulation of the cell cycle by cyclins and cyclin inhibitors

Cyclin dependent kinases (CDKs) are a family of heterodimeric serine/threonine protein kinases that drive progression through the cell cycle.[106] CDKs are the catalytic subunits and are constitutively expressed throughout each phase of the cell cycle.[108-109] CDKs depend on their specific cognate cyclin subunit for activation.[108-109] Cyclins are regulatory subunits which are expressed in a cyclical manner throughout the cell cycle.[110] Once bound together, the CDK-cyclin complexes regulates the transitions between each phase of the cell cycle.[109]

Cyclin D-CDK4, cyclin D-CDK6 and cyclin E-CDK2 complexes enable progression through the restriction point of the G_1 phase of the cell cycle.[111] Once the cell passes the G_1/S restriction point, it is committed to cell division and will undergo mitosis.[112] Mitogenic signals converge on cyclin D-CDK4 and result in temporal progression of the cell to the restriction point.[113] The restriction point is the gate keeper of the cell cycle.[113-114] For cells to pass the G_1/S restriction point, two criteria must be met. These include upregulation of cyclin E expression and hyperphosphorylation of retinoblastoma protein (pRB).[115] Cdk2 binds to cyclin E, which phosphorylates of pRB. The hyperphosphorylated pRB dissociates itself from E2F transcription factors,[115] causing free E2F transcription factors to activate proteins involved in the S phase and therefore, permitting DNA replication.[115]

Checkpoints in the cell cycle[105] mediate their actions by the activation of CDK inhibitors (CDKIs). The CDKIs inactivate cyclin-CDK complexes and therefore halt the cell cycle.[105] There are two families of CDKIs. Firstly, INK4 CDKIs are INhibitors of CDK4 and consist of four members: $p16^{INK4A}$, $p15^{INK4B}$, $p18^{INK4C}$ and $p19^{INK4D}$. INK4 inhibitors specifically prevent the binding of CDK4 and CDK6 to cyclin D, but do not bind other CDKs.[106] Secondly, the CIP/KIP family consists of three members: $p21^{CIP1}$ (Cdk Interacting Protein 1), $p27^{KIP1}$ (Kinase Inhibitory Protein 1) and $p57^{KIP2}$ (Kinase Inhibitory Protein 2), which bind CDK2 and inhibit CDK2 activity.[106] CDKIs are important in causing cell cycle arrest of unhealthy cells.

2.9.2.3 Vitamin D causes cell cycle arrest in cancer

2.9.2.3.i. G_1 arrest

Vitamin D metabolites mediate G_0/G_1 cell cycle arrest by upregulating p21 and p27 CDKIs. To date, this mechanism of action has been reported in nearly all cancer cell types treated with calcitriol and calcitriol analogues (Table 1).

Table 1. Studies identifying G_0/G_1 cell cycle arrest induced by calcitriol and/or vitamin D analogues *in vitro*

Tissue of origin	Author	Cell line(s)	Mechanism of action	Conclusion
Breast cancer	S. Jensen *et al.*[116]	MCF-7	Repression of c-myc expression (proto-oncogene) after calcitriol treatment	Reduction in cell cycle proliferation
	Chiang *et al.*[117]	MCF-1	p21 upregulation	G_0/G_1 cell cycle arrest
Ovarian cancer	Li *et al.*[118]	2008, CAOV3	p27 stabilisation cyclin E-CDK2 downregulation	G_0/G_1 cell cycle arrest
	Li *et al.*[118]	OVCAR3	p27 stabilisation	G_0/G_1 cell cycle arrest
Human head and neck squamous cells	Akutsu *et al.*[119]	SCC25 cells	Calcitriol analogue EB1089 upregulated growth repair damage factor GADD45α	G_0/G_1 cell cycle arrest
	Salehi-Tabar *et al.*[120]	SCC25 cells	Decreased expression of c-myc and c-myc target genes	G_0/G_1 cell cycle arrest
Prostate cancer	Washington *et al.*[121]	C4-2	Retinoblastoma protein (pRB)-independent G1 growth arrest	G_0/G_1 cell cycle arrest
	Bao *et al.*[122]	LNCaP, CWR22R, PC-3, CWR22R cell lines	Inhibition of Cyclin-dependent kinase-2	G_0/G_1 cell cycle arrest
	Boyle *et al.*[123]	LNCaP	Calcitriol upregulated the mRNA and protein expression of insulin-like growth factor binding protein 3, which resulted in increased expression of p21	G_0/G_1 cell cycle arrest
	Flores *et al.*[124]	LNCaP	Decreased activation of CDK2 leading to a hypophosphorylation of RB	G_0/G_1 cell cycle arrest
	Rohan *et al.*[125]	LnCaP, C4-2, RWPE-1	Downregulation of c-myc mRNA and protein expression	Growth inhibition and G_1 accumulation induced by $1,25(OH)_2D_3$ treatment
Adenoma and carcinoma colorectal cell lines	Diaz *et al.*[126]	SW620, PC/JW and HT29	Calcitriol and analogue EB1089 increased cells in G_1 in a p53 dependent manner	G_0/G_1 cell cycle arrest

The mechanisms of p21 and p27 upregulation by calcitriol are varied. A functional VDRE has been identified in the *p21* gene promoter region, enabling direct transcriptional regulation by calcitriol-VDR signalling.[127] In contrast, calcitriol improves p27 protein stability by inhibiting Skp2 activity. Skp2 is a ubiquitin-like protein responsible for the inactivation and degradation of p27.[118] These mechanisms of calcitriol regulation are illustrated in Figure 6 and lead to the inhibition of pRB phosphorylation which therefore prevents E2F activation and progression from the G_1 phase to the S phase.

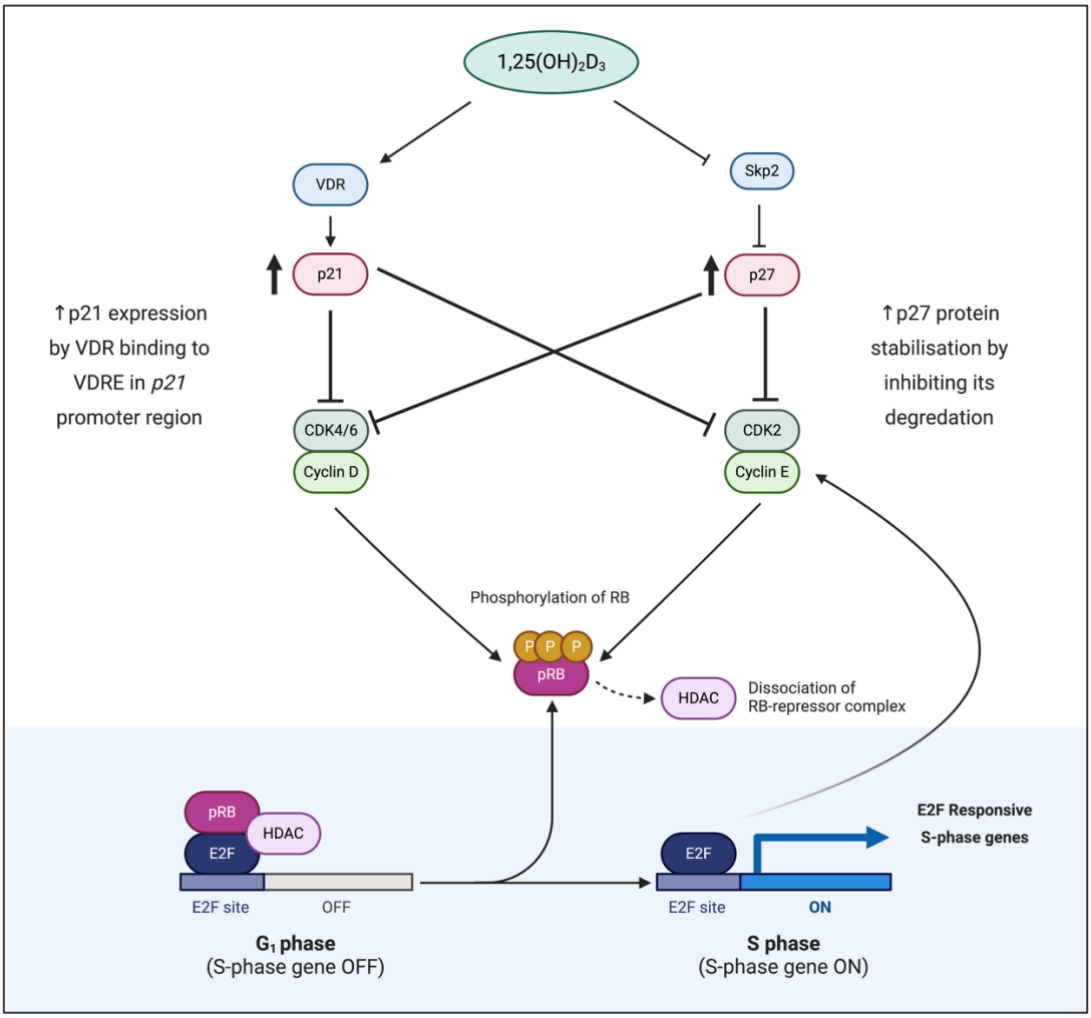

Figure 6. Calcitriol regulation of p21 and p27 expression in the G_1 phase of the cell cycle[6]

Calcitriol ($1,25(OH)_2D_3$) increases the expression of CDK inhibitors p21 and p27, which in turn suppress the activity of cyclin D-CDK4/6 and cyclin E-CDK2 complexes, respectively. Normally, cyclin D-CDK4/6 and cyclin E-CDK2 complexes phosphorylate retinoblastoma (pRB) allowing E2F transcription factors to increase expression of S-phase proteins and promote cell cycle progression. By increasing p21 and p27 expression, calcitriol prevents pRB phosphorylation and induces G_0/G_1 cell cycle arrest. (Source: personal collection). Image created using BioRender.com.

2.9.2.3.ii. G_2/M arrest

Once the cell has faithfully replicated the genome in the S phase, it enters the G_2 phase.[106] During this short growth phase, the cell continues to grow and synthesise requisite proteins for mitosis.[106] The primary objective of the G_2 checkpoint is to halt the cell cycle in the presence of DNA damage.[106] This ensures that any DNA lesions are not passaged to the daughter cells during mitosis. When DNA is damaged sensor proteins, such as Chk1 and Chk2, initiate the DNA damage response and induce cell cycle arrest.[128]

Currently, there is limited evidence of the induction of G_2/M arrest by $1,25(OH)_2D_3$, with the general consensus that G_1 cell cycle arrest is the primary target of vitamin D metabolites. However, there are a selected number of studies which have shown G_2/M cell cycle arrest in cells treated with $1,25(OH)_2D_3$. In HL60 myeloid leukaemia cells treated with $1,25(OH)_2D_3$, a G_2/M arrest was evident in cell cycle analyses.[129-130] Only one study identified a mechanistic link in $1,25(OH)_2D_3$-induced G_2/M cell cycle arrest. In ovarian cancer cell lines, $1,25(OH)_2D_3$ increased Growth arrest and DNA-Damage-Inducible alpha (GADD45α), and subsequently induced cell cycle arrest at the G_2/M phase.[131] Interestingly, a functional VDRE was identified in an exonic enhancer region of the *GADD45α* gene;[131] however, no additional studies exploring GADD45α and this VDRE in other cancer cell lines have been identified.

2.9.3 Apoptotic cell death

2.9.3.1 Apoptosis: intrinsic and extrinsic pathways

Apoptosis is a regulated mode of cell death characterised by distinct sets of morphological and biochemical changes which are well-described in the literature. Historically, apoptotic cell death was categorised purely by morphological manifestations of the cellular alteration. These features, first described by Kerr *et al.*[132] in 1972, included cytoplasmic and nuclear shrinkage (pyknosis), nuclear breakdown (karyorrhexis), nuclear membrane dissolution (karyolysis) and plasma membrane blebbing.[133] Currently, morphologic criteria, while still valuable, has been augmented by biochemical evaluation of cellular changes. The biochemical parameters provide evidence for early and late apoptotic biomarkers that culminate in terminal caspase activation and commitment to apoptosis.[134]

Apoptosis can be triggered by two distinct, but not mutually exclusive, signalling pathways that are activated extrinsically or intrinsically. The extrinsic pathway of apoptosis is initiated by an apoptogenic signal which binds a death receptors located on the plasma membrane.[135] In contrast, the intrinsic pathway of apoptosis is predominantly mediated by a diverse array of internal stressors which drive permeabilization of the outer mitochondrial membrane.[136-137] Thus, whereas the extrinsic pathway involves the activation of transmembrane receptors by an appropriate ligand; the intrinsic apoptosis pathway is activated by organelle damage and oncogenic stressors.[136-137] Regardless of how apoptosis is initiated, both intrinsic and extrinsic pathways converge upon activation of terminal caspases -3 and -7.[134]

The extrinsic pathway of apoptosis, also referred to as the death-receptor pathway, is activated at the plasma membrane by either death receptors or dependence receptors.[138] Death receptor signalling depends on the binding of the receptors' cognate ligand/s. For example, Fas ligand (FasL) on activated T-cells binds to the cell membrane receptor Fas (FasR) resulting in apoptotic death of the Fas-expressing cell.[139] On the other hand, dependence receptors are activated when the extracellular concentration of their specific ligand drops below a critical threshold.[138] An example of this is Patched1 which is activated when the level of trophic factor Sonic Hedgehog

critically declines.[140] Death receptors contain an intracellular Death Domain which allow for the activation of intracellular death signalling pathway, upon ligand binding.[140] Death receptors are normally homotrimeric. Upon Fas ligand binding, these death receptors oligomerise and recruit other intracellular adaptor proteins, such as pro-caspase 8 and FAS-associated protein with a death domain (FADD) forming an oligomeric death-inducing signalling complex (DISC).[141] DISC formation leads to caspase-8 formation and caspase-8 subsequently cleaves and activates caspase-3 and -7.[141]

In contrast, the intrinsic pathway, also termed mitochondrial apoptosis, is activated by a plethora of stimuli emanating from within the cell, such as DNA damage. Cells are generally able to withstand these intracellular perturbations in order to maintain homeostasis and prevent cellular demise.[134] The difference between cell survival and cell death is a balance between anti-apoptotic and pro-apoptotic proteins of the B-cell lymphoma (BCL-2) family of proteins.[134] Once the balance of the pro-death to pro-life signal shifts in favour of cell death, a subset of the BCL-2 family pro-apoptotic proteins form pores in the outer mitochondrial membrane (OMM). This results in the release of apoptogenic factors, such as cytochrome C (Cyt C), from the inter-membrane space into the cytosol.[134,142]

In the cytosol, Cyt C and a cytosolic adaptor protein called apoptotic peptidase activating factor 1 (APAF1) assemble the apoptosome.[134] The apoptosome is a supramolecular platform that is primarily responsible for cleaving pro-caspase-9 to active caspase-9.[143] Caspase-9 is an initiator caspase which proteolytically activates downstream effector caspase-3 and caspase-7.[134] Activation of the effector caspases in apoptosis precipitates many of the biochemical and morphological hallmarks of apoptosis, such as internucleosomal DNA fragmentation, karyorrhexis and externalisation of phosphatidylserine (PS).[144-145]

According to the current understanding, widespread mitochondrial outer membrane permeabilization (MOMP) is irreversible and represents the “point of no return” in intrinsic apoptosis.[143] Pore-forming pro-apoptotic proteins of the Bcl-2 family consist of BCL-2 associated X, apoptosis regulator (BAX), BCL-2 antagonist/killer 1 (BAK) and BCL-2 family apoptosis regulator (BOK).[146-147] Conversely, pro-survival anti-apoptotic

BCL-2 proteins include BCL-2 itself, BCL-2 like 1 (BCL-XL), BCL-2 family apoptosis regulator (MCL1), BCL-2 like 2 protein (BCL-W), and BCL-2 related protein A1 (BFL-1).[146-147] Under healthy conditions, anti-apoptotic proteins block pro-apoptotic BCL-2 proteins by binding and inhibiting them.[146-147] During apoptotic signalling, however, the expression of pro-apoptotic proteins increases relative to the anti-apoptotic proteins.[135] This culminates in the unbound pro-apoptotic proteins perforating the OMM to initiate the intrinsic apoptotic pathway.

The proteolytic activity of effector caspases precipitates intrinsic apoptosis once a point-of-no-return has been trespassed.[148] Caspases target a diverse range of substrates, such as nuclear lamins,[149-150] phospholipid support proteins[151-152] and DNase-bound inhibitor proteins.[153-154]

2.9.3.2 DNA damage and DNA damage repair in apoptosis

Eukaryotic cells mitigate genotoxic stress by a regulated and co-ordinated signalling pathway, termed the DNA damage response (DDR) pathway. DDR is responsible for the recognition, signalling and repair of double stranded breaks (DSBs) in cells. [155] The DDR pathway is triggered by aberrant DNA structures induced by replication stress or DNA damage, and like classic signal transduction pathways, these signals trigger transducers and further-downstream effectors.

In mammalian cells, ataxia-telangiecsta mutated (ATM) and ATM-and-Rad3 related (ATR) kinases are master regulators of DNA signalling and orchestrate a large network of proteins and cellular processes to mitigate DNA damage.[156] ATM and ATR are the most upstream DNA protein kinases, and phosphorylate downstream effectors at serine/threonine/glutamic acid motifs to halt cell cycle progression, recruit DNA repair enzymes and induce cellular senescence or apoptosis.[157-158] ATM is primarily activated by double strand DNA breaks (DSBs) and ATR responds to a broader range of DNA lesions including DSBs and DNA lesions that disrupt DNA replication and single stand DNA breaks.[156]

In response to DSBs, ATM is rapidly activated and localises to sites of DNA damage. The mechanism of the activation of ATM is still unclear; however, evidence suggests

that the Mre11-Rad50-Nbs1 (MRN) protein complex is involved in sensing DSBs.[159] Once activated, ATM triggers the DDR events at the chromatin flanking the DSBs by phosphorylation of histone variant H2A.X at Ser-139 to produce γH2A.X.[160] DSB detection of γH2A.X foci is about 100-fold more sensitive marker for DNA damage and is more reliable than other repair proteins that are present in cells, even when DNA is not damaged.[161] For example, it can detect DSBs at radiation doses as low as 1 mGy, which corresponds to one focus in every 30 cells.

During apoptosis, terminal caspases degrade proteins required for structural integrity, and also activate other degradation enzymes, such as DNases.[153-154] These enzymes target and cleave DNA at linker regions between oligonucleosomes producing DNA fragments of 180 bp (and multiples of 180 bp), which generate a characteristic “ladder” pattern on agarose gel electrophoresis.[162] DNA damage activates a series of intracellular machinery, such as ATM and γH2A.x which aim to repair DNA.

2.9.3.3 Summary: key morphological and biochemical biomarkers of apoptosis

Apoptotic cell death is characterised by a defined set of biochemical and morphological sequence of events that culminate in cell death.[134,142] Some of the hallmark features of apoptosis, such as phosphatidylserine (PS) exposure, and the activation of pro-apoptotic BCL-2 proteins may not necessarily progress to cell death.[148] Events at special time-points define points-of-no return which definitively commit the cell to an apoptotic fate.[142] For example, nuclear condensation is generally considered a point of no return which commits unhealthy cells to apoptosis. The sequential progression of the key parameters in apoptosis are illustrated in Figure 7.

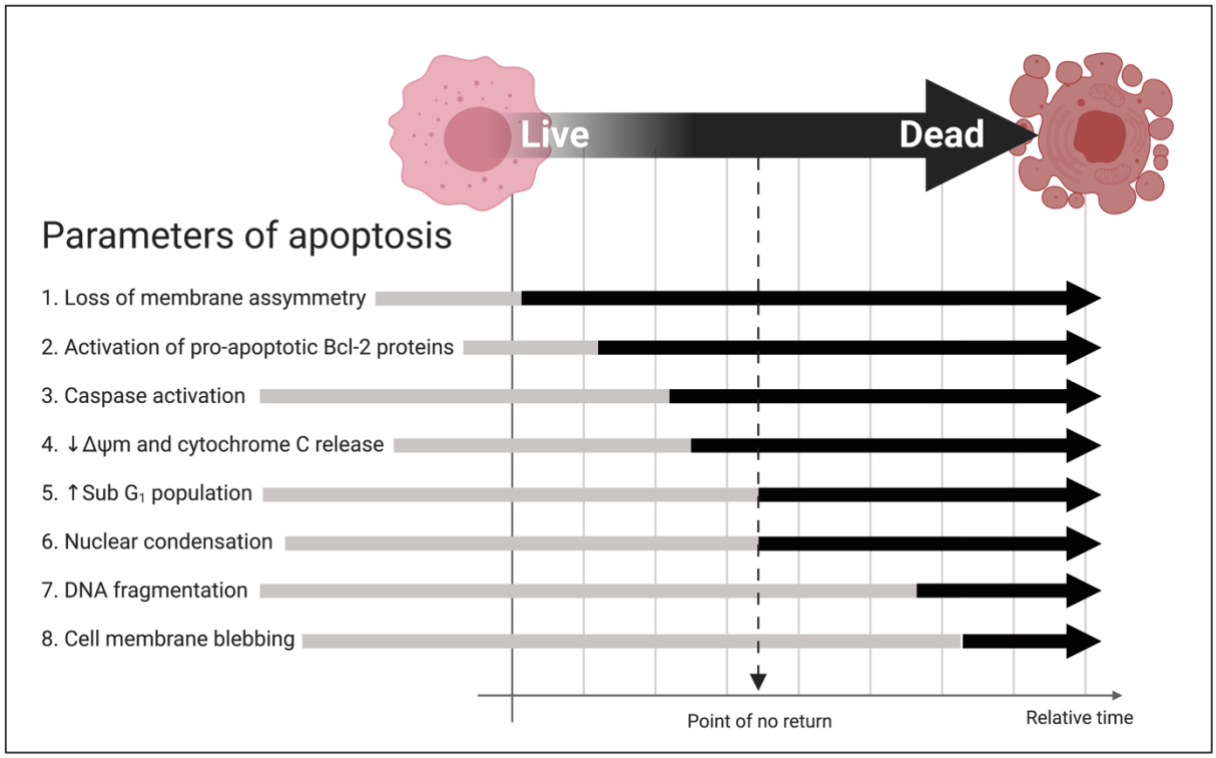

Figure 7. Biochemical and morphological parameters present during apoptotic cell death[163]

Biochemical and morphological features of apoptosis are typically expressed in a sequential manner. The length of arrows indicates the relative duration of each event. The point of no return is a defined time point characterised by cellular events that commit cells to apoptosis. (Source: personal collection; adapted from Abcam Apoptosis Guide[163]). Image created using BioRender.com.

2.9.3.4 The induction of apoptosis by vitamin D in cancer cell lines

The role of vitamin D in apoptotic induction is well reported and several underlying mechanisms have been identified. The most widely reported mechanism of apoptotic induction by vitamin D metabolites is the upregulation of pro-apoptotic BCL-2 proteins and suppression of antiapoptotic BCL-2 proteins.[6,97] This shifts the balance between pro-apoptosis and anti-apoptosis resulting in apoptotic cell death. This mechanism of action has been reported *in vitro* across multiple cell lines, for example, LNCaP prostate cancer cell line,[164] myeloid leukaemia K562 cell line[165] and metastatic lymphocyte SW480-ADH cell line.[166]

Additional pro-apoptotic mechanisms of vitamin D metabolites have also been identified. In a gastric cancer cell line, HGC-27, VDR was shown to upregulate phosphatase and tensin homologue deleted on chromosome 10 (PTEN) expression and induce apoptosis. PTEN is a tumour suppressor gene that suppresses protein kinase B activity and therefore promotes apoptosis.[167] In addition, in colorectal cancer

cell line, MIP101, 1,25$(OH)_2D_3$ treatment enhanced VDR expression and increased basal and chemotherapy-induced apoptosis by increasing the expression of secreted protein acidic and rich in cysteine (SPARC) gene and protein levels.[168] In breast cancer cell lines, mRNA microarray analyses revealed increased expression in mRNA encoding DAP-3 (death associated protein 3), caspase-8 and FADD-like apoptosis regulator (CFKAR) and numerous caspases (-3, -4, -6, -8) induced by 1,25$(OH)_2D_3$ treatment of MCF-7 and MDAMB-231 cell lines.[169] In addition, vitamin D analogue Ro3528 induced programmed cell death 4 (PDCD4) mRNA expression, and induced apoptosis in breast cancer cells.[170] These studies therefore suggest that vitamin D induces pro-apoptotic cell death regulators at a gene transcription level.

The role of vitamin D and the DDR pathway has predominantly been investigated with respect to the anti-oxidant defence mechanisms of calcitriol. Vitamin D metabolites have been shown to reduce the biological impact of reactive oxygen species (ROS) and consequently prevent DNA damage of the cell.[171-172] DNA damage and loss of repair mechanisms is a hallmark feature of carcinogenesis.[62] Calcitriol has been shown to induce several enzymes involved in anti-oxidant defence, including thioredoxin reductase, superoxide dismutase1 and 2 and glucose-6-phosphate-dehydrogenase in several cancer cell lines.[169-170,173-174] The intricacies of the anti-oxidant mechanisms of vitamin D will not be explored further as they are beyond the scope of this review.

With respect to apoptosis, the role of calcitriol and DNA damage has been demonstrated in a few studies. Galbiati *et al.*[175] demonstrated significant increase in DNA damage marker, *GADD45* gene, and induction of apoptosis in mouse insulinoma βTC_3 cells treated with 1000 nM calcitriol for 48 hours. Additionally, Jung *et al.*[176] demonstrated significant increase in DNA damage, assessed by a commercial DNA fragmentation enzyme-linked immunosorbent assay (ELISA) kit, in human ovarian cancer cell lines (SKOV3, OVCAR3, and OVCA433) treated with 50 µM 1,25$(OH)_2D_3$. Furthermore, in microarray studies in breast cancer cells, 1,25$(OH)_2D_3$ treatment modulated expression of genes which encode proteins involved in DNA repair and apoptosis, such as p53, RAD23 homolog B, PCNA and DAP1α.[166,169] Taken together, these findings indicate that calcitriol may prevent carcinogenesis by inducing apoptosis and augmenting the DDR pathway.

2.9.4 Autophagic cell death

2.9.4.1 The biology of autophagic cell death

Autophagy is a regulatory process that maintains energy and nutrient homeostasis within the cell.[177] Autophagy is characterised by the degradation and recycling of molecular building blocks mediated by lysosomal degradation. There are three known types of autophagic processes that occur in mammalian cells, namely, micro-autophagy, chaperone–mediated autophagy (CMA) and macro-autophagy.[178] Micro-autophagy and CMA are less commonly studied in mammalian cells. Briefly, in micro-autophagy, cytoplasmic content is directly engulfed by the lysosome and in CMA specialised chaperone proteins, which recognise lysosomal membrane receptors, shuttle cargo for degradation to lysosomes.[179] Macroautophagy (hereafter referred to as autophagy) is the best-characterised autophagy pathway.[178] It mediates degradation of cytosolic cargo, via engulfment of cargo by a double-membraned phagosome, that is presented to the lysosome for degradation.[180]

Autophagy is a co-ordinated intracellular event of more than 30 autophagy-related (Atg) proteins.[179] The process of autophagy (Figure 8) is a sequence of several discrete steps: (1) initiation and nucleation of the pre-autophagosomal membrane (phagophore), (2) autophagosome closure, (3) maturation of autophagosome by fusion with the lysosome to form the autolysosome, (4) degradation of cargo by acidic lysosomal enzymes and (5) cytosolic release of molecular building blocks by lysosomal membrane permeases.[181] Autophagy can either be classified as selective, where specific organelles are sequestrated into the autophagosome, or non-selective, which refers to “bulk” sequestration of cytoplasmic content into the autophagosome.[179] These classifications can be further divided into “basal autophagy” or “induced autophagy” subclasses, which are based on the absence or presence autophagy-inducing stimuli, respectively.[179]

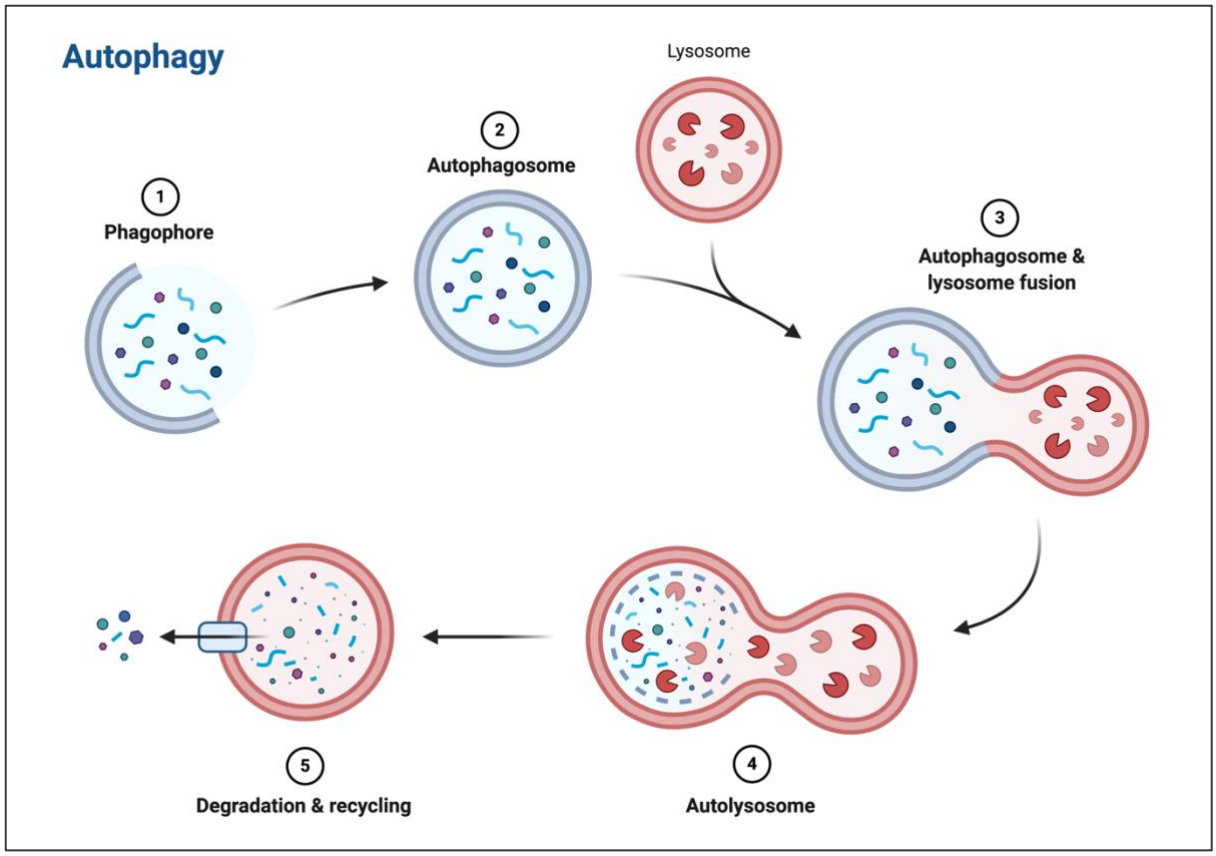

Figure 8. Intracellular process of autophagy[179]

Autophagy consists of a series of five discrete steps. Firstly, a phagophore emerges after autophagic signalling and begins to slowly elongate. In step 2, the mature phagophore forms a double membrane autophagosome. The autophagosome fuses with an acidic lysosome (step 3) in the cytosol to form a mature autolysosome (step 4). The acidic lysosome breaks down the cargo and expels molecular building blocks (step 5), such as amino acids and nucleotides, for reuse by the cell. (Source: personal collection). Image created using BioRender.com.

Autophagy is stimulated by a number of factors, including nutrient starvation, reactive oxygen speciation, DNA damage and hypoxia.[182] Mammalian target of rapamycin complex 1 (mTORC1) is a protein complex of that inhibits autophagy and is constitutively bound to another protein complex called the Atg1/ULK1 complex.[183] In starvation or energy depletion, mTORC1 dissociates from the ULK1 complex, which permits the ULK1 complex to initiate autophagosome nucleation and elongation.[179] The ULK complex activates Beclin 1, which subsequently binds to class III phosphatidylinositol 3-kinase (PI3 kinase) complex of proteins, and initiates the formation of the single membrane phagophore.[182]

Elongation of the single-membraned phagophore to a mature double-membraned autophagosome requires two ubiquitin-like protein lipidation systems.[182] These

systems include the microtubule-associated protein light chain 3B-I (LC3B) system and the Atg12 system, both of which undergo a series of lipidation reactions facilitated by ubiquitin E1, E2 and E3.[178] After these multi-step reactions are complete, the LC3B and Atg12 systems form LC3-II and the Atg12-Atg5-Atg16 complex, respectively, on the outside surface of the autophagosome.[179] Once the autophagosome enclosure is complete Atg12-Atg5-Atg16 complex dissociates from the autophagosome, whereas LC3-II remains covalently bound to the membrane.

The fact that LC3-II remains bound to the autophagosome membrane makes it a useful marker for autophagic flux.[178] Upon autophagic induction, cytosolic LC3-I is cleaved and binds to phosphatidylethanolamine to form autophagosome-bound LC3-II. Hence, assays which investigate autophagic flux measure the ratio of cytosolic LC3-I to autophagosome-bound LC3-II.[178] An increase in LC3-II levels is considered a biomarker of active autophagy.[178] Therefore, autophagic flux is often measured by standard assays used for protein measurement, including Western blotting, flow cytometry, or fluorescent microscopy of LC3 proteins.[178]

Once the autophagosome is complete, LC3-II attached to the outer membrane, detaches and the autophagosome fuses with the lysosome to form the autolysosome.[179] The lysosome contains numerous hydrolases, proteinases and lipases. The inner-autophagosome together with the engulfed cargo are degraded and released into the cytosol for recycling.

The role of autophagy in cancer is controversial with evidence to support tumour suppression and tumour promotion.[181,183-184] The principle role of autophagy is to remove damaged organelles and toxic aggregates, however; accumulation of degraded material and toxins promote instability and tumorigenesis.[180] From a mechanistic standpoint, autophagy suppresses tumorigenesis by removing toxic protein aggregates, and damaged organelles thereby mitigating oxidative stress and preventing DNA damage.[180] However, cancerous cells can exploit the autophagic mechanism to overcome hypoxic and nutrient limiting conditions, and in this way facilitate cell survival – and in some cases, even promote tumour resistance to cancer therapy.[184]

2.9.4.2 Vitamin D and autophagic cell death

Current data on the role of vitamin D on autophagic cell death are limited. De Masters *et al.*[185] demonstrated an increase presence of acidic compartments in breast cells exposed to 2Gy ionizing radiation and calcitriol analogue, EB1089, but not in breast cancer cells exposed to either treatment alone. The presence of the acidic compartments was assessed by staining cells with acridine orange . Acridine orange is a lysosomotropic agent which changes from green to red fluorescence in the presence of acidic intracellular compartments.[178] An increase in the number of intracellular acidic compartments indicates the presence of lysosomes or autolysosomes in cells and supports the induction of autophagic cell death.[178] In another study, the calcitriol analogue, EB1089, induced autophagy in MCF-7 breast cancer cells by enhancing protein levels of autophagy inducer, beclin-1.[186] In addition, breast cancer cells treated with 100 nM $1,25(OH)_2D_3$ induced autophagic cell death, and an autophagic transcriptional signature, including increased expression of genes encoding LC3, SQSTM1 and beclin-1.[187] These studies therefore identify the potential role of both synthetic and activated calcitriol in the induction of autophagy-related death in breast cancer cell lines.

Furthermore, mTOR activity was reduced in HL-60 leukaemia cells after treatment with $1,25(OH)_2D_3$, leading to mTOR dissociation from the ULK-1 complex and subsequent induction of autophagic cell death.[188] In head and neck squamous carcinoma (SCC25) cell line, 100 nM $1,25(OH)_2D_3$ induced autophagic cell death in a p19-dependent manner.[189] p19 is a CDK inhibitor whose expression is upregulated by calcitriol treatment.[189] These two studies therefore implicate the mTOR and p19 in the initiation of autophagic cell death in calcitriol treated leukaemia and squamous carcinoma cell lines, respectively.

Despite limited data on the role of vitamin D in the induction of autophagic cell death in cancer cells and tissue, the role of vitamin D in the induction of autophagic death is promising.[190] Further research on vitamin D metabolites in autophagic cell death are needed to characterise the role of vitamin D in this mode of cell death.

2.9.5 Necrotic cell death

Necrosis is a form of cell death that is radically different from apoptosis in biochemical and morphological aspects.[191] Necrosis is typically triggered when cells experience extreme acute environmental or genetic insults and is characterised by extensive cell swelling, distension of various organelles, clumping and random DNA degradation and extensive plasma membrane endocytosis.[191] Historically, necrosis was considered as a form of 'accidental cell death,' however, this view is in revision as both the onset and occurrence of necrosis can be genetically determined.

Necrosis can be initiated by the binding of ligands to specific plasma membrane proteins (in similar manner to extrinsic apoptosis). A stereotypical biochemical signal cascade of events in the induction necrosis has not been completely elucidated. Current findings suggest that limited set of cathepsin and calpain protease enzymes are involved in the activation of necrosis.[192-193] Additionally, necrosis is accompanied by early signs of mitochondrial dysfunction – reactive oxygen speciation, swelling and ATP depletion – and perinuclear clustering of organelles.[192,194]

To date, there have been no studies demonstrating the role of cholecalciferol or other vitamin D metabolites in the induction of necrosis. However, during late stages of apoptosis, cells may assume a necrotic morphotype (secondary necrosis),[195] and therefore undergoing calcitriol-induced apoptosis cells may demonstrate a necrotic morphology. The investigation vitamin D's effect on necrotic cell death is therefore an area of evolving research.

2.10 Vitamin D and cervical cancer *in vitro*

Cervical cancer cells express the VDMS.[10-11] Friedrich *et al.*[11] demonstrated localised expression of VDR, 25-hydroxylase, 1α-hydroxylase, and 24- hydroxylase genes in both healthy and cancerous cervical tissue. Kloss *et al.*[10] showed that cervical adenocarcinoma cell line, HeLa, expressed 25-hydroxylase, 1α-hydroxylase and 24-hydroxylase enzymes by reverse transcription PCR.[10] In addition, the authors demonstrated that calcidiol and calcitriol increased the expression of genes encoding the 24-hydroxylase enzyme.[10] Based on the fact that these cells responded to calcitriol and calcidiol treatments, and increased 24-hydroxylase catabolic enzyme, it was hypothesised that cervical cancer cells express a functional VDMS that is capable of autocrine synthesis and catabolism of $1,25(OH)_2D_3$. However, no additional studies on the potential of autocrine $1,25(OH)_2D_3$ metabolism have been reported. Furthermore, no study has demonstrated the expression of the VDMS in the SiHa cell line.

Three studies have investigated the role of calcitriol on the SiHa cell line. Firstly, calcitriol-treated SiHa cells showed a significant decrease in cell proliferation which was mediated by downregulation of the Human Ether a go-go 1 Potassium ion channel.[196] The second study[197] demonstrated an increase in Dicer expression, which augmented miRNA-498 and inhibited cell proliferation in calcitriol-treated SiHa cells. In the third study, RNA helicase DDX5 was upregulated in SiHa cells treated with calcitriol. RNA helicase DDX5 is a co-activator for various transcription factors, including VDR, involved in cell differentiation. The authors hypothesised that RNA helicase DDX5 may play a role in the pro-differentiating effects of calcitriol.[198]

Furthermore, there are limited *in vitro* studies investigating the role of cholecalciferol in cancer cell lines. However, studies which have investigated the anti-cancer actions of cholecalciferol have yielded promising results in prostate and thyroid cancer lines.[78,199] In addition, a recent paper published by our research group demonstrated significant decrease in parameters of cell health, and the induction of apoptosis in a metastatic cervical cancer cell line, CaSki, treated with cholecalciferol.[200] The intracellular regulation of the VDMS by cholecalciferol and the anti-cancer action of cholecalciferol in SiHa cells are novel areas for investigation.

3. Aims and objectives

3.1 Aims

The aim of this study was to investigate the potential mechanistic anti-cancerous actions of cholecalciferol on a cervical squamous carcinoma cell line, SiHa.

3.2 Objectives

The objectives of this study were:

- To evaluate cholecalciferol's action on cell count on SiHa cell line using the crystal violet assay.
- To assess the viability of cholecalciferol on SiHa cells using the trypan blue exclusion dye exclusion and Muse™ cell count and viability assays. To determine cholecalciferol's cell proliferation action on SiHa cell line using the Ki67 assay.
- To evaluate cell cycle progression of SiHa control and experimental cultures using the Muse™ Cell Cycle assay.
- To assess apoptotic cell death in SiHa control and experimental cultures by mitochondrial membrane potential, phosphatidylserine externalisation, effector caspase activation and DNA damage
- To assess autophagic cell death in SiHa control and experimental cultures by flow cytometric quantitation of microtubule-associated proteins 1A/1B light chain 3B-II (LC3-II)
- To assess necrotic cell death in cholecalciferol-treated in SiHa control and experimental cultures by lactate dehydrogenase (LDH) release assay.
- To identify changes in gross morphology of SiHa cell cultures treated with cholecalciferol brightfield microscopy of haematoxylin and eosin (H&E) stained cultures
- To identify changes in SiHa cell ultrastructure by transmission electron microscopy

- To quantify mRNA expression of the vitamin D metabolising enzymes and vitamin D receptor in SiHa control and experimental cultures using qPCR
- To quantify protein expression of the vitamin D metabolising enzymes and vitamin D receptor in SiHa control and experimental cultures using Western Blots

4. Materials and methods

4.1 Basic cell culture techniques

4.1.1 Materials

Basal Medium Eagle (BME) and trypsin-EDTA (Ethylenediaminetetraacetic acid) were obtained from Highveld Biological (Johannesburg, South Africa). Heat-inactivated foetal bovine serum (FBS), 96-well plates, 15 ml tubes, 50 ml tubes and 75 cm^2 culture flasks were purchased from Separations (Randburg, Johannesburg, South Africa). 25 cm^2 culture flasks and 6-well culture plates were supplied by Whitehead Scientific (Johannesburg, South Africa). Amphotericin B solution and penicillin-streptomycin was purchased from Thermo Fisher Scientific (Waltham, Massachusetts, United States of America). Consumables such as 200 µl yellow tips, 1000 µl blue tips, 1.5 ml Eppendorf tubes and gloves were purchased from Lasec (Cape Town, South Africa). Dimethyl sulfoxide (DMSO) (#889551) were obtained from Merck (Darmstadt, Germany). Cholecalciferol (#C9756) and absolute ethanol (99.8%; #24102) were purchased from Sigma-Aldrich (St Louis, Missouri, United States of America).

4.1.2 Cell line and cell culturing

The SiHa cell line (HTB-35™) was purchased from the American Type Culture Collection (ATCC; Manassas, Virginia, USA). SiHa cell cultures were grown and maintained in 75 cm^2 tissue culture flasks in a humidified water-jacketed incubator (Astec, Kasuya, Fukuoka, Japan) at 37°C, 5% CO_2 atmosphere. Cells were cultured in Basal Medium Eagle (BME) supplemented with 10% foetal calf serum (FCS), 1% penicillin-streptomycin (10,000 U/mL), 1% L-glutamine (200 mM) and 2.5mg/L amphotericin B. Cells were washed with 1X phosphate buffered saline solution (PBS) to remove toxic waste and restore physiological pH. Cell culture fluid was replaced every three days to replenish nutrients and essential growth factors and maintain exponential cell growth.[201]

Once cell cultures reached approximately 80% confluency, cells were passaged to new flasks with a typical split ratio of 1:3. Passaging is the dilution and transfer of cells from one flask to another.[201] To passage cells, the cells were first washed with 1X PBS to remove the serum (which neutralizes the action of the trypsin) and cell debris,[202] and the flask was incubated with trypsin for 2-3 minutes in a 37 ˚C incubator. The flasks were inspected under a Zeiss Axiovert 40CFL phase contrast microscope (Zeiss, Oberkochen, Germany) at low power to identify cell rounding. Once the cells were rounded, 0.25% trypsin-EDTA (Ethylenediaminetetraacetic acid) solution was removed, and fresh pre-warmed medium was added to the flask. This solution was then aliquoted and split into three flasks. Thereafter, the cells were returned to the incubator to allow for re-attachment and growth.

4.1.3 Cryopreservation and retrieval of cells

To preserve healthy cell cultures and maintain manageable numbers of cell cultures, excess cultures were cryopreserved. During cryopreservation, cells are suspended in a specialised medium solution and stored at -80 ºC for short-term storage or the vapour phase in a liquid nitrogen Dewar (Thermo Fisher Scientific, Waltham, Massachusetts, United States of America) for long-term storage. The preservation medium was constituted from 80% FCS, 10% DMSO and 10% BME. For cryopreservation, cells were resuspended in the preservation medium and aliquoted into 1.5ml cryotubes. These tubes were then placed in cryoboxes in the -80 ºC freezer. Then, after a minimum of four hours, the cryoboxes were transferred to the vapour phase of a liquid nitrogen Dewar.

To recover cells from liquid nitrogen cryopreservation, the cryotube was withdrawn and rapidly thawed at room temperature. The 1 ml stock cell solution was resuspended in 3 ml BME, centrifuged to remove the toxic DMSO (in the freeze medium) and plated into a 25 cm^2 flask with 5 ml of pre-warmed BME.

4.1.4 Seeding cells for experiments

Cells were seeded from working stock in approximately 80% confluent 75cm^2 flasks. Briefly, the medium was discarded, and adherent cells were washed with 1 × PBS. The cells were incubated with 0.25% trypsin-EDTA solution at 37 ºC and 5% CO_2 in the humidified incubator for 5 minutes. Thereafter, the trypsin solution was removed, and cells were resuspended in fresh cell culture medium. The cell suspension was mixed by gently aspirating with a pipette a 20 µl sample taken. This was diluted in a 1:5 ratio with 1X PBS and then 20 µl of this soluton was further diluted in a 1:1 ratio with trypan blue solution. Trypan blue served two functions: firstly, the dye penetrated non-viable cells; thus they appeared blue under a microscope, while viable cells remained yellow, and secondly, the dye provided a contrast medium allowing for easy identification of cells.[203] Cells were manually counted using a Fuch's-Rosenthal haemocytometer (depth 0.2mm, 1 mm^2; Weber Scientific, England) and the number of cells per millilitre (ml) in the cell suspension was calculated using the equation below:

$$\text{Seeding Density (cells/ml)} = \frac{\text{average cell count in 4 quadrants X } 10^4}{\text{Dilution Factor}}$$

The cell suspension was diluted with fresh medium to an appropriate seeding density. The seeding density and final volume of cell suspension for each flask or cell culture plate are tabulated in Table 2.

Table 2. List of the appropriate seeding density for each experiment in the most suitable cell culture plate for the experiment.

Culture plate or flask type	Volume of cell culture fluid	Seeding density	Experiment
96-well culture plate	0.2 ml	5 000 cells/well	Crystal violet, MTT, LDH, Autophagy LC3 assay
6-well culture plate	3 ml	15 000 cells/ml	H & E staining, trypan blue exclusion, all flow cytometry assays (except the autophagy LC3 assay)
25 cm^2 culture flask	5 ml	100 000 cells/ml	TEM, qPCR, Western blots

4.1.5 Determination of optimal treatment range and incubation period

Cholecalciferol treatments ranging between 10^{-4} – 10^{-10} M were used to establish growth inhibition curves at 24 hours, 48 hours and 72 hours, and the cell count at each time point was analysed by the crystal violet assay. The range of cholecalciferol treatments was informed by a previously published study by Tokar *et al.*[78] The GI_{50} studies (Appendix A) guided the subsequent experimental treatment concentration range used in this study. The maximum treatment concentration selected was the GI_{30} as it was cost-effective and feasible, as fresh cholecalciferol treatments were prepared for each experiment due to photo-lability of cholecalciferol.

The optimal incubation period was determined by performing cell count and cell viability analyses by crystal violet, and cell viability by trypan blue exclusion assay, and the Muse™ Count and Viability assay. SiHa control and experimental cultures were incubated for 24 hours, 48 hours and 72 hours. The methodology of these experiments is discussed in subsequent sections in the Methods chapter. Significant change in count and viability were analysed and the optimal incubation period was determined at 72 hours. All further experiments in this study were thus performed at 72-hour incubation.

4.1.6 Control and experimental cultures

After cells were seeded, a 16-hour overnight attachment protocol was followed. Control and experimental cell cultures were incubated for 72 hours in an incubator equilibrated at 37°C with 5% CO_2 atmosphere. All experiments utilised the same design which consisted of medium and ethanol solvent controls and a range of cholecalciferol treatments (26 nM, 104 nM, 260 nM and 2600 nM). The solvent control was treated with 0.1% (v/v) ethanol which corresponded to the highest cholecalciferol treatment (2600 nM). For cholecalciferol treatments, a stock solution of $1x10^{-3}$ M cholecalciferol was freshly prepared in analytical grade ethanol and this solution was diluted in fresh medium to obtain the final cholecalciferol treatment concentrations.

The parameters of cell health, cell death, gross and ultrastructural cellular morphology, and gene and protein expression of the VDMS were subsequently investigated using control and experimental cultures (Figure 9).

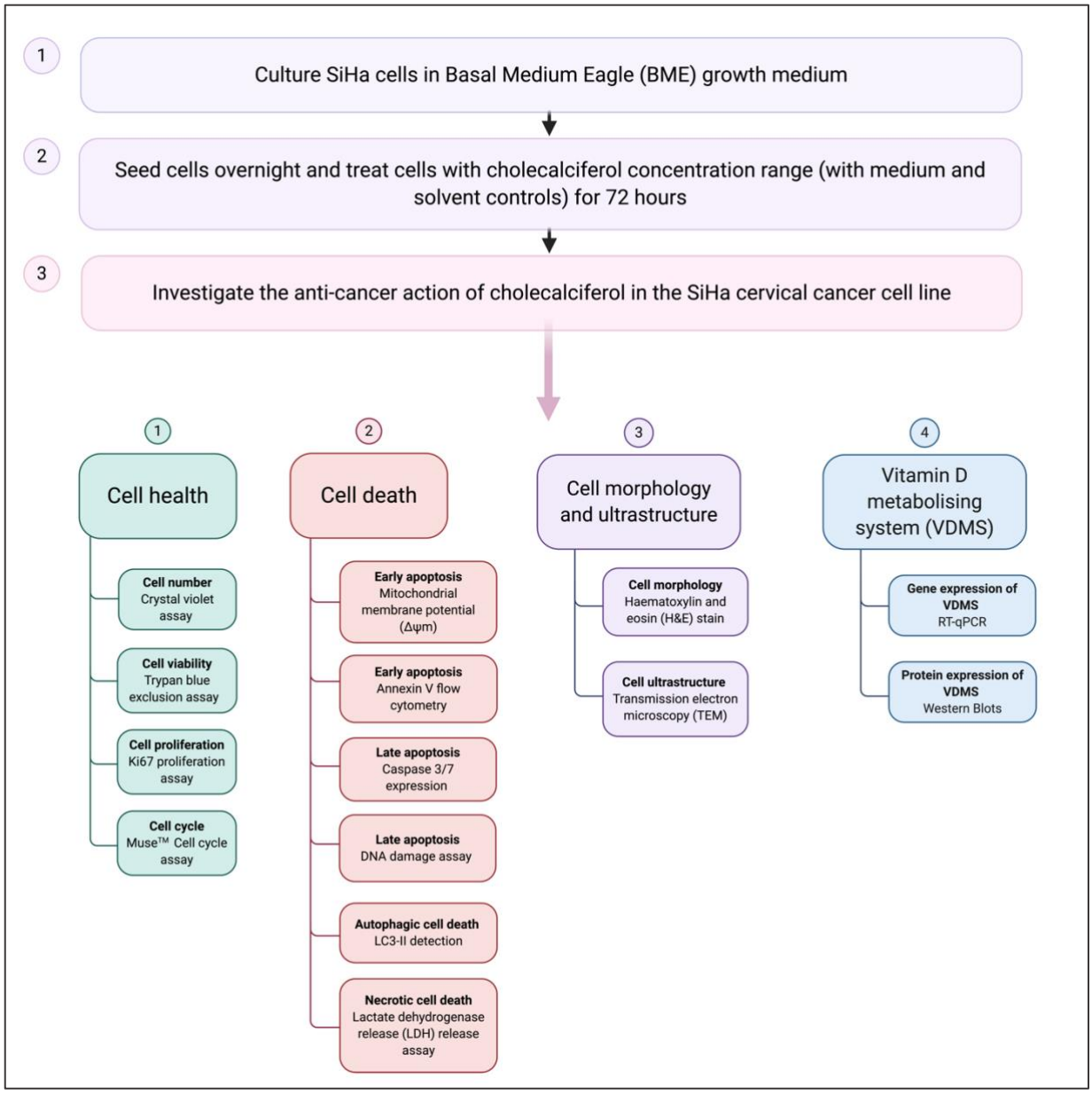

Figure 9. A simplified outline of methodological techniques aligned with each research objective in this study. Image created using BioRender.com.

4.2 Cell health assays

4.2.1 Crystal violet assay

4.2.1.1 Principle of the assay

During cell death adherent cells detach from the base of the cell culture plate. In the crystal violet assay, damaged or dead cells are sloughed from the base of the plate. This can be used for the indirect assessment of cell death and differences in cell proliferation rate of treated cell cultures.[204] Crystal violet is a triarylmethane dye that binds DNA and proteins of cells. The amount of dye binding to the cells correlates to cell number, which is determined using spectrophotometry.[205]

4.2.1.2 Materials and method

Glutaraldehyde (#111308) and Triton X-100 (#9002931) was purchased from Sigma Aldrich (St Louis, Missouri, United States of America). Crystal violet staining powder was purchased from Merck (Darmstadt, Germany). The preparation of crystal violet staining solution used in this assay is listed in Appendix B.

The cell culture fluid was removed, and each well was thoroughly washed with 1 × PBS to remove dead cells and extracellular protein in the culture fluid. Care was taken to preserve the cells still attached on the base of the well. The cells were fixed with 100 µl of 1 % glutaraldehyde (Sigma Aldrich) for 15 minutes and then stained with 100 µl of 0,1 % crystal violet solution (Sigma Aldrich; refer to Appendix A for recipe) at room temperature for 30 minutes. The dye was removed, and the 96-well plate was gently submerged in a bath with running tap water to wash off excess dye. Excess water was gently aspirated from each well and the plates were left to air dry at room temperature overnight. Three washes were performed. The stain was solubilised with 0,2% Triton-X 100 solution at room temperature for 30 minutes. The absorbance was read on an EL_x800 Universal Microplate Reader (Bio-Tek Instruments Inc., Vermont, United States of America) at 570nm. Cell counts, from absorbencies obtained, were calculated with the following formulae:

1. Blank correction= OD_{570} of treatment wells – OD_{570} of wells without cells

2. $$\text{Cell count (\%)} = \frac{\text{Blank corrected } OD_{570} \text{ of medium and treated wells}}{\text{Blank corrected } OD_{570} \text{ of solvent control well}} \times 100$$

4.2.2 Trypan blue exclusion assay

4.2.2.1 Principle of the assay

The trypan blue dye exclusion assay provides a manual count of viable cells. Trypan blue is a vital dye which enters cells with compromised cell membranes,[206] staining them blue. Conversely, live cells have intact cell membranes that exclude the dye and appear yellow.[206] Viable and non-viable cells are manually counted under a microscope using a haemocytometer and cell viability is then determined.

4.2.2.2 Materials and method

Trypan blue dye was obtained from Bio-Rad (California, United States of America). This assay also required a Fuch's-Rosenthal haemocytometer (depth 0.2mm, 1 mm^2) which was obtained from Weber Scientific (Hamilton, New Jersey, United States of America) and a Zeiss Axiovert 40CFL (Zeiss, Oberkochen, Germany) light microscope was used to view cells.

The cell culture fluid was removed, the cells were washed with 1 × PBS and detached using trypsin-EDTA. The cells were resuspended in fresh cell culture medium and were gently aspirated to create a homogenous single-cell suspension. Then, 20 µl of the sample was extracted and added to 80 µl of 1 × PBS (1:4 ratio). This mixture was further diluted at a 1:1 ratio with 20 µl trypan blue dye and this solution was loaded onto an Fuch's-Rosenthal haemocytometer and examined immediately under a 10X magnification. Cell viability was calculated using the following formula:[203]

$$\text{Viable cells (\%)} = \left[1 - \left(\frac{\text{Number of blue cells}}{\text{Total number of cells}}\right)\right] \times 100$$

4.2.3 Count and viability assay

4.2.3.1 Principle of flow cytometry and the Muse Cell Analyser™

Flow cytometry measures multiple physical and biochemical characteristics of a population of cells in a single-cell manner.[207] A flow cytometer consists of three key components: a fluidics system, an optics and detection system and a signal processing system, such as a computer.[207]

The fluidics system uses hydrodynamic focusing to direct cells and particles in suspension into a single stream towards the light source.[207-208] After hydrodynamic focusing, each particle passes through the optics system which consists of one or more beams of light. The light is scattered as the cell moves through a fixed laser beam and this scattered light provides information on cell size and shape. Secondly, if cell surface antigens or intracellular proteins are tagged, fluorescent light provides quantitative and qualitative data on the presence of these tags.[207-208] Finally, light signals from scattered light and excited fluorophores are detected by photomultiplier tubes which generate an electric current from the light signal. The light signal is decoded by the computer and displayed as plots or histograms.[207-208]

The Muse Cell Analyser™ detects two fluorescent parameters in addition to forward scatter. [209] The instrument uses a 532 nm emission laser and yellow 576/28 nm and red 680/30 nm detection channels making it compatible with a broad range of fluorophores. [209] Furthermore, the Muse Cell Analyser™ uses optimised assays which provide quantitative and qualitative data at single cell level. In this study, all flow cytometric analyses were conducted on the Muse Cell Analyser™ using Muse™ assays.

4.2.3.2 Principle of the Muse™ Count & Viability assay

The Muse™ Count & Viability assay is similar to trypan blue dye exclusion in principle; however, it allows for automated counting of a large sample size (2000 events per sample). The assay uses propidium iodide (PI) dye which enters dead cells and intercalates with DNA.[210] The PI dye is impermeant to healthy cells.[211] The dye fluoresces once it is bound to DNA and the fluorescence emission signal is quantified and expressed as percentage of viable cells in each sample by the Muse™ Cell Analyser.[210]

4.2.3.3 Materials and method

The Muse™ Count & Viability kit (#MCH100102) which contains Muse™ count and viability reagent was purchased from Merck (Darmstadt, Germany); a Muse™ Cell Analyser (Darmstadt, Germany) was also used in this method. No reagent preparation is required for this assay as all reagents are provided in the kit.

The cells were washed with 1X PBS and harvested using trypsin and prepared as per the manufacturer's instructions for suspension in 1ml of growth medium. Cells were re-washed and re-suspended in 1X PBS. Thereafter, 200 µl of cells in suspension and 200 µl of the Muse™ count and viability reagent were added to a new eppendorf tube. The tubes were incubated for 5 minutes at room temperature in the dark and analysed on the Muse™ Cell Analyser (Merck, Darmstadt, Germany) at the manufacturer's prescribed excitation and emission wavelengths (Appendix C).[54] Cell viability was measured by the instrument and expressed as percentage viable and non-viable populations.

4.3 Ki67 cell proliferation assay

4.3.1 Principle of the assay

The Muse™ Ki67 cell proliferation assay uses flow cytometry to assess the expression of a highly specific cell proliferation marker, Ki67. The Ki67 nuclear protein is only expressed during the active phases of the cell cycle: Gap1, Synthesis, Gap2, and Mitosis phases. It is not expressed in the quiescent, G_0 phase.[212] While the biological relevance and function of this protein is unclear its expression is highly concordant with active cell cycling.[212] This close relation to the cell cycle distinguishes Ki67 as an excellent marker for proliferating cells that has become a mainstay in assessing cell proliferation and drug cytostatic function.[212-213]

4.3.2 Materials and method

Muse™ Ki67 Proliferation kit (#MCH100114) contains Fixation Buffer, Assay Buffer, Permeabilisation Solution and Muse™ Hu IgG1-PE and were purchased from Merck (Darmstadt, Germany). Muse™ Fixation and Assay buffers were prepared according to the manufacturer's instructions (Appendix D).

The samples were harvested with trypsin and resuspended in 1X PBS. Thereafter, 200ul of cell suspension from each sample was transferred to an eppendorf tube and 50 µl of 1X Fixation Buffer added to each tube. The tubes were mixed and incubated for 15 minutes at room temperature. Next, 150 µl of 1X Assay Buffer was added to each tube, the tubes were centrifuged, and the supernatant removed. Thereafter, 100 µl of Permeabilisation solution was added to each tube, mixed and incubated for 15 minutes at room temperature. Subsequently, 100 µl of 1X Assay Buffer was added to each tube, centrifuged, and the supernatant removed. Next, 50 µl of 1X Assay Buffer was added to each tube, mixed and incubated for 15 minutes at room temperature. After 15 minutes 10 µl of Muse™ Hu Ki67-PE was added to each tube and incubated for 30 minutes at room temperature. Lastly, 150 µl of 1X Assay Buffer was added to each tube and analysed on the Muse™ Cell Analyser (Merck, Darmstadt, Germany) at the manufacturer's prescribed excitation and emission wavelengths (Appendix C). The Muse Cell Analyser™ measured the percentage of cells that expressed Ki67.[213]

4.4 Cell cycle analysis

4.4.1 Principle of the assay

The cell cycle consists of four sequential phases: Gap1, Synthesis, Gap2 and Mitosis.[114] As the cell cycle progresses, chromosomal DNA duplicates and this can be used to discriminate cells in the different phases of the cell cycle.[202,214]

The Muse™ Cell Cycle Assay quantifies the percentage of cells in each phase of the cell cycle by measuring the DNA quantity in each cell. The assay uses a premixed reagent containing PI DNA intercalating dye and RNAses. Once the dye binds to DNA it emits fluorescent light that is detected by the Muse Cell Analyser™ (Merck, Darmstadt, Germany). The Muse Cell Analyser™ provides a one parameter histogram plot based on DNA content of each cell in the sample population and displays the percentage of cells in each phase of the cell cycle (G_0/G_1; S; and G_2/M).[215] The Sub-G_1 population percentage is calculated by subtracting the sum of all phases by 100 i.e. sub-G_1 (%) = 100 – (G_1/G_0 + S + G_2/M) The sub-G_1 phase appears as a broad distinguishable peak on the histogram plot and represents cells undergoing necrosis or apoptosis, nuclear fragments; clumps of chromosomes and micronuclei.[216]

4.4.2 Materials and method

Muse™ Cell cycle assay kit (#MCH100106) which contains Muse™ cell cycle reagent was purchased from Merck (Darmstadt, Germany). No reagent preparation was required for this assay. All reagents were provided in the kit. The positive control culture was treated with actinomycin D at a final concentration of 0.1 µg/ml.

The cells were gently vortexed while 1 ml of ice-cold ethanol (70%) was added in a drop-wise manner to the tubes. The cells were incubated at -20°C for 4 hours and then stained. For staining, the cells were first centrifuged at 300 x*g* for 5 minutes and washed with 1X PBS. Thereafter, 200 µl of cell suspension from each tube was transferred into new eppendorf tubes and 200 µl of Muse™ Cell Cycle reagent was added to each tube and incubated for 20 minutes at room temperature in the dark. Samples were then analysed on the Muse™ Cell Analyser™ at the manufacturer's

prescribed excitation and emission wavelengths (Appendix C). Data were presented as percentages of the cell populations from each phase of the cell cycle.

4.5 Assessment of apoptosis

4.5.1 Mitochondrial membrane potential (ΔΨm) assay

4.5.1.1 Principle of the assay

Mitochondrial membrane potential (ΔΨm) was assessed using The Muse™ Mito Potential assay. The Mito Potential reagent is a tetramethylrhodamine ethyl ester (TMRE) based red-orange fluorescent dye, which is positively charged, and cell-permeant. Healthy mitochondria have a negative charge and the positively charged dye accumulates in mitochondria and produces a high fluorescent signal. Conversely, non-viable cells have depolarised membranes, which do not sequester the dye and, therefore, display a low fluorescent signal. This assay also uses a cell impermeant 7-aminoactinomycin D (7-AAD) dead cell marker that intercalates DNA of dead cells and produces a positive fluorescent signal.

4.5.1.2 Materials and method

The MitoPotential reagent and 7-AAD dead cell marker are provided in the Muse™ MitoPotential Assay kit (#MCH100110; Merck, Darmstadt, Germany). The Muse™ MitoPotential Dye was prepared fresh by diluting (1:1000) in 1X assay buffer. The positive control culture was treated with actinomycin D at a final concentration of 0.1 µg/ml.

SiHa cells were harvested using trypsin and resuspended in 1X PBS solution. Thereafter, a 100 µl sample from the cell suspension was removed and added to an eppendorf tube. Thereafter, 95µl of the Mito Potential working solution was added to each tube and cells were incubated in Mito Potential dye for 20 minutes at 37 ºC and 5% CO_2. After the incubation, 5µl of 7-AAD reagent was added to each tube and samples were incubated for 5 minutes at room temperature. Samples were then analysed using the Muse™ Cell Analyser (Merck, Darmstadt, Germany) at the

manufacturer's prescribed excitation and emission wavelengths (Appendix C). Data were expressed as percentages of live, depolarised mitochondrial potential, depolarised mitochondrial potential/dead cells and dead cells.

4.5.2 Annexin V detection assay

4.5.2.1 Principle of the assay

Once apoptosis is initiated, the internal leaflet of the cell double membrane externalises to the outside surface of the cell membrane.[217-218] This is a hallmark of early-stage apoptosis. Phosphatidylserine (PS) is a protein that is normally only expressed on the internal leaflet of the plasma membrane. [219] In apoptosis, it is externalised to the exterior surface of the plasma membrane. PS exposure is assessed by annexin V which has a very high affinity for PS (K_d ~ 10^{-7}–10^{-8} M).[219] The expression of PS on the external surface of the cell membrane was assessed by phycoerythrin (PE) tagged annexin V using the Muse™ flow cytometric assay.[220] The kit also uses 7-aminoactinomycin D (7-AAD) as a dead cell marker. The dead cell marker allows for the discrimination of live and apoptotic cells from dead cells. 7-AAD is a membrane-impermeable DNA stain that only stains dead cells.

4.5.2.2 Materials and method

Actinomycin D (#50760) was purchased from Sigma Aldrich (St Louis, Missouri, United States of America). Muse™ Annexin V & Dead cell assay kit (#MCH100105) which contains Muse™ Annexin V & Dead Cell reagent was purchased from Merck (Darmstadt, Germany). No reagent preparation was required for this assay. All reagents were provided in the kit. The positive control culture was treated with actinomycin D at a final concentration of 0.1 µg/ml.

Cells were harvested with trypsin and prepared according to manufacturer's instructions.[220] Cells were washed with 1X PBS and 100 µl of the Muse™ Annexin V & Dead Cell reagent, equilibrated to room temperature, was added to 100 µl of the cell suspension. The tubes were mixed by vortexing at medium speed and then incubated for 20 minutes at room temperature in the dark. Thereafter the tubes were analysed

on the Muse Cell Analyser™ (Merck, Darmstadt, Germany) at the manufacturer's prescribed excitation and emission wavelengths (Appendix C). Data were expressed as percentages of cells in the four categories: live cells; early apoptosis, late apoptosis; and dead cells.

4.5.3 Caspase 3/7 detection assay

4.5.3.1 Principle of the assay

Caspases (cysteinyl-directed aspartate-specific proteases) are widely expressed cysteine proteases synthesised as inactive pro-enzymes that are proteolytically activated by apoptogenic signals.[217-218,221] There are two main types of caspases involved in apoptosis: initiator caspases and downstream effector (terminal) caspases.[218] Initiator caspases (caspase-8 and caspase-9) primarily initiate apoptosis by proteolytically cleaving and activating effector caspases.[218] Effector caspases (caspase-3 and caspase-7) have broad catalytic activity and precipitate the biochemical and morphological hallmarks of apoptosis.[217]

According to the manufacturer,[222] the Muse™ caspase 3/7 reagent, contains a proprietary dye called NucView™, which is non-toxic to the cell and permeable to the cell membrane. NucView™ is a DNA binding dye that is conjugated to a DEVD (peptide sequence Asp-Glu-Val-Asp) substrate.[223-224] When the dye is bound to DEVD, the dye does not bind DNA and no fluorescent signal is produced. In apoptotic cells, cleavage of the DEVD substrate by effector caspases -3 and -7 release the dye, allowing it to bind to DNA and emit a fluorescent signal. An increase in the emission intensity indicates increased caspase activity.[223-224] In addition, 7-AAD detected any damage to the integrity of the cell membrane and discriminated live and apoptotic from dead cells.[222]

4.5.3.2 Materials and method

Actinomycin D (#50760) was purchased from Sigma Aldrich (St Louis, Missouri, United States of America). Muse™ Caspase 3/7 assay kit (#MCH100108) which contains Muse™ Caspase-3/7 working solution and a 7-AAD working solution, was purchased

from Merck (Darmstadt, Germany). The positive control culture was treated with actinomycin D at a final concentration of 0.1 µg/ml. Muse™ Caspase-3/7 and 7-AAD working solutions were prepared according to the manufacturer's instructions and are described in Appendix E.

The cell samples were prepared according to the manufacturer's instructions.[222] Firstly, the cells were harvested using trypsin and washed with 1X PBS. Thereafter, 50 µl cell suspension was added to eppendorf tubes. Next, 5 µl of Muse™ Caspase-3/7 working solution was added to each eppendorf tube and the tubes were subsequently incubated for 30 minutes at 37°C in an incubator equilibrated at 5% CO_2. After incubation, 150 µl 7-AAD working solution was added to each Eppendorf tube and samples were immediately analysed on the Muse™ Cell Analyser (Merck, Darmstadt, Germany) at the manufacturer's prescribed excitation and emission wavelengths (Appendix C). Data were expressed as percentages of cells in the four categories: live cells; late apoptosis, apoptosis/dead; and dead cells.

4.5.4 DNA damage analysis

4.5.4.1 Principle of the assay

DNA damage can be triggered by genotoxic agents and is also a feature of late apoptosis. During apoptosis, effector caspases activate DNase enzymes which cleave DNA at linker regions between oligonucleosomes.[153-154] In response to DNA damage, ATM kinase rapidly dissociates from its homodimer form and becomes phosphorylated on serine 1981.[156] ATM then triggers numerous downstream effectors, including the histone variant H2A.X. ATM phosphorylates H2A.X, at serine 139 to form γH2AX.[156] The extent of DNA damage is tightly correlated to γH2AX expression, therefore, γH2AX is a reliable biomarker of DNA damage.[225]

The Muse™ Multi-Colour DNA Damage Kit measures the extent of DNA damage by two conjugated antibodies: phosphor-specific ATM(Ser1981)-PE and phosphor-specific histone γH2A.X-PECy5. [226]

4.5.4.2 Materials and method

The Muse™ Multi-colour DNA damage assay kit (#MCH200107; Merck, Darmstadt, Germany) contains all reagents and antibodies used in this assay and reagent preparation is described in Appendix F.

SiHa control and experimental cultures were harvested using trypsin and washed using 1X PBS. Thereafter, the cells were resuspended in 1X PBS and 100µl of the cell suspension was added to an Eppendorf tube containing 100 µl of 1X Assay buffer. Cells were fixed by 50µl fixation buffer added to each sample and incubated for 10 minutes on ice. Thereafter, the samples were centrifuged, and the supernatant was discarded. The cells were permeabilised by adding equal parts of premiumisation buffer and 1X assay buffer to a total volume of 100 µl. Samples were incubated on ice for 10 minutes. After incubation, cells were washed and resuspended in 90µl assay buffer and 10 µl of the anti-body cocktail solution was added to each sample. Samples were incubated in the dark for 30 minutes at room temperature. Following incubation, samples were centrifuged, the supernatant was discarded, and cells were resuspended in 200 µl 1x assay buffer. Samples were analysed for DNA damage using the Muse™ Cell Analyser at the manufacturer's prescribed excitation and emission wavelengths (Appendix C).which enumerated the activation of each DNA damage marker and calculated total DNA damage and double-strand DNA breaks.[226]

4.6 Autophagy detection assay

4.6.1 Principle of the assay

Autophagy is characterised by the fusion of acidic lysosomes with autophagosomes.[179] Autophagosomes are double-membraned intracellular structures which surround and engulf damaged or destroyed organelles. Several key proteins work in concert to initiate, elongate and complete autophagosome formation. A key protein, which has been shown to be a reliable marker of autophagy, is microtubule-associated protein 1A/1B light chain 3B (LC3B).[178] LC3-I is responsible for elongation of the phagophore. Once the phagophore is enclosed, it matures to form the autophagosome and concomitantly LC3-I is cleaved to form LC3-II.[182] The formation

of LC3-II is thus a marker for the both the presence and activation of autophagy and autophagic cell death.[182]

This assay used two reagents to protect LC3-II and discriminate LC3-I from LC3-II, respectively. The first is a plasma membrane permeabilisation solution, which selectively extracts cytosolic LC3-I, while protecting autophagic LC3-II, allowing for its detection.[227] The second reagent (Autophagy reagent A), prevented the lysosomal degradation of LC3-II.[227] Therefore, LC3-II is trapped in the autophagosomes and remains intact. The fluorescence of LC3-II was measured by the Muse Cell Analyser™ using an anti-LC3 mouse monoclonal antibody conjugated to Alexa Fluor®555.[227]

4.6.2 Materials and method

The Muse™ Autophagy LC3-antibody-based kit (#200109) that contains autophagy reagent A, autophagy reagent B, anti-LC3 AlexaFluor®555 and an assay buffer was purchased from Merck (Darmstadt, Germany). Autophagy reagent A, autophagy reagent B, anti-LC3 AlexaFluor® 555, and 1X assay buffer were prepared according to the manufacturer's instructions. The positive control culture was treated with 200 nM rapamycin for six hours to induce autophagy.[228] Rapamycin induces autophagy by inhibiting mTORC, a key regulator in autophagic flux.[229]

Following 72 hours, all SiHa cell cultures were washed with 1 × PBS, harvested using trypsin and resuspended in 1 × PBS in eppendorf tubes. Thereafter, the tubes were centrifuged at 300 x*g* for 2 minutes at 4 ºC. The supernatant was discarded and 5 µl of Anti-LC3 AlexaFluor® 555 and 95 µl of Autophagy reagent B was added to each tube and incubated in the dark and on ice for 30 minutes. After incubation, the tubes were centrifuged at 300 x*g* for 5 minutes at 4°C, the supernatant was removed, and cells were resuspended in 200µl of 1X Assay Buffer and analysed on the Muse™ Cell analyser (Merck, Darmstadt, Germany) with the manufacturer's prescribed excitation and emission wavelengths (Appendix C). The Muse™ Cell analyser quantified LC3-II positive cells which indicated autophagic death[227] and expressed data on a one-parameter histogram plot.

4.7 Necrosis detection assay

4.7.1 Principle of the assay

During necrotic cell death, cell membranes are ruptured,[218] leading to the release of intracellular proteins and enzymes, such as lactate dehydrogenase (LDH), into the cell culture medium.[148] This enzyme is present in almost all cells and in the first step of this assay, LDH catalyses the oxidation of lactate to pyruvate and produces reduced nicotinamide adenine dinucleotide (NADH). In this assay, a tetrazolium salt is used to measure the quantity of LDH in the cell culture fluid. Firstly, LDH catalyses lactate to pyruvate and produces reduced nicotinamide adenine dinucleotide (NADH).[230] Secondly, the newly formed NADH converts the tetrazolium salt into a coloured formazan product in the presence of an electron receptor.[230] This product is quantified using a spectrophotometer and provides a direct measure of the percentage of necrotic cells present in each well.[230] Cell cytotoxicity was calculated as a percentage (%) of the solvent control, after correction with the blank well (complete culture medium only).

4.7.2 Materials and method

Acetic acid (#27225), Triton X-100 (#9002931), 2-p-iodophenyl-3-p-nitrophenyl-5-phenyl tetrazolium chloride (INT) (#146689), N-methylphenazonium methyl sulfate (PMS) (#299116), nicotinamide adenine dinucleotide (NAD) (#53849), lactic acid (#69775), tris base (#77861) and HCl (#7647010) was purchased from Sigma-Aldrich (St. Louis, Missouri, United States of America). The preparation of the buffers used in this assay is described in Appendix G.

At 72 hours, 10 µl of the 10X lysis solution was added to the maximum LDH release wells and the volume correction control wells, and the 96-well plates was returned to a humidified incubator at 37°C, 5% CO_2 for 45 minutes. Thereafter, the 96-well plate was centrifuged at 400 x*g* for 5 minutes, and 50 µl of the supernatant from each well was carefully transferred to a clean 96-well plate, to ensure that no cell material was transferred. Next, 50 µl of reconstituted 2X LDH assay buffer was added to each well of supernatant and the solution was mixed by gently shaking of the 96-well plates for

30 seconds. The samples were incubated at room temperature for 30 minutes protected from light. Afterwards, 50 µl of acetic acid was added to each well and the solutions mixed by gently shaking the plate for 30 seconds. Lastly, the absorbance of the wells were measured at 490 nm using an ELx800 Universal Microplate Reader (Bio-Tek Instruments Inc., Vermont, United States of America) and the percentage (%) of cytotoxicity was calculated[230] for each experimental culture using the formula below:[230]

$$Cell\ cytoxicity\ (\%) = \frac{\text{Absorbance of test well } - \text{ absorbance of untreated well}}{\text{Absorbance of maximum LDH release well } - \text{ Absorbance of untreated well}}\ X\ 100$$

4.8 Analysis of cell morphology

Morphological characteristics of modes of cell death was assessed using bright field microscopy with haematoxylin and eosin (H & E) staining and Transmission Electron Microscopy (TEM).

4.8.1 Brightfield microscopy using haematoxylin and eosin (H&E) staining

4.8.1.1 Principle of the assay

Haematoxylin and eosin (H&E) is one of the most widely used histological stains. The major oxidisation product of haematoxylin, haematin, stains nuclear material. In the H&E stain, sodium iodate rapidly oxidises Mayer's Haematoxylin to haematein.[231] Haematin itself has a poor affinity for tissue and is inadequate as a nuclear stain without the presence of a metal cation mordant.[232] The mordant confers a net positive charge to the dye and enables it to bind to anionic tissue sites such as nuclear chromatin.[231] Haematoxylin stains the cell nuclei blue-black and eosin stains the cytoplasm varying shades and intensities of pink.[232] Eosin is a fluorescent, xanthene dye which binds to salts with eosinophilic compounds containing positive charges. Eosin Y is the most widely used type of eosin and is soluble in water and alcohol.[232] The majority of the differentiation of eosin staining occurs in the subsequent tap water wash, and to a lesser extent, during dehydration by a graded series of alcohol.[232]

4.8.1.2 Materials and method

Coverslips for microscopy (Z692263), Bouin's fixative (#HT10-1-32), ethanol (#64175), Mayer's Haematoxylin solution (#MHS32), eosin Y, xylol (#HX68132961), resin, and microscope slides (S8902) were purchased from Sigma-Aldrich (St. Louis, Missouri, United States of America). Ethanol dilutions, Mayer's Haematoxylin solution, 1% eosin and xylol were prepared according to current protocols in molecular biology.[71] Reagent preparation is described in Appendix H.

Control and experimental SiHa cell cultures were seeded on heat-sterilised coverslips placed in 6-well plates. After 72 hours, the coverslips were removed and placed in staining dishes. The cells were washed with 1X PBS and then fixed with Bouin's solution for 30 minutes. Thereafter, cells were dehydrated for 20 minutes with 70% ethanol. Then, coverslips were rinsed with tap water and stained with Mayer's Haematoxylin solution for 20 minutes. The coverslips were rinsed with 70% ethanol and then incubated for 15 minutes with 1% eosin Y solution.[233] A graded series of dehydration steps were performed with increasing concentrations of ethanol (70%, 96% and 100%), twice for 5 minutes. The coverslips were then washed with xylol (Merck, Darmstadt, Germany) and mounted onto microscope slides with Entellan® mounting reagent (Merck) and left to dry overnight. The slides were viewed and photographed with a Zeiss Axiovert 40CFL (Zeiss, Oberkochen, Germany) light microscope.

Qualitative analysis was performed to identify morphological features of cell death, morphology of cells and features of mitosis (Appendix I). In addition, micrographs were semi-quantitatively analysed for features of apoptosis (Appendix J) using the Cell Counter plug-in on Fiji (ImageJ) software (National Institute of Health, Bethesda, Maryland, USA).[234] Fifteen micrographs (consisting of five images per biological repeat; and averaging approximately 1800 cells per sample) were used to analyse each sample. The apoptotic features (Appendix J) were manually counted and expressed as number of apoptotic features (±SEM) present in each image. The number of apoptotic features for each sample were summated from each 15-micrograph sample set. Apoptotic cells for each sample was expressed as a percentage (±SEM) and calculated by dividing the count of apoptotic cells by the total

cell count. A similar approach was used (as for the semi-quantification of apoptosis) to enumerate the number of cells which showed features of giant multi-nucleated cells (Appendix I).

4.8.2 Transmission electron microscopy

4.8.2.1 Principle of the assay

Transmission electron microscopy (TEM) allows researchers to identify ultrastructure and subcellular components of cells in normal and disease states. The fundamental principle underlying TEM is that electrons pass through thinly sliced section of embedding media containing cells to give an image of the specimen.[232] Before cells can be viewed by TEM they are passed through a series of tissue processing steps to protect delicate cells from the harsh internal environment of the electron microscope.[235] In TEM, a double fixation process is used to preserve cell ultrastructure. Cells are first fixed with an aldehyde, such as glutaraldehyde to stabilise proteins and then osmium tetroxide is used a secondary stain to retain lipids and enhance contrast. [232] Dehydration reactions using ethanol help remove water from the cells. Following dehydration, cells are embedded in epoxy resin which is immiscible with water. Thereafter, the epoxy resin is left to harden overnight with gentle heat (approximately 60 ºC).[232] After hardening, the epoxy resin is cut into blocks and 80 nm thin slices are sectioned using an ultramicrotome. This thickness is important as the electron beam is only capable of effectively penetrating a resin section to a depth of approximately 100 nm.[232]

4.8.2.2 Materials and method

All reagents were prepared by the Electron Microscopy Unit, University of Pretoria, Pretoria, South Africa. Standard protocols made available from the electron microscopy unit (Hatfield campus) of the University of Pretoria were employed in the cell preparation of TEM. These protocols are based on Sambrook *et al.* and Huang *et al.* [67,68] Sodium phosphate buffer (0.075M), glutaraldehyde, osmium tetroxide, ethanol quetol, and uranyl acetate were supplied by the Electron Microscopy Unit, University

of Pretoria, Pretoria, South Africa. The preparation of buffers and the embedding medium are described in Appendix K.

After 72 hours incubation, SiHa cells were trypsinised and washed with 1X PBS. The cells were then centrifuged at 800 x*g* for 5 minutes to form a pellet. The pellet was washed with 0.075 M sodium phosphate buffer and the cells were fixed in 2.5% glutaraldehyde in 0.075M phosphate buffer for 1 hour. Thereafter, cells were rinsed three times with 0.075M phosphate buffer and fixed with osmium tetroxide for 30 minutes. Thereafter, cells were dehydrated with a graded series of ethanol (30%, 50%, 70%, 90%, and 100%), thrice for each concentration. Subsequently, cells were infiltrated with 50% quetol in ethanol for 1 hour and then with 100% quetol for 4 to 6 hours. Thereafter, the resin was incubated at 60ºC overnight to polymerise and harden. Once polymerized, excess resin was trimmed off the resin blocks in order to expose the tissue for sectioning. Ultra-thin sections were prepared using an ultramicrotome and sections were placed onto copper support grids. The support grids contrasted were contrasted with 4% uranyl acetate for 10 minutes, rinsed with distilled water and counter stained with lead citrate. Micrographs were captured on JOEL JEM 2100F (JOEL Ltd., Tokyo, Japan) transmission electron microscope located at the Electron Microscopy Unit (University of Pretoria, South Africa).[67,68] The images were qualitiatively analysed and ultrastructural features of cell death and cellular abnormalities identified according to criteria tabulated in Appendix L.

4.9 Analysis of gene and protein expression

4.9.1 Quantitative polymerase chain reaction (qPCR)

4.9.1.1 Principle of the assay

In quantitative reverse transcription PCR (RT-qPCR), RNA is reverse-transcribed into cDNA which is amplified in the PCR reaction to determine gene expression. In real-time PCR (qPCR), DNA amplification and PCR detection steps are combined to provide feedback on amplification during the PCR run.[236-237] The real-time instrument quantifies PCR amplification by measuring fluorescent signals emitted from fluorescent reporter dyes at each cycle.[236-237] Fluorescent signals after each cycle are plotted onto a quantitation plot, which takes the shape of a sigmoidal curve.[236] As DNA amplifies, the signal increases and the graph changes from an initial linear phase to a log linear phase of amplification.[236,238] At this stage, the signal is above the background threshold and this point is referred to as the threshold cycle (Ct).[238] The Ct values obtained from each tube in a PCR run can then be analysed to determine changes to gene expression in control and experimental cell cultures.[239-240]

Post-PCR melt curves are performed to identify amplified products and distinguish them from primer dimers and other small amplification artifacts.[241] At the DNA melting temperature (Tm), half of the DNA helical structure is lost.[242] DNA products have a distinct Tm based on their size and GC content.[238] The melt curve begins at a temperature lower than the Tm of the products and ends at a temperature above the Tm. During melt curve analysis, the thermal cycler continuously monitors the fluorescence of each sample as the temperature increases. At the start of the melt curve, there is an abundance of PCR products as double-strand DNA, thus a high fluorescent signal by SYBR Green which binds to double-strand DNA. When the Tm of the PCR product is reached, double-stranded DNA denatures, and the fluorescent dye is released. This provides an accurate Tm for every single amplified product, and multiple peaks suggest nonspecific primer pairs or suboptimal PCR conditions. Melting peaks are generated by the change in gradient of the DNA melt curve. The peaks are plotted by as negative differential (–dF/dT) versus temperature and the profile is analogous to PCR bands separated by gel electrophoresis.[241]

4.9.1.2 Materials and overview of the assay

Nuclease-free (PCR) water (#P442) was purchased from Top-Bio (Vestec, Czech Republic). iTaq™ Universal SYBR(R) Green Supermix (#172-5121) and cDNA synthesis kit (iScript Reverse Transcriptase Supermix for RT-qPCR (#1708840) was purchased from Bio-Rad (California, United States of America). Ethanol (#64175) and isopropanol (#34965) were purchased from Sigma-Aldrich (St. Louis, Missouri, United States of America). Forward and reverse primers for VDR, CYP2R1, CYP27A1, CYP27B1 and CYP24A1 were purchased from Inqaba Biotec (Johannesburg, South Africa). Qiazol® lysis reagent (#79306) was purchased from Qiagen (Germantown, Maryland, United States of America). Chloroform (#1024451000) was purchased from Merck (Darmstadt, Germany).

The differential gene expression was performed by a sequence of five steps described in Figure 12. These steps included the following sequential progression: RNA isolation, RNA purification, reverse transcription of RNA to cDNA and finally, qPCR, using specific primers to genes of interest in cDNA derived from the control and experimental cultures (Figure 10).

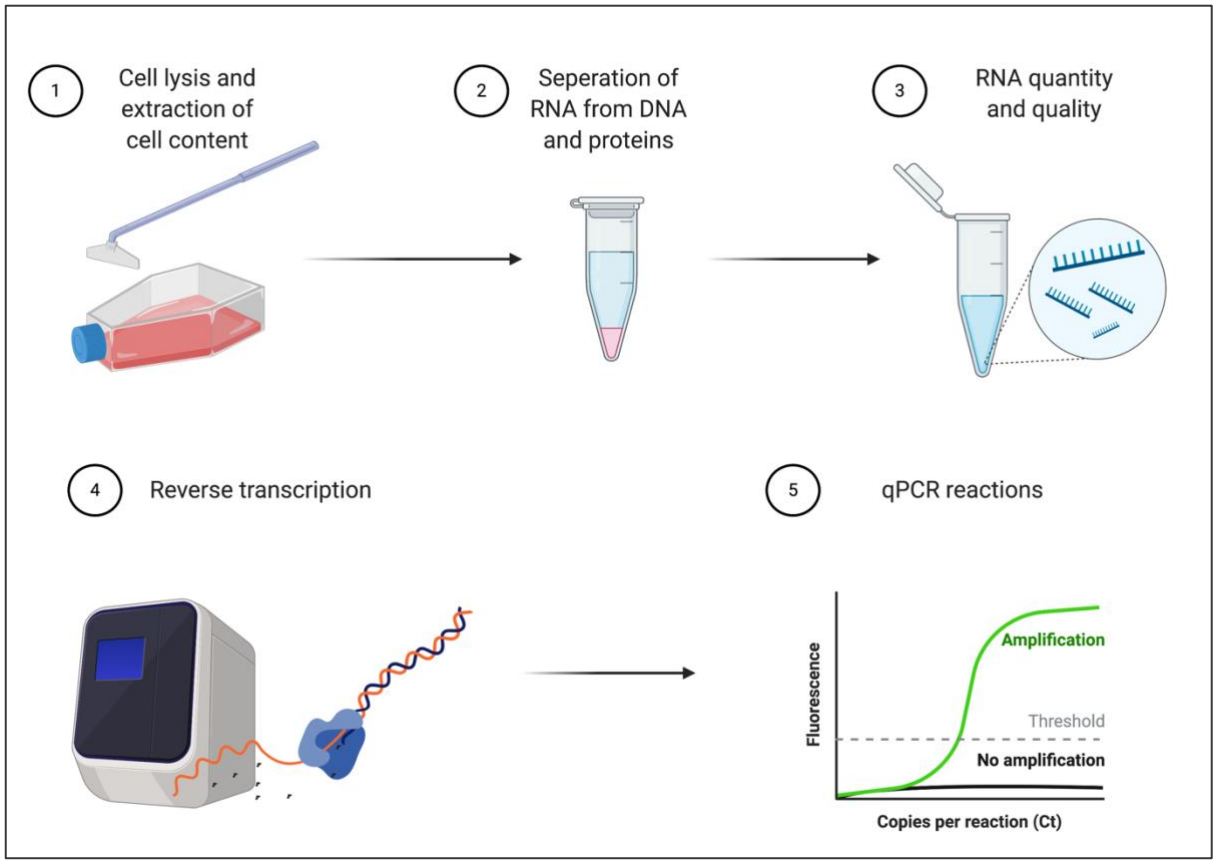

Figure 10. Overview of the steps performed to identify differential expression of genes of the VDMS in control and experimental SiHa cells (Source: personal collection). Image created using BioRender.com.

4.9.1.3 RNA isolation, purification and quantification

A manual RNA isolation protocol was followed to isolate and purify total RNA in SiHa cells.[243] Briefly, SiHa cell cultures were washed with ice-cold 1X PBS and 500µl of Qiaziol lysis reagent (Qiagen) was added to each flask and incubated for five minutes at room temperature. Thereafter, cells were scraped off using a rubber policeman and collected into an eppendorf tube. Then, 100 µl chloroform was added to each tube. The tubes were vortexed for 15 seconds and centrifuged 12 000 x*g* for 15 minutes at 4°C. Thereafter, approximately 250 µl of the colourless aqueous phase was carefully extracted and placed into a new tube. The rest of the tube contained DNA and proteins and discarded. Subsequently, 250 µl of isopropanol was added to each tube and the tubes were mixed by vortexing for 10 seconds and centrifuged at 12 000 xg for 20 minutes at 4°C. The supernatant was then discarded and 500 µl of ice-cold 75%

ethanol was added to each tube to precipitate the RNA. Thereafter, tubes were centrifuged at 7 400 x*g* for 15 minutes at 4°C.

Next, the aqueous phase was transferred carefully to new tubes, and 250 µl of isopropanol will be added. The tubes were then vortexed for 15 seconds and stored at -80°C for 1 hour. Subsequently, cells were centrifuged at 12 000 xg for 20 minutes at 4°C. The ethanol was then removed, and samples were left to air dry for 5 to 10 minutes. Thereafter, the RNA was resuspended in 10 µl of nuclease-free water and tubes were placed on ice. Total RNA was quantified using a NanoDrop spectrophotometer (Nandrop2000, Thermo Fisher, Massachusetts, United States of America). RNA quality encompasses both its purity (absence of DNA and protein and inhibitors) and integrity.[241] A ratio of 2.0 is considered ideal and ratios less than 1.8 indicate the presence of contaminants. If RNA yield was low and of poor quality (A260/A280 < 1.8)[238] then RNA was not transcribed into DNA and the RNA was discarded. The RNA extraction and isolation steps are illustrated in Figure 11.

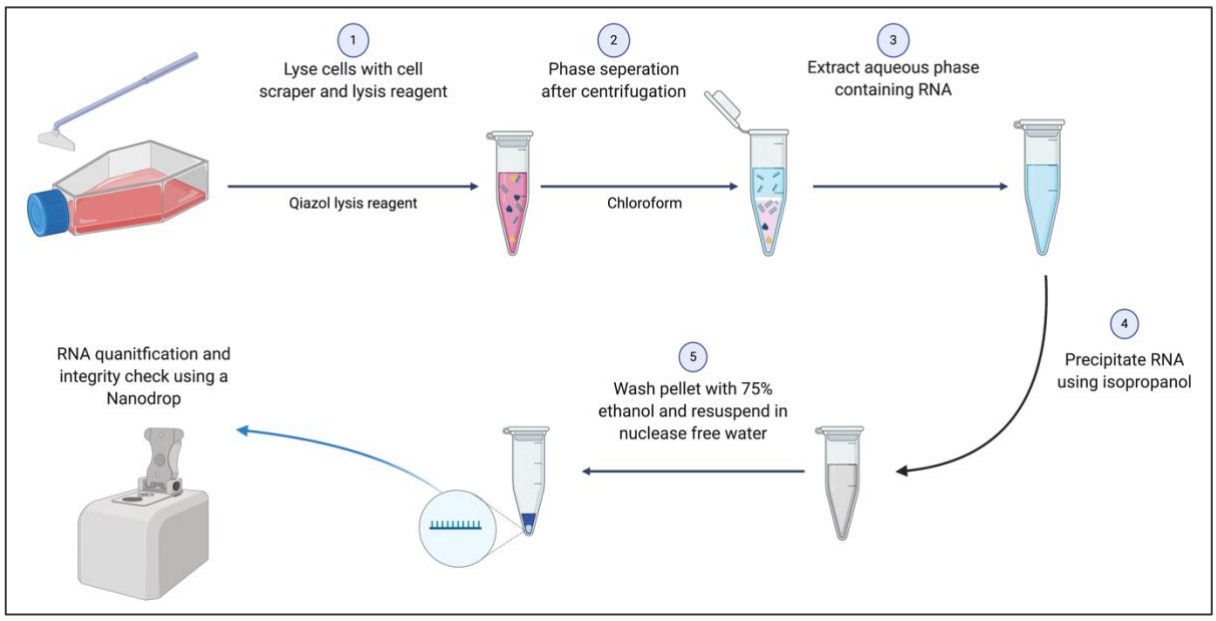

Figure 11. Manual RNA isolation protocol using QIAzol lysis reagent (Source: Personal collection). Image created using BioRender.com.

4.9.1.4 cDNA synthesis

RNA concentration was standardised to 200 ng/µl with nuclease free water for cDNA synthesis. cDNA was synthesised using the iScript Reverse Transcriptase Supermix

(Bio-Rad) as per the manufacturer's instructions with the following thermal profile: priming, 5 minutes at 25ºC; reverse transcription, 20 minutes at 46ºC and RT inactivation, 1 minute at 95 ºC. The cDNA synthesis reaction consisted of one cycle and was performed using the RotorGene Q Thermal Cycler (Germantown, Maryland, United States of America). Once the reaction was complete, cDNA was stored at -20 ºC until PCR reactions were performed.

4.9.1.5 Optimisation of PCR reactions

Assay optimisation improves sensitivity, specificity and reproducibility over a wider linear dynamic range of the qPCR segment of the assay.[241] The optimal conditions (primer concentration and annealing temperature) of qPCR reactions for each primer pair were determined using SiHa cells propagated in medium only. The concentration of the primer pairs ranged from 100nM - 700nM (Appendix M). The Tm calculator by Thermo Fisher[244] informed the determination of annealing temperature of each primer pair. If needed temperatures were adjusted at two degrees below the annealing temperature (Ta) until the optimal temperature was determined. The optimal temperature was informed by both amplification plots and melt curves.[241]

Furthermore, efficiency reactions were also performed after PCR conditions were optimised. PCR efficiency reactions (Appendix N) revealed amplification rates between 90-110% and thus permitted the use of the comparative Ct analysis method described by Livak and Schmittgen.[239]

4.9.1.6 qPCR reaction

The PCR reactions for each gene of interest was performed on the Qiagen Rotor-Gene Q 5Plex PCR thermocycler (Qiagen, Hilden, Germany) using iTaq Universal SYBR Green Supermix. The sequences of each primer pair and optimised PCR conditions of each primer pair are included in Appendix M. Post-PCR melt curve analysis was performed after all PCR runs to confirm the presence of a single PCR product.

The thermal cycling profile for optimisation reactions were as follows: denaturation at 95℃ for 15 seconds, annealing temperature was primer-specific for 15 seconds, and

extension at 72 ºC for 10 seconds. The cycling profile set for 40 cycles in all experiments. Post-qPCR melt curve analysis was conducted at 65-95℃ at 0.5 ºC increments and 5 seconds per step.

The threshold was set at the logarithmic phase of the quantitation plot on the Rotor-Gene Q software (Qiagen, Hilden Germany) to obtain Ct values for each reaction tube. The Ct values were used to calculate relative gene expression based on the comparative Ct method described by Livak and Schmittgen.[239] The housekeeper 18s rRNA was used as an internal control and all Ct values were expressed relative to the solvent control.

The calculations used to determine relative gene expression are detailed below:

1. $\Delta Ct = Ct_{\text{target gene}} - Ct_{\text{18s gene}}$
2. $\Delta\Delta Ct = \Delta Ct - \text{average } \Delta Ct_{\text{Solvent control}}$
3. Fold Change = $2^{-\Delta\Delta Ct}$

If $2^{-\Delta\Delta Ct}$ was < 1, then relative gene expression was calculated by taking the negative inverse, as described below:

4. Fold change = $-\frac{1}{2^{-\Delta\Delta Ct}}$

4.9.2 Western blots

4.9.2.1 Principle of the assay

Western blotting is used to identify the expression level of a protein of interest. The Western blot technique consists of three elements: (i) protein fractionation by size using gel electrophoresis, (ii) transfer of the fractionated proteins on the gel to a robust membrane support and (iii) probing the membrane with tagged-antibodies in order to identify and quantitate protein expression.[245]

Firstly, cell lysates are denatured in gel loading buffer containing sodium dodecyl sulfate (SDS) detergent.[245-246] This produces a uniformly negative charge and removes higher protein structure, so proteins will be separated primarily by molecular weight using SDS-PAGE (sodium dodecyl sulphate polyacrylamide gel electrophoresis).[246] Proteins migrate from the negative to the positive electrode of the running apparatus by size.[247] Smaller proteins will migrate further down the gel in comparison to larger proteins. The gel loading buffer, which denatures proteins also contains tracking dyes, such as bromophenol blue, to determine protein migration through the gel. This guides the researcher and prevents proteins from running over.[245-246]

After SDS-PAGE, proteins are migrated to a solid support such as polyvinylidene fluoride (PVDF) membrane which binds proteins with high affinity.[246] The electric field is parallel to the surface of the gel and membrane sandwich and the sandwich is oriented with the gel on the negative electrode and the membrane on the positive electrode. Protein bands therefore migrate from the negative electrode to the positive electrode.[245,247]

After the transfer process, the membrane is blocked with a blocking solution. The blocking solution reduces non-specific binding of antibodies to off-target proteins on the membrane and enhances the specificity and selectivity of the antibody, increasing the signal–to–noise ratio for detection of the target.[248] After blocking, the membrane is probed with a primary antibody against the protein of interest. The primary antibody has and subsequently probed with a secondary antibody which has an enzyme, such

as horseradish peroxidase (HRP), conjugated to it.[247] The proteins can then be detected using enhanced chemiluminescence (ECL)[247] and semi-quantified by densitometric analysis.

4.9.2.2 Materials and overview of the assay

Mammalian protein extraction buffer (MPER; # 78501), Halt™ Protease Inhibitor Cocktail, EDTA-Free (#87785), 2-mercaptoethanol (#M3148), MOPS running buffer (# M1254), methanol (#34860) and TWEEN®-20 (# P1379) were purchased from Sigma-Aldrich (St. Louis, Missouri, United States of America). Pierce™ BCA protein assay kit (#23225), NuPAGE™ 4-12% Bis-Tris protein gels (# NP0335BOX), Trizma ® base (#77816), glycine (#G8898), Pierce™ Western Blotting ECL substrate kit (#32106) and 4X NuPAGE™ LDS buffer (# NP0008) were purchased from Thermo Fisher Scientific (MA, United States of America). Sodium lauryl sulphate (#30175) were purchased from BDH Chemicals Ltd. (Poole, England). Immuno-Blot® PVDF Membranes for protein blotting (#162-0177) and Precision Plus Protein standards (#1610374) were purchased from Bio-Rad (California, United States of America. Bovine serum albumin (BSA) (#2217C303) were purchased from VWR lab products PVT. Ltd. (Bengaluru, India). The preparation of buffers for the Western blot are listed in Appendix O.

A six-step process was followed in Western Blot experiments to analyse protein extracts from SiHa cell cultures (Figure 12).

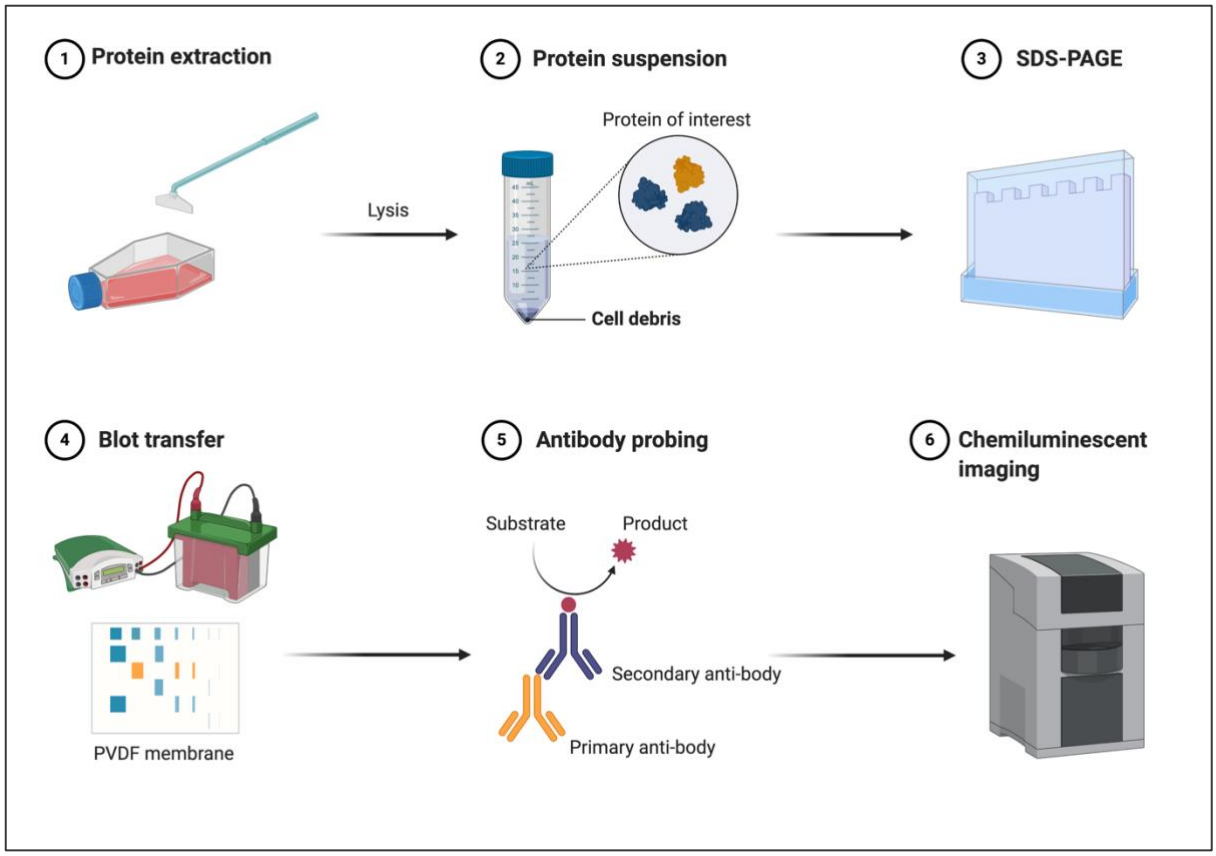

Figure 12. Overview of workflow for Western Blot experiments (Source: personal collection). Image created using BioRender.com.

4.9.2.3 Cell lysis and protein extraction

After 72-hour treatment with cholecalciferol, crude protein lysates were extracted from SiHa cells using 500 µl ice-cold MPER mammalian protein extraction buffer supplemented with protease inhibitors (Halt™ Protease Inhibitor Cocktail, EDTA-Free; 1:100 ratio). The flasks were incubated at room temperature for 5 minutes on ice and then cells were scraped from the flask using a cell scraper. Cell lysates were collected into Eppendorf tubes and cell debris was pelleted by centrifugation at 14 000 x*g* and 4°C for 15 minutes. Thereafter, the supernatant containing total protein was carefully extracted, aliquoted and stored at -80 ºC.

4.9.2.4 Protein quantification

Pierce™ BCA protein assay kit (Thermo Fisher) was used to determine the protein concentration of each sample. A working stock solution to quantify the protein was

prepared following the enhanced protocol described by the manufacturer. Briefly, the working stock solution consisted of 50 parts of BCA reagent A to 1-part BCA reagent B (50:1) and 2 ml of this solution was aliquoted into a separate tube for each sample. To each tube, 100 µl of the total protein extracts were added and the mixture was and incubated at 60°C for 30 minutes. Thereafter, all tubes were cooled to room temperature and a 200 µl sample of this mixture was added to a 96-well plate. Optical density was measured at 562 nm using an EL_x800 Absorbance Reader (BioTek Instruments Inc., Vermont, United States of America).

Calibration curves (Appendix P) to standardise protein concentration to 15 µg/lane for Western Blot experiments were established using bovine serum albumin (BSA) protein standards (250 µg/ml, 125 µg/ml, 50 µg/ml, 25 µg/ml, 5 µg/ml, and 0 µg/ml) provided in the Pierce™ BCA protein assay kit. The straight-line equation (y = mx + c) of the BCA standard curve was employed to calculate the x-value (protein concentration) from the measured Absorbance (y-value).

4.9.2.5 Denaturation of proteins

15µg of protein was denatured using a reducing loading buffer. The loading buffer consisted of 4X NuPAGE™ LDS buffer (25% of total volume) and reducing agent β-mercaptoethanol (2.5% of final volume). The proteins in the loading buffer were boiled at 95 ºC for 7 minutes, and then 25 µl of the sample was loaded onto each lane of NuPAGE™ 4-12% Bis-Tris protein gels.

4.9.2.6 SDS-PAGE

Samples were loaded onto NuPAGE™ 4-12% Bis-Tris protein gels with a relevant pre-stained standard molecular weight protein marker (Precision Plus protein standards; 10–250 kD) in lane 1 subjected to electrophoresis. Electrophoresis was performed at room temperature at 200 V for 50 minutes in 1X MOPS running buffer (Appendix O) diluted in deionised H_2O.[249]

4.9.2.7 Membrane transfer

Separated proteins were transferred to polyvinylidene fluoride (PVDF) membranes after SDS-PAGE for 90 minutes at 110 V at 4 °C. Before the transfer sandwich was prepared, the PVDF membrane was pre-wetted and activated in 100% methanol and then placed in 1X transfer buffer (Appendix O). The gel and membrane were stacked and oriented so that the gel is on the cathode and the PVDF membrane is on the anode (Figure 13).[250]

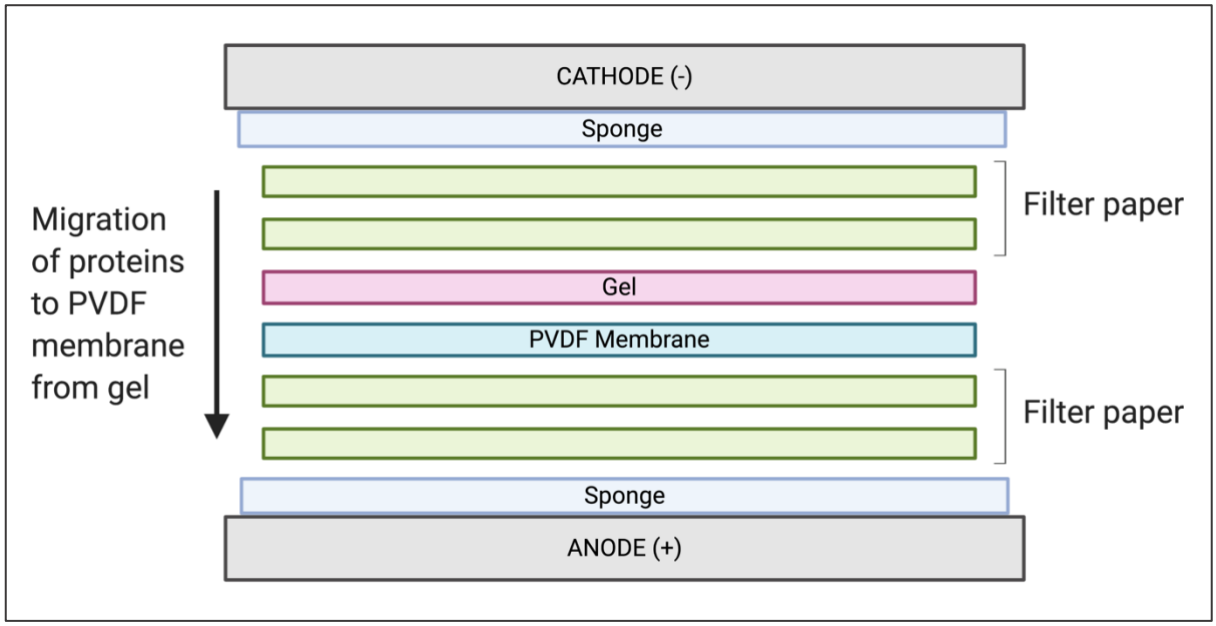

Figure 13. The wet transfer sandwich orientation

Negatively charged proteins in the gel are placed near the cathode and the membrane is placed on the positive, anode, side of the sandwich as indicated by the downwards arrow. Sponges (in blue) and filter paper (green) help support the sandwich and help ensure the gel and membrane remain in close contact. (Source: personal collection). Image created using BioRender.com.

4.9.2.8 Membrane blocking and antibody probing

After the transfer, PVDF membranes were washed in deionised water and then blocked with 2.5% BSA in 0.2% PBS-Tween® 20, agitated at room temperature for 1 hour. Thereafter, membranes were washed three times with 0.2% PBS-Tween® 20 for 10 minutes each.

The membranes were then probed with the primary antibody for the protein of interest overnight at 4°C. Primary antibodies were appropriately diluted (Appendix Q) in a 0,2%

PBS-Tween® 20 solution which contained 2.5% BSA and 0.02% sodium azide. The housekeeper protein used was β-actin protein and was used as a loading control.

The next day, primary antibody solutions were removed and stored at 4 ºC and membranes were washed three times with 0.2% PBS-Tween® 20 for 10 minutes each. Membranes were agitated at room temperature for 1 hour in compatible secondary antibody cocktail. The secondary antibody solution consisted of horseradish peroxidase (HRP)-conjugated-anti-rabbit antibody (1:10 000) in 0.2% PBS-Tween® 20 containing 2.5% BSA. After visualisation of the protein of interest, the membranes were washed three times for 10 minutes each with 0.2% PBS-Tween® 20. Then, the membrane was probed with HRP-conjugated anti-β-actin antibody (1:5 000) in 0.2% PBS-TWEEN® 20 containing 2.5% BSA for 1 hour at room temperature. The antibody incubation conditions for western blots are listed in Appendix Q.

4.9.2.9 Membrane visualisation and densitometric analysis

Proteins were visualised by HRP activation using Pierce™ enhanced chemiluminescent (ECL) reagent and images captured by a ChemiDoc™ XRS$^+$ Imaging System (Bio-Rad Laboratories Inc., California, United States of America). Protein blots were densitometrically analysed using the Image Lab version 6.0 (Bio-Rad Laboratories, Inc., CA, USA) software. Protein quantity was determined by the software and protein expression in each lane was normalised to the corresponding β-actin expression. Semi-quantitative analysis was conducted on three biological repeats.

4.10 Statistics

All statistical testing of data and the study design, including sample size, were determined in consultation with the faculty statistician to ensure adequate statistical powering of the study. A copy of the clearance letter from the faculty statistician is provided in Appendix S.

4.10.1 Sample size

Each experiment comprised nine flasks, resulting from three biological repeats each with three technical repeats and may be seen as independent. Experimental (treated cultures) and control cultures were run in each experiment. The most conservative analysis was a two-way analysis of variance (ANOVA) with the following factors: treatments (6 experimental cultures) and biological repeats (3 parent flasks) with interaction. This analysis yielded 36 degrees of freedom for residual, which exceeded the norm of 30 degrees of freedom, and hence the sample size was adequate for experiments.

4.10.2 Quantitative data analysis

Quantitative data were presented using descriptive summary statistics [means and standard error of mean (SEM)] and reported by treatment for each parameter. Data analysis was conducted by both assuming the nine flasks were independent and also where biological repeats were specified as the random component. From the latter analysis, the assumption for the first analysis could/may be confirmed. The first ANOVA for a two-factor design which considered treatment (6 experiment cultures) and biological repeats (3 parent flasks) along with the interaction term. The second analysis employed mixed-effects maximum likelihood repression with fixed effect treatment and parent flasks as specified as the random component. All testing was done at the 0.05 level of significance. Statistical analysis was performed using GraphPad Prism v8.x software for Windows (GraphPad Software, La Jolla, California, United States of America, www.graphpad.com).

4.10.3 Qualitative and semi-quantification data analysis for microscopy studies

All microscopy on control and experimental cultures were performed on three biological repeats and analysed qualitatively for representative morphological features of cell growth and cell death. In addition, as described in the Methods section (4.8.1.2), percentage apoptotic cells and giant multi-nucleated cells were analysed by one way

ANOVA and Bonferroni post hoc testing at a significance of <0.05 using GraphPad Prism v8.x software for Windows (GraphPad Software, La Jolla, California, United States of America, www.graphpad.com).

5. Results

5.1 Optimal incubation period for cholecalciferol treatments in SiHa cells determined by cell enumeration and viability

The optimal incubation period for cholecalciferol in SiHa cells was determined by preliminary cell count and cell viability experiments. These studies were conducted over 24-hour intervals for 72 hours. A significant decrease in cell count and viability was identified at 72 hours in cultures treated with 2600 nM cholecalciferol. Cell count was significantly decreased at 2600 nM (72.88 ± 2.46 %) treatment in comparison with medium (101.00 ± 4.10 %; p = 0.004) and solvent (100 ± 3.59 %; p = 0.011) controls (Figure 14.C) in the crystal violet assay.

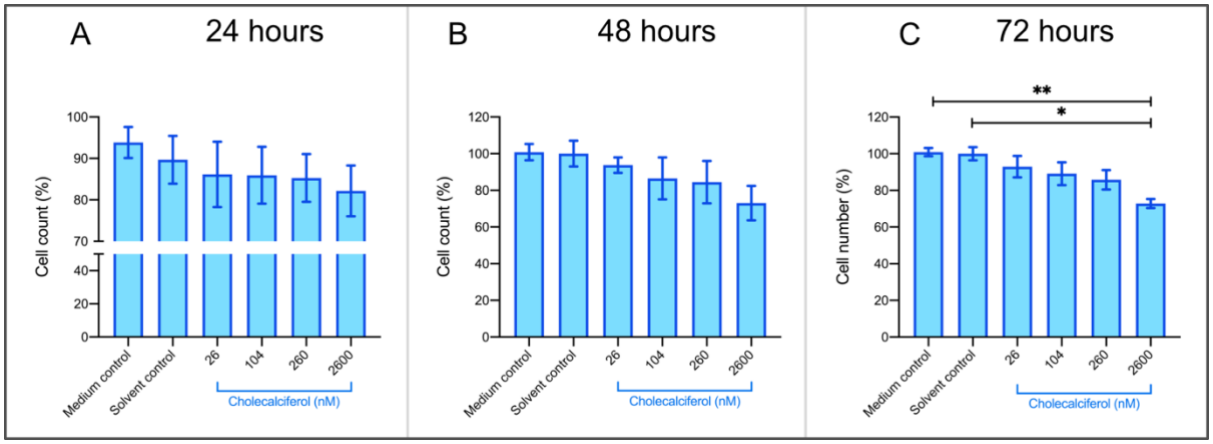

Figure 14. Cell count using the crystal violet assay

Cell counts of control and experimental SiHa cultures incubated with cholecalciferol for 24 hours (A), 48 hours (B) and 72 hours (C). At 72 hours, a significant decrease in cell count was observed at 2600 nM in comparison with the medium and solvent controls. All assays were repeated three times, and each measured in triplicate and $p < 0.05$ was considered statistically significant. ** $p < 0.01$; * $p < 0.05$.

Cell viability decreased in both semi-quantitative trypan blue and quantitative Muse™ Count and Viability assays at 2600 nM in comparison with controls and 26 nM and 104 nM treatments. Cholecalciferol significantly reduced cell viability at 2600 nM (82.04 ± 1.79 %) in comparison with the medium (93.71 ± 1.21 %; $p < 0.0001$) and solvent (93.31 ± 1.13 %; $p < 0.0001$) controls and, 26 nM (89.71 ± 0.65 %; p = 0.0033) and 104 nM (88.47 ± 1.08 %; p = 0.0236) treatments in the trypan blue dye exclusion assay (Figure 15.C). In the quantitative Muse™ Count and Viability assay, a significant

decrease in cell viability was observed at 2600 nM (88.07 ± 1.57 %) treatment in comparison with the medium (95.11 ± 1.07 %; p = 0.004) and solvent (95.34 ± 0.84 %; p = 0.003) controls, and 26 nM (94.24 ± 0.62 %; p = 0.017) treatment (Figure 16.C).

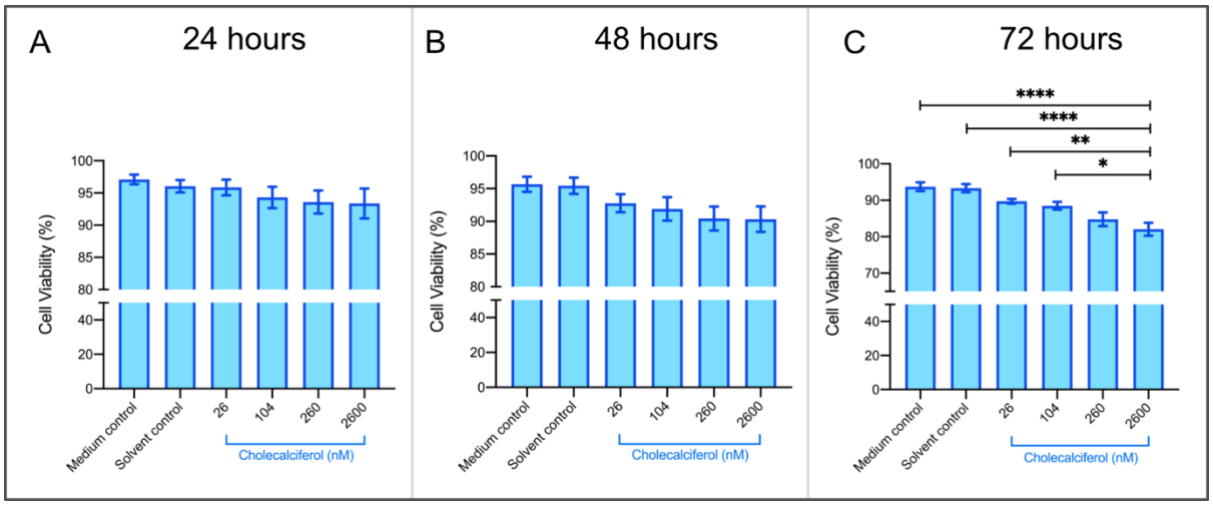

Figure 15. Cell viability semi-quantified by trypan blue dye exclusion in SiHa control and experimental cultures at 24, 48 and 72 hours

Cells were quantified at 24 hours (A), 48 hours (B) and 72 hours (C). No significant changes to cell viability was observed at 24- and 48-hours but a significant decrease in cell viability was observed at 72 hours at 2600 nM. All assays were performed on three biological repeats and each measured in triplicate and $p < 0.05$ was considered statistically significant. * $p < 0.05$; ** $p < 0.01$; **** $p < 0.0001$.

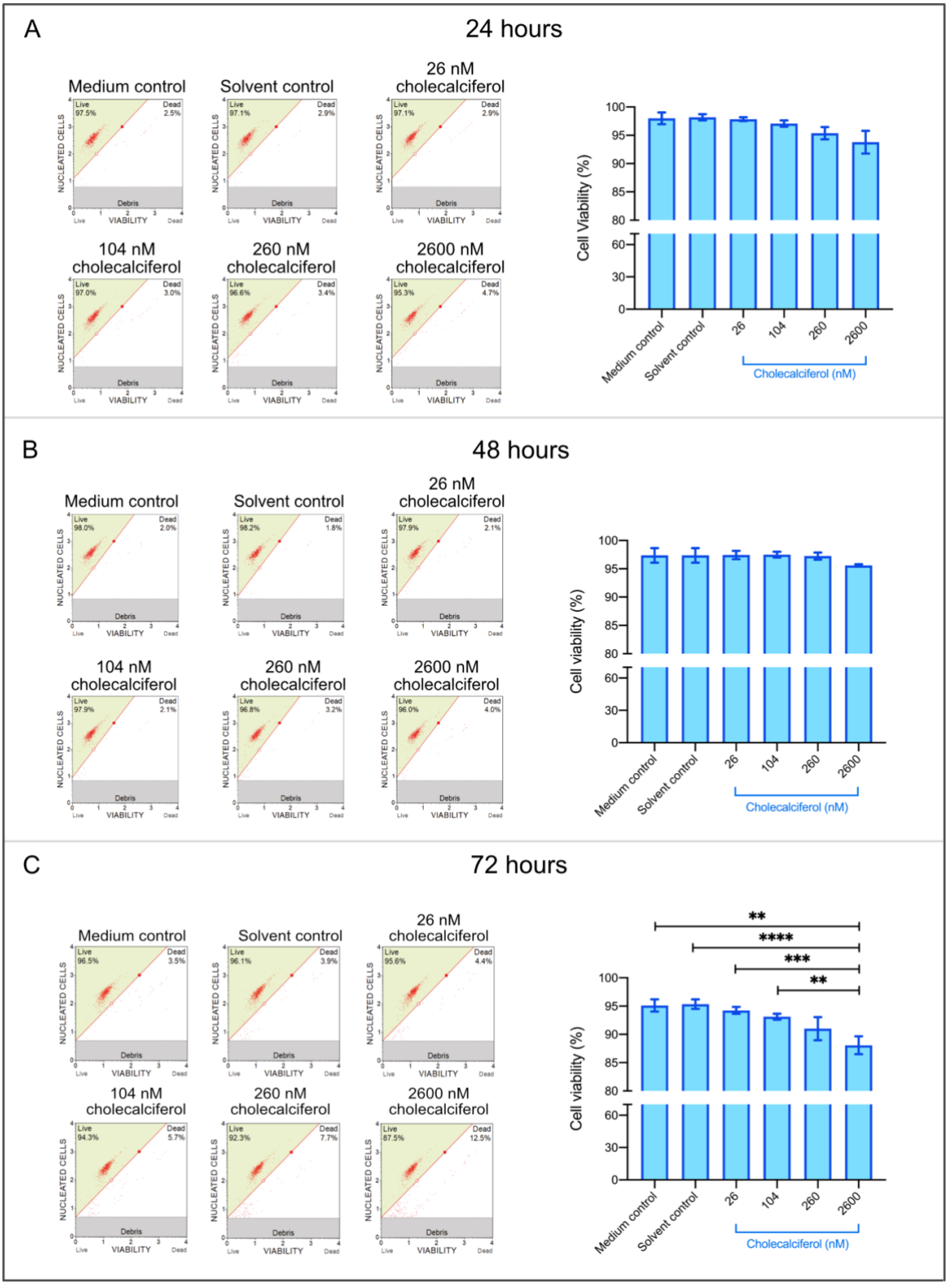

Figure 16. Cell viability in SiHa control and experimental cell cultures at 24, 48 and 72 hours

Cell viability assessed by Muse™ Count and viability assay for 24 hours (A), 48 hours (B) and 72 hours (C) with a range of cholecalciferol treatments. At 72 hours, a significant decrease in cell viability was identified in SiHa cells treated with 2600 nM cholecalciferol in comparison with the medium and solvent controls, and 26 nM and 104 nM treatments. All assays were performed independently three times and in triplicate. * $p < 0.05$; ** $p < 0.001$; *** $p < 0.0001$ and **** $p < 0.00001$.

Thus, 72-hour incubations were found to be optimal, as cell count and cell viability were significantly decreased at 2600 nM treatment. Therefore, all further experiments were conducted over a 72-hour incubation period.

5.2 Cell proliferation measured by Ki67 proliferation marker expression

Expression of the Ki67 nuclear antigen is closely associated with cell proliferation.[212] Cell proliferation was investigated using the Muse™ Ki67 Cell Proliferation kit. No significant change in Ki67 nuclear antigen expression was observed between control and experimental SiHa cultures (Figure 17).

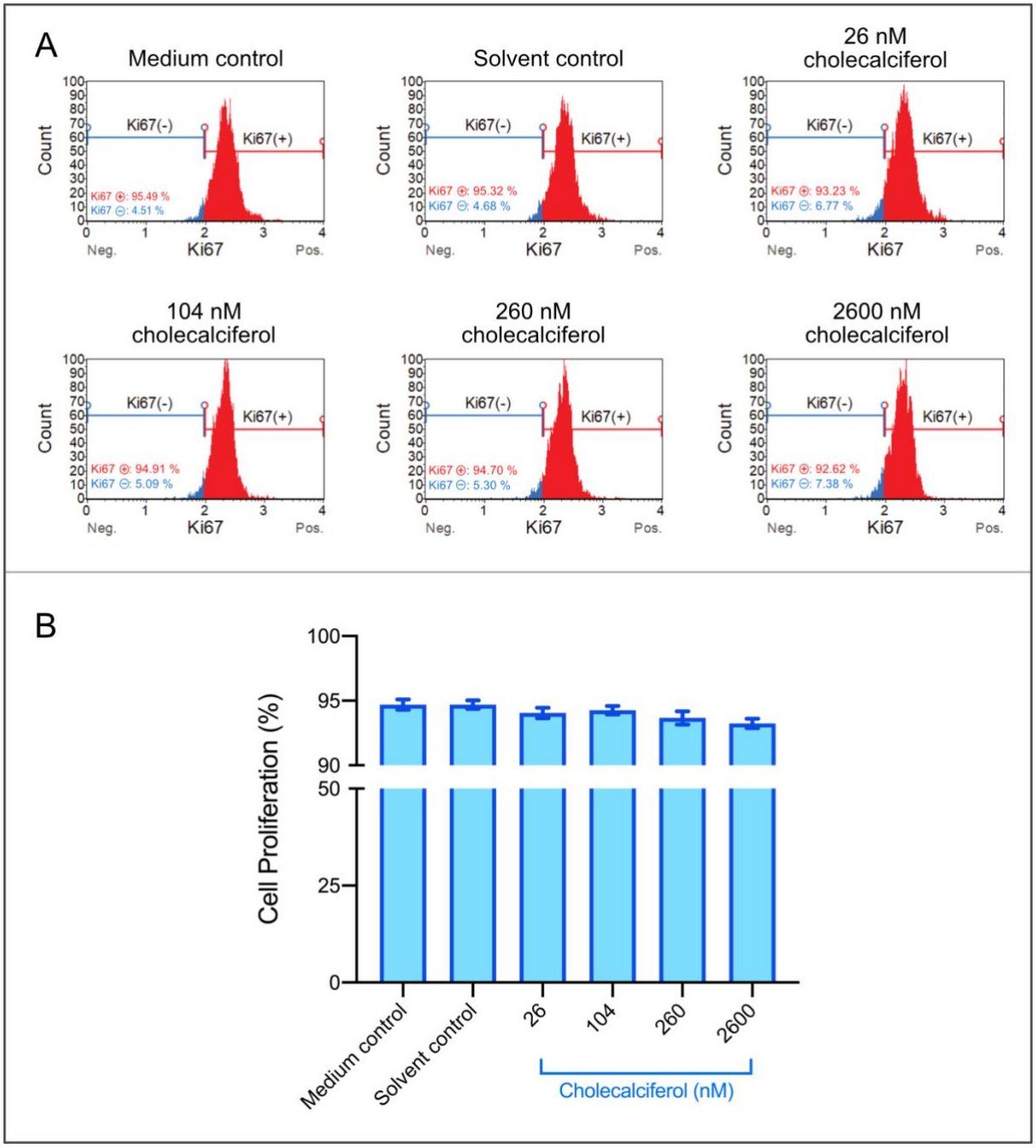

Figure 17. Effects of cholecalciferol Ki67 cell proliferation marker in SiHa cells

Representative Muse™ single-parameter histogram plots of each cell culture (A) and cell proliferation in SiHa control and experimental cell cultures (B). Data are represented as mean ± SEM and significant difference was determined when $p < 0.05$. No significant change in Ki67 expression was observed between the control and treatment cultures.

5.3 Cell cycle analysis using Muse™ Cell Cycle assay

The cell cycle profile identifies cells in different phases of the cell cycle, based on DNA content of each cell.[251] The cell cycle profile, analysed by the Muse™ Cell Cycle assay, identified significant increases in the sub-G_1 cell population at 2600 nM. A significant

increase in the sub-G_1 phase of the cell cycle was observed at 2600 nM (9.90 ± 0.65 %) treatment in comparison with the medium (0.93 ± 0.18 %; $p < 0.0001$) and solvent (1.03 ± 0.15 %; $p < 0.0001$) controls, and 26 nM (0.87 ± 0.30 %; $p < 0.0001$), 104 nM (1.07 ± 0.20 %; $p < 0.0001$) and 260 nM (2.50 ± 1.10 %; $p < 0.0001$) treatments (Figure 17.B). In addition, here was no evidence of cell cycle arrest at G_1/G_0 and G_2/M across the treatment range, as cells did not accumulate in either G_1/G_0 or G_2/M phases of the cell cycle (Figure 18.C, D and E).

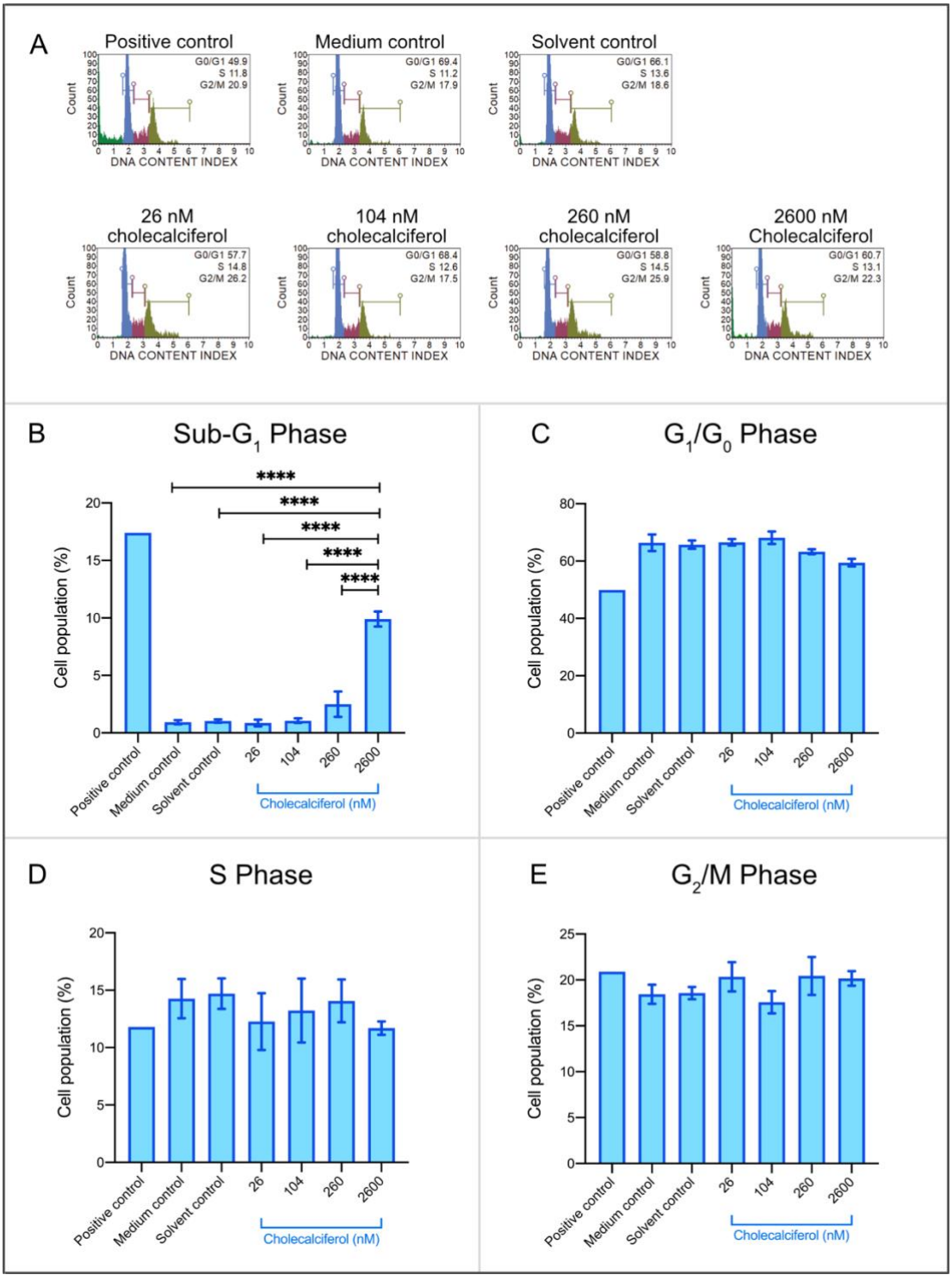

Figure 18. Effects of cholecalciferol on the cell cycle profile SiHa control and experimental cultures

Single-parameter cell cycle histograms (A), Sub- G_1phase (B), G_1/G_0 phase (C), S phase (D), and the G_2/M phase (E). Data are represented mean ± SEM and $p < 0.05$ was considered significantly different. Statistical analysis was conducted on three independent repeats. A significant increase sub-G_1 phase was observed at 2600 nM treatment in comparison with all cultures. **** $p < 0.0001$.

5.4 Biochemical investigation of modes of cell death

Modes of cell death investigated include apoptosis, autophagic cell death and necrosis. Biochemical markers for early and late stages of apoptosis were investigated using flow cytometry. Early-stage apoptotic markers measured mitochondrial membrane potential and phosphatidylserine (PS) externalisation. Late-stage markers quantified terminal caspase (caspase-3 and -7) activity and DNA damage markers (H2A.x and ATM). Autophagic cell death was assessed by quantification of LC3-II expression and necrotic cell death assessed by quantification of LDH release.

5.4.1 Biochemical markers of early apoptosis

5.4.1.1 Mitochondrial membrane potential measured by Muse™ Mito Potential assay

Mitochondrial health is a biomarker of overall cell health and decreased mitochondrial health is regarded as an early marker of apoptosis.[252] Mitochondrial membrane potential ($\Delta\Psi m$) was assessed using the Muse™ Mito Potential assay. In this assay, healthy mitochondria sequester the Mito Potential dye and dead cells stain positive with cell impermeant dead cell marker, 7-AAD.

A significant decrease was observed in the live cell population (Figure 19.B) at 2600 nM treatment (84.45 ± 1.7 %) in comparison with medium (94.39 ± 1.12 %; p = 0.0008) and solvent (94.09 ± 0.70; p = 0.0011) controls; and 26 nM (94.23 ± 0.32 %; p = 0.0009) and 104 nM (92.67 ± 0.58 %; p = 0.0043) treatments was observed. This finding was accompanied by a significant increase in cells with depolarised $\Delta\Psi m$ (Figure 19.C) at 2600 nM treatment (14.7 ± 1.28 %) in comparison with medium (3.97 ± 1.76 %; p = 0.0058) and solvent (5.14 ± 1.06 %; p = 0.0145) controls; and 26 nM (4.69 ± 1.05 %; p = 0.0102) and 104 nM (6.47 ± 1.96 %; p = 0.0431) treatments. These findings demonstrate a significant decrease in $\Delta\Psi m$ at 2600 nM treatment of cholecalciferol in SiHa cells.

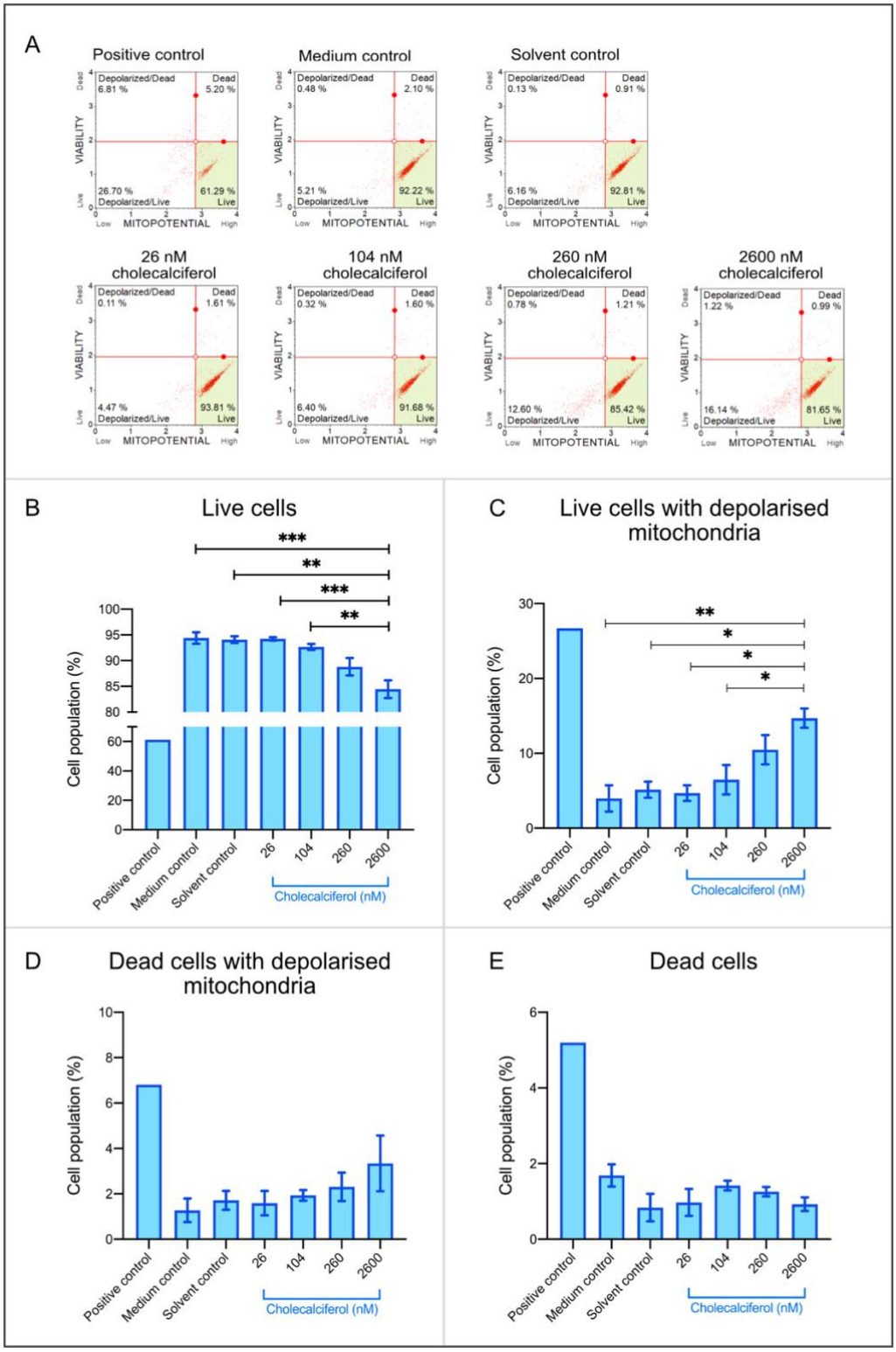

Figure 19. Mitochondrial membrane potential (ΔΨm) in SiHa control and experimental cell cultures

Representative two-parameter plots of events captured on the Muse™ Cell Analyser (A), live cells (B), live cells with depolarised mitochondrial membranes (C), dead cells with depolarised membranes (D) and dead cells (E). Statistical analysis was performed on three independent biological replicates. Values are expressed as mean ± SEM and $p < 0.05$ was considered statistically significant. Cholecalciferol significantly decreased live cells and increased cells with decreased ΔΨm at 2600 nM (A and B, respectively). * $p < 0.05$; ** $p < 0.01$; *** $p < 0.001$; **** $p < 0.0001$.

5.4.1.2 Phosphatidylserine (PS) externalisation using the Muse™ Annexin V detection assay

An early biochemical feature of apoptotic cell death is PS externalisation.[142] PS externalisation to the outer membrane (PS flip-pattern) was detected in apoptotic cells by the Muse™ Annexin V & Dead Cell Assay. Additionally, a cell impermeant dead cell marker, 7-AAD, was used as an indicator of cell membrane integrity.

A significant decrease was observed in the live cell population at 2600 nM (90.19 ± 1.12 %) in comparison with medium control (95.56 ± 0.35 %; p = 0.0027), solvent control (95.43 ± 0.31 %; p = 0.0035) and 26 nM treatment (94.88 ± 0.98 %; p = 0.0111; Figure 20.B). Cells in early apoptosis were significantly increased at 2600 nM (7.59 ± 0.26 %) in comparison with medium (2.38 ± 0.43 %; p = 0.0351) and solvent (2.53 ± 0.24 %; p = 0.0439) controls and 26 nM treatment (2.25 ± 0,80 %; p = 0.0112; Figure 20.C). Furthermore, an increase in late-stage apoptosis (Figure 20.D) was also observed at only 2600 nM treatment (3.40 ± 1.13 %) comparison with the medium control (0.53 ± 0.10 %; p = 0.0353). These data collectively show a decrease in live cells and an increase in PS externalisation in SiHa cells treated with 2600 nM cholecalciferol.

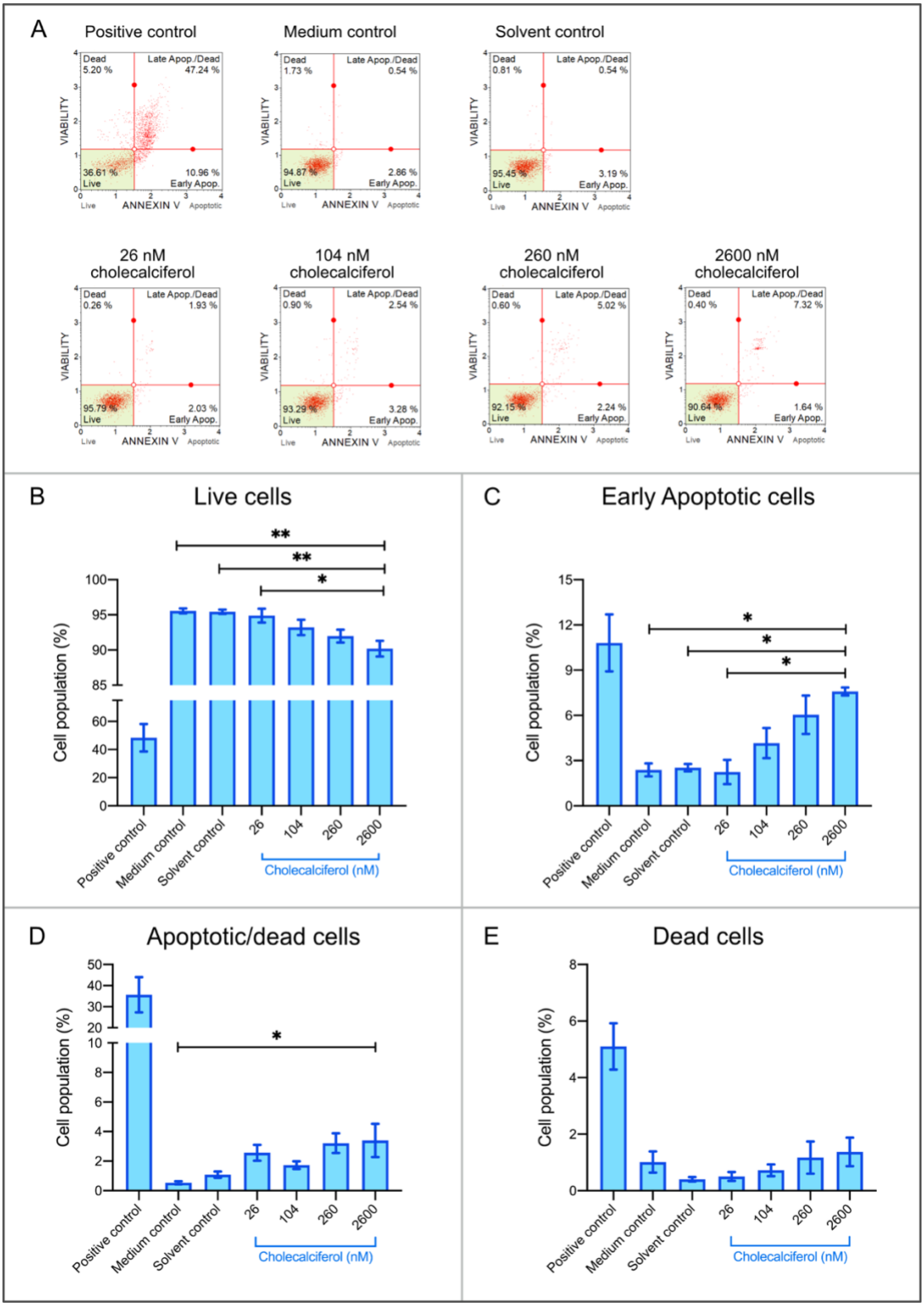

Figure 20. Annexin V binding in SiHa control and experimental cell cultures

Representative two-parameter dot-plot Muse™ diagrams (A), live cells (B), early apoptotic cells (C), apoptotic and dead cells (D) and dead cells (E). Live cells were significantly decreased, and apoptotic cells were significantly increased at 2600 nM cholecalciferol treatment (B and C, respectively). Statistical analysis was performed on three independent repeats. Data are expressed as mean ± SEM and $p < 0.05$ was considered statistically significant. * $p < 0.05$; ** $p < 0.01$.

5.4.2 Biochemical markers of late apoptosis

5.4.2.1 Caspases -3 and -7 activity in cholecalciferol-treated SiHa cells

The activation of terminal caspases (caspases -3 and -7) is a hallmark of late apoptosis.[142] This was investigated using the Muse™ Caspase 3/7 assay. A significant decrease in the live cell population (Figure 21.B) at 2600 nM (89.48 ± 0.53 %) was observed in comparison with medium control (94.53 ± 0.53 %; p = 0.0009), solvent control (94.01% ± 0.5 %; p = 0.0025) and 26 nM treatment (94.15 ± 1.15 %; p = 0.0018). These findings were accompanied by a significant increase in caspases-3 and -7 activity at 2600 nM (4.99 ± 0.30 %) comparison with medium control (1.71 ± 0.42 %; p = 0.0136) and 104 nM (2.24 ± 0.439 %; p = 0.0473; Figure 21.C). In summary, a significant increase in activated terminal caspases were observed at 2600 nM cholecalciferol treatment.

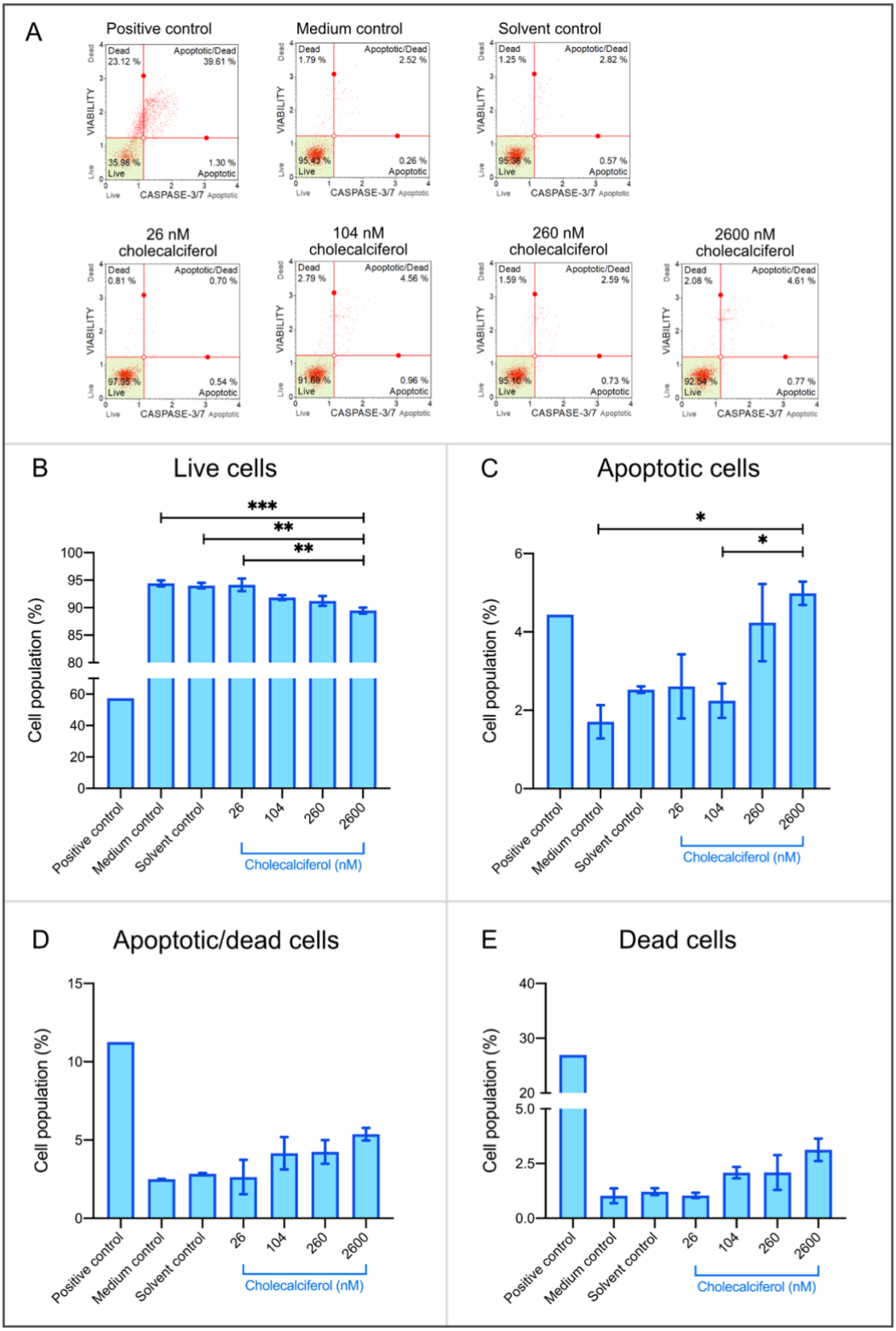

Figure 21. Activation of caspases -3 and -7 activation in SiHa control and experimental cell cultures

Representative two-parameter dot-plots of each cell culture (A), live cells (B), live cells with activated caspase-3/7 (C), dead cells with active caspases (D) and dead cells (E). At 2600 nM cholecalciferol, live cells were significantly decreased, and apoptotic cells were increased. Statistical analysis was performed on three independent repeats. Values are expressed as mean ± SEM and $p < 0.05$ was considered statistically significant. * $p < 0.05$; ** $p < 0.01$; *** $p < 0.001$.

5.4.2.2 Double-stranded and total DNA damage in cholecalciferol-treated SiHa cells

Nuclear fragmentation and DNA damage occurs during apoptosis after terminal caspase activation.[142] DNA damage was assessed using the Muse™ Multi-colour DNA damage assay which quantified phosphorylated ATM enzyme and H2A.X histone (γ-H2A.X) protein. Double-strand DNA breaks (DSBs) were identified by dual staining of phosphorylated ATM and γ-H2A.X; and total DNA damage included both single strand DNA lesions and DSBs identified by dual staining and individual staining of each marker, respectively.

The Muse™ Multi-colour DNA damage assay showed significant decrease in the live cell population at 2600 nM (90.10 ± 1.50 %) in comparison with the medium (98.46 ± 0.41 %; p = 0.001) and solvent (97.44 ± 0.70 %; p = 0.004) control cultures, and 26 nM (95.56 ± 0.76 %; p = 0.040) and 104 nM (96.45 ± 1.12 %; p = 0.014) treatments (Figure 22.B). Double-stranded DNA breaks were identified by dual activation of ATM and H2A.X markers, indicated in the top-right quadrant of each two-parameter plot (Figure 22.A). There was a significant increase in cells with double-stranded DNA breaks at 2600 nM (2.63 ± 1.01 %) in comparison with the medium control (0.52 ± 0.37 %; p = 0.046; Figure 22.C). Additionally, cells with total DNA damage significantly increased at 2600 nM treatment (9.90 ± 1.45 %) in comparison with medium (1.60 ± 0.78 %; p = 0.001) and solvent (2.56 ± 0.70 %; p = 0.004) controls, and 26 nM ± 0.76%; *p* = 0.039) and 104 nM (3.55 ± 1.19 %; p = 0.013) treatments (Figure 22.D). These findings, therefore, demonstrated increased DSBs and single-strand DNA lesions in SiHa cell cultures treated with 2600 nM cholecalciferol.

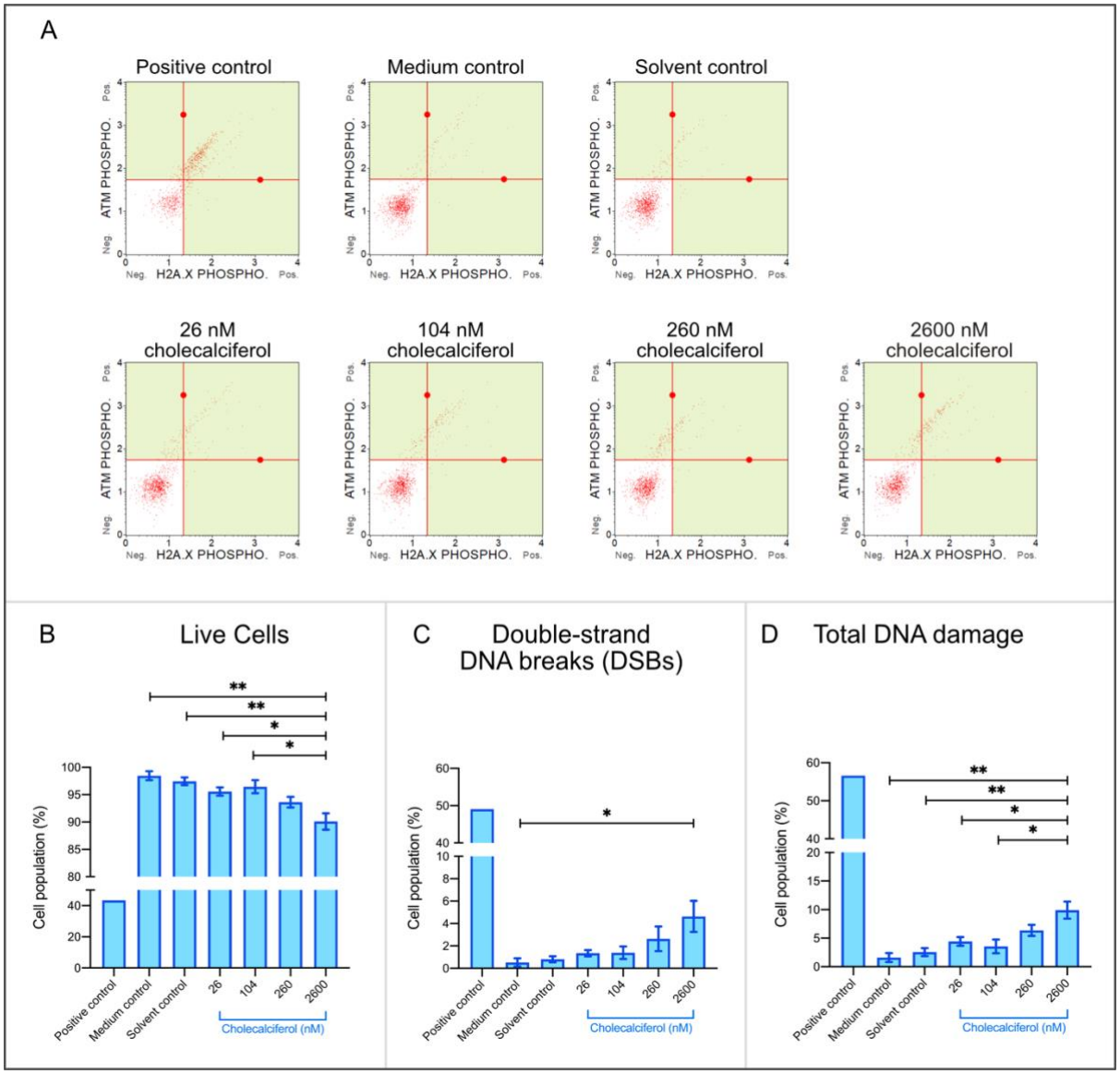

Figure 22. DNA damage in SiHa control and experimental cell cultures

Muse™ two-parameter dot-plots (A), live cells (B), cells with double stranded DNA breaks (C) and cells with total DNA damage (D). A significant decrease in live cells was observed at 2600 nM treatment in comparison with medium and solvent controls, and 26 nM and 104 nM treatments. A significant increase in double stranded DNA breaks was identified at 2600 nM treatment in comparison with the medium control. Total DNA damage was significantly increased at 2600 nM treatment in comparison with the medium and solvent controls, and 26 nM and 104 nM treatments. Statistical analysis was conducted on three independent biological replicates. Values are expressed as mean ± SEM and $p < 0.05$ was considered statistically significant. * $p < 0.05$; ** $p < 0.01$.

5.4.3 Autophagic cell death

During autophagy, cytosolic LC3 protein migrates to the autophagosome where it undergoes post-translational modifications to form LC3-II.[142] LC3-II is a specific marker for autophagy induction. Induction of autophagic cell death in SiHa cell

cultures, assessed by the Muse™ LC3-II detection assay, determined mean autophagy intensity based on fluorescence of the LC3-II marker in each sample. There was no significant increase in LC3-II expression between control and experimental cultures (Figure 23.B). This suggested that cholecalciferol did not induce autophagic cell death in SiHa cell cultures.

Positive control cultures were treated with rapamycin, which targets a key modulator of autophagic induction. mTOR.[229] Positive control cultures demonstrated two distinct populations of cells with distinct peaks on the one-parameter histogram plot (Figure 23.A). The first peak (left) of this graph overlaps with the solvent control (grey overlay) and represents LC3-II expression in Siha cells at baseline. The second peak (right), which is broader and tented identified a second cell population with increased LC3-II protein levels. These cells were undergoing autophagy. In contrast, the one-parameter histogram plots (Figure 23.A) of cholecalciferol treated cultures did not show a second cell population and there was no significant increase in LC3-II expression in experimental cultures (Figure 23.B). This suggests that cholecalciferol did not induce autophagic cell death in SiHa cell cultures.

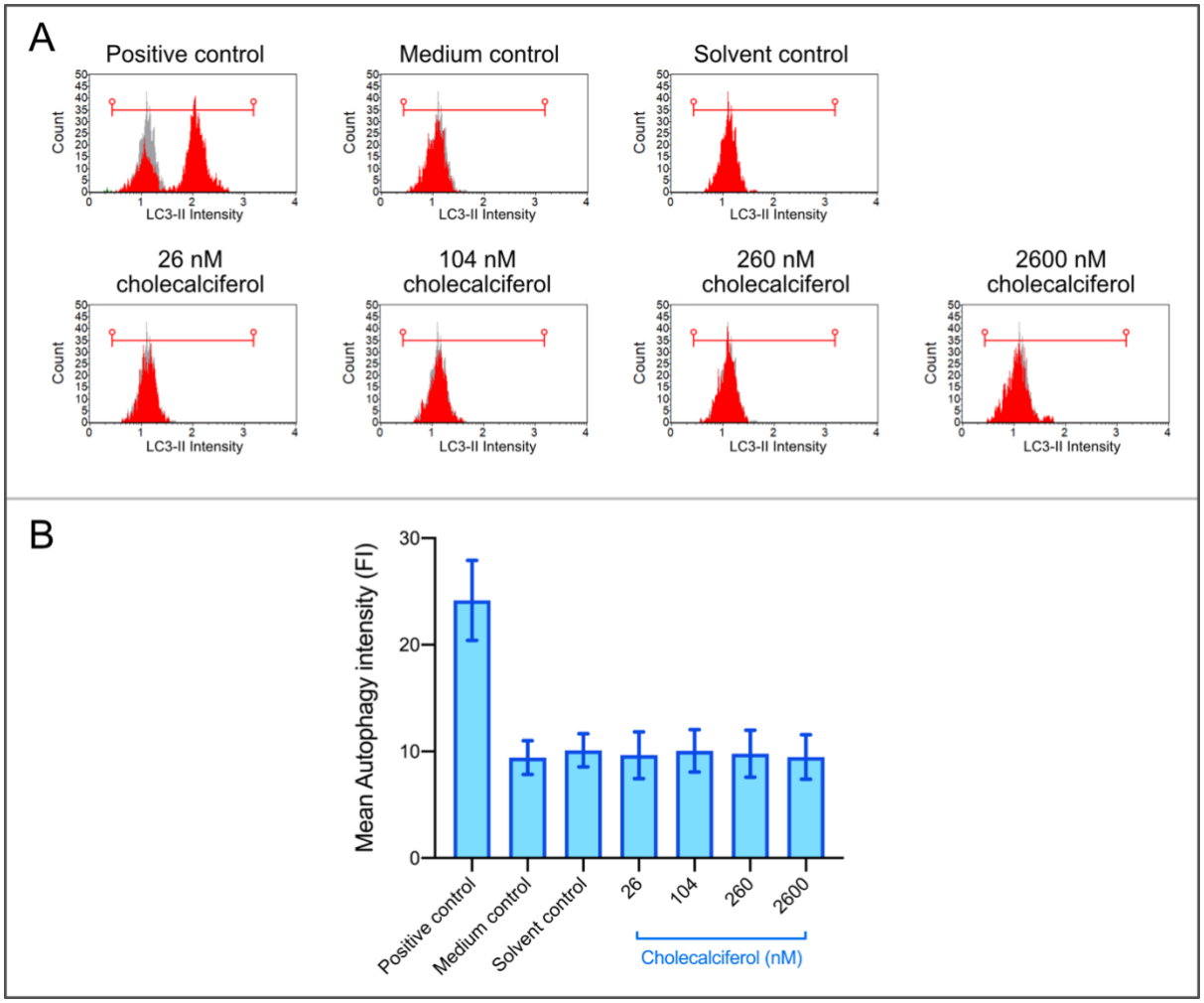

Figure 23. LC3-II intensity detected the induction of autophagic cell death

A representative sample of Muse™ one-parameter histogram plots of LC3-II intensity (A) and mean autophagy intensity (B). Statistical analysis was performed on three independent biological replicates. Values are expressed as mean ± SEM and $p < 0.05$ was considered statistically significant. No significant change was observed in LC3-II fluorescence intensity (FI) between control and experimental cultures.

5.4.4 Necrotic cell death based on LDH release

During necrosis, the cell membrane permeabilises and intracellular content is released into the cell culture medium.[230] Necrotic cell death was quantified by assaying the amount of intracellular LDH enzyme released into the culture. There was no significant change in necrotic cell death observed by LDH release across the treatment range (Figure 24).

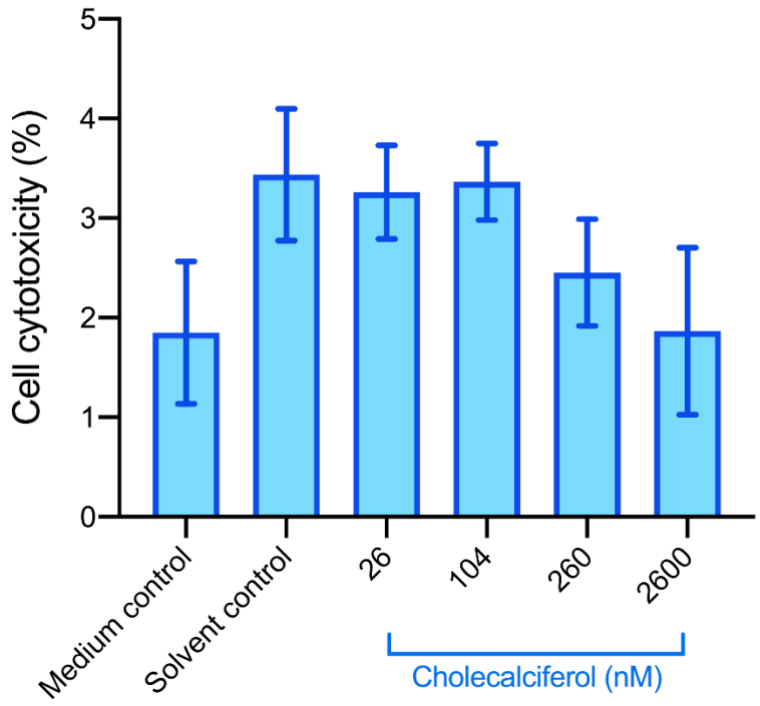

Figure 24. Necrotic cell death assessed using the lactate dehydrogenase (LDH) release assay

No significant changes in LDH release were identified between control and experimental cell cultures. Absorbance values for each well were subtracted from the blank control (medium only well) and released LDH was calculated relative to the solvent control and expressed as a percentage (%). Bar graph indicates statistical analysis of independent experiments repeated three times in triplicate. Data are represented mean ± SEM and significant difference was determined when $p < 0.05$.

5.5 Cell morphology and cell ultrastructure of cholecalciferol-treated SiHa cells

Cell morphology was qualitatively investigated using light microscopy of H&E stained SiHa cell cultures. Additionally, morphological features of apoptosis and giant multinuclear cells were semi-quantified from light micrographs. Ultrastructure of SiHa cells was examined using transmission electron microscopy.

5.5.1 Qualitative assessment of cell morphology using brightfield microscopy

5.5.1.1 Cell morphology in control and experimental cultures

Medium and solvent control cultures demonstrated cells in interphase with intact cell membranes and nuclear envelopes, oval-shaped nuclei, small distinct nucleoli (visible as dark dots within the nucleus) and homogenous eosinophilic (pink-stained) cytoplasm. At 26 nM, 104 nM and 260 nM treatments, cells showed similar morphological features as in control cultures. Furthermore, all stages of mitotic cellular division were present in the aforementioned control and treatment cultures (Figure 25). Cells in prophase presented with a dense, dark nucleus and dissolved nuclear membrane. Cells in metaphase showed chromosomes aligned at the equator forming a metaphase plate. An anaphase bridge appeared in cases where chromosomes separated from the equator and telophase showed a clear separation of chromosomes with the presence of cell membrane invagination.

In contrast, cells treated with 2600 nM cholecalciferol treatments demonstrated classical morphological features consistent with apoptosis. These included cell condensation and nuclear fragmentation (karyorrhexis) and the presence of membrane blebs and apoptotic bodies (Figure 25.F and Figure 26).

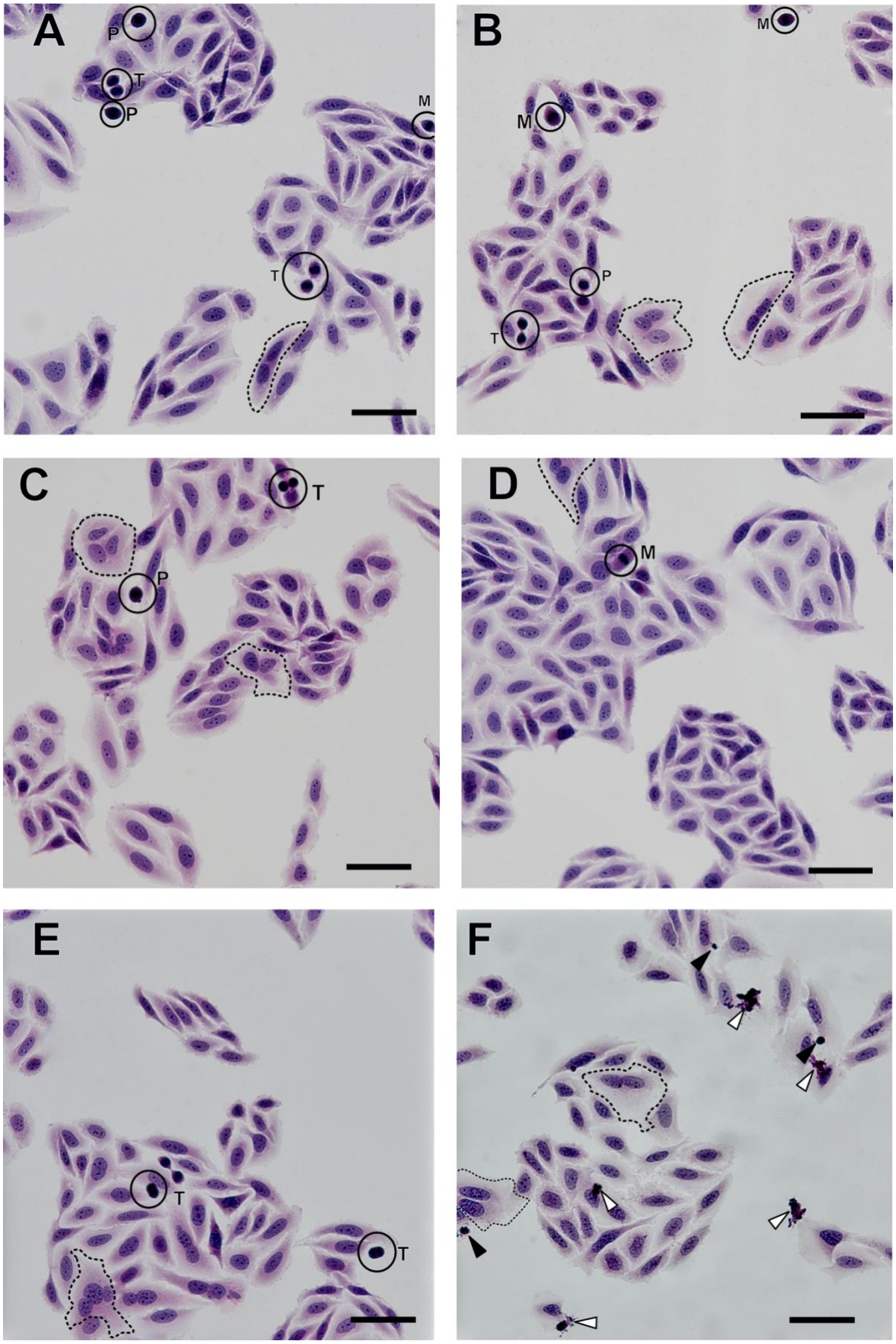

Figure 25. Light microscopy images of haematoxylin and eosin (H&E) stained SiHa cultures

(continued) Medium control (A), solvent control (B), and 26 nM (C), 104 nM (D), 260 nM (E) and 2600 nM (F) treatments of cholecalciferol. Features of mitosis (encircled) were identified in control cultures, and cells treated with 26 nM, 104 nM and 260 nM cholecalciferol. The stages of mitosis are indicated by letters: prophase (P), metaphase (M) and telophase (T). Features of apoptosis were evident at 2600 nM treatment. Features of apoptosis identified include nuclear condensation and cell shrinkage (black arrowheads) and membrane blebbing with apoptotic bodies (white arrowheads) were observed at 2600 nM treatment. Scale bar = 50 µm.

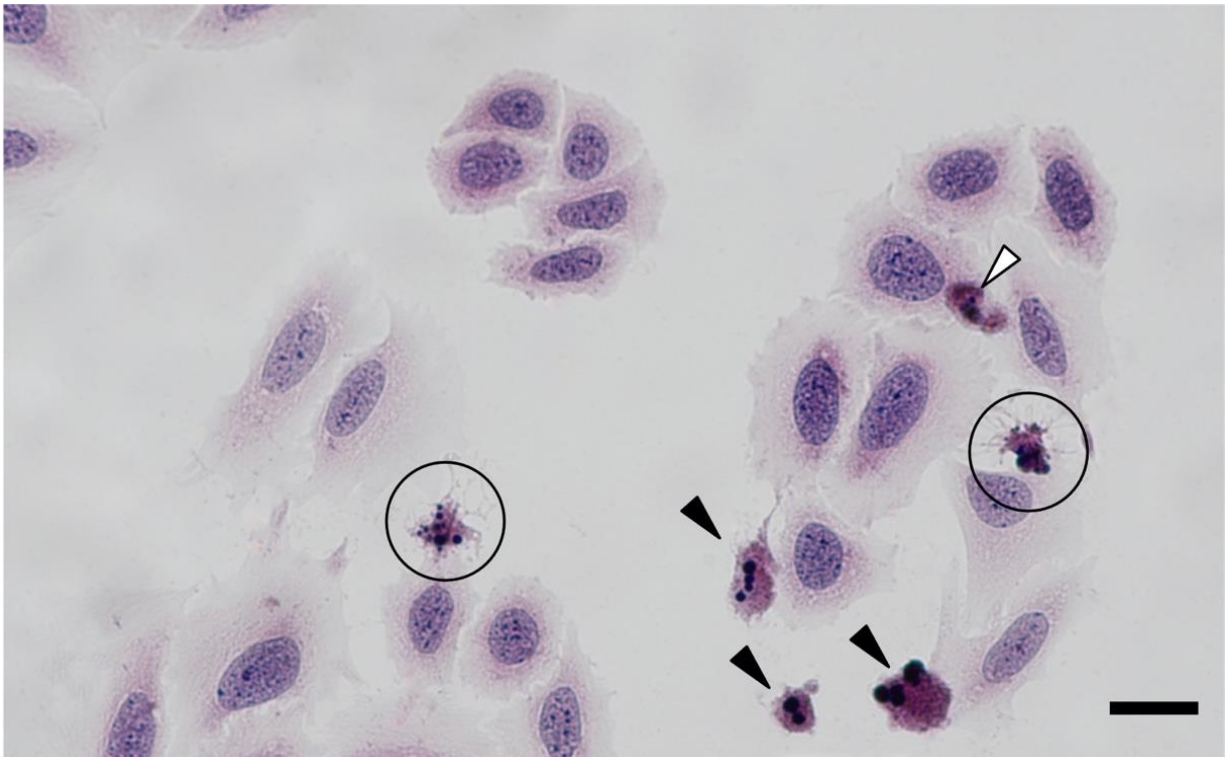

Figure 26. Brightfield micrograph of H&E stained SiHa cells treated with 2600 nM cholecalciferol

Morphological features of apoptosis, including cell condensation (white arrowhead) and cells with fragmented nuclei (black arrowheads) were present at 2600 nM cholecalciferol treatment. Some cells demonstrated multiple morphological features of apoptosis (circled) such as apoptotic bodies, nuclear fragmentation and membrane blebbing. Scale bar: 20 µm.

In addition, giant multinucleated cells were present in control and experimental cultures (Figure 27). These cells are larger in size and have at least two distinct nuclei. The cells in all cultures appeared larger in size in comparison with surrounding cells. The giant multinucleated cells occurred within cell islands (Figure 27.B), on the periphery of cell islands (Figure 27.A, D and F) or isolated between cell islands (Figure 27.E) and contained two to six nuclei in each giant cell. The cytoplasm of these cells stained a normal to paler eosinophilic pink-stain in comparison with surrounding cells, and the intact basophilic nuclei contained one- six nucleoli/nucleus. Features of mitoses and apoptosis were not visualised in giant multinucleated cells.

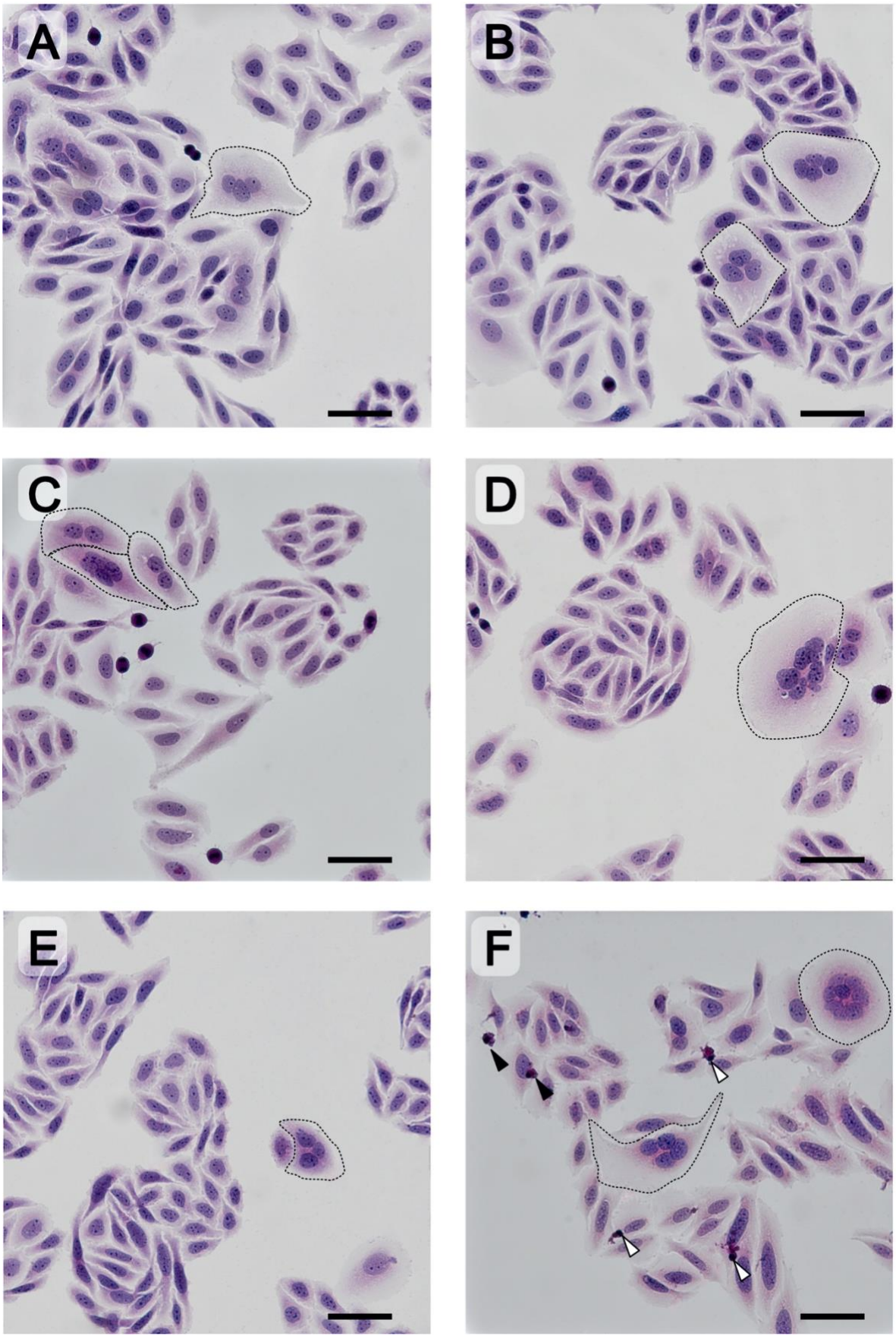

Figure 27. Giant multinucleated cells (outlined) present in control and experimental SiHa cell cultures

(continued) Medium control (A), solvent control (B), 26 nM (C), 104 nM (D), 260 nM (E) and 2600 nM (F). Giant multinucleated cells (outlined by black stippled dots) appeared larger with an eosinophilic cytoplasm and multiple, distinct nuclei present in each cell. Features of mitosis are not indicated for clarity. Features of apoptosis are indicated at 2600 nM: shrunken cells (black arrowheads) and membrane blebbing (white arrowheads). Scale bar: 50µm.

5.5.1.2 Semi-quantitative analysis of apoptotic features and giant multinucleated cells

For semi-quantitative analysis of brightfield micrographs, 15 images were analysed for each of the control and experimental SiHa cell cultures. This was comprised of five micrographs from three independent experiments for each cell culture. The number of cells with morphological features of apoptosis, and giant multinucleated cell count were semi-quantified. The criteria used to identify morphological features and as described in the materials and methods (section 4.8.1.2).

Cell membrane blebbing, nuclear fragmentation and the presence of apoptotic bodies were individually enumerated for positive features of apoptosis. The total apoptotic cells were enumerated as a summary measure of cells containing one or more individual features of apoptosis. Giant multinucleated cells were enumerated on the basis of simultaneously meeting two essential criteria: enlarged cells in comparison with surrounding cells, and cells that showed two more distinct nuclei.

Cell counts (Figure 28) revealed a significant increase in apoptotic features at 2600 nM treatment (12.40 ± 2.47 %) in comparison with medium (0.42 ± 0.17 %; $p < 0.0001$) and solvent (0.40 ± 0.16 %; $p < 0.0001$) control cultures, and 26 nM (0.26 ± 0.16 %; $p < 0.0001$), 104 nM (0.26 ± 0.13 %; $p < 0.0001$) and 260 nM (0.89 ± 0.33 %; $p < 0.0001$) experimental cultures.

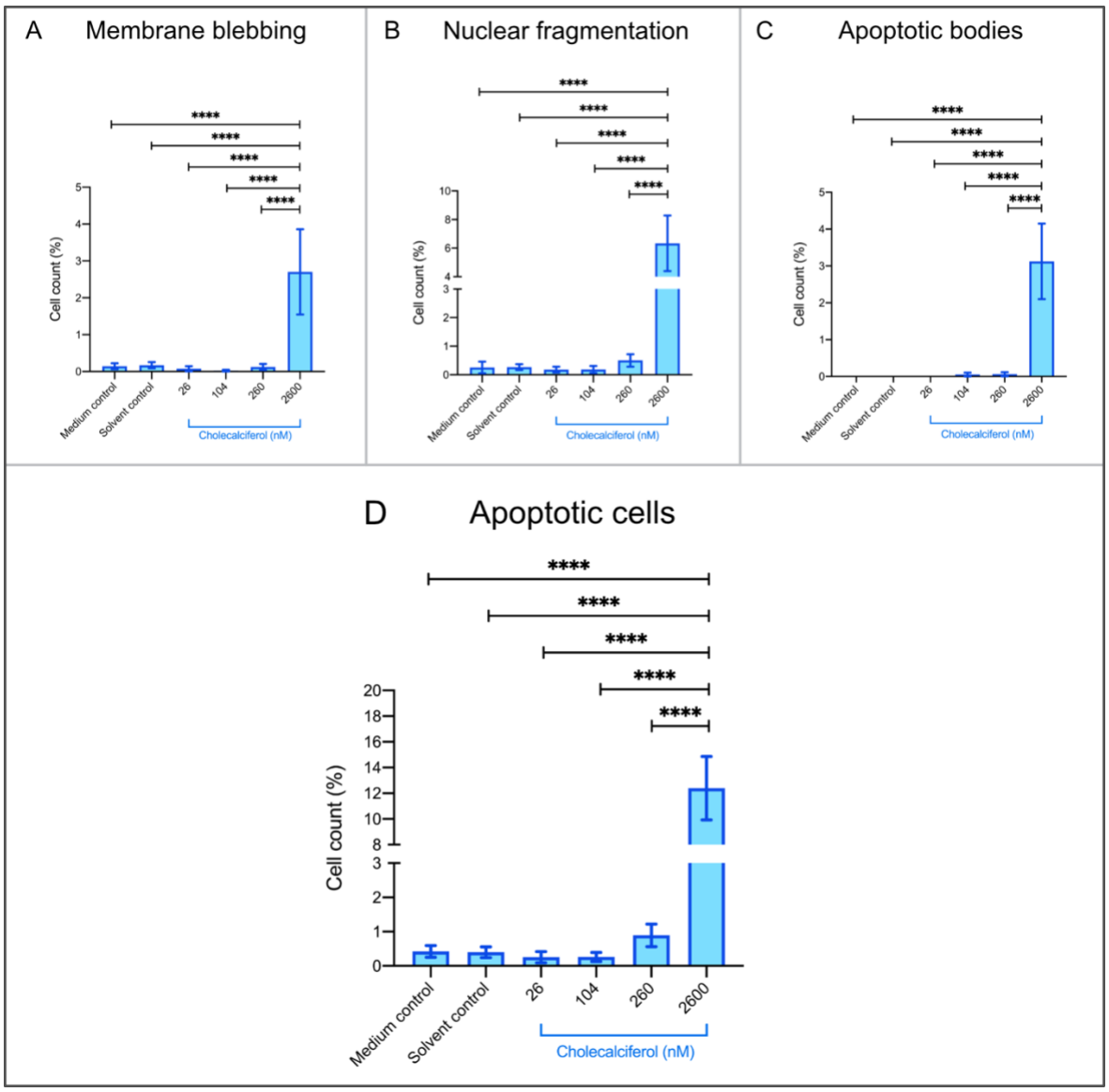

Figure 28. Semi-quantification of morphological features of apoptosis in SiHa control and experimental cultures.

Semi-quantification of features of apoptosis: apoptotic bodies (A), membrane blebbing (B) and nuclear fragmentation (C); and cumulative number of apoptotic cells in control and experimental cultures (D). A significant increase in apoptotic cellular features and total apoptotic cells was observed at 2600 nM treatment in comparison with controls and 26 nM, 104 nM and 260 nM treatments. Bars represent mean ± SEM from 15 micrographs selected for each sample. Cell count was calculated as a percentage of cells showing individual apoptotic features (A-C) and total apoptotic cells with one or more apoptotic features (D) for control and experimental SiHa cultures. One-way ANOVA was used to identify significant differences and $p < 0.05$ was considered significant. **** $p < 0.0001$.

Furthermore, giant multinucleated cells present in all cell cultures identified no significant change in the percentage of cell count between control and experimental cultures (Figure 29).

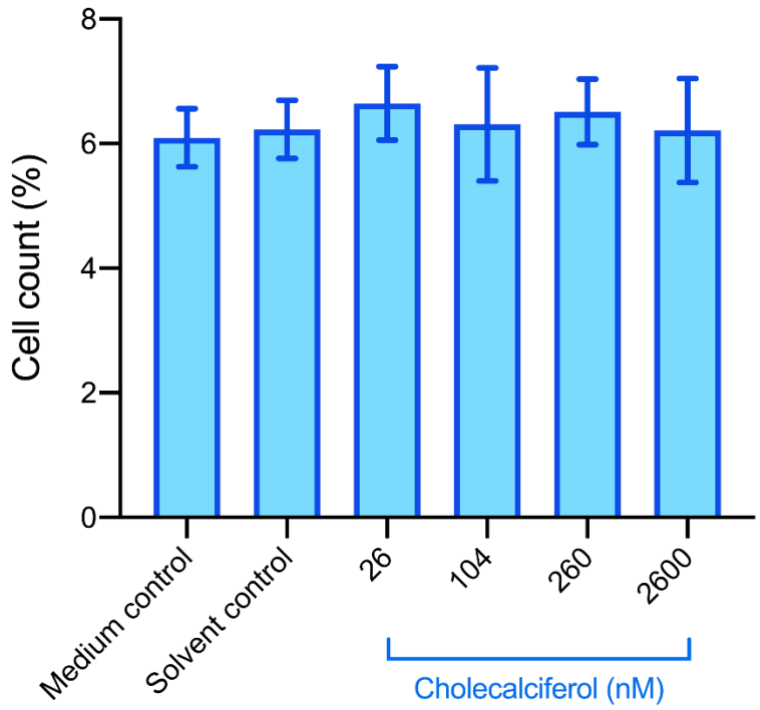

Figure 29. Giant multinucleated cells in SiHa cell cultures

Giant multinucleated cells were enumerated from 15 brightfield micrographs of each SiHa cell culture and expressed as a percentage of total cell count. Bars represent mean ± SEM from 15 micrographs selected for each sample. One-way ANOVA was used to identify significant differences and $p < 0.05$ was considered significant. No significant change to the number of giant multinucleated cells in all cell cultures was identified.

5.5.2 Cell ultrastructure assessed using transmission electron microscopy (TEM)

Transmission electron microscopy was used to investigate ultrastructural features of control and experimental SiHa cell cultures. Medium and solvent control cultures showed healthy cells with an intact cell membrane and an intact nuclear membrane with a prominent nucleus (Figure 30.A-B). Similarly, cell cultures treated with 26 nM, 104 nM and 260 nM demonstrated healthy cells with intact cell and nuclear membranes (Figure 30.C-E).

Cells treated with 2600 nM cholecalciferol demonstrated morphological features consistent with apoptosis. In Figure 30.F, the representative micrograph showed a shrunken cell with membrane blebbing, apoptotic bodies and nuclear fragmentation. Additionally, no ultrastructural features of necrosis and autophagic cell death were observed across the treatment range.

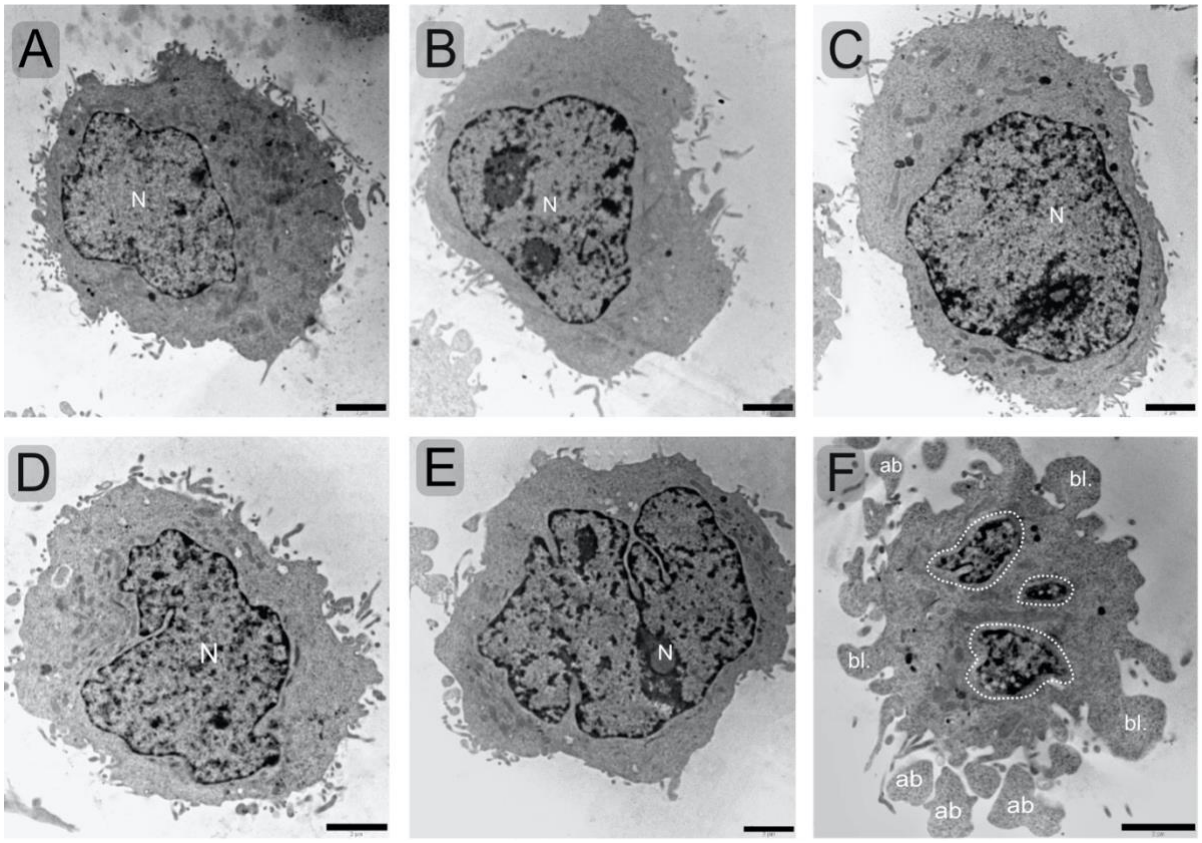

Figure 30. Transmission electron micrographs of SiHa control and experimental cultures

cholecalciferol treatment. Medium and solvent controls and 26 nM, 104 nM and 260 nM treatments showed healthy cells with intact cell membranes and nuclei (N) while cells treated with 2600 nM cholecalciferol demonstrated cell membrane blebbing (bl.) and apoptotic bodies (ab). In addition, the 2600 nM treatment group showed cells with fragmented nuclei (white outline). Scale bar: 2 µm.

At high magnification, cell cultures treated with 2600 nM cholecalciferol showed damaged mitochondria. Two mitochondrial abnormalities were apparent in these cell cultures: dark, electron-dense mitochondria and electron-lucent mitochondria with disarranged and dilated cristae (Figure 31.B). Diseased mitochondria are associated with poor cell health and is an early feature of apoptosis. In contrast, healthy mitochondria (Figure 31.A) demonstrated regularly interspaced cristae and typical electron density.

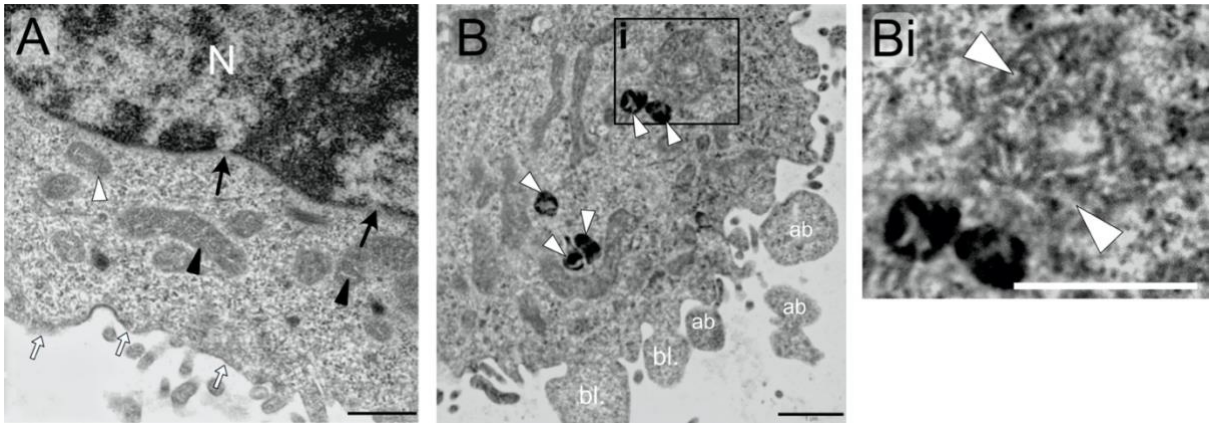

Figure 31. Transmission electron micrographs in solvent control and 2600 nM cholecalciferol treatment in SiHa

Solvent control (A) and 2600 nM treatment (B) showed normal cellular appearance and apoptotic morphology, respectively. The solvent control demonstrated mitochondria with intact outer membranes and regularly interspaced cristae (black arrowheads). Nucleus (N), nuclear pores (black arrow) and intact cell membranes (white arrows) were also evidenced in (A). In contrast, 2600 nM cholecalciferol treatment showed mitochondria with electron-dense matrix (white arrowheads) and dilated cristae (Bi, inset, white arrows). membrane blebs (bl.) and apoptotic bodies (ab) were also observed in (B). Scale bar: 500 nm (A); 1µm (B) and (B.i).

In summary, ultrastructural features associated with apoptosis were only observed in cell cultures treated with 2600 nM cholecalciferol. These features included fragmented nuclei, membrane blebbing and apoptotic bodies and damaged mitochondria. In contrast, healthy cells were observed in controls and all other treatment cultures. Furthermore, no ultrastructural features associated with autophagic cell death or necrosis were identified in all cell cultures.

5.6 Evaluation of gene and protein expression of the VDMS

Gene and protein expression of the vitamin D activating enzymes (CYP2R1, CYP27A and CYP27B1), vitamin D inactivating enzymes (CYP24A1) and the vitamin D receptor (VDR) and were quantified by qPCR and Western blots respectively.

5.6.1 Effects of cholecalciferol on gene and protein expressions of the 25-hydroxylases (CYP2R1 and CYP27A1) in SiHa cell line

Cholecalciferol is activated to 25(OH)D_3 by 25-hydroxylase enzymes (CYP2R1 and CYP27A1) and the effect of cholecalciferol on gene and protein expression of the 25-hydroxylases were investigated.

The CYP2R1 is the major 25-hydroxylase enzyme in the body.[253] *CYP2R1* mRNA transcripts showed significant fold increase at 2600 nM (5.52 ± 0.80) in comparison with medium (1.37 ± 0.003; $p < 0.0001$) and solvent (0.33 ± 0.68; $p < 0.0001$) controls, and 26 nM (-1.35 ± 0.01; $p < 0.0001$) and 104 nM (1.30 ± 0.02; $p < 0.0001$) treatments (Figure 32.A). Additionally, *CYP2R1* mRNA expression was significantly increased in fold at 260 nM (2.30 ± 0.02) in comparison with the solvent control ($p = 0.0049$) and 26 nM treatment ($p < 0.0001$; Figure 32.A).

A significant fold increase in protein expression at 2600 nM (1.33 ± 0.09) in comparison with the solvent control (1.00 ± 0.00; $p = 0.021$) and 26 nM treatment (0.93 ± 0.08; $p = 0.005$) was identified by Western blots (Figure 32.C). However, there was no significant increase in CYP2R1 protein expression at 260 nM treatment (Figure 32.C).

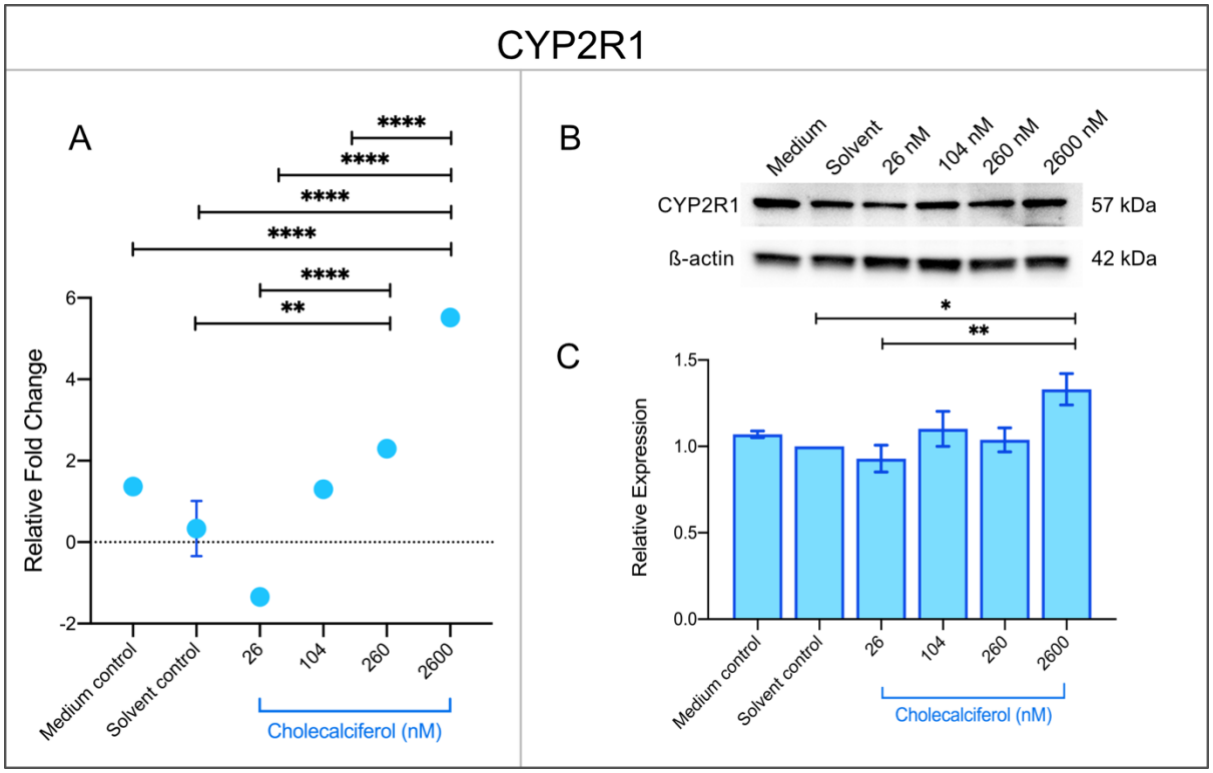

Figure 32. Gene and protein expression of CYP2R1 in SiHa control and experimental cultures

qPCR analysis of CYP2R1 gene expression (A), a representative Western blot of CYP2R1 protein expression (B) and semi-quantitative analysis of CYP2R1 protein in SiHa control and experimental cultures (C). qPCR data are presented as mean ± SEM for a representative of three independent experiments conducted in triplicate, and Western blot data presented as mean ± SEM of three independent experiments. qPCR data were analysed using the delta-delta Ct method and gene expression was normalised to 18s housekeeper expression. Protein expression was normalised to β-actin loading control. Gene and protein expressions were calculated as a fold change relative to solvent control. Data were analysed by one-way ANOVA and $p < 0.05$ was considered statistically significant. * $p < 0.05$; ** $p < 0.01$; **** $p < 0.0001$.

The CYP27A1 is a minor 25-hydroxylase enzyme.[253] qPCR did not identify significant changes in *CYP27A1* expression across the treatment range (Figure 33.A). CYP27A1 protein expression was not detected by Western blots in all SiHa cell cultures (Figure 33.B and Figure 33.C). These data indicate that either the expression of this enzyme is below the detectable limits of the Western blot, or that SiHa cells express very low levels of CYP27A1 protein.

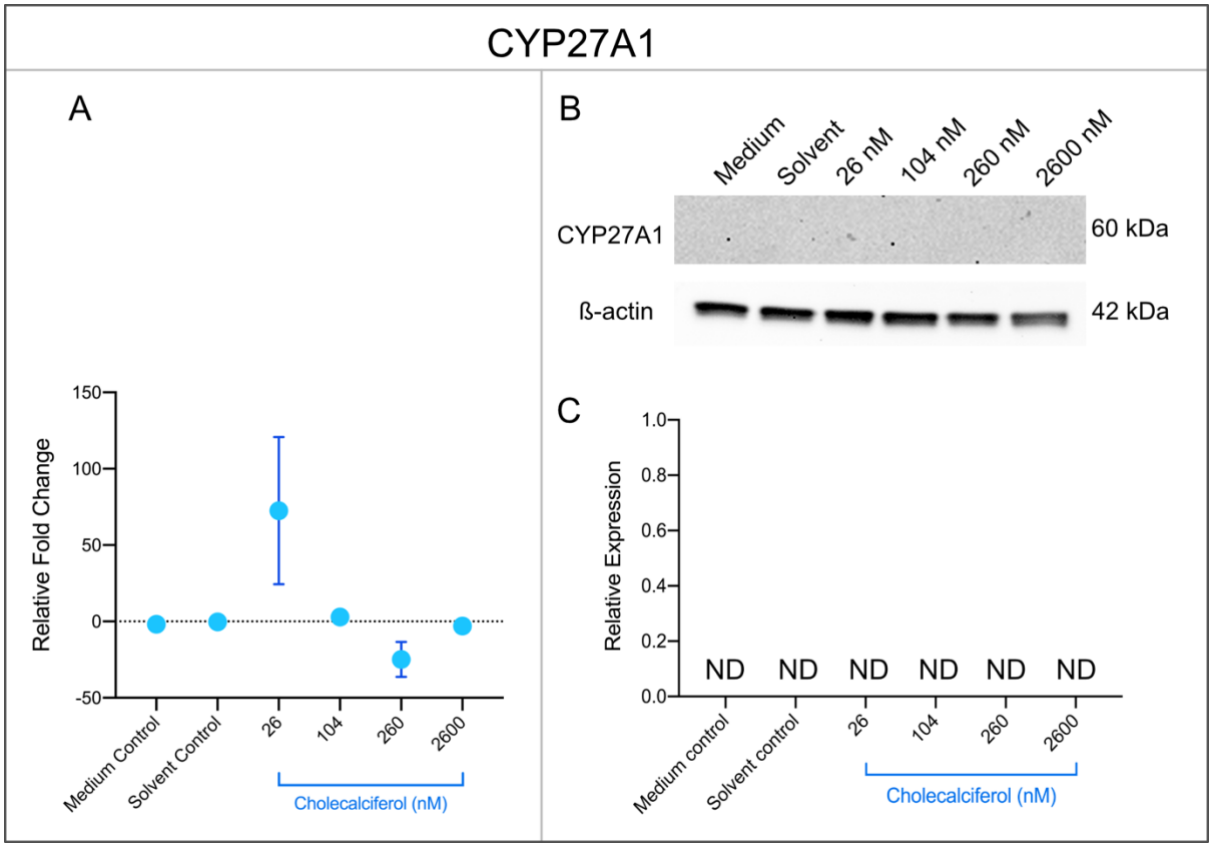

Figure 33. Gene and protein expressions of CYP27A1 enzyme in SiHa cell cultures treated with cholecalciferol

qPCR analysis of *CYP27A1* gene expression (A), a representative Western blot of CYP27A1 protein expression (B) and semi-quantitative analysis of CYP27A1 protein in SiHa control and experimental cultures (C). qPCR data are presented as mean ± SEM for a representative of three independent experiments conducted in triplicate and Western blot data presented as mean ± SEM of three independent biological replicates. qPCR data were analysed using the delta-delta Ct method and gene expression was normalised to 18s housekeeper expression. Protein expression was normalised to β-actin loading control. Gene and protein expressions were calculated as a fold change relative to solvent control. Data were analysed by one-way ANOVA and $p<0.05$ was considered statistically significant.

Hence, these findings taken together suggests that 25-hydroxylation of cholecalciferol in SiHa cells is predominantly mediated by the CYP2R1 enzyme, and not by the minor CYP27A1 enzyme. Furthermore, significant CYP2R1 upregulation in expression is demonstrated only at 2600 nM treatment in SiHa cells.

5.6.2 Effects of cholecalciferol on gene and protein expressions of 1α-hydroxylase (CYP27B1) in SiHa cell line

CYP27B1 is the only 1, α- hydroxylase in the VDMS and catalyses the formation of the most biologically potent vitamin D metabolite, $1,25(OH)_2D_3$.[253] Figure 34.A demonstrates a significant fold decrease in *CYP27B1* gene expression was observed in SiHa cells treated with 260 nM (-2.11 ± 0.08; p = 0.047) and 2600 nM (-2.87 ± 0.27; p = 0.003) in comparison with solvent control (-0.33 ± 0.78). A significant fold decrease in CYP27B1 protein expression was observed at 2600 nM treatment (0.50 ± 0.05) in comparison with the medium (1.01 ± 0.13; p = 0.028) and solvent (1.00 ± 0.00; p = 0.031) controls (Figure 34.B and 34.C). Thus, gene and protein data are congruent as they both show a significant decrease in gene transcripts and protein expression of CYP27B1 in SiHa cells treated with 2600 nM cholecalciferol.

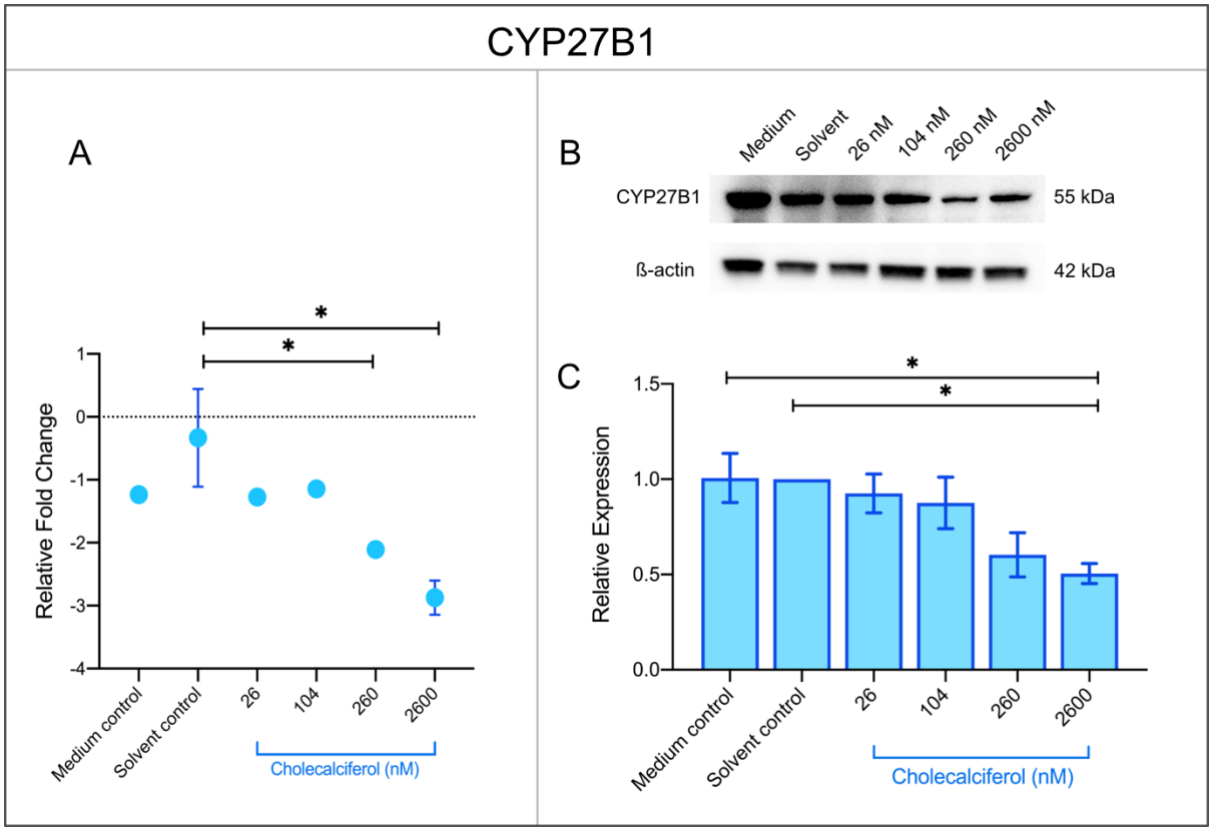

Figure 34. CYP27B1 gene and protein expression in SiHa cells

qPCR analysis of *CYP27B1* gene expression (A), a representative Western blot of CYP27B1 protein expression (B) and semi-quantitative analysis of CYP27B1 protein in SiHa control and experimental cultures (C). qPCR data are presented as mean ± SEM for a representative of three independent experiments conducted in triplicate; and Western blot data presented as mean ± SEM of three independent biological replicates. qPCR data were analysed using the delta-delta Ct method and gene expression was normalised to 18s housekeeper expression. Protein expression was normalised to β-actin loading control. Gene and protein expressions were calculated as a fold change relative to solvent control. Data were analysed by one-way ANOVA and $p < 0.05$ was considered statistically significant. * $p < 0.05$

5.6.3 Effects of cholecalciferol on gene and protein expressions of VDR in SiHa cell line

The biological activity of $25(OH)D_3$ and $1,25(OH)_2D_3$ is mediated by VDR, thus it is central to transducing intracellular signalling of the vitamin D metabolites.[42] *VDR* gene expression was significantly increased in fold change in cell cultures treated with 2600 nM cholecalciferol (1.98 ± 0.13) in comparison with the medium control (-0.38 ± 0.76; p = 0.033; Figure 35.A). Furthermore, a significant fold increase in VDR protein expression was observed at 2600 nM (1.85 ± 0.13) in comparison with medium (1.02 ± 0.11; p = 0.048) and solvent (1.00 ± 0.00; p = 0.04) controls (Figure 35.B and 35.C).

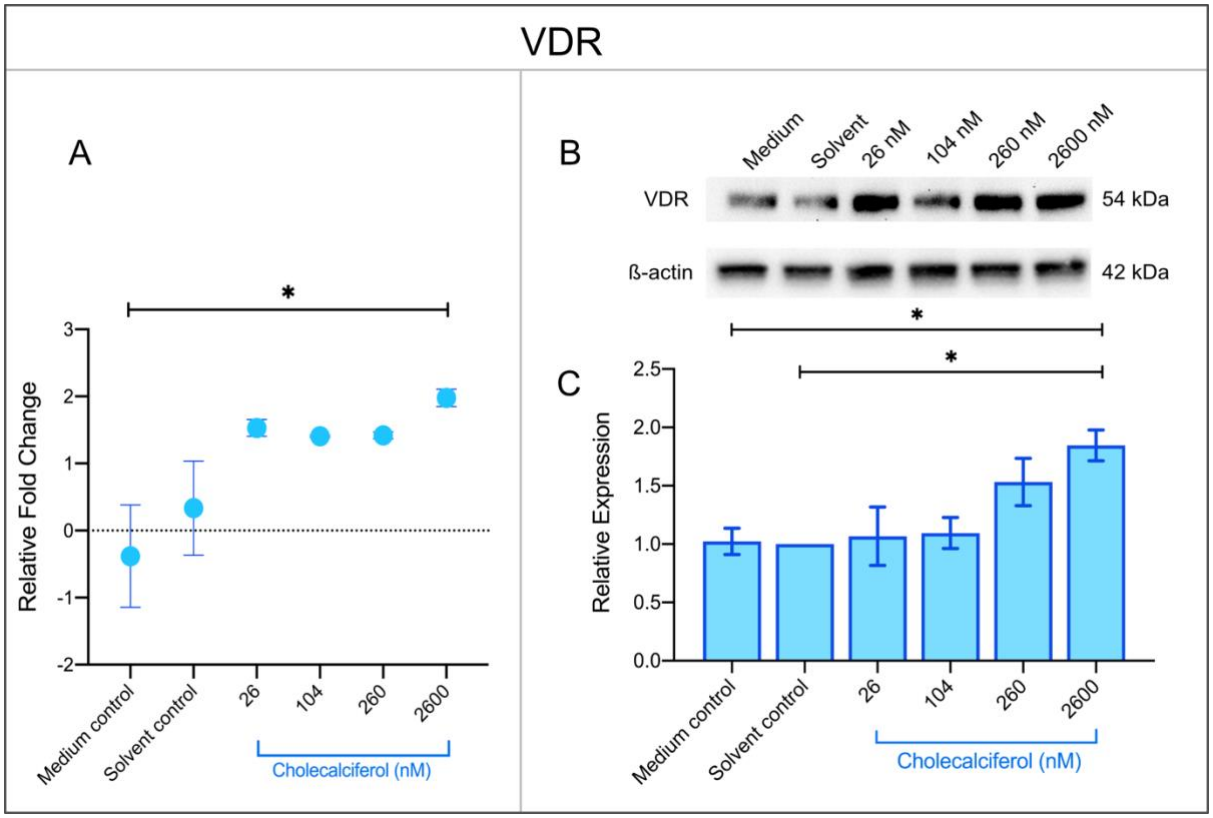

Figure 35. Vitamin D receptor (VDR) gene and protein expression in SiHa control and experimental cultures

qPCR analysis of *VDR* gene expression (A), a representative Western blot of VDR protein expression (B) and semi-quantitative analysis of VDR protein in SiHa control and experimental cultures (C). qPCR data are presented as mean ± SEM for a representative of three independent experiments conducted in triplicate; and Western blot data presented as mean ± SEM of three independent experiments. qPCR data were analysed using the delta-delta Ct method and gene expression was normalised to 18s housekeeper expression. Protein expression was normalised to β-actin loading control. Gene and protein expressions were calculated as a fold change relative to solvent control. Data were analysed by one-way ANOVA and $p < 0.05$ was considered statistically significant. * $p < 0.05$

5.6.4 Effects of cholecalciferol on gene and protein expressions of 24-hydroxylase (CYP24A1) in SiHa cell line

$25(OH)D_3$ and $1,25(OH)_2D_3$ are inactivated by CYP24A1, which maintains intracellular vitamin D homeostasis.[40] *CYP24A1* gene expression was significantly increased in fold at 2600 nM treatment (8.38 ± 0.81) in comparison with the medium (1.66 ± 0.03; $p < 0.0001$) and solvent (0.33 ± 0.72; $p < 0.0001$) controls, and 26 nM (2.37 ± 0.34; $p < 0.0001$) and 104 nM (3.49 ± 0.21; $p = 0.0002$) treatments (Figure 36.A). Additionally, a significant increase in gene expression was also observed at 260 nM (7.74 ± 0.25) in comparison with the medium ($p < 0.0001$) and solvent ($p < 0.0001$) controls, and 26 nM ($p < 0.0001$) and 104 nM ($p = 0.0007$) treatments (Figure 36.A). CYP24A1 protein

expression was significantly increased in fold only at 2600 nM treatment (1.50 ± 0.12) in comparison with the medium control (0.85 ± 0.03; p = 0.0274) and 104 nM (0.83 ± 0.15; p = 0.0206) treatment (Figure 36.B and 36.C).

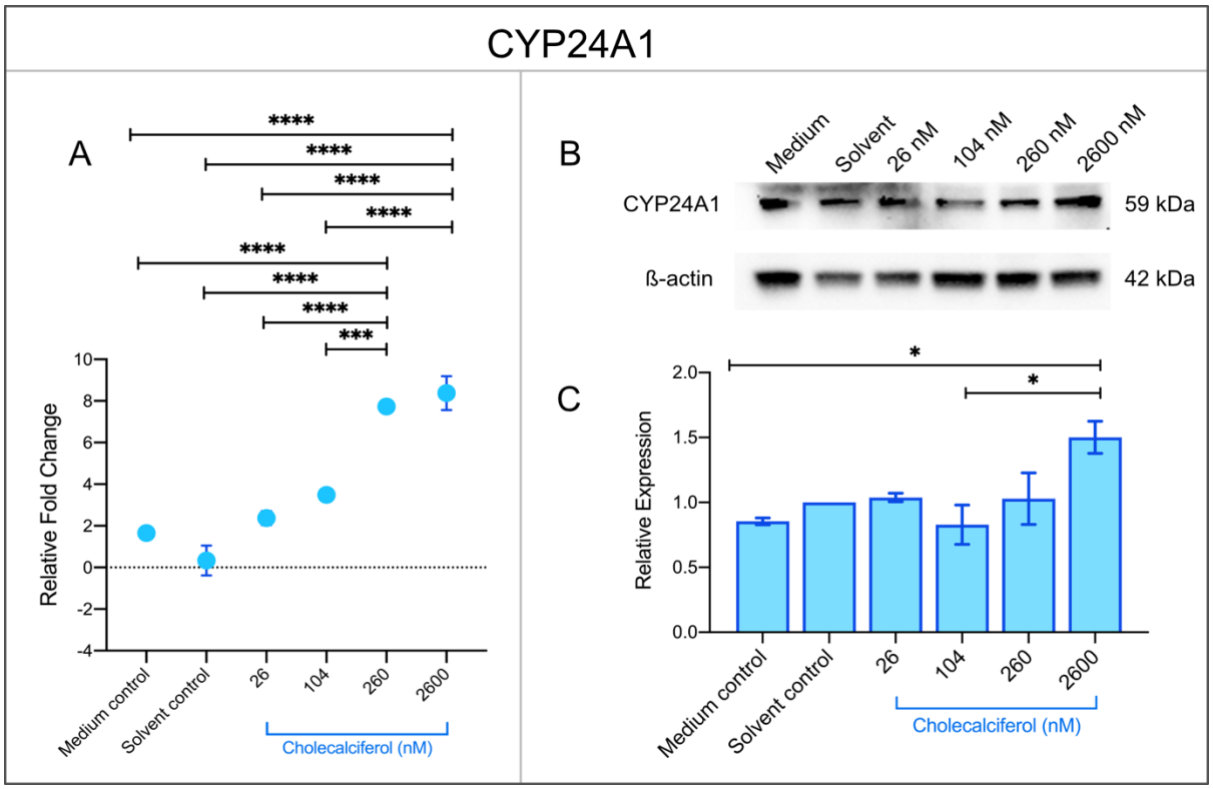

Figure 36. Effects of cholecalciferol on CYP24A1 gene and protein expression in SiHa control and experimental cultures

qPCR analysis of *CYP24A1* gene expression (A), a representative Western blot of CYP24A1 protein expression (B) and semi-quantitative analysis of CYP24A1 protein in SiHa control and experimental cultures (C). qPCR data are presented as mean ± SEM for a representative of three independent experiments conducted in triplicate; and Western blot data presented as mean ± SEM of three independent biological replicate. qPCR data were analysed using the delta-delta Ct method and gene expression was normalised to 18s housekeeper expression. Protein expression was normalised to β-actin loading control. Gene and protein expressions were calculated as a fold change relative to solvent control. Data were analysed by one-way ANOVA and p<0.05 was considered statistically significant. * $p < 0.05$; **** $p < 0.0001$

5.6.4.1 A summary of the effects of cholecalciferol on the VDMS in SiHa cells

In summary, evaluation of gene and protein expression of the VDMS showed increased expression levels of CYP2R1 and CYP24A1 and decreased levels of CYP27B1 at the 2600 nM treatment. In addition, CYP27A1 protein expression was not detected in SiHa cells. Furthermore, VDR protein expression was significantly

upregulated at high treatment dose 2600 nM. It is also noteworthy that although upregulation of CYP2R1, CYP27B1, CYP24A1 gene transcripts was observed at 260 nM treatments, the protein expression was not significantly increased.

6. Discussion

6.1 Rationale for investigating the anti-cancer actions of vitamin D in cervical cancer

Observational, preclinical and clinical studies suggest that vitamin D deficiency increases the risk of developing cancer.[5-6] The mechanisms of anti-cancer action of the vitamin D metabolites, for example, pro-apoptosis, anti-proliferation and anti-metastatic actions have also been demonstrated *in vitro*.[6] However, the roles of vitamin D metabolites in cervical cancer are poorly studied. Cervical cancer disproportionately affects low- and middle-income counties disproportionately,[12] where it is a major health burden.[3] This study aimed to characterise the anti-cancer actions of a vitamin D precursor, cholecalciferol, in a high-grade cervical cancer cell line, SiHa.

6.2 Cholecalciferol inhibited cell count and viability in the SiHa cell line

The concentration of cholecalciferol that inhibited SiHa cell growth by 50% (GI_{50}) was determined to be 5.089 x 10^{-6} M by cell count using the crystal violet assay. Various GI_{50} concentrations of cholecalciferol, measuring different endpoints, have been reported in cancer cell lines. In prostate cancer cell lines, the GI_{50} concentration was determined by cell viability using the 3-(4,5-dimethylthiazol-2-yl)-2–5-diphenyltetrazolium bromide (MTT) assay. The concentration between the two cell lines was variable in RWPE-2-W99 and RWPE-1 cell lines and was calculated at 3.8x10^{-6} M and 6.4 x 10^{-6} M, respectively.[78] However, the GI_{50} concentration between two thyroid cancer cell lines was similar and was calculated at 1.68 x 10^{-5} M and 1.38 x 10^{-5} M in TPC1 and C643 cell lines, respectively, using the thymidine incorporation cell proliferation assay.[199] It is noteworthy that these studies determined GI_{50} concentrations using cell viability and cell proliferation studies, respectively. In contrast, cell count was measured in this study. These variabilities in GI_{50} in prostate and thyroid cancer cell lines in comparison to the SiHa cell line demonstrate cell-specific growth inhibition. An alternative explanation is that the differences observed

in GI_{50} between these studies may be a consequence of the different cell health endpoints measured in each of these studies.

On the background of the GI_{50} calculations, this study further employed a wide treatment range at sub-GI_{50} concentrations (26 nM, 104 nM and 260 nM) and a maximum GI_{30} concentration (2600 nM). The rationale for this was to broadly assess the anti-cancer actions of cholecalciferol and the effects of these treatment concentrations on the VDMS in the SiHa cell line. Furthermore, the maximum treatment GI_{30} concentration was selected because it was cost-effective as fresh treatment was prepared for each experiment in this study.

The optimal incubation period of the experimental cultures by cell count and viability both identified significant inhibition at 72 hours at 2600 nM cholecalciferol treatment. The use of multiple cell health endpoints avoids the erroneous interpretation of data,[204,211] therefore, both cell count and viability were evaluated. Crystal violet enumerates cell count by binding to DNA and proteins and is insensitive to cell viability.[205] Cell viability was assessed semi-quantitatively and flow cytometrically using trypan blue and propidium iodide, respectively. These are vital dyes which only stain dead cells.[254] The qualitative assessment of trypan blue using a haemocytometer, however; has been reported to overestimate cell viability.[204,255] Therefore, the Muse™ Cell Count and Viability assay, which analysed a 1000 cell events per sample, facilitated quantitative analysis of cell viability[210] and improved the accuracy of cell viability assessment. All three assays were in agreement and showed significant decrease in cell count and cell viability at 2600 nM cholecalciferol treatment at 72 hours only in the SiHa cell line. Therefore, all experiments were conducted at 72-hour incubations.

The effect of cholecalciferol on cancer cell count and viability is not well reported as there is limited literature investigating anti-cancer action of this pro-hormone. In a previous study by our research group, we showed significant decrease in both cell count and cell viability in the metastatic cervical cancer CaSki cell line at 260 nM and 2600 nM treatments of cholecalciferol at 72 hours incubation.[200] In comparison, this study showed a significant decrease in cell count and cell viability at 2600 nM treatment only, indicating a cell-specific response to cholecalciferol treatment in

cervical cancer cell lines. Similarly, variable responses in cell count and viability to calcitriol treatment of cancer cell lines have been reported.[256] Cell count of MCF-7 breast cancer cells was significantly impaired by 10 nM and 100 nM treatments of calcitriol compared to the solvent control at 96 hours.[257] Cell viability was assessed using a tetrazolium salt assay in gastric cancer cell lines (SNU1 and SNU638) and cholangiocarcinoma cell lines (HuCCT1 and SNU1079), treated with a range of calcitriol concentrations for 96 hours. A cell-specific response to calcitriol treatment was observed.[258] While all cell lines in the study showed a significant decrease in cell viability at 10 µM treatments only; the SNU1079 cholangiocarcinoma cell line showed significant decrease in cell viability across the treatment range (10 µM, 1 µM, 0,1 µM and 0.001 µM).[258] Together, these studies demonstrate a variable cell line specific response to calcitriol treatments.

6.3 Cholecalciferol did not decrease Ki67 expression in SiHa cells

The anti-proliferative action of $1,25(OH)_2D_3$ is the earliest reported anti-cancer action[79] and is well documented in *in vitro* studies.[6,79,97-98] Chiang *et al.*[117] demonstrated a significant reduction in Ki67 expression and cell proliferation in FaDu and SCC-25 squamous carcinoma cell lines treated with 10^{-8} M, 10^{-7} M and 10^{-6} M calcitriol concentrations in comparison to the vehicle control.

While these studies highlight the anti-proliferative role of activated vitamin D, calcitriol, in cancer cell lines; the anti-proliferative role of vitamin D precursor, cholecalciferol, remains unclear. This study did not show evidence of anti-proliferation by cholecalciferol in the SiHa cell line by flow cytometric Ki67 analysis. Ki67 is a reliable marker for the identification of proliferating cells[259] and is clinically utilised for prognosis and diagnosis by staining cancer biopsy tissue.[212] Therefore, this finding suggests that the observed decrease in cell count and viability by cholecalciferol is not mediated by the inhibition of cell proliferation. This finding is supported by cholecalciferol treatment of the CaSki metastatic cervical cancer cell line, which also did not demonstrate an anti-proliferative effect.[200] In contrast, cholecalciferol treatment of the HeLa cervical cancer cell line demonstrated inhibition of cell proliferation at 2600 nM cholecalciferol treatment.[77] Therefore, these studies show varied responses by

cervical cancer cell lines to cholecalciferol treatment, and demonstrate cell-specific anti-proliferation response.

6.4 Cholecalciferol did not disrupt cell cycling but increased the sub-G_1 population of SiHa cells

Abnormalities in cell cycle progression have been documented in cancer cell lines treated with vitamin D metabolites. The most commonly reported cell cycle abnormality by $1,25(OH)_2D_3$ *in vitro* is G_0/G_1 cell cycle arrest.[59,260] During the G_1 phase, the cell is most sensitive to growth signals as it prepares for cell division by increasing transcription and translation of essential DNA synthesis proteins.[106] Cells arrested in this phase are unable to enter the S phase and synthesise proteins and DNA required for cell division.[106] The most common mechanisms of G_0/G_1 arrest by vitamin D metabolites is the upregulation of CDKIs, p21 and p27, which collectively cause hypophosphorylation of tumour suppressor pRB, resulting in cell cycle arrest.[97-98] In contrast to the widely reported G_0/G_1 arrest, Jiang *et al.*[131] reported G_2/M arrest through p53-independent induction of GADD45 stress protein in an ovarian cancer cell line (OVCAR3) by 10^{-7} M calcitriol treatment. In this study, cholecalciferol did not induce cell cycle arrest at either the G_0/G_1 or the G_2/M phases of the cell cycle. The absence of cell arrest is further supported by insignificant change in Ki67 expression in all experimental SiHa cell treatments in this study. The absence of cell cycle arrest is also corroborated by brightfield microscopic findings which identified cells in various stages of cell division (prophase, metaphase, anaphase and telophase) present in control and all experimental cultures.

The role of cholecalciferol on cell cycle perturbation in cervical cancer cell lines is variable. The findings in this study are consistent with cholecalciferol treatment of CaSki cervical cancer cell line, which showed no evidence of a cell cycle arrest.[200] In contrast, a significant G_0/G_1 cell cycle arrest was observed in HeLa cells treated with 2600 nM cholecalciferol.[77] Notably, the aforementioned studies[77,200] both show that cervical cancer cell lines treated with cholecalciferol have an increased sub-G_1 phase of the cell cycle.

The sub-G_1 phase of the cell cycle analysis was also significantly increased in SiHa cells treated with 2600 nM cholecalciferol in this study. The sub-G_1 phase analysed by the Muse Cell Analyser™ was visualised as a broad peak representing hypodiploid cells.[162] It is distinct from the narrow G_1 phase peak of diploid DNA cells.[162] The sub-G_1 phase represents cells at various stages of necrosis or apoptotic cell death, but may also include nuclear fragments, clumps of chromosomes and micronuclei or nuclei with normal DNA content (2N) but different chromatin structure (which reduce the accessibility of the fluorochrome to DNA).[216] Therefore, a definitive conclusion of apoptosis or any other mode of cell death cannot be made based on an increased sub-G_1 phase alone, and demonstration of biochemical and morphological hallmarks of cell death are required to identify a mode of cell death.[137,148]

6.5 Cholecalciferol upregulated early and late biochemical and morphological markers of intrinsic apoptosis in SiHa cell line

Apoptosis is a form of regulated cell death (RCD).[142] Apoptosis is initiated by the intrinsic or extrinsic pathway, which are triggered by different stimuli.[134] The extrinsic apoptosis pathway is triggered by a ligand-induced activation of cell membrane proteins of the death receptor family.[137] In contrast, the intrinsic pathway is triggered by a variety of internal stressors within the cell, such as replication stress, reactive oxygen speciation and mitochondrial perturbations.[142] Irrespective of how apoptosis is initiated, both signal transduction pathways converge on terminal caspase activation – the latter activation is a hallmark of apoptotic cell death.[137,261]

In this study, biochemical and morphological features of apoptosis were observed in SiHa cells treated with 2600 nM cholecalciferol. The biochemical features included significant decrease in mitochondrial membrane potential, significant increases in PS flip pattern, terminal caspase activation and expression of DNA damage markers (γH2A.x and phosphorylated ATM). Additionally, brightfield microscopy and ultrastructural analysis of SiHa experimental cultures demonstrated morphological and ultrastructural features of apoptosis: nuclear condensation and fragmentation, cell membrane blebbing and the formation of apoptotic bodies. Semi-quantification of apoptotic cell morphology showed significant increase in features of apoptosis and

total apoptotic cell number at 2600 nM cholecalciferol treatment of SiHa cells. These findings will be further explored in the context of the underlying physiology, to clarify the sequence and linkage of individual apoptotic cellular events induced by cholecalciferol in SiHa cell line.

6.5.1 Cholecalciferol induced mitochondrial damage in SiHa cell line

Mitochondrial health is a useful indicator of cell health.[136] Here, 2600 nM cholecalciferol treatment in SiHa cells significantly decreased $\Delta\Psi m$ and induced abnormal mitochondrial ultrastructure. The abnormal mitochondria showed two distinct characteristics: electron-lucent mitochondria with dilated cristae or dark, electron-dense cristae, and thickened electron-dense outer mitochondrial membranes. Electron lucent mitochondria with dilated cristae have been reported in HeLa cells treated with an apoptosis-inducing agent, etoposide. Using correlative light and electron microscopy, Sun *et al.*[262] demonstrated that these mitochondrial abnormalities are associated with early apoptosis. Electron-dense mitochondria are the manifestation of thickened inner and outer membranes, and studies suggest this may disrupt the electron transport chain and impair ATP synthesis.[262-263] Mitochondrial abnormalities are critical in the initiation of intrinsic apoptosis, and failure of cells to survive mitochondrial perturbations can cause apoptosis.[137,142]

The findings hereafter explain how the 2600 nM cholecalciferol treatment in SiHa cells induces irreversible mitochondrial insult leading to the induction of intrinsic apoptosis. Intrinsic apoptosis is induced by irreversible and widespread mitochondrial outer membrane permeabilisation (MOMP).[264] This event is carefully regulated by two types of proteins from the BCL-2 family. These are pro-apoptotic (BAX, BAK and BOK) and anti-apoptotic proteins (BCL-2, BCLXL and MCL1).[134] Pro-apoptotic proteins form pores across the outer mitochondrial membrane (OMM),[146-147] whereas anti-apoptotic proteins sequester pro-apoptotic proteins and prevent their pore-forming activity.[146] In response to apoptotic stimuli, pro-apoptotic proteins perforate the OMM resulting in the release of Cyt C into the cytosol.[146-147] Under normal conditions, Cyt C resides in the inter-mitochondrial membrane space and shuttles electrons in the mitochondrial respiratory chain[265-267] of healthy mitochondria. However, during apoptosis, Cyt C is released into the cytosol and binds to apoptotic peptidase activating factor 1 (APAF1)

which drives the assembly of the apoptosome,[268] a supramolecular platform that activates caspase-9,[134] and initiates the caspase cascade. Thus, mitochondria play a central role in the induction of intrinsic apoptosis, and this study demonstrated that cholecalciferol induced mitochondrial abnormality.

This finding of cholecalciferol initiating intrinsic apoptosis by favouring pro-apoptotic protein balance that can disrupt mitochondrial function is supported by studies which have demonstrated the activation of apoptosis by vitamin D metabolites in cancer cell lines.[97,117,126] Studies on numerous *in vitro* cancer cell lines show that vitamin D metabolites upregulate the pro-apoptotic and suppress the anti-apoptotic proteins in the BCL-2 protein family.[269-271] For example, in MCF-7 breast cancer cell line $1,25(OH)_2D_3$ induced intrinsic apoptosis by increased translocation of pro-apoptotic BAX protein to mitochondria which lead to increased Cyt C in the cytosol.[272] In addition, LNCaP prostate cancer cell line revealed abrogation of calcitriol induced apoptosis in cells overexpressing BCL-2.[164] Furthermore, Kizildag *et al.*[165] demonstrated that 50 nM $1,25(OH)_2D_3$ treatment activated intrinsic apoptosis by the suppression of anti-apoptotic genes (*BCL-2* and *BCL-XL*) and the stimulation of pro-apoptotic gene (*BAX*) in K562 chronic myeloid leukaemia cell line. Taken together, these findings highlight the role of $1,25(OH)_2D_3$ in the modulation of gene and protein expression of the BCL-2 protein family and mitochondrial perturbation in the induction of intrinsic apoptosis in cancer cell lines.

6.5.2 Cholecalciferol induced phosphatidylserine externalisation in SiHa cells

Phosphatidylserine (PS) externalisation was significantly increased in SiHa cells treated with 2600 nM cholecalciferol. Translocation of PS to the outer leaflet of the cell's lipid bilayer is an early event of apoptosis.[148,219] This process enables phagocytosis of apoptotic cells *in vivo* and can be a useful marker for early apoptosis *in vitro*.[219] Annexin V, a recombinant PS-binding protein with high specificity for PS,[219] was used in this study to detect externalised PS.[220]

In this study, induction of a PS flip pattern in SiHa cells treated with 2600 nM cholecalciferol was observed. The increase in PS exposure in this study is also supported by significant increase in PS exposure in CaSki cervical cancer cells treated with 260 nM and 2600 nM cholecalciferol.[200] $1,25(OH)_2D_3$ is also observed to induce PS externalisation. Narvaez *et al.*[272] observed that $1,25(OH)_2D_3$ induced the intrinsic pathway of apoptosis, by upregulation of BAX, and PS exposure in MCF-7 breast cancer cell lines.

The PS flip pattern supports the earlier observation of damaged mitochondria, and collectively these two observations implicate cholecalciferol in the induction of early-stage apoptosis. However, it should be noted that PS exposure is a reversible event[217,273] and specificity of PS externalisation is not specific for apoptosis.[274-275] Therefore, additional terminal biomarkers of cell death should be used to corroborate early stage apoptosis experimental observations.[137,142]

6.5.3 Cholecalciferol induced terminal caspase activation in SiHa cell line

Caspases are central components of apoptotic response and irreversibly commit the cell to die.[137,142] This study demonstrated significantly increased activity of terminal caspases, caspase-3 and caspase-7, in SiHa cells treated with 2600 nM cholecalciferol. The caspase cascade consists of a series of proteolytic enzymes. All caspases are synthesised as inactive zymogens that undergo proteolytic activation during apoptosis.[141] Two major functional classes of caspases exist. Initiator caspases consist of caspase-8, -9 and -10. In contrast, the terminal group of effector caspases consist of the caspase-3, -6 and -7 family.[134,141] The initiator caspases receive and propagate death signals from the intrinsic and extrinsic apoptosis pathways[134] and proteolytically activate downstream effector (or terminal) caspases in a cascade-like manner.[276] These caspases have a broad catalytic activity,[277] as they inactivate some proteins and activate other enzymes such as DNases which degrade nuclear DNA.[276,278]

Caspase activation has been demonstrated in other *in vitro* studies investigating the role of vitamin D metabolites on apoptosis. An increase in caspase-3 activity was observed in NCI-H929 human myeloma cells treated with 1×10^{-7} M calcitriol analogue EB1089 for 72 hours.[279] Furthermore, the proteolytic activity of caspase-3 was demonstrated by the cleavage of poly-(ADP-ribose) polymerase (PARP) protein which is a substrate for activated caspase-3.[276] In addition, an increase in the sub-G_1 phase of the cell cycle and downregulation of BCL-2 were observed. Kim *et al.*[280] showed significant activation of both initiator caspase-9 and effector caspase-3 and BCL-2 and BCL-XL downregulation in Ishikawa endometrial carcinoma cells treated with 2.5 µM $1,25(OH)_2D_3$. These findings were consistent with decreased cell viability, by MTT measurement, and suggest apoptotic mode of cell death in this endometrial cell line. In addition, the findings of this study are supported by significantly increased effector caspase activity in a metastatic cervical cancer CaSki cell line treated with 260 nM and 2600 nM cholecalciferol.[200] The effector caspase activation in SiHa cells treated with 2600 nM cholecalciferol in this study, strongly implicates apoptosis cell death as a mechanism for the decreased cell count and viability, and increased sub-G_1 phase of cells in the cell cycle.

The broad catalytic activity of effector caspases precipitates intrinsic apoptosis and commits the cell to an irreversible apoptotic fate.[148] The diverse range of caspase substrates also explains several other characteristic features of apoptosis and those identified in biochemical and morphological analyses of this study. Caspases cleave a plethora of cytoskeletal proteins, such as nuclear lamins, resulting in nuclear shrinking and budding[149-150] – consistent with the morphological features of brightfield and TEM microscopy in SiHa cells treated with 2600 nM cholecalciferol in this study. Recent evidence suggests that effector caspases increase activation of proteins that promote the PS flip pattern, for example, phospholipid scramblases[151-152] and also inhibits mediators of PS internalisation, for example, phospholipid flippases.[281] Furthermore, caspases induce DNases,[282] which cleave DNA and the consequence of DNA cleavage is the activation of biochemical DNA damage markers. Therefore, the multiple catalytic substrates of effector caspases can account for the biochemical and morphological changes observed in SiHa cells treated with 2600 nM cholecalciferol.

6.5.4 Cholecalciferol induced significant DNA damage in SiHa cell line

Another key finding of this study was the significant induction of DNA damage in SiHa cells treated with 2600 nM cholecalciferol. During apoptosis, effector caspases activate DNase via cleavage of its inhibitor ICAD/DFF45.[153-154] DNases cleave DNA at linker regions between oligonucleosomes producing DNA fragments of multiples of 180 base pairs, which appear as the classic apoptotic 'DNA ladder' when DNA fragments are subjected to agarose gel electrophoresis.[162,282] ATM is an upstream DDR kinase enzyme that is activated by DSBs. Upon activation, ATM phosphorylates numerous downstream targets such as γH2A.X, which localise at sites of DNA damage and recruit DNA damage repair complexes to DSB foci. γH2A.X is specific to DNA damage and a reliable marker for the investigation of DNA damage.[225] Galbiati *et al.*[175] demonstrated significant increase in DNA damage marker, *GADD45* gene, and induction of apoptosis in mouse insulinoma βTC_3 cells treated with 1000 nM calcitriol for 48 hours. Additionally, Jung *et al.*[176] demonstrated significant increase in DNA damage, assessed by a commercial DNA fragmentation enzyme-linked immunosorbent assay (ELISA) kit, in human ovarian cancer cell lines (SKOV3, OVCAR3, and OVCA433) treated with 50 μM $1,25(OH)_2D_3$. Therefore, the DNA damage observed in SiHa cells treated with 2600 nM cholecalciferol is supported by these studies and demonstrates the role of activated vitamin D in the induction apoptosis and DNA damage *in vitro*.

6.5.5 Summary: cholecalciferol treatment induced intrinsic apoptosis in SiHa cell line

In summary, this study showed an induction of intrinsic apoptosis in SiHa cells treated with 2600 nM cholecalciferol. Damaged mitochondria were demonstrated by biochemical and TEM analyses. Severe perturbation to mitochondrial function is an important induction step of the intrinsic pathway. Consequently, significant PS flipping, karyorrhexis, blebbing, apoptotic body formation, DNA damage and terminal caspase activity were noted. Therefore, apoptotic cell death is biochemically and morphologically supported by cholecalciferol treatment of SiHa cells.

6.6 Cholecalciferol treatment did not induce autophagic cell death and necrosis in SiHa cell line

Insignificant change in LC3-II expression demonstrated that cholecalciferol did not induce autophagic cell death across the treatment range. Furthermore, no ultrastructural features of autophagic cell death were observed in TEM images. These findings are supported by a study on cholecalciferol in CaSki cell line, which did not identify significant increase in LC3-II expression. In contrast, calcitriol analogue (EB1089) demonstrated Beclin-1 dependent autophagic cell death accompanied by DNA fragmentation and chromatin condensation in MCF-7 breast cancer cell lines.[186] Furthermore, activation of the VDR by 100 nM $1,25(OH)_2D_3$ showed an autophagic transcriptional signature in breast cancer cell lines (MCF-7, ZR-75-1, MDA-MB-453, MCF-12A, MDA-MB231, and HMEC).[187] These data collectively suggest that autophagic cell death may be a less commonly induced mode of cell death by the vitamin D metabolites and is absent in cholecalciferol treated SiHa cell line.

In this study, cholecalciferol did not demonstrate necrotic cell death evidenced by the LDH release assay and the absence of morphological features of necrosis in brightfield and TEM micrographs. A necrotic phenotype may be acquired during *in vitro* end-stage apoptosis, as it leads to complete breakdown of the plasma membrane.[148] The 7-AAD dead cell marker used in all flow cytometric apoptosis assays was not significantly changed, indicating that cholecalciferol did not induce necrotic cell death or secondary necrosis. The literature however does not support necrosis death mode in cholecalciferol or other vitamin D metabolite treatments in cancer cell lines.

6.7 Cholecalciferol did not increase or decrease the large multinucleated (LMNC) sub-population in SiHa cells

Large multinucleated cells (LMNC), also referred to as giant multinucleated cells, have been described in cancer cell lines and cancer tissues; however, their role in tumorigenesis is uncertain.[283] The cells are thought to originate from cell division or cell fusion.[283]

The giant multinucleated cells observed in this study are consonant with classical morphological features of LMNCs, as morphological analysis showed cellular enlargement, multiple nuclei and persistent survival in culture without multiplication.[284] In this study the LMNCs demonstrated insignificant change with cholecalciferol treatment across the treatment range. These cells were not identified in growth arrest as evidenced by the low LMNC numbers by semi-quantification of the cells by light microscopy. The ATCC note that approximately 24% of SiHa cell line are hyper-triploid and contain a chromosomal number of 71,[36] however; the frequency of LMNCs are not mentioned. This study suggests that cholecalciferol does not change the cell number and growth characteristics of this minor sub-population of SiHa cells, and that this sub-population contributes to approximately 6-7% of the total SiHa population.

Literature does not report evidence of vitamin D and its metabolites exerting anti-cancer actions in on LMNCs in established cancers and early dysplastic cells. The heterogeneity of sub-populations of cells in cancers can cause resistance to therapies and result in relapse and metastasis.[285] Although these LMNCs do not form colonies they are none-the less biologically viable and metabolically active,[285] and thus may be important in cancer growth and metastases. Further studies exploring the effects of the various vitamin D metabolites in cervical cancer can yield a more comprehensive answer to resolving the role of vitamin D (and its metabolites) on the metabolism of LMNC and the potential anti-cancer actions exerted on LMNC in cervical cancer cell lines and cervical tissue.

6.8 Cholecalciferol induced perturbations of gene and protein expression in the VDMS in SiHa cell line

6.8.1 The VDMS in cervical tissue

Vitamin D exerts its genomic action by binding to its receptor, VDR. The activation of the vitamin D pro-hormone, cholecalciferol, occurs by two sequential hydroxylation steps consisting of 25-hydroxylation to produce $25(OH)D_3$, followed by 1α-hydroxylation of $25(OH)D_3$ to synthesise the most biological active metabolite, $1,25(OH)_2D_3$.[5,253] Activated vitamin D metabolites, $25(OH)D_3$ and $1,25(OH)_2D_3$ bind to

VDR to elicit a genomic response, and metabolites are inactivated by 24-hydroxylation catabolic pathways. These activating and inactivating enzymes together with VDR constitute an interacting autocrine system – the VDMS, which maintains autocrine vitamin D homeostasis.[8] This study demonstrated expression of an autocrine VDMS in SiHa cell line. The results from qPCR and Western blot analyses of the VDMS will be further explored to elucidate a possible mechanism of cholecalciferol-mediated apoptosis in SiHa cells.

The expression of the VDMS in cancer cell lines *in vitro* is not well demonstrated in the literature. Whilst isolated studies on the effects of calcitriol have demonstrated the expression of VDR and CYP24A1 in SiHa cells,[196-197] the expression of a full VDMS is yet to be reported in the SiHa cell line. The gene expression of 25-hydroxylase and 1α-hydroxylase enzymes have been reported in malignant gynaecological cell lines. Kloss *et al*.[10] showed that cervical adenocarcinoma cell line, HeLa, and the ovarian cancer cell line, OVCAR-3, expressed both 25-hydroxylase and 1α-hydroxylase enzymes by real-time PCR analysis. In addition, the study also demonstrated that calcidiol and calcitriol increased the expression of genes encoding 25-hydroxylase and 1α-hydroxylase enzymes.[10] A different research group, led by Friedrich *et al.*[11] identified localised expression of VDR, 25-hydroxylase, 1α-hydroxylase, and 24-hydroxylase in both healthy and cancerous cervical tissue. These findings provide evidence of the expression of VDMS in cervical tissue and cervical cancer cell lines. Since the expression of these enzymes and the VDR were increased in these experimental studies by calcidiol and calcitriol treatments, it suggests that cervical tissue and cervical cancer cell lines metabolise vitamin D precursors at an autocrine level.

6.8.2 Cholecalciferol induces significant CYP2R1 gene and protein expression in SiHa cell line

The first activation step of biologically inactive cholecalciferol is hydroxylation of carbon-25, which is catalysed by 25-hydroxylase enzymes (CYP2R1 and CYP27A1) to produce 25(OH)D_3.[5] This study showed a significant increase in CYP2R1 gene and protein expression in SiHa cells treated with 2600 nM cholecalciferol. In contrast, no

significant change in *CYP27A1* gene expression was noted, and CYP27A1 protein was not detected by Western blots. There are six known cytochrome P450 enzymes capable of 25-hydroxylation of cholecalciferol;[8] however, CYP2R1 is considered the major 25-hydroxylase enzyme, due to its specificity for both vitamin D_3 and D_2 and comparable enzymatic catalytic efficiency and K_m for both substrates.[8] The minor 25-hydroxylase, CYP27A1 is mainly responsible for the production of bile acids and only 25-hydroxylates vitamin D_3 and not D_2.[253] The extent of other 25-hydroxylase enzymes in the activation of vitamin D precursors remains unclear.[37] A study on serum 25(OH)D_3 levels in mice showed a greater than 50% reduction in the production of 25(OH)D_3 in mice with *CYP2R1* knockout,[286] suggesting that 25-hydroxylation of cholecalciferol is predominantly catalysed by CYP2R1. This study also demonstrates the redundant capacity to synthesise 25(OH)D_3 from cholecalciferol precursor by the minor 25 hydroxylase enzymes.[37,253] In this study, the upregulation of CYP2R1 gene and protein expression in SiHa cells treated with 2600 nM cholecalciferol may mediate 25-hydroxylation of cholecalciferol. In contrast, as protein expression of CYP27A1 was not detected, it suggests that this CYP enzyme has a limited or minor role in activating cholecalciferol precursor in the SiHa cell line. These findings, therefore, are consistent with the dominant role of CYP2R1 catalysing 25-hydroxylation in healthy tissue, which is also retained in the cancerous cervical cell line, SiHa.

In this study, the novel finding of 25-hydroxylase, CYP2R1, in the SiHa cell line is consistent with studies that showed 25-hydroxylase enzyme expression in cervical cancer cell lines and cervical cancer patient biopsies.[10-11] However, the authors do not specifically provide the identity of the CYP 25-hydroxylase that was analysed, so it is unclear which specific 25-hydroxylase enzyme was measured. In an independent study,[77] however, basal gene and protein expression of both CYP2R1 and CYP27A1 enzymes were observed in the HeLa cell line; however, 2600 nM treatment of cholecalciferol only increased CYP27A1 gene and protein expression, and not CYP2R1 expression. In contrast, an increase in CYP2R1 and undetectable CYP27A1 expression were observed in SiHa cells in this study. Thus, these findings suggest that cervical cancer cell lines exhibit cell line specific gene and protein expression of the 25-hydroxylases; and furthermore, that these CYP enzymes are differentially upregulated in response to cholecalciferol treatment in a cell-specific manner amongst the cervical cancer cell lines.

6.8.3 Cholecalciferol significantly downregulated CYP27B1 gene and protein expression in SiHa cell line

25(OH)D_3 is further hydroxylated to the most biologically potent vitamin D metabolite, 1,25(OH)$_2D_3$, by 1α-hydroxylase (CYP27B1).[8] In contrast to the numerous 25-hydroxylases, CYP27B1 is the only known 1α-hydroxylase in the VDMS.[253] This study identified a significant decrease in CYP27B1 gene and protein expression in SiHa cells at 2600 nM treatment of cholecalciferol. Although an increase in CYP2R1 was observed in this study, there was no associated increase in CYP27B1 expression in SiHa cells, which suggests that there is limited or no intracellular production of 1,25(OH)$_2D_3$ in SiHa cells treated with 2600 nM. Thus, based on these findings, it is unclear if 1,25(OH)$_2D_3$ and/or 25(OH)D_3 are responsible for the observed anti-cancer actions of cholecalciferol in the SiHa cell line. It may be hypothesised that SiHa cells produce 25(OH)D_3 from cholecalciferol treatment; however, the increased 25(OH)D_3 is not further hydroxylated to 1,25(OH)$_2D_3$ due to the decreased CYP27B1 expression in SiHa cells. Therefore, further experiments are warranted to quantify 25(OH)D_3, and 1,25(OH)$_2D_3$ in cholecalciferol treated SiHa cells.

The extrarenal regulation of CYP27B1 in cancers is unclear and can be at variance to mineral and skeletal health homeostasis.[37] Renal 1,25(OH)$_2D_3$ production is regulated by PTH, FGF23 and 1,25(OH)$_2D_3$ itself.[5] In states of hypocalcaemia, PTH stimulates CYP27B1 whereas increased 1,25(OH)$_2D_3$, phosphate levels and FGF23 downregulate CYP27B1.[37] Renal CYP27B1 is autoregulated by a VDRE site located near the *CYP27B1* gene promoter –VDR binds to the VDRE when 1,25(OH)$_2D_3$ is abundant to inhibit its expression.[287-288] In contrast to the renal system, the extrarenal CYP27B1 in cancerous and non-cancerous tissue is not regulated by calciotropic hormones (PTH and vitamin D), but by tissue-specific factors,[289-291] such as pro-inflammatory cytokines in macrophages.[292] Furthermore, expression of CYP27B1 is inversely correlated with the degree of cancer progression, with decreased expression in poorly differentiated tumours of the lung, prostate, colon, parathyroid, and skin.[80-84,293] This inverse relationship between CYP27B1 expression and tumour grade suggests that local production of 1,25(OH)$_2D_3$ may be important for cancer prevention

in specific tissues. Further mechanistic studies are warranted to clarify the regulation of cholecalciferol treated SiHa cells.

6.8.4 Cholecalciferol significantly upregulated VDR gene and protein expression in SiHa cell line

Vitamin D receptor (VDR) is a transcription factor belonging to the nuclear hormone superfamily and is expressed in almost all tissues of the human body.[6] VDR mediates the genomic action of vitamin D metabolites in cells by dimerising to RXR, which then activates vitamin D response elements (VDREs) in the promoter region of genes responsible for cell growth and differentiation.[5] VDR expression is well documented in numerous cell lines, and the presence of VDR in tumour cells is a prerequisite for the anti-cancer actions of $1,25(OH)_2D_3$;[260] however, as described in the literature review, multiple mechanisms attenuate VDR expression during tumorigenesis.

In this study, significant upregulation of VDR gene and protein was observed in SiHa cells treated with 2600 nM cholecalciferol. VDR gene and/or protein expression has been observed in healthy and malignant cervical cancer tissue[11,294] and cervical cancer cell lines.[10] The increased VDR expression observed in this study suggests that VDR ligands (vitamin D metabolites, $25(OH)D_3$ and/or $1,25(OH)_2D_3$) are synthesised at an autocrine level and stimulate the expression of VDR. Furthermore, the observed anti-cancer actions in this study may be mediated by the vitamin D metabolites ($25(OH)D_3$ and/or $1,25(OH)_2D_3$) complexed to VDR and RXR to form $25(OH)D_3$-VDR-RXR and/or $1,25(OH)_2D_3$-VDR-RXR trimeric complex. Consequently, it is likely that the translocation of this trimeric complex into the nucleus exerts genomic actions on genes that regulate intrinsic apoptosis. Since VDR expression level was significantly increased in this study, it would suggest that SiHa cells retain intact expression for VDR, which is responsive to cholecalciferol treatment.

6.8.5 Cholecalciferol significantly upregulated CYP24A1 gene and protein expression in SiHa cell line

This study demonstrated significant upregulation in CYP24A1 gene and protein expression in SiHa cells treated with 2600 nM cholecalciferol. Activated vitamin D metabolites, $25(OH)D_3$ and $1,25(OH)_2D_3$, are inactivated by CYP24A1 in multi-step reactions.[40] CYP24A1 catalyses the inactivation of vitamin D metabolites by either 24-oxidation or 23-hydroxylation pathways which produce in inactive calcitroic acid or biologically active $1\alpha,25R(OH)_2D_3$-26,23S-lactone, respectively.[37,40] Therefore, labelling CYP24A1 as a purely catabolic enzyme in vitamin D metabolism is a misnomer. For example, the first metabolite of the 24-oxidation pathway, $1,24,25(OH)_3D_3$, has substantial affinity for VDR with approximately 10% biological activity of $1,25(OH)_2D_3$.[295] These vitamin D metabolites retain agonist action and may bind to VDR. These partial VDR agonist metabolites may therefore also contribute to the observed anti-cancer action observed in this study.

CYP24A1 expression is increased at high concentration of $1,25(OH)_2D_3$ which leads to the catabolism of $1,25(OH)_2D_3$.[5] The *CYP24A1* gene promoter region contains two VDRE sites, and *CYP24A1* expression is increased upon binding of VDR to these sites.[289] The observed increase in *CYP24A1* gene expression together with an increase in VDR expression in SiHa cells at 2600 nM cholecalciferol treatments suggest that ligand-activated VDR binds to VDREs in *CYP24A1* promoter that may cause the increased *CYP24A1* expression observed in SiHa cells. This increased gene activity corresponds to increased CYP24A1 protein translation and subsequently degradation of active vitamin D metabolites in SiHa cells. The role of catabolism by CYP24A1 of $25(OH)D_3$, $1,25(OH)_2D_3$ and other vitamin D metabolites in SiHa cells require further clarification.

Several studies have demonstrated that *CYP24A1* expression is aberrantly increased in cancer cells. Spontaneous upregulation of *CYP24A1* correlates with poor clinical outcome[11] in these cancers and endows tumour cells with resistance to the anti-cancer actions of $1,25(OH)_2D_3$; and therefore, *CYP24A1* is considered a candidate oncogene.[6,86] There is considerable tissue-specific variability in the mechanism of

CYP24A1 upregulation in clinical and *in vitro* studies, as discussed in the literature review. Most importantly, VDR is often downregulated in these cancers with upregulated *CYP24A1* expression.[60] Future studies investigating independent regulation of CYP24A1 is needed to clarify the relationship of CYP24A1 expression and calcitriol-VDR dependent regulation in cholecalciferol-treated SiHa cell line.

6.9 A proposed mechanism of cholecalciferol action on the VDMS and induction of intrinsic apoptosis in SiHa cell line

A hypothesised explanation for the observations in this study is based on the expression of the VDMS and the significant increase in apoptosis in cholecalciferol treated SiHa cell line (Figure 37; steps 1-6). SiHa cells treated with 2600 nM cholecalciferol demonstrated a significant increase CYP2R1 25-hydroxylase enzyme levels. At this treatment, CYP2R1 catalysed the conversion of cholecalciferol precursor to calcidiol ($25(OH)D_3$) (step 1). As the protein expression of CYP27B1 is not upregulated, it is suggested that calcidiol is not converted to calcitriol ($1,25(OH)_2D_3$) (step 2). Furthermore, the significantly increased CYP24A1 catabolises vitamin D metabolites, calcidiol and calcitriol, resulting in predominantly inactive metabolites (step 3); which may attenuate VDR signalling. The observed apoptotic cell death is most likely mediated directly by $25(OH)D_3$ (step 4), which binds to the significantly increased VDR protein (step 4) and promotes apoptotic gene expression in SiHa cells (step 5). A less likely alternative is the direct binding of cholecalciferol to VDR which results in apoptosis (step 6); an experimental finding reported in one study which investigated cholecalciferol treatment on melanoma cell line at very high cholecalciferol treatment concentration (10^{-4} M).[296]

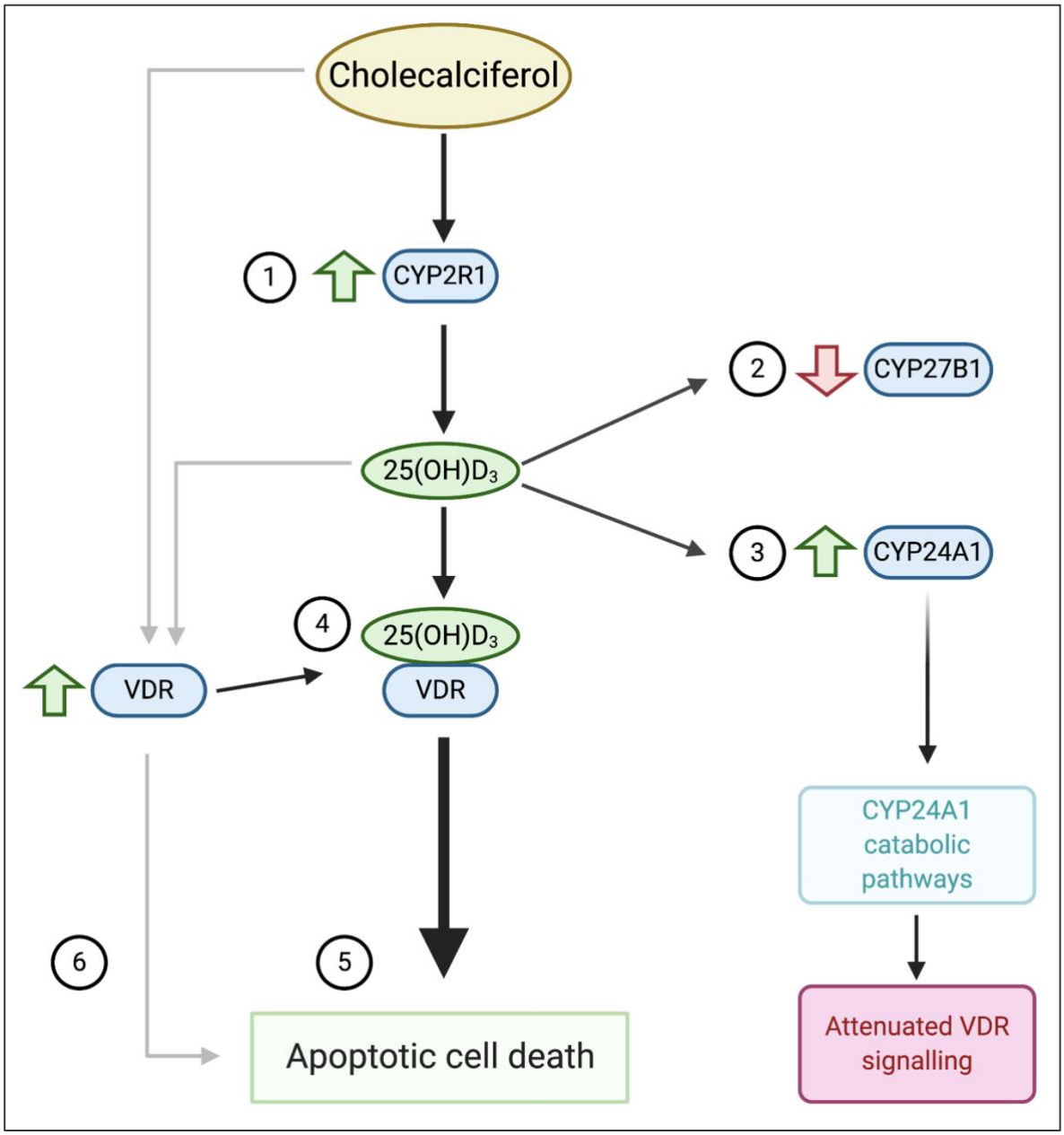

Figure 37. Proposed hypothesis for the induction of apoptosis by cholecalciferol in the SiHa cell line. (Source: personal collection). Image created using BioRender.com.

6.10 Limitations of the study

A potential limitation of this study is that the enzymatic machinery of the novel alternate vitamin D metabolising pathway catalysed by CYP11A1 was not investigated.[297] A key product of CYP11A1 enzyme is 20(OH)D which can be hydroxylated by CYP24A1 to produce $20,24(OH)_2D$ and $20,25(OH)_2D$. These metabolites have been shown to be more potent in suppressing melanoma tumour growth than $1,25(OH)_2D_3$.[298] Furthermore, the receptors of 20-hydroxylated vitamin D metabolites are RORα and

RORγ, and their expression is inversely correlated with melanoma progression and directly correlated with cancer prognosis.[298] In addition to melanoma, CYP11A1 expression has been reported in colon, kidney, lung, liver, prostate and uterine corpus endometrial carcinoma. Furthermore, RORα and RORγ are positively correlated with breast, lung and liver cancer.[299-302] Therefore, the CYP11A1 pathway is an enticing alternative vitamin D metabolising pathway which may influence the observed pro-apoptotic actions observed in cholecalciferol treated SiHa cells. The regulation of this pathway by cholecalciferol in SiHa cells warrants further investigation.

A further limitation of this study is that the vitamin D metabolites were not quantified to tie-in with the gene and protein expression profiles of the VDMS. Method development using chromatographic analytical techniques, for example, liquid chromatography mass spectrometry (LCMS)[303-304] may overcome the barrier of sensitively and specifically detecting vitamin D metabolite profiles at the cellular level,[303] and thus contribute to an enhanced understanding of the VDMS.

7. Conclusion

In conclusion, this study showed that SiHa cells treated with 2600 nM treatment of cholecalciferol undergo significant inhibition of cell growth and viability, associated with intrinsic apoptosis. The induction of intrinsic apoptosis was demonstrated by decreased mitochondrial membrane potential, significant PS externalisation, significant effector caspase activity, and morphological and ultrastructural features of apoptosis that included nuclear damage, cellular condensation, membrane blebbing, and apoptotic body formation.

Furthermore, CYP2R1 gene and protein expression was increased in SiHa cells at 2600 nM cholecalciferol treatment. This finding was accompanied by decreased CYP27B1 gene and protein expression, and increased VDR and CYP24A1 gene and protein expression at 2600 nM. Interestingly, no detectable CYP27A1 protein expression was noted. Collectively, these findings suggest an increase in $25(OH)D_3$ production, without further conversion to $1,25(OH)_2D_3$, as the enzyme responsible for the conversion, CYP27B1, was downregulated. $25(OH)D_3$, therefore, may bind to VDR and upregulate *CYP24A1* expression. Thus, the observed pro-apoptotic actions of cholecalciferol may potentially be mediated by $25(OH)D_3$ in SiHa cells treated with 2600 nM cholecalciferol.

In addition, other modes of cell death, *viz.* necrosis and autophagic cell death, were not observed by biochemical and morphological analyses. Furthermore, cholecalciferol treatments did not inhibit cell proliferation nor cause an abnormal cell cycle profile in SiHa cells.

The limitations of this study are that the vitamin D metabolites produced in SiHa cells treated with cholecalciferol were not measured, and that the novel CYP11A1-mediated alternate pathway was not explored. Future studies should consider the measurement of intracellular vitamin D metabolites synthesised and catabolised in cholecalciferol treated SiHa cell line. In addition, the potential role of the CYP11A1 pathway should be investigated, as the observed anti-cancer actions may be in-part mediated by CYP11A1 metabolites.

This study contributes to a niche body of knowledge on the *in vitro* anti-cancer actions of vitamin D metabolites in cervical cancer, with special exploration of cholecalciferol on apoptosis and the VDMS in an *in vitro* cervical cancer cell line, SiHa. Future studies exploring the VDMS in other cervical cancer cell lines and quantifying the metabolites produced can provide further insight into autocrine regulation of early vitamin D precursor effects on apoptosis in cervical cancer. In addition, these *in vitro* mechanistic studies can pave a pathway for exploring potential prevention and adjunctive treatment modalities of cholecalciferol and other vitamin D metabolites in cervical cancer patients with dysplasia and malignant disease, respectively.

8. References

1. Arbyn M, Weiderpass E, Bruni L, de Sanjosé S, Saraiya M, Ferlay J, *et al*. Estimates of incidence and mortality of cervical cancer in 2018: A worldwide analysis. Lancet Glob Health. 2020; 8(2):e191-e203. doi:10.1016/s2214-109x(19)30482-6

2. Cohen PA, Jhingran A, Oaknin A, Denny L. Cervical cancer. The Lancet. 2019; 393(10167):169-82. doi:10.1016/S0140-6736(18)32470-X

3. Jordaan S. MP, Simoens C., Bogers J. Challenges and progression of policies on cervical cancer in South Africa. Health Care: Current Reviews. 2017; 5(1)

4. International Agency for Research on Cancer (IARC) [Internet]. The Global Cancer Observatory: South Africa. Lyon, France: World Health Organisation (WHO); 2018 [accessed 10 October 2020]. Available from: https://gco.iarc.fr/today/data/factsheets/populations/710-south-africa-fact-sheets.pdf.

5. Holick MF. Vitamin D deficiency. N. Engl. J. Med. 2007; 357(3):266-81. doi:10.1056/NEJMra070553

6. Feldman D, Krishnan AV, Swami S, Giovannucci E, Feldman BJ. The role of vitamin D in reducing cancer risk and progression. Nat. Rev. Cancer. 2014; 14(5):342-57. doi:10.1038/nrc3691

7. Holick MF. Chapter 4 - Photobiology of vitamin D. In: Feldman D, editor. Vitamin D (fourth edition): Academic Press; 2018. p. 45-55.

8. Jenkinson C. The vitamin D metabolome: An update on analysis and function. Cell Biochem. Funct. 2019; 37(6):408-23. doi:10.1002/cbf.3421

9. Reichrath J, Rafi L, Muller SM, Mink D, Reitnauer K, Tilgen W, *et al*. Immunohistochemical analysis of 1,25-dihydroxyvitamin D_3 receptor in cervical carcinoma. Histochem. J. 1998; 30(8):561-7. doi:10.1023/a:1003283117492

10. Kloss M, Fischer D, Thill M, Friedrich M, Cordes T, Salehin D, *et al*. vitamin D, calcidiol and calcitriol regulate vitamin D metabolizing enzymes in cervical and ovarian cancer cells. Anticancer Res. 2010; 30(11):4429-34.

11. Friedrich M, Rafi L, Mitschele T, Tilgen W, Schmidt W, Reichrath J. Analysis of the vitamin D system in cervical carcinomas, breast cancer and ovarian cancer. Recent Results Cancer Res. 2003; 164:239-46.

12. Bray F, Ferlay J, Soerjomataram I, Siegel RL, Torre LA, Jemal A. Global cancer statistics 2018: GLOBOCAN estimates of incidence and mortality worldwide for 36

cancers in 185 countries. CA Cancer J. Clin. 2018; 68(6):394-424. doi:doi:10.3322/caac.21492

13. [Internet]. Cervical cancer. World Health Organisation; 2018 [accessed 12 October 2018]. Available from: http://www.who.int/cancer/prevention/diagnosis-screening/cervical-cancer/en/.

14. IARC Handbooks of cancer prevention. Volume 10: Cervix cancer screening. Lyon: IARC Press, International Agency for Research on Cancer; 2005.

15. Bray F, Carstensen B, Møller H, Zappa M, Žakelj MP, Lawrence G, *et al*. Incidence trends of adenocarcinoma of the cervix in 13 European countries. Cancer Epidemiol. Biomarkers Prev. 2005; 14(9):2191-9. doi:10.1158/1055-9965.Epi-05-0231

16. Bray F, Loos AH, McCarron P, Weiderpass E, Arbyn M, Møller H, *et al*. Trends in cervical squamous cell carcinoma incidence in 13 European countries: Changing risk and the effects of screening. Cancer Epidemiol. Biomarkers Prev. 2005; 14(3):677-86. doi:10.1158/1055-9965.Epi-04-0569

17. Bray F, Lortet-Tieulent J, Znaor A, Brotons M, Poljak M, Arbyn M. Patterns and trends in human papillomavirus-related diseases in Central and Eastern europe and Central Asia. Vaccine. 2013; 31:H32-H45. doi:https://doi.org/10.1016/j.vaccine.2013.02.071

18. Denny L. Cervical cancer in South Africa: An overview of current status and prevention strategies. CME: Continuing Med. Ed. J. 2010; 28(2):70-3.

19. Cogliano V, Baan R, Straif K, Grosse Y, Secretan B, El Ghissassi F, *et al*. Carcinogenicity of human papillomaviruses. The Lancet. Oncology. 2005; 6(4):204.

20. Frumovitz M [Internet]. Invasive cervical cancer: Epidemiology, risk factors, clinical manifestations, and diagnosis. UpToDate; 2019 [updated December 21, 2017; accessed 1 March 2019]. Available from: https://www.uptodate.com/contents/small-cell-neuroendocrine-carcinoma-of-the-cervix?source=related_link.

21. Woodman CB, Collins SI, Young LS. The natural history of cervical HPV infection: Unresolved issues. Nat. Rev. Cancer. 2007; 7(1):11-22. doi:10.1038/nrc2050

22. Wright JD [Internet]. Cervical intrepithelial neoplasia: Terminology, incidence, pathogenesis, and prevention. UpToDate; 2019 [updated January 2019; accessed 1 March 2019]. Available from: https://www.uptodate.com/contents/cervical-intraepithelial-neoplasia-terminology-incidence-pathogenesis-and-prevention.

23. Balasubramaniam SD, Balakrishnan V, Oon CE, Kaur G. Key molecular events in cervical cancer development. Medicina (Kaunas, Lithuania). 2019; 55(7):384. doi:10.3390/medicina55070384

24. Yim EK, Park JS. The role of HPV E6 and E7 oncoproteins in HPV-associated cervical carcinogenesis. Cancer Res. Treat. 2005; 37(6):319-24. doi:10.4143/crt.2005.37.6.319

25. Schwarz E, Freese UK, Gissmann L, Mayer W, Roggenbuck B, Stremlau A, *et al*. Structure and transcription of human papillomavirus sequences in cervical carcinoma cells. Nature. 1985; 314(6006):111-4. doi:10.1038/314111a0

26. Schiffman M, Castle PE, Jeronimo J, Rodriguez AC, Wacholder S. Human papillomavirus and cervical cancer. Lancet. 2007; 370(9590):890-907. doi:10.1016/s0140-6736(07)61416-0

27. Watson RA. Human papillomavirus: Confronting the epidemic – A urologist's perspective. Rev. Urol. 2005; 7(3):135-44.

28. Winer RL, Kiviat NB, Hughes JP, Adam DE, Lee SK, Kuypers JM, *et al*. Development and duration of human papillomavirus lesions, after initial infection. J Infect. Dis. 2005; 191(5):731-8. doi:10.1086/427557

29. Feldman S, Goodman A, Peipert J [Internet]. Screening for cervical cancer. UpToDate; 2020 [accessed 3 October 2020]. Available from: https://www-uptodate-com.uplib.idm.oclc.org/contents/screening-for-cervical-cancer?search=cervical%20cancer%20screening&source=search_result&selectedTitle=1~120&usage_type=default&display_rank=1#H1.

30. Penson R, Lee L [Internet]. Prevention of cervical cancer. London: BMA House; 2019 [accessed 10 September 2020]. Available from: https://bestpractice-bmj-com.uplib.idm.oclc.org/topics/en-gb/259/prevention#referencePop50.

31. Gustafsson L, Pontén J, Bergström R, Adami HO. International incidence rates of invasive cervical cancer before cytological screening. Int. J Cancer. 1997; 71(2):159-65. doi:10.1002/(sici)1097-0215(19970410)71:2<159::aid-ijc6>3.0.co;2-#

32. Huh WK, Ault KA, Chelmow D, Davey DD, Goulart RA, Garcia FA, *et al*. Use of primary high-risk human papillomavirus testing for cervical cancer screening: Interim clinical guidance. Obstet. Gynecol. 2015; 125(2):330-7. doi:10.1097/aog.0000000000000669

33. Practice bulletin no. 168: Cervical cancer screening and prevention. Obstet. Gynecol. 2016; 128(4):e111-30. doi:10.1097/aog.0000000000001708

34. Jordaan S, P M, K R, Simoens C, Bogers J-P. A review of cervical cancer in South Africa: Previous, Current and Future. Health Care: Current Rev. 2016; 04 doi:10.4172/2375-4273.1000180

35. Mbulawa ZZA, van Schalkwyk C, Hu N-C, Meiring TL, Barnabas S, Dabee S, *et al*. High human papillomavirus (HPV) prevalence in South African adolescents and young women encourages expanded HPV vaccination campaigns. PloS one. 2018; 13(1):e0190166-e. doi:10.1371/journal.pone.0190166

36. (ATCC) ATCC [Internet]. Siha (ATCC® HTB-35™). American Type Cell Culture (ATCC); [accessed 27 February 2019]. Available from: https://www.atcc.org/products/all/HTB-35.aspx.

37. Bikle DD. vitamin D: Newer concepts of its metabolism and function at the basic and clinical level. Journal of the Endocrine Society. 2020; 4(2) doi:10.1210/jendso/bvz038

38. Takeyama K, Kitanaka S, Sato T, Kobori M, Yanagisawa J, Kato S. 25-hydroxyvitamin D3 1alpha-hydroxylase and vitamin D synthesis. Science. 1997; 277(5333):1827-30. doi:10.1126/science.277.5333.1827

39. Zehnder D, Bland R, Williams MC, McNinch RW, Howie AJ, Stewart PM, *et al*. Extrarenal expression of 25-hydroxyvitamin D_3-1 alpha-hydroxylase. J Clin. Endocrinol. Metab. 2001; 86(2):888-94. doi:10.1210/jcem.86.2.7220

40. St-Arnaud R, Jones G. Chapter 6 - CYP24A1: Structure, function, and physiological role. In: Feldman D, editor. Vitamin D (fourth edition): Academic Press; 2018. p. 81-95.

41. Gupta RP, He YA, Patrick KS, Halpert JR, Bell NH. CYP3A4 is a vitamin D-24- and 25-hydroxylase: Analysis of structure function by site-directed mutagenesis. The Journal of clinical endocrinology and metabolism. 2005; 90(2):1210-9. doi:10.1210/jc.2004-0966

42. Pike JW, Meyer MB, Lee SM, Onal M, Benkusky NA. Chapter 9 - Genome-wide perspectives on vitamin D receptor–mediated control of gene expression in target cells. In: Feldman D, editor. vitamin D (fourth edition): Academic Press; 2018. p. 141-74.

43. Bouillon R, Pauwels S. Chapter 7 - The vitamin D-binding protein. In: Feldman D, editor. vitamin D (fourth edition): Academic Press; 2018. p. 97-115.

44. Jones KS, Assar S, Harnpanich D, Bouillon R, Lambrechts D, Prentice A, *et al*. 25(OH)D_2 half-life is shorter than 25(OH)D_3 half-life and is influenced by DBP concentration and genotype. J Clin. Endocrinol. Metab. 2014; 99(9):3373-81. doi:10.1210/jc.2014-1714

45. Holick MF. 25-OH-vitamin D assays. J Clin. Endocrinol. Metab. 2005; 90(5):3128-9. doi:10.1210/jc.2005-0162

46. Vieth R, Holick MF. Chapter 57B - The IOM—Endocrine Society controversy on recommended vitamin D targets: In support of the Endocrine Society position. In: Feldman D, editor. vitamin D (fourth edition): Academic Press; 2018. p. 1091-107.

47. Bouillon R, Rosen C. Chapter 57a - the IOM–Endocrine Society controversy on recommended vitamin D targets: In support of the IOM position. In: Feldman D, editor. vitamin D (fourth edition): Academic Press; 2018. p. 1065-89.

48. Amrein K, Scherkl M, Hoffmann M, Neuwersch-Sommeregger S, Köstenberger M, Tmava Berisha A, *et al*. vitamin D deficiency 2.0: An update on the current status worldwide. Eur. J. Clin. Nutr. 2020; doi:10.1038/s41430-020-0558-y

49. Marshall W, Lapsley M, Day A, Shipman K. Calcium, phosphate and magnesium. Clinical chemistry. 9 ed: Elsevier; 2020. p. 255-71.

50. DeLuca HF. Evolution of our understanding of vitamin D. Nutr Rev. 2008; 66(10 Suppl 2):S73-87. doi:10.1111/j.1753-4887.2008.00105.x

51. Pike JW, Meyer MB. Fundamentals of vitamin D hormone-regulated gene expression. J Steroid. Biochem. Mol. Biol. 2014; 144 Pt A:5-11. doi:10.1016/j.jsbmb.2013.11.004

52. Pike JW, Meyer MB, Martowicz ML, Bishop KA, Lee SM, Nerenz RD, *et al*. Emerging regulatory paradigms for control of gene expression by 1,25-dihydroxyvitamin D3. J Steroid. Biochem. Mol. Biol. 2010; 121(1-2):130-5. doi:10.1016/j.jsbmb.2010.02.036

53. Ramagopalan SV, Heger A, Berlanga AJ, Maugeri NJ, Lincoln MR, Burrell A, *et al*. A chip-seq defined genome-wide map of vitamin D receptor binding: Associations with disease and evolution. Genome Res. 2010; 20(10):1352-60. doi:10.1101/gr.107920.110

54. Mizwicki MT, Norman AW. Chapter 16 - Vitamin D sterol/Vitamin D receptor conformational dynamics and nongenomic actions. In: Feldman D, editor. Vitamin D (fourth edition): Academic Press; 2018. p. 269-92.

55. Huhtakangas JA, Olivera CJ, Bishop JE, Zanello LP, Norman AW. The vitamin D receptor is present in caveolae-enriched plasma membranes and binds 1 alpha,25(OH)$_2$-vitamin D$_3$ *in vivo* and *in vitro*. Mol Endocrinol. 2004; 18(11):2660-71. doi:10.1210/me.2004-0116

56. Chen J, Olivares-Navarrete R, Wang Y, Herman TR, Boyan BD, Schwartz Z. Protein-disulfide isomerase-associated 3 (PDIA3) mediates the membrane response

to 1,25-dihydroxyvitamin D_3 in osteoblasts. J Biol. Chem. 2010; 285(47):37041-50. doi:10.1074/jbc.M110.157115

57. Boyan BD, Sylvia VL, Dean DD, Pedrozo H, Del Toro F, Nemere I, *et al*. 1,25-$(OH)_2D_3$ modulates growth plate chondrocytes via membrane receptor-mediated protein kinase C by a mechanism that involves changes in phospholipid metabolism and the action of arachidonic acid and PGE2. Steroids. 1999; 64(1-2):129-36. doi:10.1016/s0039-128x(98)00099-3

58. Igor NS. 1,25-dihydroxyvitamin D_3 and type 2 diabetes: Ca^{2+}-dependent molecular mechanisms and the role of vitamin D status. Horm. Mol. Biol. Clin. Investig. 2016; 26(1):61-5. doi:https://doi.org/10.1515/hmbci-2015-0069

59. Christakos S, Dhawan P, Verstuyf A, Verlinden L, Carmeliet G. vitamin D: Metabolism, molecular mechanism of action, and pleiotropic effects. Physiol. Rev. 2016; 96(1):365-408. doi:10.1152/physrev.00014.2015

60. Jeon S-M, Shin E-A. Exploring vitamin D metabolism and function in cancer. Exp. Mol. Med. 2018; 50(4):20-. doi:10.1038/s12276-018-0038-9

61. The Human Protein Atlas [Internet]. Metabolics - vitamin D metabolism. 2020 [accessed 1 October 2020]. Available from: https://www.proteinatlas.org/ENSG00000186104-CYP2R1/tissue/metabolic/Vitamin+D+metabolism.

62. Hanahan D, Weinberg Robert A. Hallmarks of cancer: The next generation. Cell. 2011; 144(5):646-74. doi:10.1016/j.cell.2011.02.013

63. Fleet JC. Chapter 20 - Regulation of intestinal calcium and phosphate absorption. In: Feldman D, editor. Vitamin D (fourth edition): Academic Press; 2018. p. 329-42.

64. Al-Azhri J, Zhang Y, Bshara W, Zirpoli G, McCann SE, Khoury T, *et al*. Tumor expression of vitamin D receptor and breast cancer histopathological characteristics and prognosis. Clin. Cancer Res. 2017; 23(1):97-103. doi:10.1158/1078-0432.Ccr-16-0075

65. Brożyna AA, Jozwicki W, Janjetovic Z, Slominski AT. Expression of vitamin D receptor decreases during progression of pigmented skin lesions. Hum. Pathol. 2011; 42(5):618-31. doi:10.1016/j.humpath.2010.09.014

66. Lopes N, Sousa B, Martins D, Gomes M, Vieira D, Veronese LA, *et al*. Alterations in vitamin D signalling and metabolic pathways in breast cancer progression: A study of vdr, CYP27B1 and CYP24A1 expression in benign and malignant breast lesions. BMC cancer. 2010; 10:483-. doi:10.1186/1471-2407-10-483

67. Wang Y, Shi J, Chai K, Ying X, Zhou BP. The role of snail in EMT and tumorigenesis. Curr. Cancer Drug Targets. 2013; 13(9):963-72. doi:10.2174/15680096113136660102

68. Mittal MK, Myers JN, Misra S, Bailey CK, Chaudhuri G. *In vivo* binding to and functional repression of the VDR gene promoter by slug in human breast cells. Biochem. Biophys. Res. Commun. 2008; 372(1):30-4. doi:10.1016/j.bbrc.2008.04.187

69. Peña C, García JM, Silva J, García V, Rodríguez R, Alonso I, *et al*. E-cadherin and vitamin D receptor regulation by Snail and ZEB1 in colon cancer: Clinicopathological correlations. Hum. Mol. Genet. 2005; 14(22):3361-70. doi:10.1093/hmg/ddi366

70. DeSmet ML, Fleet JC. Constitutively active Ras signaling reduces 1,25 dihydroxyvitamin D-mediated gene transcription in intestinal epithelial cells by reducing vitamin D receptor expression. J Steroid. Biochem. Mol. Biol. 2017; 173:194-201. doi:10.1016/j.jsbmb.2017.01.008

71. Zhang Z, Kovalenko P, Cui M, Desmet M, Clinton SK, Fleet JC. Constitutive activation of the mitogen-activated protein kinase pathway impairs vitamin D signaling in human prostate epithelial cells. J Cell. Physiol. 2010; 224(2):433-42. doi:10.1002/jcp.22139

72. Solomon C, White JH, Kremer R. Mitogen-activated protein kinase inhibits 1,25-dihydroxyvitamin D_3-dependent signal transduction by phosphorylating human retinoid x receptor alpha. J Clin. Invest. 1999; 103(12):1729-35. doi:10.1172/jci6871

73. Stambolsky P, Tabach Y, Fontemaggi G, Weisz L, Maor-Aloni R, Siegfried Z, *et al*. Modulation of the vitamin D_3 response by cancer-associated mutant p53. Cancer cell. 2010; 17(3):273-85. doi:10.1016/j.ccr.2009.11.025

74. Mohri T, Nakajima M, Takagi S, Komagata S, Yokoi T. MicroRNA regulates human vitamin D receptor. Int J Cancer. 2009; 125(6):1328-33. doi:10.1002/ijc.24459

75. Essa S, Denzer N, Mahlknecht U, Klein R, Collnot EM, Tilgen W, *et al*. VDR microRNA expression and epigenetic silencing of vitamin D signaling in melanoma cells. J Steroid Biochem Mol Biol. 2010; 121(1-2):110-3. doi:10.1016/j.jsbmb.2010.02.003

76. Marik R, Fackler M, Gabrielson E, Zeiger MA, Sukumar S, Stearns V, *et al*. DNA methylation-related vitamin D receptor insensitivity in breast cancer. Cancer Biol. Ther. 2010; 10(1):44-53. doi:10.4161/cbt.10.1.11994

77. Pather Y, Marais S, Joubert AM, Mercier AE, Punchoo R, editors. Cholecalciferol induces cell cycle arrest and apoptosis in HeLa cell line. 56th Annual Conference of

the Microscopy Society of Southern Africa; 2019; Cape Town, South Africa: Council for Scientific and Industrial Research; 2019.

78. Tokar EJ, Webber MM. Cholecalciferol (Vitamin D3) inhibits growth and invasion by up-regulating nuclear receptors and 25-hydroxylase (CYP27A1) in human prostate cancer cells. Clin. Exp. Metastasis. 2005; 22(3):275-84. doi:10.1007/s10585-005-8393-z

79. Fleet JC, DeSmet M, Johnson R, Li Y. Vitamin D and cancer: A review of molecular mechanisms. Biochem. J. 2012; 441(1):61-76. doi:10.1042/BJ20110744

80. Brożyna AA, Jóźwicki W, Jochymski C, Slominski AT. Decreased expression of CYP27B1 correlates with the increased aggressiveness of ovarian carcinomas. Oncology Rep. 2015; 33(2):599-606. doi:10.3892/or.2014.3666

81. Hsu J-W, Yasmin-Karim S, King MR, Wojciechowski JC, Mickelsen D, Blair ML, *et al*. Suppression of prostate cancer cell rolling and adhesion to endothelium by 1α,25-dihydroxyvitamin D_3. Am. J Pathol. 2011; 178(2):872-80. doi:https://doi.org/10.1016/j.ajpath.2010.10.036

82. Segersten U, Correa P, Hewison M, Hellman P, Dralle H, Carling T, *et al*. 25-hydroxyvitamin D_3-1alpha-hydroxylase expression in normal and pathological parathyroid glands. J Clin. Endocrinol. Metab. 2002; 87(6):2967-72. doi:10.1210/jcem.87.6.8604

83. Chen TC, Holick MF, Lokeshwar BL, Burnstein KL, Schwartz GG. Evaluation of vitamin D analogs as therapeutic agents for prostate cancer. Recent Results Cancer Res. 2003; 164:273-88. doi:10.1007/978-3-642-55580-0_20

84. Mawer EB, Hayes ME, Heys SE, Davies M, White A, Stewart MF, *et al*. Constitutive synthesis of 1,25-dihydroxyvitamin D_3 by a human small cell lung cancer cell line. J Clin. Endocrinol. Metab. 1994; 79(2):554-60. doi:10.1210/jcem.79.2.8045976

85. Hummel DM, Fetahu IS, Gröschel C, Manhardt T, Kállay E. Role of proinflammatory cytokines on expression of vitamin D metabolism and target genes in colon cancer cells. J Steroid Biochem. Mol. Biol. 2014; 144 Pt A:91-5. doi:10.1016/j.jsbmb.2013.09.017

86. Albertson DG, Ylstra B, Segraves R, Collins C, Dairkee SH, Kowbel D, *et al*. Quantitative mapping of amplicon structure by array CGH identifies CYP24 as a candidate oncogene. Nat. Genetics. 2000; 25(2):144-6.

87. Höbaus J, Hummel DM, Thiem U, Fetahu IS, Aggarwal A, Müllauer L, *et al*. Increased copy-number and not DNA hypomethylation causes overexpression of the candidate proto-oncogene CYP24A1 in colorectal cancer. International journal of cancer. 2013; 133(6):1380-8. doi:10.1002/ijc.28143

88. Meijer GA, Hermsen MA, Baak JP, van Diest PJ, Meuwissen SG, Beliën JA, *et al*. Progression from colorectal adenoma to carcinoma is associated with non-random chromosomal gains as detected by comparative genomic hybridisation. J. Clin. Pathol. 1998; 51(12):901-9. doi:10.1136/jcp.51.12.901

89. Komagata S, Nakajima M, Takagi S, Mohri T, Taniya T, Yokoi T. Human CYP24 catalyzing the inactivation of calcitriol is post-transcriptionally regulated by miR-125b. Mol. Pharmacol. 2009; 76(4):702-9. doi:10.1124/mol.109.056986

90. Borkowski R, Du L, Zhao Z, McMillan E, Kosti A, Yang C-R, *et al*. Genetic mutation of p53 and suppression of the mir-17~92 cluster are synthetic lethal in non-small cell lung cancer due to upregulation of vitamin D signaling. Cancer Res. 2015; 75(4):666-75. doi:10.1158/0008-5472.CAN-14-1329

91. Luo W, Yu W-D, Ma Y, Chernov M, Trump DL, Johnson CS. Inhibition of protein kinase Ck2 reduces CYP24A1 expression and enhances 1,25-dihydroxyvitamin D_3 antitumor activity in human prostate cancer cells. Cancer Res. 2013; 73(7):2289-97. doi:10.1158/0008-5472.CAN-12-4119

92. Luo W, Karpf AR, Deeb KK, Muindi JR, Morrison CD, Johnson CS, *et al*. Epigenetic regulation of vitamin D 24-hydroxylase/CYP24A1 in human prostate cancer. Cancer Res. 2010; 70(14):5953-62. doi:10.1158/0008-5472.CAN-10-0617

93. Ramnath N, Nadal E, Jeon CK, Sandoval J, Colacino J, Rozek LS, *et al*. Epigenetic regulation of vitamin D metabolism in human lung adenocarcinoma. J Thorac. Oncol. 2014; 9(4):473-82. doi:10.1097/JTO.0000000000000114

94. Garland CF, Garland FC. Do sunlight and vitamin D reduce the likelihood of colon cancer? Int. J Epidemiol. 1980; 9(3):227-31. doi:10.1093/ije/9.3.227

95. Colston K, Colston MJ, Feldman D. 1,25-dihydroxyvitamin D_3 and malignant melanoma: The presence of receptors and inhibition of cell growth in culture. Endocrinology. 1981; 108(3):1083-6. doi:10.1210/endo-108-3-1083

96. Giammanco M, Di Majo D, La Guardia M, Aiello S, Crescimannno M, Flandina C, *et al*. vitamin D in cancer chemoprevention. Pharm Biol. 2015; 53(10):1399-434. doi:10.3109/13880209.2014.988274

97. Trump D, Aragon-Ching J. Vitamin D in prostate cancer. Asian J Androl. 2018; 20(3):244-52. doi:10.4103/aja.aja_14_18

98. Campbell MJ, Trump DL. Vitamin D receptor signaling and cancer. Endocrinol. Metab. Clin. North Am. 2017; 46(4):1009-38. doi:https://doi.org/10.1016/j.ecl.2017.07.007

99. Lointier P, Wargovich MJ, Saez S, Levin B, Wildrick DM, Boman BM. The role of vitamin D_3 in the proliferation of a human colon cancer cell line *in vitro*. Anticancer Res. 1987; 7(4B):817-21.

100. Gross M, Kost SB, Ennis B, Stumpf W, Kumar R. Effect of 1,25-dihydroxyvitamin D_3 on mouse mammary tumor (Gr) cells: Evidence for receptors, cellular uptake, inhibition of growth and alteration in morphology at physiologic concentrations of hormone. J Bone Miner. Res. 1986; 1(5):457-67. doi:10.1002/jbmr.5650010510

101. Skowronski RJ, Peehl DM, Feldman D. vitamin D and prostate cancer: 1,25 dihydroxyvitamin D_3 receptors and actions in human prostate cancer cell lines. Endocrinology. 1993; 132(5):1952-60. doi:10.1210/endo.132.5.7682937

102. Eelen G, Verlinden L, van Camp M, van Hummelen P, Marchal K, de Moor B, *et al*. The effects of 1alpha,25-dihydroxyvitamin D_3 on the expression of DNA replication genes. J Bone. Miner. Res. 2004; 19(1):133-46. doi:10.1359/jbmr.0301204

103. Hedlund TE, Moffatt KA, Miller GJ. vitamin D receptor expression is required for growth modulation by 1 alpha,25-dihydroxyvitamin D_3 in the human prostatic carcinoma cell line ALVA-31. J Steroid Biochem. Mol.. 1996; 58(3):277-88. doi:10.1016/0960-0760(96)00030-1

104. Zhuang SH, Schwartz GG, Cameron D, Burnstein KL. Vitamin D receptor content and transcriptional activity do not fully predict antiproliferative effects of vitamin D in human prostate cancer cell lines. Mol. Cell Endocrinol. 1997; 126(1):83-90. doi:10.1016/s0303-7207(96)03974-3

105. Williams GH, Stoeber K. The cell cycle and cancer. J Pathol. 2012; 226(2):352-64. doi:10.1002/path.3022

106. Malumbres M. 4 - Control of the cell cycle. In: Niederhuber JE, Armitage JO, Kastan MB, Doroshow JH, Tepper JE, editors. Abeloff's Clinical Oncology (sixth edition). Philadelphia: Content Repository Only; 2020. p. 56-73.e5.

107. Studzinski GP, Gocek E, Coffman F, Danilenko M. Chapter 96 - Effects of vitamin D derivatives on differentiation, cell cycle, and apoptosis in hematological malignancies. In: Feldman D, editor. Vitamin D (fourth edition): Academic Press; 2018. p. 761-99.

108. Sánchez I, Dynlacht BD. New insights into cyclins, CDKs, and cell cycle control. Semin Cell Dev Biol. 2005; 16(3):311-21. doi:https://doi.org/10.1016/j.semcdb.2005.02.007

109. Deshpande A, Sicinski P, Hinds PW. Cyclins and CDKs in development and cancer: A perspective. Oncogene. 2005; 24(17):2909-15. doi:10.1038/sj.onc.1208618

110. Morgan DO. Cyclin-dependent kinases: Engines, clocks, and microprocessors. Annu. Rev. Cell. Dev. Biol. 1997; 13:261-91. doi:10.1146/annurev.cellbio.13.1.261

111. Malumbres M, Barbacid M. Mammalian cyclin-dependent kinases. Trends Biochem. Sci. 2005; 30(11):630-41. doi:https://doi.org/10.1016/j.tibs.2005.09.005

112. Sherr CJ, Roberts JM. Living with or without cyclins and cyclin-dependent kinases. Genes & Development. 2004; 18(22):2699-711. doi:10.1101/gad.1256504

113. Cobrinik D. Pocket proteins and cell cycle control. Oncogene. 2005; 24(17):2796-809. doi:10.1038/sj.onc.1208619

114. Kastan MB, Bartek J. Cell-cycle checkpoints and cancer. Nature. 2004; 432(7015):316.

115. Nevins JR. The RB/E2F pathway and cancer. Hum. Mol. Genet. 2001; 10(7):699-703. doi:10.1093/hmg/10.7.699

116. Jensen SS, Madsen MW, Lukas J, Binderup L, Bartek J. Inhibitory effects of 1alpha,25-dihydroxyvitamin D_3 on the G_1-S phase-controlling machinery. Mol. Endocrinol. 2001; 15(8):1370-80. doi:10.1210/mend.15.8.0673

117. Chiang K-C, Yeh C-N, Chen S-C, Shen S-C, Hsu J-T, Yeh T-S, *et al*. MART-10, a new generation of vitamin D analog, is more potent than 1α,25-dihydroxyvitamin D_3 in inhibiting cell proliferation and inducing apoptosis in ER+ MCF-7 breast cancer cells. J. Steroid Biochem. 2013; 139:54-60. doi: 10.1016/j.jsbmb.2013.10.005.

118. Li P, Li C, Zhao X, Zhang X, Nicosia SV, Bai W. $p27^{kip1}$ stabilization and G_1 arrest by 1,25-dihydroxyvitamin D_3 in ovarian cancer cells mediated through down-regulation of cyclin e/cyclin-dependent kinase 2 and Skp1-cullin-F-box protein/Skp2 ubiquitin ligase. J Biol. Chem. 2004; 279(24):25260-7. doi:10.1074/jbc.M311052200

119. Akutsu N, Lin R, Bastien Y, Bestawros A, Enepekides DJ, Black MJ, *et al*. Regulation of gene expression by 1alpha,25-dihydroxyvitamin D_3 and its analog EB1089 under growth-inhibitory conditions in squamous carcinoma cells. Mol. Endocrinol. 2001; 15(7):1127-39. doi:10.1210/mend.15.7.0655

120. Salehi-Tabar R, Nguyen-Yamamoto L, Tavera-Mendoza LE, Quail T, Dimitrov V, An B-S, *et al*. vitamin D receptor as a master regulator of the c-myc/Mxd1 network. Proc. Natl. Acad. Sci. USA. 2012; 109(46):18827-32. doi:10.1073/pnas.1210037109

121. Washington MN, Kim J-S, Weigel NL. 1α,25-dihydroxyvitamin D_3 inhibits c4-2 prostate cancer cell growth via a retinoblastoma protein (RB)-independent G_1 arrest. The Prostate. 2011; 71(1):98-110. doi:10.1002/pros.21226

122. Bao BY, Hu YC, Ting HJ, Lee YF. Androgen signaling is required for the vitamin D-mediated growth inhibition in human prostate cancer cells. Oncogene. 2004; 23(19):3350-60. doi:10.1038/sj.onc.1207461

123. Boyle BJ, Zhao XY, Cohen P, Feldman D. Insulin-like growth factor binding protein-3 mediates 1 alpha,25-dihydroxyvitamin D(3) growth inhibition in the LnCaP prostate cancer cell line through p21/waf1. J Urol. 2001; 165(4):1319-24.

124. Flores O, Wang Z, Knudsen KE, Burnstein KL. Nuclear targeting of cyclin-dependent kinase 2 reveals essential roles of cyclin-dependent kinase 2 localization and cyclin E in vitamin D-mediated growth inhibition. Endocrinology. 2010; 151(3):896-908. doi:10.1210/en.2009-1116

125. Rohan JN, Weigel NL. 1alpha,25-dihydroxyvitamin D_3 reduces c-myc expression, inhibiting proliferation and causing G_1 accumulation in c4-2 prostate cancer cells. Endocrinology. 2009; 150(5):2046-54. doi:10.1210/en.2008-1395

126. Diaz GD, Paraskeva C, Thomas MG, Binderup L, Hague A. Apoptosis is induced by the active metabolite of vitamin D_3 and its analogue EB1089 in colorectal adenoma and carcinoma cells: Possible implications for prevention and therapy. Cancer Res. 2000; 60(8):2304-12.

127. Liu M, Lee MH, Cohen M, Bommakanti M, Freedman LP. Transcriptional activation of the CDK inhibitor p21 by vitamin D_3 leads to the induced differentiation of the myelomonocytic cell line u937. Genes Dev. 1996; 10(2):142-53. doi:10.1101/gad.10.2.142

128. Smith J, Tho LM, Xu N, Gillespie DA. The ATM-Chk2 and ATR-Chk1 pathways in DNA damage signaling and cancer. Adv Cancer Res. 2010; 108:73-112. doi:10.1016/b978-0-12-380888-2.00003-0

129. Studzinski GP, Rathod B, Rao J, Kheir A, Wajchman HJ, Zhang F, *et al*. Transition to tetraploidy in 1,25-dihydroxyvitamin D_3-resistant HL60 cells is preceded by reduced growth factor dependence and constitutive up-regulation of Sp1 and Ap-1 transcription factors. Cancer Res. 1996; 56(23):5513-21.

130. Godyn JJ, Xu H, Zhang F, Kolla S, Studzinski GP. A dual block to cell cycle progression in HL60 cells exposed to analogues of vitamin D. Cell Proliferation. 1994; 27(1):37-46. doi:10.1111/j.1365-2184.1994.tb01404.x

131. Jiang F, Li P, Fornace AJ, Jr., Nicosia SV, Bai W. G_2/M arrest by 1,25-dihydroxyvitamin D_3 in ovarian cancer cells mediated through the induction of

GADD45 via an exonic enhancer. J Biol Chem. 2003; 278(48):48030-40. doi:10.1074/jbc.M308430200

132. Kerr JF, Wyllie AH, Currie AR. Apoptosis: A basic biological phenomenon with wide-ranging implications in tissue kinetics. Br. J Cancer. 1972; 26(4):239-57. doi:10.1038/bjc.1972.33

133. Galluzzi L, Maiuri MC, Vitale I, Zischka H, Castedo M, Zitvogel L, *et al*. Cell death modalities: Classification and pathophysiological implications. Cell Death Differ. 2007; 14(7):1237-43. doi:10.1038/sj.cdd.4402148

134. Galluzzi L, Linkermann A, Kepp O, Kroemer G. 5 - pathophysiology of cancer cell death. In: Niederhuber JE, Armitage JO, Kastan MB, Doroshow JH, Tepper JE, editors. Abeloff's Clinical Oncology (sixth edition). Philadelphia: 2020. p. 74-83.e4.

135. Green DR, Llambi F. Cell death signaling. Cold Spring Harb Perspect Biol. 2015; 7(12) doi:10.1101/cshperspect.a006080

136. Galluzzi L, Kepp O, Kroemer G. Mitochondrial regulation of cell death: A phylogenetically conserved control. Microbial. Cell (Graz, Austria). 2016; 3(3):101-8. doi:10.15698/mic2016.03.483

137. Galluzzi L, Bravo-San Pedro JM, Vitale I, Aaronson SA, Abrams JM, Adam D, *et al*. Essential versus accessory aspects of cell death: Recommendations of the NCCD 2015. Cell Death Differ. 2015; 22(1):58-73. doi:10.1038/cdd.2014.137

138. Fulda S, Debatin KM. Extrinsic versus intrinsic apoptosis pathways in anticancer chemotherapy. Oncogene. 2006; 25(34):4798-811. doi:10.1038/sj.onc.1209608

139. Nagata S. Fas ligand-induced apoptosis. Annu. Rev. Genet. 1999; 33(1):29-55.

140. Tartaglia LA, Ayres TM, Wong GH, Goeddel DV. A novel domain within the 55 kD TNF receptor signals cell death. Cell. 1993; 74(5):845-53. doi:10.1016/0092-8674(93)90464-2

141. Riedl SJ, Shi Y. Molecular mechanisms of caspase regulation during apoptosis. Nat. Rev. Mol. Cell Biol. 2004; 5(11):897-907. doi:10.1038/nrm1496

142. Galluzzi L, Vitale I, Aaronson SA, Abrams JM, Adam D, Agostinis P, *et al*. Molecular mechanisms of cell death: Recommendations of the Nomenclature Committee on Cell Death 2018. Cell Death Differ. 2018; 25(3):486-541. doi:10.1038/s41418-017-0012-4

143. Mishra AP, Salehi B, Sharifi-Rad M, Pezzani R, Kobarfard F, Sharifi-Rad J, *et al*. Programmed cell death, from a cancer perspective: An overview. Mol Diagn. Ther. 2018; 22(3):281-95. doi:10.1007/s40291-018-0329-9

144. Sakahira H, Enari M, Nagata S. Cleavage of CAD inhibitor in CAD activation and DNA degradation during apoptosis. Nature. 1998; 391(6662):96-9. doi:10.1038/34214

145. Julien O, Wells JA. Caspases and their substrates. Cell Death Differ. 2017; 24(8):1380-9. doi:10.1038/cdd.2017.44

146. Moldoveanu T, Follis AV, Kriwacki RW, Green DR. Many players in BCL-2 family affairs. Trends Biochem. Sci. 2014; 39(3):101-11. doi:10.1016/j.tibs.2013.12.006

147. Shamas-Din A, Kale J, Leber B, Andrews DW. Mechanisms of action of BCL-2 family proteins. Cold Spring Harb. Perspect. Biol. 2013; 5(4):a008714. doi:10.1101/cshperspect.a008714

148. Kroemer G, Galluzzi L, Vandenabeele P, Abrams J, Alnemri ES, Baehrecke EH, *et al*. Classification of cell death: Recommendations of the Nomenclature Committee on Cell Death 2009. Cell Death Differ. 2009; 16(1):3-11. doi:10.1038/cdd.2008.150

149. Buendia B, Santa-Maria A, Courvalin JC. Caspase-dependent proteolysis of integral and peripheral proteins of nuclear membranes and nuclear pore complex proteins during apoptosis. J Cell. Sci. 1999; 112(11):1743-53.

150. Lindenboim L, Zohar H, Worman HJ, Stein R. The nuclear envelope: Target and mediator of the apoptotic process. Cell Death Discov. 2020; 6:29. doi:10.1038/s41420-020-0256-5

151. Suzuki J, Imanishi E, Nagata S. Exposure of phosphatidylserine by Xk-related protein family members during apoptosis. J. Biol. Chem. 2014; 289(44):30257-67. doi:10.1074/jbc.M114.583419

152. Suzuki J, Imanishi E, Nagata S. Xkr8 phospholipid scrambling complex in apoptotic phosphatidylserine exposure. Proc. Natl. Acad. Sci. USA. 2016; 113(34):9509-14. doi:10.1073/pnas.1610403113

153. Nagata S. Apoptotic DNA fragmentation. Exp. Cell. Res. 2000; 256(1):12-8. doi:10.1006/excr.2000.4834

154. Nagata S, Nagase H, Kawane K, Mukae N, Fukuyama H. Degradation of chromosomal DNA during apoptosis. Cell Death Differ. 2003; 10(1):108-16. doi:10.1038/sj.cdd.4401161

155. Stucki M, Clapperton JA, Mohammad D, Yaffe MB, Smerdon SJ, Jackson SP. Mdc1 directly binds phosphorylated histone H2Ax to regulate cellular responses to DNA double-strand breaks. Cell. 2005; 123(7):1213-26.

156. Maréchal A, Zou L. DNA damage sensing by the ATM and ATR kinases. Cold Spring Harb Perspect. Biol. 2013; 5(9) doi:10.1101/cshperspect.a012716

157. Matsuoka S, Ballif BA, Smogorzewska A, McDonald ER, 3rd, Hurov KE, Luo J, *et al*. ATM and ATR substrate analysis reveals extensive protein networks responsive to DNA damage. Science. 2007; 316(5828):1160-6. doi:10.1126/science.1140321

158. Stokes MP, Rush J, Macneill J, Ren JM, Sprott K, Nardone J, *et al*. Profiling of UV-induced ATM/ATR signaling pathways. Proc. Natl. Acad. Sci. USA. 2007; 104(50):19855-60. doi:10.1073/pnas.0707579104

159. Uziel T, Lerenthal Y, Moyal L, Andegeko Y, Mittelman L, Shiloh Y. Requirement of the Mrn complex for ATM activation by DNA damage. Embo J. 2003; 22(20):5612-21. doi:10.1093/emboj/cdg541

160. Redon C, Pilch D, Rogakou E, Sedelnikova O, Newrock K, Bonner W. Histone H2A variants H2Ax and H2Az. Curr. Opin. Genet. Dev. 2002; 12(2):162-9. doi:10.1016/s0959-437x(02)00282-4

161. Mah LJ, El-Osta A, Karagiannis TC. γH2Ax: A sensitive molecular marker of DNA damage and repair. Leukemia. 2010; 24(4):679-86. doi:10.1038/leu.2010.6

162. Riccardi C, Nicoletti I. Analysis of apoptosis by propidium iodide staining and flow cytometry. Nat Protoc. 2006; 1(3):1458-61. doi:10.1038/nprot.2006.238

163. Abcam [Internet]. Apoptosis: Tools for cell death series 1. 2018 [accessed 10 October 2020]. Available from: https://docs.abcam.com/pdf/kits/apoptosis-analysis-guide.pdf.

164. Blutt SE, McDonnell TJ, Polek TC, Weigel NL. Calcitriol-induced apoptosis in LnCaP cells is blocked by overexpression of BCL-2. Endocrinology. 2000; 141(1):10-7. doi:10.1210/endo.141.1.7289

165. Kizildag S, Ates H, Kizildag S. Treatment of k562 cells with 1,25-dihydroxyvitamin D3 induces distinct alterations in the expression of apoptosis-related genes BCL2, Bax, Bclxl, and p21. Ann Hematol. 2010; 89(1):1-7. doi:10.1007/s00277-009-0766-y

166. Pálmer HG, Sánchez-Carbayo M, Ordóñez-Morán P, Larriba MJ, Cordón-Cardó C, Muñoz A. Genetic signatures of differentiation induced by 1alpha,25-dihydroxyvitamin D_3 in human colon cancer cells. Cancer Res. 2003; 63(22):7799-806.

167. Pan L, Matloob AF, Du J, Pan H, Dong Z, Zhao J, *et al*. Vitamin D stimulates apoptosis in gastric cancer cells in synergy with trichostatin a/sodium butyrate-induced and 5-aza-2′-deoxycytidine-induced PTEN upregulation. FEBS J. 2010; 277(4):989-99. doi:doi:10.1111/j.1742-4658.2009.07542.x

168. Taghizadeh F, Tang MJ, Tai IT. Synergism between vitamin D and secreted protein acidic and rich in cysteine-induced apoptosis and growth inhibition results in increased susceptibility of therapy-resistant colorectal cancer cells to chemotherapy. Mol. Cancer Ther. 2007; 6(1):309-17. doi:10.1158/1535-7163.Mct-06-0517

169. Swami S, Raghavachari N, Muller UR, Bao YP, Feldman D. Vitamin D growth inhibition of breast cancer cells: Gene expression patterns assessed by cDNA microarray. Breast Cancer Res. Treat. 2003; 80(1):49-62. doi:10.1023/A:1024487118457

170. Lee HJ, Liu H, Goodman C, Ji Y, Maehr H, Uskokovic M, *et al*. Gene expression profiling changes induced by a novel gemini vitamin D derivative during the progression of breast cancer. Biochem. Pharmacol. 2006; 72(3):332-43. doi:10.1016/j.bcp.2006.04.030

171. Fedirko V, Bostick RM, Long Q, Flanders WD, McCullough ML, Sidelnikov E, *et al*. Effects of supplemental vitamin D and calcium on oxidative DNA damage marker in normal colorectal mucosa: A randomized clinical trial. Cancer Epidemiol. Biomarkers Prev. 2010; 19(1):280-91. doi:10.1158/1055-9965.Epi-09-0448

172. Kallay E, Pietschmann P, Toyokuni S, Bajna E, Hahn P, Mazzucco K, *et al*. Characterization of a vitamin D receptor knockout mouse as a model of colorectal hyperproliferation and DNA damage. Carcinogenesis. 2001; 22(9):1429-35. doi:10.1093/carcin/22.9.1429

173. Peehl DM, Shinghal R, Nonn L, Seto E, Krishnan AV, Brooks JD, *et al*. Molecular activity of 1,25-dihydroxyvitamin D_3 in primary cultures of human prostatic epithelial cells revealed by cDNA microarray analysis. J Steroid Biochem. Mol. Biol. 2004; 92(3):131-41. doi:10.1016/j.jsbmb.2004.07.003

174. Zhang X, Li P, Bao J, Nicosia SV, Wang H, Enkemann SA, *et al*. Suppression of death receptor-mediated apoptosis by 1,25-dihydroxyvitamin D_3 revealed by microarray analysis. J Biol. Chem. 2005; 280(42):35458-68. doi:10.1074/jbc.M506648200

175. Galbiati F, Polastri L, Thorens B, Dupraz P, Fiorina P, Cavallaro U, *et al*. Molecular pathways involved in the antineoplastic effects of calcitriol on insulinoma cells. Endocrinology. 2003; 144(5):1832-41. doi:10.1210/en.2002-221014

176. Jung YS, Kim HJ, Seo SK, Choi YS, Nam EJ, Kim S, *et al*. Anti-proliferative and apoptotic activities of müllerian inhibiting substance combined with calcitriol in

ovarian cancer cell lines. Yonsei Med. J. 2016; 57(1):33-40. doi:10.3349/ymj.2016.57.1.33

177. Denton D, Kumar S. Autophagy-dependent cell death. Cell Death & Differentiation. 2019; 26(4):605-16. doi:10.1038/s41418-018-0252-y

178. Klionsky DJ, Abdelmohsen K, Abe A, Abedin MJ, Abeliovich H, Acevedo Arozena A, *et al*. Guidelines for the use and interpretation of assays for monitoring autophagy (3rd edition). Autophagy. 2016; 12(1):1-222. doi:10.1080/15548627.2015.1100356

179. Parzych KR, Klionsky DJ. An overview of autophagy: Morphology, mechanism, and regulation. Antioxid. Redox. Signal. 2014; 20(3):460-73. doi:10.1089/ars.2013.5371

180. Santana-Codina N, Mancias JD, Kimmelman AC. The role of autophagy in cancer. Annu. Rev. Cancer Biol. 2017; 1:19-39. doi:10.1146/annurev-cancerbio-041816-122338

181. Levine B, Kroemer G. Autophagy in the pathogenesis of disease. Cell. 2008; 132(1):27-42. doi:10.1016/j.cell.2007.12.018

182. Doherty J, Baehrecke EH. Life, death and autophagy. Nat. Cell Biology. 2018; 20(10):1110-7. doi:10.1038/s41556-018-0201-5

183. Li X, He S, Ma B. Autophagy and autophagy-related proteins in cancer. Mol. Cancer. 2020; 19(1):12. doi:10.1186/s12943-020-1138-4

184. Amaravadi RK, Thompson CB. The roles of therapy-induced autophagy and necrosis in cancer treatment. Clin. Cancer Res. 2007; 13(24):7271-9. doi:10.1158/1078-0432.Ccr-07-1595

185. DeMasters G, Di X, Newsham I, Shiu R, Gewirtz DA. Potentiation of radiation sensitivity in breast tumor cells by the vitamin D_3 analogue, EB1089, through promotion of autophagy and interference with proliferative recovery. Mol. Cancer Ther. 2006; 5(11):2786-97. doi:10.1158/1535-7163.Mct-06-0316

186. Høyer-Hansen M, Bastholm L, Mathiasen IS, Elling F, Jäättelä M. vitamin D analog EB1089 triggers dramatic lysosomal changes and beclin 1-mediated autophagic cell death. Cell Death Differ. 2005; 12(10):1297-309. doi:10.1038/sj.cdd.4401651

187. Tavera-Mendoza LE, Westerling T, Libby E, Marusyk A, Cato L, Cassani R, *et al*. vitamin D receptor regulates autophagy in the normal mammary gland and in luminal breast cancer cells. Proc. Natl. Acad. Sci. U.S.A. 2017; 114(11):E2186-E94. doi:10.1073/pnas.1615015114

188. Wang J, Lian H, Zhao Y, Kauss MA, Spindel S. vitamin D_3 induces autophagy of human myeloid leukemia cells. J. Biol. Chem. 2008; 283(37):25596-605. doi:10.1074/jbc.M801716200

189. Tavera-Mendoza L, Wang T-T, Lallemant B, Zhang R, Nagai Y, Bourdeau V, *et al*. Convergence of vitamin D and retinoic acid signalling at a common hormone response element. EMBO Rep. 2006; 7(2):180-5. doi:10.1038/sj.embor.7400594

190. Høyer-Hansen M, Nordbrandt SP, Jäättelä M. Autophagy as a basis for the health-promoting effects of vitamin D. Trends Mol. Med. 2010; 16(7):295-302. doi:10.1016/j.molmed.2010.04.005

191. Syntichaki P, Tavernarakis N. Death by necrosis. Uncontrollable catastrophe, or is there order behind the chaos? EMBO Rep. 2002; 3(7):604-9. doi:10.1093/embo-reports/kvf138

192. Festjens N, Vanden Berghe T, Vandenabeele P. Necrosis, a well-orchestrated form of cell demise: Signalling cascades, important mediators and concomitant immune response. Biochim. Biophys. Acta. 2006; 1757(9-10):1371-87. doi:10.1016/j.bbabio.2006.06.014

193. Golstein P, Kroemer G. Cell death by necrosis: Towards a molecular definition. Trends Biochem. Sci. 2007; 32(1):37-43. doi:10.1016/j.tibs.2006.11.001

194. Zong WX, Thompson CB. Necrotic death as a cell fate. Genes Dev. 2006; 20(1):1-15. doi:10.1101/gad.1376506

195. Vanden Berghe T, Vanlangenakker N, Parthoens E, Deckers W, Devos M, Festjens N, *et al*. Necroptosis, necrosis and secondary necrosis converge on similar cellular disintegration features. Cell Death Differ. 2010; 17(6):922-30. doi:10.1038/cdd.2009.184

196. Avila E, Garcia-Becerra R, Rodriguez-Rasgado JA, Diaz L, Ordaz-Rosado D, Zugel U, *et al*. Calcitriol down-regulates human ether a go-go 1 potassium channel expression in cervical cancer cells. Anticancer Res. 2010; 30(7):2667-72.

197. González-Duarte RJ, Cázares-Ordoñez V, Romero-Córdoba S, Díaz L, Ortíz Vc, Freyre-González JA, *et al*. Calcitriol increases dicer expression and modifies the micrornas signature in siha cervical cancer cells. Biochem. Cell Biol. 2015; 93(4):376-84. doi:10.1139/bcb-2015-0010

198. González-Duarte RJ, Cázares-Ordoñez V, Díaz L, Ortíz V, Larrea F, Avila E. The expression of RNA helicase DDX5 is transcriptionally upregulated by calcitriol through a vitamin D response element in the proximal promoter in siha cervical cells. Mol. Cell Biochem. 2015; 410(1-2):65-73. doi:10.1007/s11010-015-2538-4

199. Bennett RG, Wakeley SE, Hamel FG, High RR, Korch C, Goldner WS. Gene expression of vitamin D metabolic enzymes at baseline and in response to vitamin D treatment in thyroid cancer cell lines. Oncology. 2012; 83(5):264-72. doi:10.1159/000342093

200. Bhoora S, Pather Y, Marais S, Punchoo R. Cholecalciferol inhibits cell growth and induces apoptosis in the caski cell line. Med. Sci. 2020; 8(1):12.

201. Masters JR, Stacey GN. Changing medium and passaging cell lines. Nat Protoc. 2007; 2(9):2276-84. doi:10.1038/nprot.2007.319

202. Freshney RI. Culture of animal cells: A manual of basic technique and specialized applications. 6th ed. ed. Hoboken, N.J.: Wiley-Blackwell; 2010.

203. Thermo Fisher [Internet]. Trypan blue exclusion. ThermoFisher Scientific; 2018 [accessed 7 April 2018]. Available from: https://www.thermofisher.com/za/en/home/references/gibco-cell-culture-basics/cell-culture-protocols/trypan-blue-exclusion.html.

204. Aslantürk Ö. *In vitro* cytotoxicity and cell viability assays: Principles, advantages, and disadvantages. 2018.

205. Feoktistova M, Geserick P, Leverkus M. Crystal violet assay for determining viability of cultured cells. Cold Spring Harb Protoc. 2016; 2016(4):pdb.prot087379. doi:10.1101/pdb.prot087379

206. Strober W. Trypan blue exclusion test of cell viability. Curr Protoc Immunol. 2001; Appendix 3:Appendix 3B. doi:10.1002/0471142735.ima03bs21

207. Adan A, Alizada G, Kiraz Y, Baran Y, Nalbant A. Flow cytometry: Basic principles and applications. Critical Reviews in Biotechnology. 2017; 37(2):163-76. doi:10.3109/07388551.2015.1128876

208. McCoy JP. Basic principles of flow cytometry. Hematology/Oncology Clinics. 2002; 16(2):229-43.

209. Luminex Corporation [Internet]. Muse™ Cell Analyser User Guide. California, United States of America Millipore Corporation; [accessed 1 October 2020]. Available from: https://www.luminexcorp.com/wp-content/uploads/2019/08/Muse-0110-7895_10-040419.pdf?x40452.

210. [Internet]. Muse™ Count & Viability Kit user's guide. [accessed 12 October 2018]. Available from: http://www.merckmillipore.com/ZA/en/product/Muse-Count-Viability-Assay-Kit-100-Tests,MM_NF-MCH100102#documentation.

211. Riss T, Niles A, Moravec R, Duellman S, Benink HA, Worzella TJ, *et al*. Cell viability assays. In: Markossian S, Sittampalam GS, Grossman A, editors. Assay guidance manual. Bethesda (MD): Eli Lilly & Company and the National Center for Advancing Translational Sciences; 2013.

212. Li, Jiang, Chen, Zheng. Ki67 is a promising molecular target in the diagnosis of cancer (review). Mol. Med. Rep. 2015; 11(3):1566-72.

213. Millipore Merck [Internet]. Muse™ Ki67 Proliferation Kit. 2018 [accessed 4 February 2018]. Available from: https://www.merckmillipore.com/ZA/en/product/Muse-Ki67-Proliferation-Kit,MM_NF-MCH100114#documentation.

214. Flow cytometry: First principles. [Internet] Hoboken: Wiley; 2004 [accessed 24 May 2019]. Available from: http://qut.eblib.com.au/patron/FullRecord.aspx?p=210528.

215. Millipore Merck [Internet]. Muse™ Cell Cycle Assay Kit. Darmstadt, Germany: Merck; [accessed 10 February 2019]. Available from: http://www.merckmillipore.com/ZA/en/product/Muse-Cell-Cycle-Assay-Kit,MM_NF-MCH100106.

216. Darzynkiewicz Z, Bedner E, Smolewski P. Flow cytometry in analysis of cell cycle and apoptosis. Semin Hematol. 2001; 38(2):179-93. doi:10.1016/s0037-1963(01)90051-4

217. Elmore S. Apoptosis: A review of programmed cell death. Toxicol. Pathol. 2007; 35(4):495-516. doi:10.1080/01926230701320337

218. Fink SL, Cookson BT. Apoptosis, pyroptosis, and necrosis: Mechanistic description of dead and dying eukaryotic cells. Infect. Immun. 2005; 73(4):1907-16. doi:10.1128/iai.73.4.1907-1916.2005

219. Demchenko AP. Beyond annexin v: Fluorescence response of cellular membranes to apoptosis. Cytotechnology. 2013; 65(2):157-72. doi:10.1007/s10616-012-9481-y

220. Millipore Merck [Internet]. Muse™ Annexin V and Dead Cell Assay Kit. Darmstadt, Germany: Merck; [accessed 10 February 2019]. Available from: http://www.merckmillipore.com/ZA/en/product/Muse-Annexin-V-and-Dead-Cell-Assay-Kit,MM_NF-MCH100105?ReferrerURL=https%3A%2F%2Fwww.google.com%2F.

221. Laux MT, Boerner E, Podbielska H, Jelen M. Apoptosis: A review. J. Med. Sci. (Faisalabad, Pakistan). 2003; 3(2):180-91.

222. Millipore Merck [Internet]. Muse™ Caspase-3/7 Assay Kit. Darmstadt, Germany: Merck; [accessed 10 February 2019]. Available from: http://www.merckmillipore.com/ZA/en/product/Muse-Caspase-3-7-Assay-Kit,MM_NF-MCH100108?ReferrerURL=https%3A%2F%2Fwww.google.com%2F.

223. Lavrik IN, Golks A, Krammer PH. Caspases: Pharmacological manipulation of cell death. J. Clin. Invest. 2005; 115(10):2665-72. doi:10.1172/jci26252

224. Porter AG, Janicke RU. Emerging roles of caspase-3 in apoptosis. Cell Death Differ. 1999; 6(2):99-104. doi:10.1038/sj.cdd.4400476

225. Tanaka T, Huang X, Halicka HD, Zhao H, Traganos F, Albino AP, *et al*. Cytometry of ATM activation and histone H2Ax phosphorylation to estimate extent of DNA damage induced by exogenous agents. Cytometry Part A. 2007; 71A(9):648-61. doi:10.1002/cyto.a.20426

226. Millipore Merck [Internet]. Muse™ Multi-color DNA Damage Kit. Darmstadt, Germany Merck; [accessed 10 September 2020]. Available from: https://www.luminexcorp.com/?wpdmdl=40957.

227. Millipore Merck [Internet]. Muse™ Autophagy LC3-Antibody Based Kit. Darmstadt, Germany: Merck; [accessed 10 February 2019]. Available from: http://www.merckmillipore.com/ZA/en/product/MuseAutophagy-LC3-antibody-based-Kit,MM_NF-MCH200109?ReferrerURL=https%3A%2F%2Fwww.google.com%2F.

228. Sotthibundhu A, McDonagh K, von Kriegsheim A, Garcia-Munoz A, Klawiter A, Thompson K, *et al*. Rapamycin regulates autophagy and cell adhesion in induced pluripotent stem cells. Stem Cell Res. Ther. 2016; 7(1):166-. doi:10.1186/s13287-016-0425-x

229. Waldner M, Fantus D, Solari M, Thomson AW. New perspectives on mTOR inhibitors (rapamycin, rapalogs and torkinibs) in transplantation. Br. J Clin. Pharmacol. 2016; 82(5):1158-70. doi:10.1111/bcp.12893

230. Chan FK, Moriwaki K, De Rosa MJ. Detection of necrosis by release of lactate dehydrogenase activity. Methods Mol. Biol. 2013; 979:65-70. doi:10.1007/978-1-62703-290-2_7

231. Fischer AH, Jacobson KA, Rose J, Zeller R. Hematoxylin and eosin staining of tissue and cell sections. Cold Spring Harb. Protoc. 2008; 2008(5):pdb.prot4986. doi:10.1101/pdb.prot4986

232. Bancroft JD, Layton C, Suvarna SK Bancroft's Theory and Practice of Histological Techniques. [Internet] [Oxford]: Churchill Livingstone Elsevier; 2013 [accessed 23 March 2019]. Available from: ClinicalKey http://www.clinicalkey.com/dura/browse/bookChapter/3-s2.0-C20090426369

233. Eosin Y solutions. Cold Spring Harb. Protoc. 2014; 2014(6):pdb.rec073718. doi:10.1101/pdb.rec073718

234. Schindelin J, Arganda-Carreras I, Frise E, Kaynig V, Longair M, Pietzsch T, *et al*. Fiji: An open-source platform for biological-image analysis. Nat. Methods. 2012; 9(7):676-82.

235. Mayer J, Giannuzzi LA, Kamino T, Michael J. TEM sample preparation and FIB-induced damage. MRS Bulletin. 2007; 32(5):400-7. doi:10.1557/mrs2007.63

236. Higuchi R, Fockler C, Dollinger G, Watson R. Kinetic PCR analysis: Real-time monitoring of DNA amplification reactions. Biotechnology (NY). 1993; 11(9):1026-30. doi:10.1038/nbt0993-1026

237. Higuchi R, Dollinger G, Walsh PS, Griffith R. Simultaneous amplification and detection of specific DNA sequences. Biotechnology (NY). 1992; 10(4):413-7. doi:10.1038/nbt0492-413

238. Pfaffl M. Quantification stratergies in real-time PCR. In: Bustin SA, editor. A-Z of quantitative PCR La Jolla, CA, USA: International University Line (IUL); 2004. p. 87-112.

239. Schmittgen TD, Livak KJ. Analyzing real-time PCR data by the comparative Ct method. Nature Protocols. 2008; 3(6):1101-8. doi:10.1038/nprot.2008.73

240. Livak KJ, Schmittgen TD. Analysis of relative gene expression data using real-time quantitative PCR and the 2−ΔΔCt method. Methods. 2001; 25(4):402-8.

241. Nolan T, Hands RE, Bustin SA. Quantification of mRNA using real-time RT-PCR. Nature Protocols. 2006; 1(3):1559-82. doi:http://dx.doi.org/10.1038/nprot.2006.236

242. ThermoFisher Scientific [Internet]. PCR basics. 2018 [accessed 3 August 2018]. Available from: https://www.thermofisher.com/za/en/home/life-science/cloning/cloning-learning-center/invitrogen-school-of-molecular-biology/pcr-education/pcr-reagents-enzymes/pcr-basics.html.

243. Chomczynski P, Sacchi N. Single-step method of RNA isolation by acid guanidinium thiocyanate-phenol-chloroform extraction. Anal. Biochem. 1987; 162(1):156-9. doi:10.1006/abio.1987.9999

244. [Internet]. Tm calculator. Thermo Fisher; [accessed 11 February 2019]. Available from: https://www.thermofisher.com/za/en/home/brands/thermo-scientific/molecular-biology/molecular-biology-learning-center/molecular-biology-resource-library/thermo-scientific-web-tools/tm-calculator.html.

245. GE Healthcare Life Sciences [Internet]. Western blotting principles and methods. Uppsala, Sweden: GE Healthcare; 2014 [accessed 12 February 2018]. Available from: https://cdn.gelifesciences.com/dmm3bwsv3/AssetStream.aspx?mediaformatid=10061&destinationid=10016&assetid=20206.

246. Abcam [Internet]. Western blot protocol. Abcam; 2018 [accessed 1 November 2018]. Available from: https://www.abcam.com/protocols/general-western-blot-protocol.

247. Jensen EC. The basics of Western blotting. Anat. Rec. 2012; 295(3):369-71. doi:10.1002/ar.22424

248. Pillai-Kastoori L, Heaton S, Shiflett SD, Roberts AC, Solache A, Schutz-Geschwender AR. Antibody validation for Western blot: By the user, for the user. J. Biol. Chem2020; 295(4):926-39. doi:10.1074/jbc.RA119.010472

249. Mahmood T, Yang PC. Western blot: Technique, theory, and trouble shooting. N Am. J. Med. Sci. 2012; 4(9):429-34. doi:10.4103/1947-2714.100998

250. Bio-Rad [Internet]. Protein blotting methods. Bio-Rad; [accessed 11 February 2019]. Available from: https://www.bio-rad.com/en-us/applications-technologies/protein-blotting-methods?ID=LUSPPSESH.

251. Darzynkiewicz Z, Huang X, Zhao H. Analysis of cellular DNA content by flow cytometry. Curr. Protoc. Immunol. 2017; 119:5.7.1-5.7.20. doi:10.1002/cpim.36

252. Finkel E. The mitochondrion: Is it central to apoptosis? Science. 2001; 292(5517):624-6. doi:10.1126/science.292.5517.624

253. Jones G, Prosser DE, Kaufmann M. Chapter 5 - The activating enzymes of vitamin D metabolism (25- and 1α-hydroxylases). In: Feldman D, editor. Vitamin D (fourth edition): Academic Press; 2018. p. 57-79.

254. Riss T, Niles A, Moravec R, Karassina N, Vidugiriene J. Cytotoxicity assays: *In vitro* methods to measure dead cells. In: Markossian S, Sittampalam GS, Grossman A, editors. Assay guidance manual. Bethesda (MD): Eli Lilly & Company and the National Center for Advancing Translational Sciences; 2019.

255. Altman SA, Randers L, Rao G. Comparison of trypan blue dye exclusion and fluorometric assays for mammalian cell viability determinations. Biotechnol. Prog. 1993; 9(6):671-4. doi:10.1021/bp00024a017

256. Yang ES, Burnstein KL. vitamin D inhibits g1 to s progression in lncap prostate cancer cells through $p27^{kip1}$ stabilization and CDK2 mislocalization to the cytoplasm. J. Biol. Chem. 2003; 278(47):46862-8. doi:10.1074/jbc.M306340200

257. Zinser GM, Tribble E, Valrance M, Urben CM, Knutson JC, Mazess RB, *et al*. 1,24(s)-dihydroxyvitamin D_2, an endogenous vitamin D_2 metabolite, inhibits growth of breast cancer cells and tumors. Anticancer Res. 2005; 25(1A):235-41.

258. Baek S, Lee Y-S, Shim H-E, Yoon S, Baek S-Y, Kim B-S, *et al*. Vitamin D_3 regulates cell viability in gastric cancer and cholangiocarcinoma. Anat. Cell Biol. 2011; 44(3):204-9. doi:10.5115/acb.2011.44.3.204

259. Scholzen T, Gerdes J. The Ki-67 protein: From the known and the unknown. J. Cell Physiol. 2000; 182(3):311-22. doi:10.1002/(sici)1097-4652(200003)182:3<311::Aid-jcp1>3.0.Co;2-9

260. Carlberg C, Muñoz A. An update on vitamin D signaling and cancer. Semin. Cancer Biol. 2020; doi:10.1016/j.semcancer.2020.05.018

261. Galluzzi L, Kepp O, Kroemer G. 5 - Pathophysiology of cancer cell death. In: Niederhuber JE, Armitage JO, Doroshow JH, Kastan MB, Tepper JE, editors. Abeloff's Clinical Oncology (fifth edition). Philadelphia: Content Repository Only; 2014. p. 69-77.e3.

262. Sun M. Correlated three-dimensional light and electron microscopy reveals transformation of mitochondria during apoptosis. Nat. Cell Biol. 2007; 9(9):1057.

263. Arismendi-Morillo G. Electron microscopy morphology of the mitochondrial network in gliomas and their vascular microenvironment. Biochim. Biophys. Acta Bioenerg. 2011; 1807(6):602-8. doi:https://doi.org/10.1016/j.bbabio.2010.11.001

264. Tait SWG, Green DR. Mitochondria and cell death: Outer membrane permeabilization and beyond. Nat. Rev. Mol. 2010; 11(9):621-32. doi:http://dx.doi.org/10.1038/nrm2952

265. Galluzzi L, Kepp O, Trojel-Hansen C, Kroemer G. Non-apoptotic functions of apoptosis-regulatory proteins. EMBO Rep. 2012; 13(4):322-30. doi:10.1038/embor.2012.19

266. Li K, Li Y, Shelton JM, Richardson JA, Spencer E, Chen ZJ, *et al*. Cytochrome c deficiency causes embryonic lethality and attenuates stress-induced apoptosis. Cell. 2000; 101(4):389-99. doi:10.1016/s0092-8674(00)80849-1

267. Liu X, Kim CN, Yang J, Jemmerson R, Wang X. Induction of apoptotic program in cell-free extracts: Requirement for dATP and cytochrome c. Cell. 1996; 86(1):147-57. doi:10.1016/s0092-8674(00)80085-9

268. Li P, Nijhawan D, Budihardjo I, Srinivasula SM, Ahmad M, Alnemri ES, *et al*. Cytochrome c and dATP-dependent formation of apaf-1/caspase-9 complex initiates an apoptotic protease cascade. Cell. 1997; 91(4):479-89. doi:10.1016/s0092-8674(00)80434-1

269. Guzey M, Kitada S, Reed JC. Apoptosis induction by 1alpha,25-dihydroxyvitamin D_3 in prostate cancer. Mol. Cancer Ther. 2002; 1(9):667-77.

270. James SY, Mackay AG, Colston KW. vitamin D derivatives in combination with 9-cis retinoic acid promote active cell death in breast cancer cells. J Mol. Endocrinol. 1995; 14(3):391-4. doi:10.1677/jme.0.0140391

271. Xu H-M, Tepper CG, Jones JB, Fernandez CE, Studzinski GP. 1,25-dihydroxyvitamin D3 protects hl60 cells against apoptosis but down-regulates the expression of the bcl-2 gene. Exp. Cell Res. 1993; 209(2):367-74. doi:https://doi.org/10.1006/excr.1993.1322

272. Narvaez CJ, Welsh J. Role of mitochondria and caspases in vitamin D-mediated apoptosis of MCF-7 breast cancer cells. J Biol. Chem. 2001; 276(12):9101-7. doi:10.1074/jbc.M006876200

273. The Cancer Genome Atlas Research N, Burk RD, Chen Z, Saller C, Tarvin K, Carvalho AL, *et al*. Integrated genomic and molecular characterization of cervical cancer. Nature. 2017; 543:378. doi:10.1038/nature21386

274. Zwaal RF, Comfurius P, Bevers EM. Surface exposure of phosphatidylserine in pathological cells. Cell Mol. Life Sci. 2005; 62(9):971-88. doi:10.1007/s00018-005-4527-3

275. Schutters K, Reutelingsperger C. Phosphatidylserine targeting for diagnosis and treatment of human diseases. Apoptosis. 2010; 15(9):1072-82. doi:10.1007/s10495-010-0503-y

276. Hengartner MO. The biochemistry of apoptosis. Nature. 2000; 407(6805):770-6. doi:10.1038/35037710

277. Nicholson DW. Caspase structure, proteolytic substrates, and function during apoptotic cell death. Cell Death Differ. 1999; 6(11):1028-42. doi:10.1038/sj.cdd.4400598

278. Earnshaw WC, Martins LM, Kaufmann SH. Mammalian caspases: Structure, activation, substrates, and functions during apoptosis. Annu. Rev. Biochem. 1999; 68:383-424. doi:10.1146/annurev.biochem.68.1.383

279. Park WH, Seol JG, Kim ES, Hyun JM, Jung CW, Lee CC, *et al*. Induction of apoptosis by vitamin D_3 analogue EB1089 in NCI-H929 myeloma cells via activation of caspase 3 and p38 MAP kinase. Br. J. Haematol. 2000; 109(3):576-83. doi:10.1046/j.1365-2141.2000.02046.x

280. Kim T-H, Park J, Lee J-S, Lee H-H. Effects of 1alpha, 25-dihydroxyvitamin D_3 on programmed cell death of ishikawa endometrial cancer cells through ezrin

phosphorylation. J Obstet. Gynaecol. Res. 2017; 37(4):503-9. doi:10.1080/01443615.2016.1271777

281. Segawa K, Kurata S, Nagata S. Human type IV P-type ATPases that work as plasma membrane phospholipid flippases and their regulation by caspase and calcium. J. Biol. Chem. 2016; 291(2):762-72. doi:10.1074/jbc.M115.690727

282. Kopeina GS, Prokhorova EA, Lavrik IN, Zhivotovsky B. Alterations in the nucleocytoplasmic transport in apoptosis: Caspases lead the way. Cell Prolif. 2018; 51(5):e12467. doi:10.1111/cpr.12467

283. Weihua Z, Lin Q, Ramoth AJ, Fan D, Fidler IJ. Formation of solid tumors by a single multinucleated cancer cell. Cancer. 2011; 117(17):4092-9. doi:10.1002/cncr.26021

284. Hayflick L, Moorhead PS. The serial cultivation of human diploid cell strains. Exp. Cell Res. 1961; 25:585-621. doi:10.1016/0014-4827(61)90192-6

285. Mirzayans R, Andrais B, Murray D. Roles of polyploid/multinucleated giant cancer cells in metastasis and disease relapse following anticancer treatment. Cancers. 2018; 10(4):118. doi:10.3390/cancers10040118

286. Zhu JG, Ochalek JT, Kaufmann M, Jones G, DeLuca HF. CYP2R1 is a major, but not exclusive, contributor to 25-hydroxyvitamin D production *in vivo*. Proc. Natl. Acad. Sci. USA. 2013; 110(39):15650-5. doi:10.1073/pnas.1315006110

287. Kong XF, Zhu XH, Pei YL, Jackson DM, Holick MF. Molecular cloning, characterization, and promoter analysis of the human 25-hydroxyvitamin D3-1alpha-hydroxylase gene. Proc. Natl. Acad. Sci. USA. 1999; 96(12):6988-93. doi:10.1073/pnas.96.12.6988

288. Murayama A, Takeyama K, Kitanaka S, Kodera Y, Hosoya T, Kato S. The promoter of the human 25-hydroxyvitamin D_3 1 alpha-hydroxylase gene confers positive and negative responsiveness to PTH, calcitonin, and 1 alpha,25$(OH)_2D_3$. Biochem. Biophys. Res. Commun. 1998; 249(1):11-6. doi:10.1006/bbrc.1998.9098

289. Hobaus J, Thiem U, Hummel DM, Kallay E. Role of calcium, vitamin D, and the extrarenal vitamin D hydroxylases in carcinogenesis. Anticancer Agents Med. Chem. 2013; 13(1):20-35.

290. Young MV, Schwartz GG, Wang L, Jamieson DP, Whitlatch LW, Flanagan JN, *et al*. The prostate 25-hydroxyvitamin D-1 alpha-hydroxylase is not influenced by parathyroid hormone and calcium: Implications for prostate cancer chemoprevention by vitamin D. Carcinogenesis. 2004; 25(6):967-71. doi:10.1093/carcin/bgh082

291. Avila E, Díaz L, Halhali A, Larrea F. Regulation of 25-hydroxyvitamin D_3 1alpha-hydroxylase, 1,25-dihydroxyvitamin D_3 24-hydroxylase and vitamin D receptor gene

expression by 8-bromo cyclic AMP in cultured human syncytiotrophoblast cells. J Steroid Biochem. Mol. Biol. 2004; 89-90(1-5):115-9. doi:10.1016/j.jsbmb.2004.03.090

292. White JH. Regulation of intracrine production of 1,25-dihydroxyvitamin D and its role in innate immune defense against infection. Arch. Biochem. Biophys. 2012; 523(1):58-63. doi:10.1016/j.abb.2011.11.006

293. Matusiak D, Benya RV. CYP27A1 and CYP24 expression as a function of malignant transformation in the colon. J Histochem. Cytochem. 2007; 55(12):1257-64. doi:10.1369/jhc.7A7286.2007

294. Friedrich M, Meyberg R, Axt-Fliedner R, Villena-Heinsen C, Tilgen W, Schmidt W, *et al*. vitamin D receptor (VDR) expression is not a prognostic factor in cervical cancer. Anticancer Res. 2002; 22(1a):299-304.

295. Tanaka Y, Castillo L, DeLuca HF. The 24-hydroxylation of 1,25-dihydroxyvitamin D_3. J Biol. Chem. 1977; 252(4):1421-4.

296. Chen TC, Persons KS, Lu Z, Mathieu JS, Holick MF. An evaluation of the biologic activity and vitamin D receptor binding affinity of the photoisomers of vitamin D_3 and previtamin D_3. J Nutr. Biochem. 2000; 11(5):267-72. doi:10.1016/s0955-2863(00)00077-2

297. Tieu EW, Tang EK, Chen J, Li W, Nguyen MN, Janjetovic Z, *et al*. Rat CYP24A1 acts on 20-hydroxyvitamin D(3) producing hydroxylated products with increased biological activity. Biochem Pharmacol. 2012; 84(12):1696-704. doi:10.1016/j.bcp.2012.09.032

298. Brożyna AA, Jóźwicki W, Skobowiat C, Jetten A, Slominski AT. RORα and RORγ expression inversely correlates with human melanoma progression. Oncotarget. 2016; 7(39):63261-82. doi:10.18632/oncotarget.11211

299. Fu RD, Qiu CH, Chen HA, Zhang ZG, Lu MQ. Retinoic acid receptor-related receptor alpha (RORα) is a prognostic marker for hepatocellular carcinoma. Tumour Biol. 2014; 35(8):7603-10. doi:10.1007/s13277-014-2007-9

300. Lekva T, Berg JP, Heck A, Lyngvi Fougner S, Olstad OK, Ringstad G, *et al*. Attenuated RORc expression in the presence of EMT progression in somatotroph adenomas following treatment with somatostatin analogs is associated with poor clinical recovery. PloS one. 2013; 8(6):e66927-e. doi:10.1371/journal.pone.0066927

301. Oh TG, Bailey P, Dray E, Smith AG, Goode J, Eriksson N, *et al*. PRMT2 and RORγ expression are associated with breast cancer survival outcomes. Mol. Endocrinol. 2014; 28(7):1166-85. doi:10.1210/me.2013-1403

302. Oh TG, Wang S-CM, Acharya BR, Goode JM, Graham JD, Clarke CL, *et al*. The nuclear receptor, RORγ, regulates pathways necessary for breast cancer metastasis. EBioMedicine. 2016; 6:59-72. doi:10.1016/j.ebiom.2016.02.028

303. Roth HJ, Schmidt-Gayk H, Weber H, Niederau C. Accuracy and clinical implications of seven 25-hydroxyvitamin D methods compared with liquid chromatography-tandem mass spectrometry as a reference. Ann. Clin. Biochem. 2008; 45(Pt 2):153-9. doi:10.1258/acb.2007.007091

304. Shah I, James R, Barker J, Petroczi A, Naughton DP. Misleading measures in vitamin D analysis: A novel LC-MS/MS assay to account for epimers and isobars. Nutrition Journal. 2011; 10(1):46. doi:10.1186/1475-2891-10-46

305. Bavle RM. Mitosis at a glance. Journal of oral and maxillofacial pathology: JOMFP. 2014; 18(Suppl 1):S2-S5. doi:10.4103/0973-029X.141175

306. Elmore SA, Dixon D, Hailey JR, Harada T, Herbert RA, Maronpot RR, *et al*. Recommendations from the inhand apoptosis/necrosis working group. Toxicol. Pathol. 2016; 44(2):173-88. doi:10.1177/0192623315625859

307. Gounden S, Phulukdaree A, Moodley D, Chuturgoon A. Increased Sirt3 expression and antioxidant defense under hyperglycemic conditions in HEP2 cells. Metab Syndr Relat Disord. 2015; 13(6):255-63. doi:10.1089/met.2014.0140

308. Blomberg Jensen M, Andersen CB, Nielsen JE, Bagi P, Jørgensen A, Juul A, *et al*. Expression of the vitamin D receptor, 25-hydroxylases, 1α-hydroxylase and 24-hydroxylase in the human kidney and renal clear cell cancer. J. Steroid Biochem. Mol. Biol. 2010; 121(1):376-82. doi:https://doi.org/10.1016/j.jsbmb.2010.03.069

Appendices

Appendix A: Growth inhibitory studies conducted over 24 hours, 48 hours and 72 hours showing the GI_{50} concentration

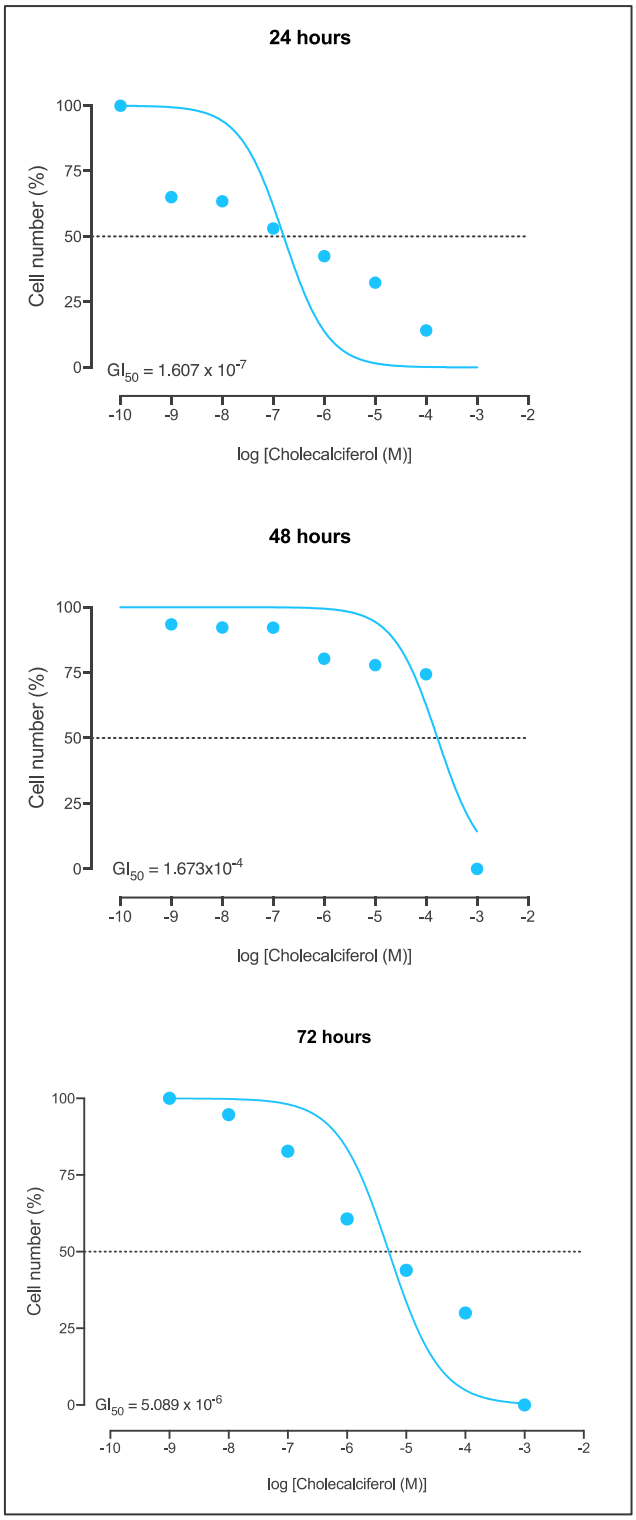

Appendix B: Crystal Violet Staining Solution (0.5%)

A. 0.5 g crystal violet powder (Sigma-Aldrich)
B. 80 mL distilled H_2O
C. 20 mL methanol
D. Dissolve crystal violet powder in H_2O and then add methanol. Store solution in the dark at room temperature.

Appendix C: Excitation and emission spectra of Muse™ Assays

		Dye 1		Dye 2	
	Assay	**Characteristic and fluorophore**	**Excitation and emission spectra**	**Characteristic and fluorophore**	**Excitation and emission spectra**
1	**Count and viability**	Cell permeant	ex: 548 nm em: 710 nm	Cell impermeant	ex: 540 nm em: 620 nm
2	**Ki67 Cell proliferation**	Phycoerythrin (PE) Conjugated anti-Ki67 antibody	Broad Em and Ex spectra	-	-
3	**Cell Cycle assay**	Propidium iodide	ex: 540 nm em: 620 nm	-	-
4	**Annexin V detection assay**	PE Conjugated anti-phosphatidylserine antibody	Broad Em and Ex spectra	Dead cell dye (7-AAD)	ex: 550 nm em: 646 nm
5	**Caspase 3/7 detection assay**	Caspase dye	ex: 565 nm em: 586 nm	Dead cell dye (7-AAD)	ex: 550 nm em: 646 nm
6	**Autophagy LC3-II detection assay**	AlexaFluor® 555 conjugated anti-LC3	ex: 555 nm em: 568 nm	-	-
7	**MitoPotential assay**	Tetramethylrhodamine, ethyl ester (TMRE)	ex: 561 nmem: 585 nm	Dead cell dye (7-AAD)	ex: 550 nmem: 646 nm
8	**Multicolour DNA Damage assay**	PE	Broad Em and Ex spectra	Pe-Cy5	ex: 565 em: 666

Appendix D: Preparation of assay and fixation buffers for the Muse™ Ki67 proliferation assay

1X Assay Buffer:

1. The Assay Buffer was supplied as a 5X concentrate that was diluted to a 1X working solution with DI water.
2. The 5X Assay Buffer concentrate was equilibrated to room temperature to dissolve any crystals that may have formed during storage.
3. 1-part 5X Assay Buffer was added to 4 parts DI water.
4. Approximately 500 µl of 1X Assay Buffer was required for each sample.
5. The solution was mixed by a gentle vortex.

1X Fixation Buffer:

1. The 1X Fixation Buffer is supplied as a 5X concentrate that was diluted to a 1X working solution with 1X PBS prior to use.
2. The 5X Fixation Buffer concentrate was equilibrated to room temperature to completely dissolve any crystals that may have formed during storage.
3. 1-part 5X Fixation Buffer was added to 4 parts 1X PBS.
4. Approximately 50 µl of 1X Fixation Buffer was required for each sample.
5. The solution was mixed by a gentle vortex.

Appendix E: Muse™ Caspase 3/7 detection assay reagents

Muse™ Caspase-3/7 Reagent working solution:

1. The Caspase-3/7 stock solution was freshly diluted with 1X PBS in a 1:8 ratio.
2. The working solution was stored on ice or at 2 to 8°C and was protected from light until use.
3. Each sample required 5 µl of the Muse™ Caspase-3/7 working solution.

Muse™ Caspase 7-AAD working solution:

1. The working solution was freshly prepared before use.
2. Add 2 µl of Muse™ Caspase 7-AAD stock solution to 148 µl of 1X Assay Buffer solution.
3. 150 µl of the Muse™ Caspase 7-AAD working solution was required for each sample.
4. The working solution was stored on ice or at 2 to 8°C and protected from light until use.

Appendix F: Muse™ Multi-Colour DNA Damage assay

Assay Buffer:

1. The Assay Buffer is supplied at 5X concentration and was diluted to 1X with deionized water prior to use.
2. The solution was stored at 4°C until required.

Antibody Working Cocktail Solution:

1. The kit contains two antibodies which were used in multiplex.
2. The antibody working cocktail solution contained equal parts anti-phospho-ATM (Ser1981) PE-conjugated and anti-phospho-Histone H2A.X (Ser139)-PECy5 conjugated antibodies.
3. Samples were stained by adding 10µl of the anti-body solution was added to each sample.

Appendix G: LDH reagent preparation

Tris Buffer, 200 mM, pH 8.0:

1. Dissolve 24.2 g Tris base in 1 L milli-Q water.
2. Adjust pH to 8.0 with hydrochloric acid.
3. Sterilize the solution by autoclave.

2X LDH assay buffer:

1. Dissolve 223 mg INT (2-p-iodophenyl-3-p-nitrophenyl-5-phenyl tetrazolium chloride), 57 mg PMS (N-methylphenazonium methyl sulphate) 575 mg NAD (nicotinamide adenine dinucleotide), and 3.2 g lactic acid in 480 mL 200 mM Tris buffer solution, pH 8.0.
2. Store the 2X LDH assay buffer in small aliquots at −20°C

10X Lysis solution: 9% Triton X-100:

1. Dissolve 9 mL Triton X-100 with 91 mL milli-Q water.

Stop solution:1 M acetic acid

Appendix H: H&E reagent preparation

1% Eosin stain:

1. Add 1.0 g of water-soluble eosin powder to 20 ml of double-distilled H_2O and mix until dissolved.
2. Then add 80 ml of 95% ethanol, and mix.
3. Store the solution at room temperature.

Each ethanol concentration for the graded series of ethanol was prepared by diluting absolute ethanol in DI water.

Appendix I: Morphological criteria assessed in control and experimental cultures by H&E stained microscopy

	Morphological criteria	**Description**
Mitosis	Prophase (late)	Chromosomes are distinctly seen, and centrioles move apart. Nuclear membrane disappears.[305]

	Metaphase	Chromosomes are lined up along the metaphase or equatorial plate. [305]
	Anaphase	Sister chromatids separate and begin to migrate to opposite poles of the cell and a cleavage furrow begins to develop.[305]
	Telophase	Terminal phase of mitosis and characterized by cytokinesis, reconstitution of nucleus and nuclear envelope, disappearance of mitotic spindle, and unwinding of chromosomes into chromatin.[305]
Cell apoptosis	Nuclear fragmentation (Karyorrhexis)	Condensation of chromatin in the nucleus and breaking down into smaller hyper-condensed fragments.[306]
	Membrane blebbing	Bulging of the plasma membrane of a cell causing irregular contour of the cell membrane.[306]
	Apoptotic bodies	Small, rounded hyperchromatic structures surrounding cells undergoing apoptosis.[306]
Cell necrosis	Cell swelling	Enlarged expanded cells. [306]
	Pale eosinophilic cytoplasm	Appear pale in colour with poor affinity to staining. [306]
Large multinucleate cells	Enlarged cells	Cells appear larger in surface area in comparison to surrounding cells.[283]
	Cells containing >2 nuclei	More than two distinct nuclei are present in the cell.[283]

Appendix J: Morphological criteria semi-quantified in control and apoptotic cells by H&E stained microscopy

	Morphological criteria	**Description**
Cell apoptosis	Nuclear fragmentation (Karyorrhexis)	Condensation of chromatin in the nucleus and breaking down into smaller hyper-condensed fragments.[306]
	Membrane blebbing	Bulging of the plasma membrane of a cell causing irregular contour of the cell membrane.[306]
	Apoptotic bodies	Small, rounded hyperchromatic structures surrounding cells undergoing apoptosis.[306]
Large multinucleated cells	Enlarged cells	Cells appear larger in surface area in comparison to surrounding cells.[283]
	Cells containing >2 nuclei	More than two distinct nuclei are present in the cell.[283]

Appendix K: Preparation of embedding solution for TEM analysis

Embedding solution preparation for 5g mixture

	5g
EmBed812	2.617g
MNA	1.767g
DDSA	0.683g
S1	0.05g

Appendix L: Ultrastructural criteria used in the assessment of control and experimental SiHa cells analysed by TEM

	Controls		Treatments (nM)			
TEM ultrastructural analysis	**Medium**	**Solvent**	**26**	**106**	**260**	**2600**
1. Apoptosis						
Cell membrane intact						
Cell membrane blebbing/apoptotic bodies						
Cell shrinkage						
Nuclear fragmentation						
2. Necrosis						
Cell membrane not intact						
Cell swelling						
Cytoplasmic vacuolation						
Mitochondrial swelling						
3. Autophagy						
Autophagic bodies						
Vacuoles						
Nuclear fragmentation						
4. Cellular abnormalities not stated above						

Appendix M: qPCR Primer optimisations

Primer sequences for the genes[307-308] investigated in this study, including sequences of the primer pairs and optimised annealing temperatures and primer concentration.

Amplicon	Forward (5' → 3')	Reverse (5' → 3')	Optimised primer concentration	Optimised annealing temperature
CYP2R1	AGA GAC CCA GAA GTG TTC CAT	GTC TTT CAG CAC AGA TGA GGT A	200 nM	58.7 ºC
CYP27A1	TGC GCC AGG CTC TGA ACC AG	TCC ACT TGG GGA GGA AGG TG	100 nM	50.0 ºC
CYP27B1	CCT GGC AGA GCT TGA ATT GCA	GGG GAA GAT GTA TAC CTT GGT	400 nM	58.5 ºC
VDR	GGA GAA AAC ACT TGT AAG TTG CT	TGG TCA GGT TGG TCT CGA ACT	100 nM	56.0 ºC
CYP24A1	CGG ACT CTT GAC AAG GCA ACA	TGA GGC GTA TTA TCG CTG GCA	400 nM	64.5 ºC
18s rRNA	ACA CGG ACA GGA TTG ACA GA	CAA ATC GCT CCA CCA ACT AA	—	—

CYP2R1

	Quantitation plot	Melt curve
100 nM	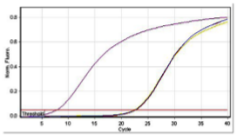	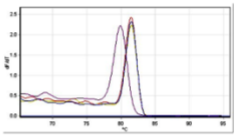
200 nM (optimal)	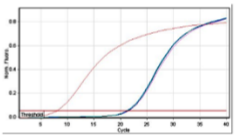	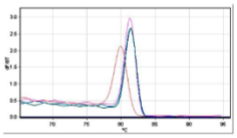
300 nM	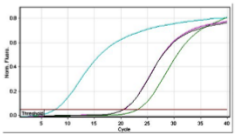	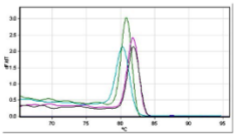
400 nM	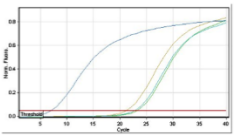	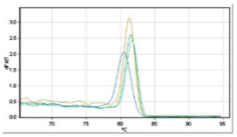
500 nM	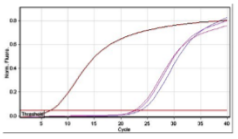	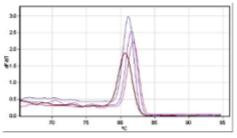
600 nM	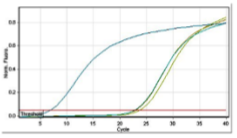	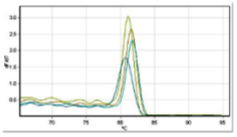
700 nM	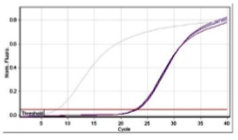	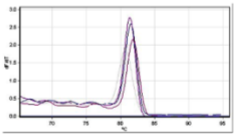
NTC	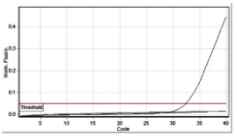	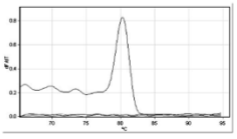

CYP27A1

	Quantitation plot	Melt curve
100 nM (optimal)	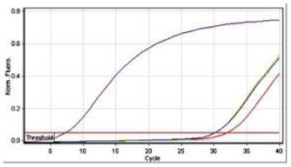	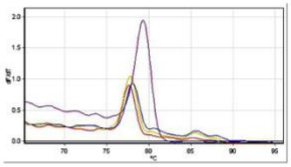
200 nM	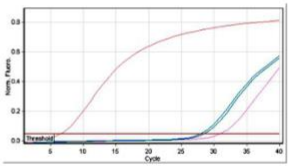	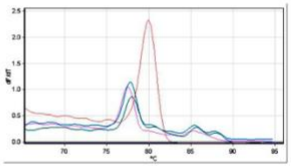
300 nM	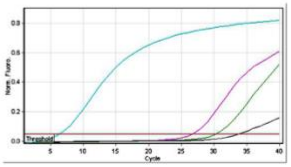	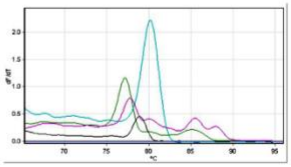
400 nM	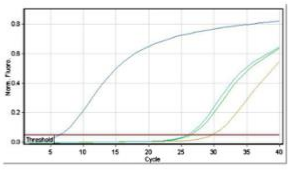	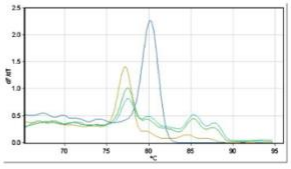
500 nM	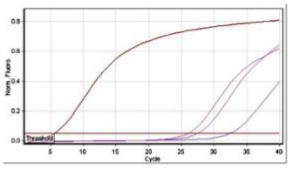	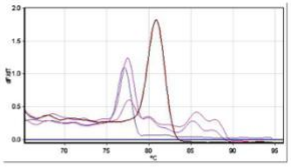
600 nM	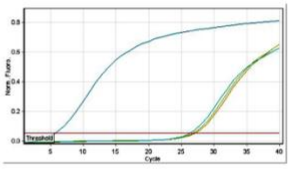	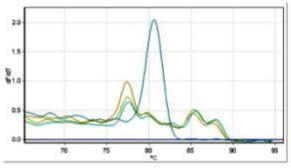
700 nM	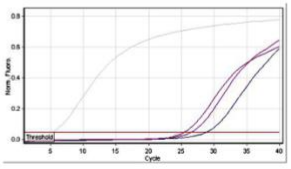	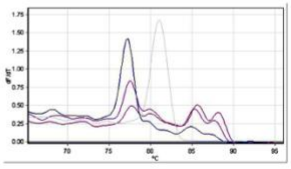
NTC	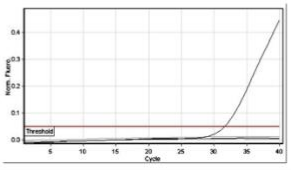	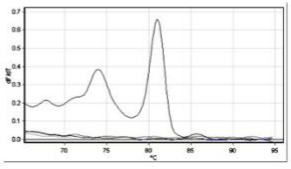

CYP27B1

	Quantitation plot	Melt curve
100 nM	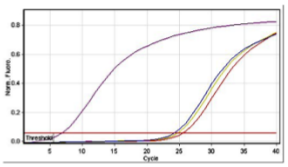	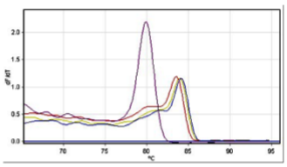
200 nM	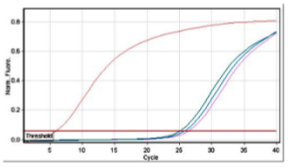	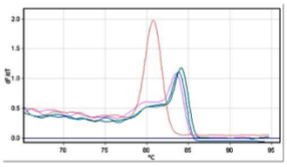
300 nM	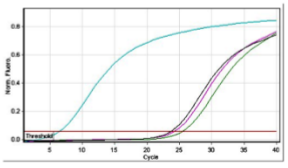	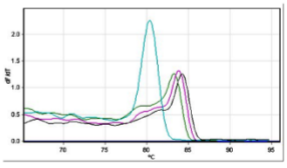
400 nM (optimal)	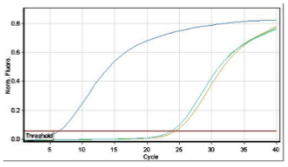	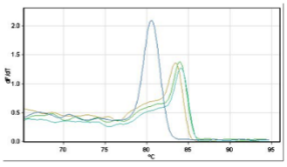
500 nM	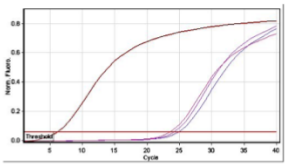	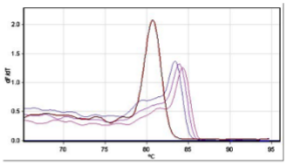
600 nM	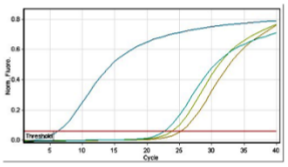	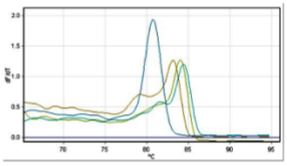
700 nM	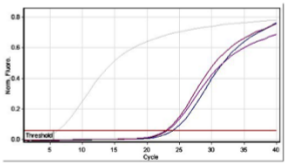	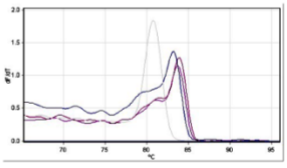
NTC	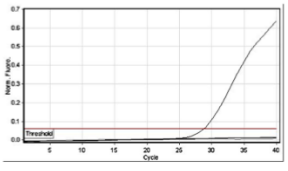	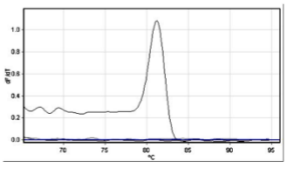

Vitamin D receptor (VDR)

	Quantitation plot	Melt curve
100 nM (optimal)	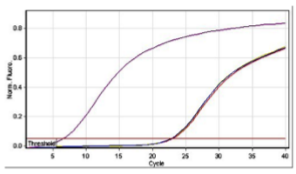	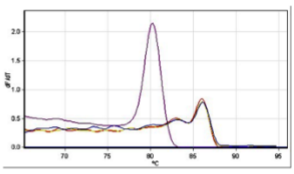
200 nM	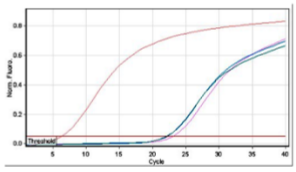	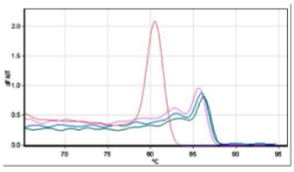
300 nM	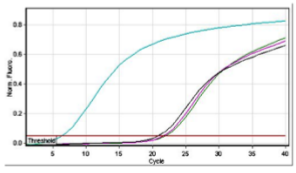	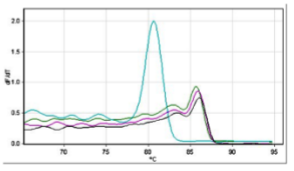
400 nM	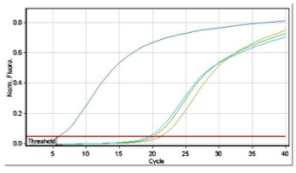	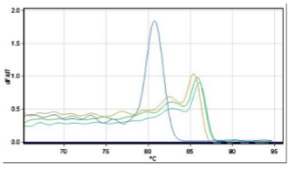
500 nM	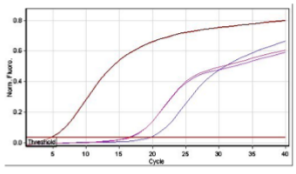	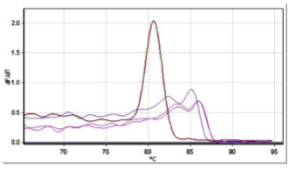
600 nM	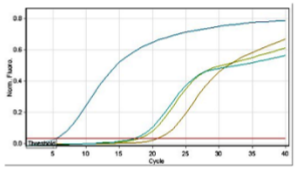	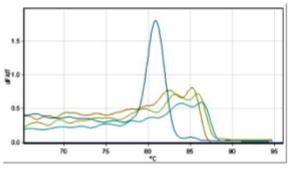
700 nM	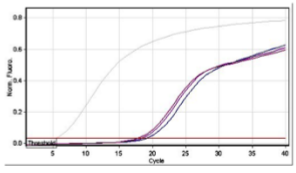	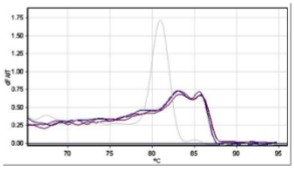
NTC	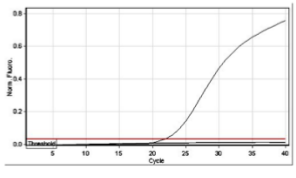	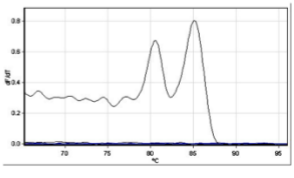

CYP24A1

	Quantitation plot	Melt curve
100 nM	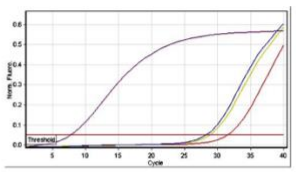	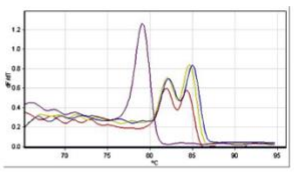
200 nM	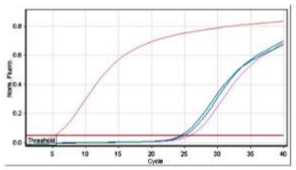	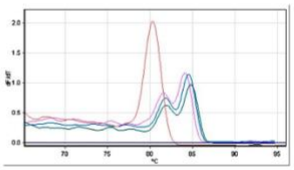
300 nM	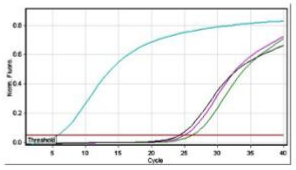	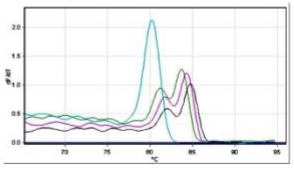
400 nM (optimal)	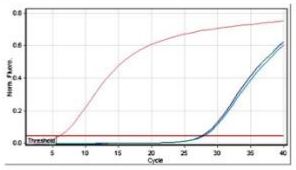	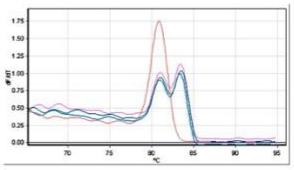
500 nM	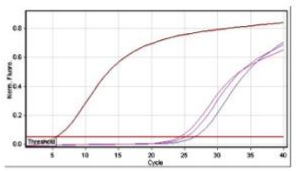	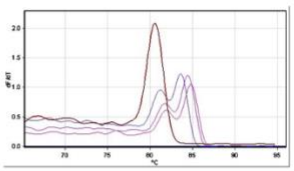
600 nM	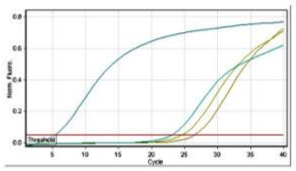	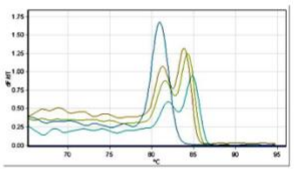
700 nM	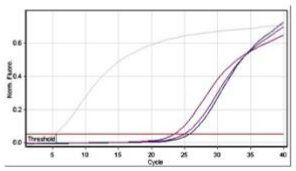	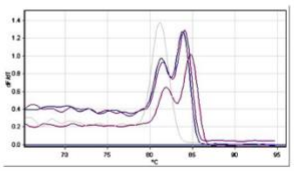
NTC	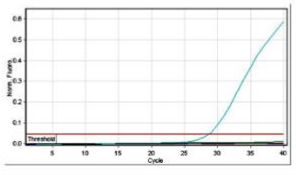	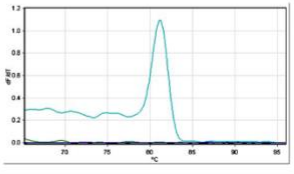

Appendix N: Efficiency plots

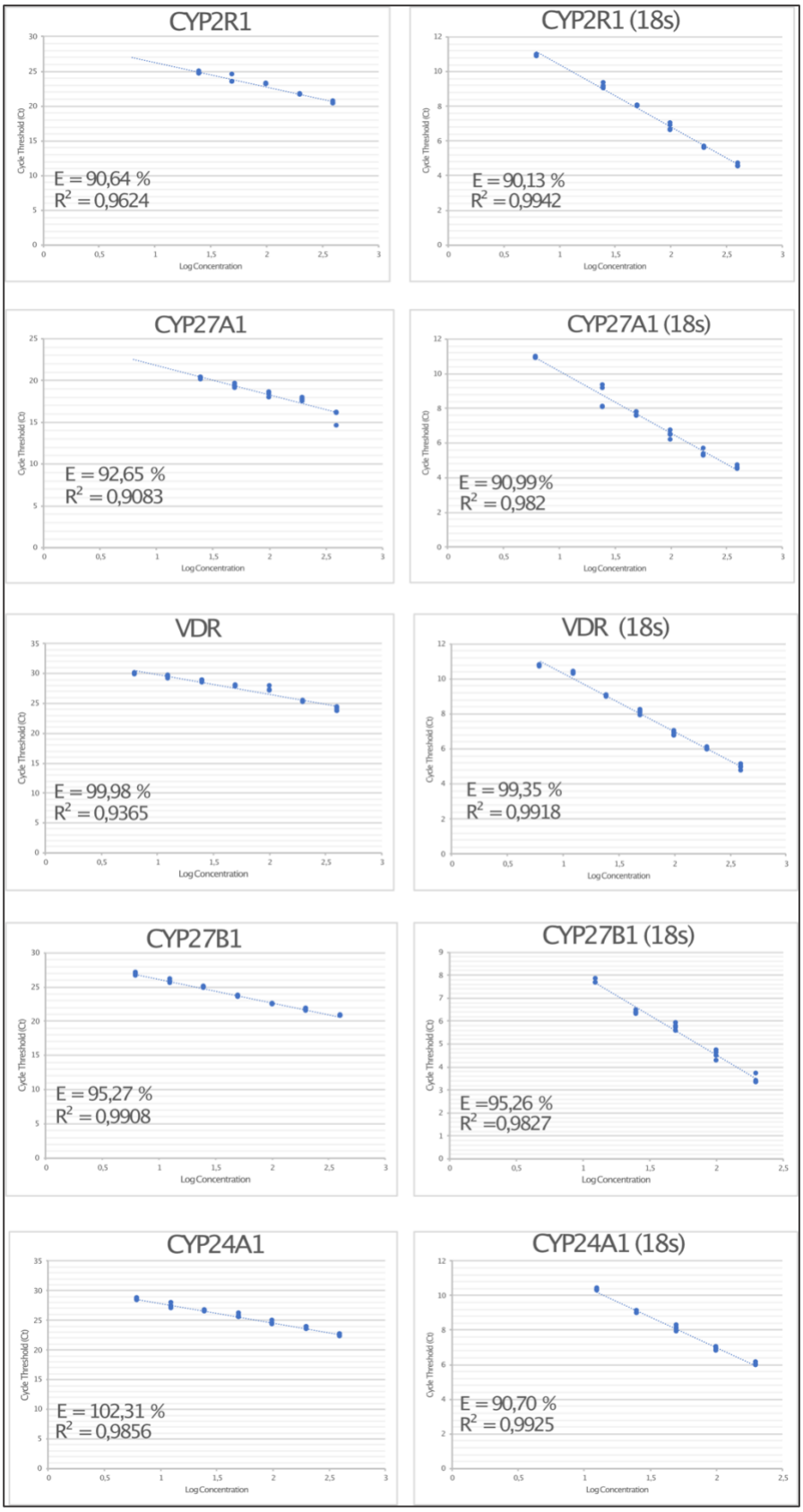

Appendix O: Western blot reagents

MOPS running buffer (20X): Add 104.6g of MOPS (50mM), 60.6g Trizma® base/Tris (50mM), 10g sodium dodecyl sulphate/sodium lauryl sulphate (0.1%) and 3g of EDTA (1 mM) to 500 ml ddH_2O. This buffer should have a pH of 7.7 and can be stored at 4°C for approximately 6 months. Dilute 20X MOPS running buffer using ddH_2O to make a 1X solution.

Transfer buffer (10X): Add 30.3g of Trizma® base (25mM) and 144g of glycine (192 mM) to 1L of ddH_2O. Transfer buffer should have a pH 8.3 and can be stored at 4°C for approximately 6 months. Dilute 10X transfer buffer using 20% MeOH to make a 1X solution. Ensure MeOH is ice-cold.

0.2% PBS-Tween: Dilute 200 µl of PBS-tween in 100 ml of PBS.

Appendix P: An example of a BCA protein assay standard curve

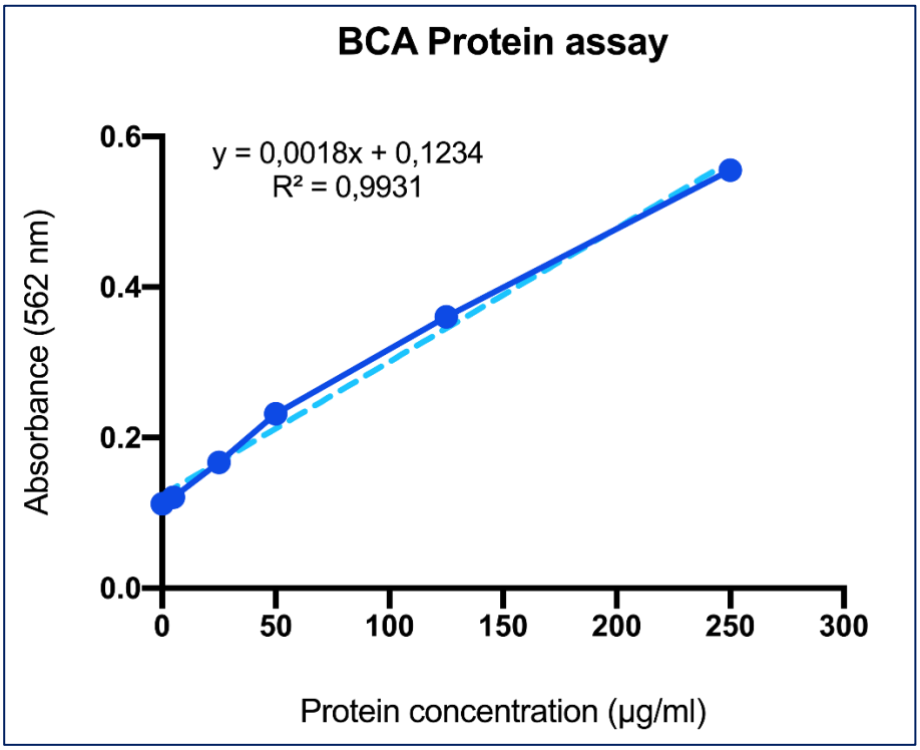

Appendix Q: Optimised antibody concentrations

Western blot antibody incubation conditions.

Protein Name	Antibody (catalogue number)	Concentration (antibody: blocking solution)	Incubation time and temperature	Blocking solution	Secondary antibody
1. CYP2R1	Anti-rabbit IgG, polyclonal CYP2R1 antibody (cat. no. #ab137634) (Abcam)	1:1000	4 ºC Overnight	0,125g BSA in 0.2% PBS-Tween	Goat Anti-Rabbit HRP-conjugated
2. CYP27A1	Monoclonal CYP27A1 antibody (cat. no. #ab126785) (Abcam)	1:500			
3. CYP27B1	Anti-rabbit IgG, monoclonal CYP27B1 antibody (cat. no. #ab206655) (Abcam)				
4. VDR	Rabbit IgG, monoclonal VDR antibody (cat. no. #12550) (Cell Signalling Technologies)				
5. CYP24A1	Polyclonal CYP24A1 antibody (cat. no. #ab175976) (Abcam)	1:1000			
6. Beta-Actin	Monoclonal anti-β-Actin−peroxidase antibody (cat. no. #A3854) (Sigma Aldrich)	1:5000	1 Hour at Room temperature	0,125g BSA in 0.2% PBS-Tween	Not Applicable-(Already HRP-Conjugated)
Secondary antibody	Goat Anti-rabbit IgG, HRP-linked antibody secondary antibody (cat. no. #E-AB-1003)	1: 5000	1 Hour at Room temperature	Not applicable	Not applicable

Appendix R: Ethics approval letter

UNIVERSITEIT VAN PRETORIA
UNIVERSITY OF PRETORIA
YUNIBESITHI YA PRETORIA

Faculty of Health Sciences

Institution: The Research Ethics Committee, Faculty Health Sciences, University of Pretoria complies with ICH-GCP guidelines and has US Federal wide Assurance.

- FWA 00002567, Approved dd 22 May 2002 and Expires 03/20/2022.
- IORG #: IORG0001762 OMB No. 0990-0279 Approved for use through February 28, 2022 and Expires: 03/04/2023.

10 June 2020

Approval Certificate
Annual Renewal

Ethics Reference No.: 141/2019
Title: Potential anticancer actions of cholecalciferol on a cervical squamous carcinoma cell line

Dear Prof T Pillay

The **Annual Renewal** as supported by documents received between 2020-05-22 and 2020-06-10 for your research, was approved by the Faculty of Health Sciences Research Ethics Committee on its quorate meeting of 2020-06-10.

Please note the following about your ethics approval:

- Renewal of ethics approval is valid for 1 year, subsequent annual renewal will become due on 2021-06-10.
- Please remember to use your protocol number (141/2019) on any documents or correspondence with the Research Ethics Committee regarding your research.
- Please note that the Research Ethics Committee may ask further questions, seek additional information, require further modification, monitor the conduct of your research, or suspend or withdraw ethics approval.

Ethics approval is subject to the following:

- The ethics approval is conditional on the research being conducted as stipulated by the details of all documents submitted to the Committee. In the event that a further need arises to change who the investigators are, the methods or any other aspect, such changes must be submitted as an Amendment for approval by the Committee.

We wish you the best with your research.

Yours sincerely

Dr R Sommers
MBChB MMed (Int) MPharmMed PhD
Deputy Chairperson of the Faculty of Health Sciences Research Ethics Committee, University of Pretoria

The Faculty of Health Sciences Research Ethics Committee complies with the SA National Act 61 of 2003 as it pertains to health research and the United States Code of Federal Regulations Title 45 and 46. This committee abides by the ethical norms and principles for research, established by the Declaration of Helsinki, the South African Medical Research Council Guidelines as well as the Guidelines for Ethical Research: Principles Structures and Processes, Second Edition 2015 (Department of Health)

Research Ethics Committee
Room 4-60, Level 4, Tswelopele Building
University of Pretoria, Private Bag x323
Gezina 0031, South Africa
Tel +27 (0)12 356 3084
Email: deepeka.behari@up.ac.za
www.up.ac.za

Fakulteit Gesondheidswetenskappe
Lefapha la Disaense tša Maphelo

Appendix S: Biostatistician clearance letter

Date: 18 / 2 /20 19

LETTER OF CLEARANCE FROM THE BIOSTATISTICIAN

This letter is to confirm that,

Name(s): Mr Sachin Bhoora

from the University of Pretoria

discussed with me the study titled Potential anticancer actions of cholecalciferol on a cervical carcinoma cell line

I hereby confirm that I am aware of the project and also undertake to assist, if possible, with the Statistical analysis of the data generated from the project.

The analytical tool(s) that will be used is (are) Descriptive statistics by treatment. Treatments will be compared using one-way ANOVA followed by post-hoc analysis for treatment differences.

to achieve the objective(s) of the study.

Name: PJ Becker **(Tel:** 012-319-2203)

Signature

Research Office,

Faculty of Health Sciences, UP

BIOSTATISTICS
Faculty of Health Sciences
Research Office
2019 -02- 18
UNIVERSITY OF PRETORIA